

# Gas-phase Fe/O and Fe/N abundances in Star-Forming Regions

## Relations between nucleosynthesis, metallicity and dust

J. E. Méndez-Delgado<sup>1</sup>, K. Kreckel<sup>1</sup>, C. Esteban<sup>2,3</sup>, J. García-Rojas<sup>2,3</sup>, L. Carigi<sup>4</sup>, A.A.C. Sander<sup>1</sup>, M. Palla<sup>5,6</sup>, M. Chruślińska<sup>7</sup>, I. De Looze<sup>8</sup>, M. Relaño<sup>9,10</sup>, S.A. van der Giessen<sup>8,9</sup>, E. Reyes-Rodríguez<sup>2,3</sup>, S. F. Sánchez<sup>11,2</sup>

<sup>1</sup> Astronomisches Rechen-Institut, Zentrum für Astronomie der Universität Heidelberg, Mönchhofstraße 12-14, D-69120 Heidelberg, Germany e-mail: jemd@uni-heidelberg.de

<sup>2</sup> Instituto de Astrofísica de Canarias, E-38205 La Laguna, Tenerife, Spain

<sup>3</sup> Departamento de Astrofísica, Universidad de La Laguna, E-38206 La Laguna, Tenerife, Spain

<sup>4</sup> Instituto de Astronomía, Universidad Nacional Autónoma de México, Ap. 70-264, 04510 CDMX, México

<sup>5</sup> Dipartimento di Fisica e Astronomia “Augusto Righi”, Alma Mater Studiorum, Università di Bologna, Via Gobetti 93/2, 40129 Bologna, Italy

<sup>6</sup> INAF-Osservatorio di Astrofisica e Scienza dello Spazio di Bologna, Via Gobetti 93/3, 40129 Bologna, Italy

<sup>7</sup> Max Planck Institute for Astrophysics, Karl-Schwarzschild-Str. 1, D-85748 Garching, Germany

<sup>8</sup> Sterrenkundig Observatorium, Ghent University, Krijgslaan 281 - S9, 9000 Gent, Belgium

<sup>9</sup> Dept. Física Teórica y del Cosmos, E-18071 Granada, Spain

<sup>10</sup> Instituto Universitario Carlos I de Física Teórica y Computacional, Universidad de Granada, E-18071 Granada, Spain

<sup>11</sup> Universidad Nacional Autónoma de México, Instituto de Astronomía, AP 106, Ensenada 22800, BC, México

August 13, 2024

### ABSTRACT

**Context.** In stars, metallicity is usually traced using Fe, while in nebulae, O serves as the preferred proxy. Both elements have different nucleosynthetic origins and are not directly comparable. Additionally, in ionized nebulae, Fe is heavily depleted onto dust grains.

**Aims.** We investigate the distribution of Fe gas abundances in a sample of 452 star-forming nebulae with [Fe III]  $\lambda$ 4658 detections and their relationship with O and N abundances. Additionally, we analyze the depletion of Fe onto dust grains in photoionized environments.

**Methods.** We homogeneously determine the chemical abundances with direct determinations of electron temperature ( $T_e$ ), considering the effect of possible internal variations of this parameter. We adopt a sample of 300 Galactic stars to interpret the nebular findings.

**Results.** We find a moderate linear correlation ( $r = -0.59$ ) between Fe/O and O/H. In turn, we report a stronger correlation ( $r = -0.80$ ) between Fe/N and N/H. We interpret the tighter correlation as evidence of Fe and N being produced on similar timescales while Fe-dust depletion scales with the Fe availability. The apparently flat distribution between Fe/N and N/H in Milky Way stars supports this interpretation. We find that when  $12+\log(\text{O}/\text{H}) < 7.6$ , the nebulae seem to reach a plateau value around  $\log(\text{Fe}/\text{O}) \approx -1.7$ . If this trend is confirmed, it would be consistent with a very small amount of Fe-dust in these systems, similar to what is observed in high- $z$  galaxies discovered by the *James Webb Space Telescope* (JWST). We derive a relationship that allows us to approximate the fraction of Fe trapped into dust in ionized nebulae. If the O-dust scales in the same way, its possible contribution in low metallicity nebulae would be negligible. After analyzing the Fe/O abundances in J0811+4730 and J1631+4426, we do not see evidence of the presence of very massive stars with  $M_{\text{init}} > 300M_{\odot}$  in these systems.

**Conclusions.** The close relation observed between the N and Fe abundances has the potential to serve as a link between stellar and nebular chemical studies. This requires an expansion of the number of abundance determinations for these elements in both stars and star-forming nebulae, especially at low metallicities.

**Key words.** ISM: abundances – ISM: dust – Galaxies: abundances – Stars: abundances – H II regions – Nucleosynthesis

## 1. Introduction

The determination of metallicity, which refers to the abundance of elements heavier than helium, and its distribution are key to understanding the formation and evolution of galaxies in the Universe. However, studies focused in the chemical composition of the ionized nebulae trace metallicity using the oxygen abundance, whereas the stars typically use iron as a proxy for this parameter. Since the nucleosynthetic origin of both elements is different, the comparison between one metallicity proxy and the other is not straightforward, being the central topic of several studies (Matteucci & Greggio 1986; Wheeler et al. 1989; Grat-

ton et al. 2000; Walcher et al. 2009; Nicholls et al. 2017; Sánchez et al. 2021; Chruślińska et al. 2024).

O is produced primarily by massive stars and mainly released into the interstellar medium (ISM) through core-collapse supernovae (CCSN) on short time-scales (Woosley et al. 2002; Chiappini et al. 2003; Kobayashi et al. 2020). Other elements like Ne, S, and Ar can also be produced by massive stars through the alpha process, which would link their relative abundances (Chiappini et al. 2003; Carigi et al. 2005; Croxall et al. 2016; Esteban et al. 2020; Rogers et al. 2022; Arellano-Córdova et al. 2024). On the other hand, the Fe-peak elements such as Fe, Ni, Cr, Mn are mostly produced by explosive nucleosynthesis, mainly in type Ia supernovae (SN-Ia) (Chiappini et al. 2003) with variable contri-

butions from massive stars (Gratton et al. 2000; Palla 2021). Due to these differences, it is expected that the abundance of Fe is not always proportional to that of O, but their relative abundance depends on the stellar formation and evolution. For instance, it is expected that in young regions of high star formation, the production of Fe would be delayed in comparison to that of O, since the former element requires a time period of at least  $\sim 40$  Myrs to form stellar systems that give rise to SN-Ia (Greggio 2005; Maoz & Mannucci 2012; Chruślińska et al. 2024).

Nitrogen is an interesting element that could serve as a bridge between stellar metallicities, usually traced via Fe, and nebular ones, commonly traced via O. Several works have pointed to two main nucleosynthetic mechanisms as the origin of N (Vila-Costas & Edmunds 1993; Henry et al. 2000; Israelian et al. 2004; Nava et al. 2006; Nicholls et al. 2017; Romano et al. 2019; Grisoni et al. 2021). N can be produced on short timescales, analogous to O, known as the primary production mechanism. On the other hand, intermediate-mass stars ( $3M_{\odot} < M < 8M_{\odot}$ ) are capable of producing N at the expense of C and O through the CNO cycle (van den Hoek & Groenewegen 1997; Henry et al. 2000; Vincenzo et al. 2016; Ventura et al. 2022), known as the secondary production mechanism. Stars more massive than those mentioned earlier may also contribute nitrogen formed through the CNO cycle (Mollá et al. 2006; Przybilla et al. 2010), although their overall contributions are expected to be smaller (Henry et al. 2000). Wolf-Rayet stars can also contaminate the ISM with nitrogen-rich ejecta through stellar winds (Meynet & Maeder 2005; Crowther 2007). The release of the main secondary-produced N requires timescales that allow the evolution of intermediate-mass stars ( $\sim 40$  Myr (Chruślińska et al. 2024)). This condition is also necessary for the formation of stellar systems that give rise to SN-Ia, producers of Fe.

There are various difficulties in analyzing Fe, N, and O relations in the nebular emission spectra of star-forming regions. In these systems, most of the Fe atoms are usually depleted into dust grains, which are able to survive in photoionized environments (Osterbrock et al. 1992; Rodríguez 1996; Izotov et al. 2006; Roman-Duval et al. 2022b,a). [Fe III] emission lines arising from the gaseous-phase iron are typically faint, up to an order of magnitude fainter than temperature-sensitive auroral lines (e.g., [O III]  $\lambda 4363$ , [N II]  $\lambda 5755$ ). Other Fe-signatures, such as those from [Fe II], can arise from starlight through fluorescent processes, further complicating their analysis (Rodríguez 1999; Verner et al. 2000). Additionally, the complex atomic structures of the Fe ions make their radiative and collisional models under nebular conditions susceptible to containing significant systematic uncertainties (Rodríguez & Rubin 2005).

Fortunately, since the pioneering work of Osterbrock et al. (1992), who determined the first gaseous Fe/H abundance in the Orion Nebula, there has been significant progress both observationally and theoretically. Studies dedicated to the properties of the faint auroral lines and ultra-faint heavy element recombination lines (RLs) have indirectly also detected multiple [Fe III] emission lines (Rodríguez 2002; Izotov et al. 2006; Esteban et al. 2009; Peimbert et al. 2007; Mesa-Delgado et al. 2009; Berg et al. 2015; Kojima et al. 2021; Méndez-Delgado et al. 2021a). On the other hand, recent atomic studies have allowed for the inference of the  $\text{Fe}^{2+}$  radiative and collisional properties with an accuracy of  $\sim 20\%$  (Mendoza et al. 2023), sufficient for reliable estimates of its ionic abundances. This opens up the possibility of accurately studying the gaseous Fe abundance in star-forming regions and its relationship with other chemical properties. Since [Fe III] lines are present even in some high-redshift galaxies, recently unveiled with the *James Webb Space Telescope*

(JWST) (Arellano-Córdova et al. 2022; Welch et al. 2024), a better understanding of this element provides additional pieces of information about the composition and chemical evolution of the Universe.

The depletion of Fe into dust grains in photoionized environments is an active research area, with important implications for other elements such as O (Jenkins 2009; Jones et al. 2017; Hensley & Draine 2023). There is no consensus on the precise chemical composition of dust in photoionized environments, but it is expected to consist mainly of the leftovers from the cool clouds where star formation initially started. In neutral clouds, it is believed that Fe exists as nano-inclusions in large silicate dust grains and other types of free-flying Fe compounds (Jones et al. 2017; Hensley & Draine 2023). If most of the Fe-rich dust grains present in photoionized environments are in the form of silicates, they could then be linked to the depletion of O. In contrast, the survival of mostly free-flying Fe compounds would decouple the depletion of Fe from that of O. Therefore, determining the Fe dust fraction and its environmental dependencies may be key to quantifying the O depletion and understanding the properties of interstellar dust.

Additionally, recent results based on the high gaseous abundances of Fe/O in low-metallicity galaxies by Kojima et al. (2021) have suggested the existence of very massive stars with  $M_{\text{init}} > 300M_{\odot}$  in these systems. The presence of such stars would imply the need for inclusion in photoionization models (Goswami et al. 2021, 2022; Watanabe et al. 2024), which in turn could help us to understand the existence of intense He II lines in low-metallicity photoionized systems (López-Sánchez & Esteban 2009; Schaerer et al. 2019).

Given the importance of the gas phase Fe abundances and its relation with other elements as O and N in several physical phenomena, we examine in this study the largest sample of star-forming regions, both Galactic and extragalactic, from the literature with precise determinations of Fe, O, and N. We further adopt stellar chemical abundances from the literature to compare and discuss in the context of the results from ionized nebulae. Following the methodology of the DEep Spectra of Ionized REgions Database (DESIREd) project (Méndez-Delgado et al. 2023a), we have uniformly analyzed 452 optical spectra from Galactic and extragalactic star-forming regions, including the Sunburst Arc, a high-redshift system ( $z = 2.37$ ), recently observed with the JWST (Welch et al. 2024). We have directly determined their ionic abundances of  $\text{Fe}^{2+}/\text{H}^+$ ,  $\text{N}^+/\text{H}^+$ ,  $\text{O}^+/\text{H}^+$ ,  $\text{O}^{2+}/\text{H}^+$ , through precise calculations of their electron density and temperature ( $n_e, T_e$ ), while also considering the effects of temperature inhomogeneities (Peimbert 1967; Peimbert & Costero 1969; Bergerud et al. 2020; Cameron et al. 2023; Méndez-Delgado et al. 2023b).

In Sec. 2, we describe our observational sample of both stars and nebulae. In Sec. 3, we outline the methodology used to calculate the physical conditions and chemical abundances of the analyzed nebular sample. Additionally, Sec. 4 is dedicated to detailing the issues involved in calculating the total gaseous abundance of Fe, owing to discrepancies between photoionization models and direct determinations of  $\text{Fe}^{3+}$  abundance. In Sec. 5, we present the nebular and stellar Fe/O and Fe/N distributions from our sample. These results and their implications for various astrophysical topics are discussed in Sec. 6. Finally, in Sec. 7, we summarize our findings.

## 2. Observational sample

As part of the DESIRED project (Méndez-Delgado et al. 2023a), we compile all reported emission line intensities, corrected by reddening, from Table D.2. This constitutes a subset of what an extended version of DESIRED encompasses ( $\sim 2000$  optical spectra with direct determinations of  $T_e$ ). We standardize the formats, providing individual notes for each line in case of observational defects or blends. This enables a uniform and consistent analysis of the entire database in a straightforward fashion. Analysis codes and the standardized spectra will be presented in a forthcoming paper. DESIRED aims to be a collaborative project that facilitates the analysis of deep spectra from photoionized regions, including H II regions, planetary nebulae and Herbig-Haro objects beyond partial compilations of a limited number of emission lines.

The extension of the original DESIRED sample (Méndez-Delgado et al. 2023a) brings additional complications due to the different observational conditions present in the literature. For example, at low spectral resolution, lines typically used in density diagnostics such as [Ar IV]  $\lambda 4711$  can be blended with He I  $\lambda 4713$ , or other temperature-sensitive lines like [O III]  $\lambda 4363$  can be mixed with [Fe II]  $\lambda 4360$ . In all these cases, we have placed special emphasis and added cautionary notes when compiling this information in the DESIRED format. These notes are considered to discard lines with observational problems from the analysis of physical conditions, analogous to the approach established by Méndez-Delgado et al. (2023a). In addition to handling notes, we consider additional tests to ensure the quality of the data. For example, we verify that [O III]  $\lambda 5007/\lambda 4959$ , [S III]  $\lambda 9531/\lambda 9069$ , and [N II]  $\lambda 6584/\lambda 6548$  are consistent with theoretical values within 20%; otherwise, they are discarded. This is described in higher detail in Sec. 3.

The selected data for this article present reliable detections (with errors smaller than 40%) of the [Fe III]  $\lambda 4658$  line, which is the most suitable line for determining the  $\text{Fe}^{2+}/\text{H}^+$  abundances due to its relatively high intensity (Rodríguez 2002; Mesa-Delgado et al. 2009; Méndez-Delgado et al. 2021a) and because it originates from some of the best-known atomic transitions (Mendoza et al. 2023). Additionally, a sub-sample of the data contains detections of [Fe III]  $\lambda 4702$ , another relatively bright and well-known line. More importantly, these observations contain at least one detection of the following auroral/nebular intensity ratios: [O III]  $\lambda 4363/\lambda 5007$ , [N II]  $\lambda 5755/\lambda 6584$ , and [S III]  $\lambda 6312/\lambda 9069$ . These ratios are highly sensitive to  $T_e$  and are insensitive to density up to values of  $n_e \sim 10^4 \text{ cm}^{-3}$  (Froese Fischer & Tachiev 2004; Tayal 2011). A good determination of  $T_e$  is critical for obtaining reliable chemical abundances in optical spectra, given the exponential dependence of line emissivity of the collisionally excited lines (CELs) on this parameter (Osterbrock & Ferland 2006). In Fig. 1 we show the position of the sample of H II regions used in the present study in the Baldwin-Phillips-Terlevich (BPT) diagram (Baldwin et al. 1981), showing that we have not included regions with hard ionizing sources, which are usually to the right of the Kauffmann et al. (2003) line. The observational sample covers a metallicity range from  $12+\log(\text{O}/\text{H}) \approx 6.9$  to  $12+\log(\text{O}/\text{H}) \approx 8.9$  ( $r^2 = 0$ , Peimbert 1967).

Additionally, we adopt Galactic stellar abundances available for Fe, O, and N from B-type stars (Nieva & Przybilla 2012; Weßmayer et al. 2022) and other dwarf stars, including metal-poor ones (Carretta et al. 2000; Israelian et al. 2004; Cayrel et al. 2004; Ecuivillon et al. 2004; Spite et al. 2006; Bensby et al. 2013; Magrini et al. 2018; Amarsi et al. 2019). We exclude stars that

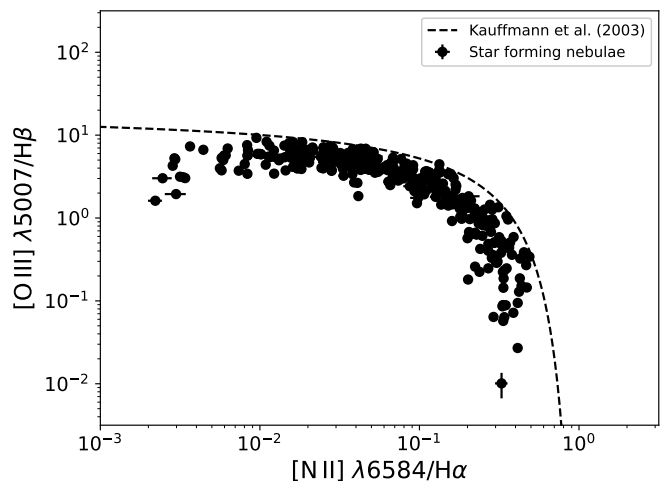


**Fig. 1.** BPT diagram of the selected nebular spectra. The dashed line represents the empirical relation by Kauffmann et al. (2003) that distinguishes between star-forming regions and active galactic nuclei (AGNs).

have undergone mixing with deep layers of the star, thereby affecting the observed CNO abundances from Carretta et al. (2000) and Spite et al. (2006). We add a 0.40 dex correction to the Fe abundances in the stars from Spite et al. (2006) for 3D/NLTE effects (Spite et al. 2006; Kobayashi et al. 2020).

The selected B-type stars represent the present-day chemical composition of the ISM, and their elemental abundances could ideally be compared to those of H II regions. However, in practice, this is not the case. Detailed studies of the O/H abundances from ionizing stars in Galactic H II regions (Simón-Díaz et al. 2006; Simón-Díaz & Stasińska 2011; García-Rojas et al. 2014) show systematically higher abundances of  $\sim 0.2$  dex in comparison to the nebular determinations when using CELs and the so-called “direct method” (Dinerstein 1990; Peimbert et al. 2017). If instead of nebular CELs, ultra-faint heavy element RLs are used, the discrepancies practically disappear, which is interpreted as evidence in favor of an inhomogeneous nebular temperature structure (Peimbert 1967; Carigi et al. 2005; García-Rojas & Esteban 2007; Méndez-Delgado et al. 2022a; Esteban et al. 2022). Other giant B-type stars may exhibit large chemical variations in CNO abundances due to strong mixing processes, complicating their direct comparison with H II regions element by element (Trundle et al. 2007; Hunter et al. 2007; Przybilla et al. 2010; Garcia et al. 2014). This will be further discussed in Sec. 6.3. The metal-poor Galactic stars do not reflect the current composition of the ISM, but rather part of its chemical past if they are not polluted by their own evolution. This is the case with our selected sample of dwarf stars. Their inclusion allows us to understand the evolution of Fe/O and Fe/N abundances with respect to O/H and N/H.

Overall, the number of low-metallicity stars with simultaneous determinations of N and Fe in the literature is relatively limited. A primary challenge often encountered is the detection of N abundance indicators, which remain faint even at solar metallicities (Asplund 2005; Amarsi et al. 2020, 2021). Additionally, the determination of Fe can be problematic, particularly in the case of hotter massive stars. For stars with  $T_{\text{eff}} \gtrsim 24 \text{ kK}$ , corresponding approximately to the spectral type B0.5, there are no optical Fe lines (e.g., Thompson et al. 2008) and instead the iron forest at UV wavelengths has to be analyzed, which is chal-



lenging. Even in the B-star regime, the Fe lines are generally weak and high-quality (high S/N, high resolution) spectra are required. Hence, many studies examining abundances in massive stars resort to determine CNO abundances, but adopt a solar or solar-scaled Fe abundance by default (e.g., Martins et al. 2015; Bragança et al. 2019).

### 3. Nebular physical conditions and chemical abundances

#### 3.1. Electron density and temperature

To determine the physical conditions of the gas, we use *PyNeb* 1.1.18 (Luridiana et al. 2015) with the atomic dataset presented in Table D.1 and the H I effective recombination coefficients from Storey & Hummer (1995). We first employ the *getCrossTemDen* routine with line intensity ratios sensitive to  $n_e$  and  $T_e$ . We test density-sensitive diagnostics such as [S II]  $\lambda 6731/\lambda 6716$ , [O II]  $\lambda 3726/\lambda 3729$ , [Cl III]  $\lambda 5538/\lambda 5518$ , [Fe III]  $\lambda 4658/\lambda 4702$ , and [Ar IV]  $\lambda 4740/\lambda 4711$  with temperature-sensitive diagnostics including [N II]  $\lambda 5755/\lambda 6584$ , [O III]  $\lambda 4363/\lambda 5007$ , [Ar III]  $\lambda 5192/\lambda 7135$ , and [S III]  $\lambda 6312/\lambda 9069$ .

Firstly, each density-sensitive diagnostic is cross-correlated with all available temperature diagnostics using a Monte Carlo experiment of 100 points to propagate uncertainties in line intensities. For each convergence, a value of  $n_e$  and  $T_e$  and their associated uncertainties are obtained. The average  $n_e$ , weighted by the inverse square of the error of the different convergences, is adopted as the representative value of the diagnostic (e.g.,  $n_e([\text{O II}] \lambda 3726/\lambda 3729)$ ). This approach enables us to consider the small temperature dependence of density diagnostics under typical nebular conditions.

Once the density for each diagnostic is established, we follow the criteria suggested in Sec. 5 by Méndez-Delgado et al. (2023a) to estimate a global average density. If  $n_e([\text{S II}] \lambda 6731/\lambda 6716) < 100 \text{ cm}^{-3}$ , we adopt  $n_e = 100 \pm 100 \text{ cm}^{-3}$ . If  $100 \text{ cm}^{-3} \leq n_e([\text{S II}] \lambda 6731/\lambda 6716) < 1000 \text{ cm}^{-3}$ , we adopt the average between  $n_e([\text{S II}] \lambda 6731/\lambda 6716)$  and  $n_e([\text{O II}] \lambda 3726/\lambda 3729)$ . If  $n_e([\text{S II}] \lambda 6731/\lambda 6716) \geq 1000 \text{ cm}^{-3}$ , we adopt the averages of  $n_e([\text{S II}] \lambda 6731/\lambda 6716)$ ,  $n_e([\text{O II}] \lambda 3726/\lambda 3729)$ ,  $n_e([\text{Cl III}] \lambda 5538/\lambda 5518)$ ,  $n_e([\text{Fe III}] \lambda 4658/\lambda 4702)$ , and  $n_e([\text{Ar IV}] \lambda 4740/\lambda 4711)$ . In cases where it is not possible to determine the density, such as in the spectra reported by Izotov et al. (2006), we adopt  $n_e = 100 \pm 100 \text{ cm}^{-3}$ .

Although there is temperature stratification (i.e., a representative temperature for each ionization volume, Stasińska 1978; Osterbrock & Ferland 2006; Peimbert et al. 2017; Berg et al. 2021), the possible existence of density stratification is not obvious among the different density diagnostics of H II regions (Méndez-Delgado et al. 2023a). These diagnostics have non-uniform sensitivities with  $n_e$ , and are susceptible to systematic biases (Peimbert 1971; Rubin 1989; Tsamis et al. 2003; Méndez-Delgado et al. 2022a). The impact of these density biases is small in optical spectra if a good determination of  $T_e$  is adopted (up to 0.1 dex if auroral lines are used to determine ionic abundances; Méndez-Delgado et al. 2023b; Rickards Vaught et al. 2024) but critical in chemical abundance studies with fine structure infrared CELs (Rubin 1989; Tsamis et al. 2003; Stasińska et al. 2013; Méndez-Delgado et al. 2024). Therefore, as a good approximation, adopting the global average density value, we estimate the temperatures  $T_e([\text{N II}] \lambda 5755/\lambda 6584)$ ,  $T_e([\text{O III}] \lambda 4363/\lambda 5007)$ ,

$T_e([\text{Ar III}] \lambda 5192/\lambda 7135)$ , and  $T_e([\text{S III}] \lambda 6312/\lambda 9069)$  using the *getTemDen* routine from PyNeb.

Being a critical parameter, we exercise strict control over the determination of  $T_e$ . In addition to excluding lines with errors larger than 40%, we compare the observed line intensity ratios of nebular transitions with their theoretical predictions. Lines arising from the same upper atomic level (e.g., [O III]  $\lambda \lambda 5007, 4959$ , [S III]  $\lambda \lambda 9531, 9069$ , [N II]  $\lambda \lambda 6584, 6548$ ) have fixed relative intensities given by the Einstein radiative coefficients, regardless of the physical conditions of the gas (Storey & Zeppen 2000). If the observed line intensity ratios differ by more than 20% from the theoretical predictions, their use for determining  $T_e$  is discarded. In the particular case of [S III]  $\lambda \lambda 9531, 9069$ , when  $\lambda 9531/\lambda 9069 < 2.47$ , it is assumed that [S III]  $\lambda 9531$  is affected by telluric absorption bands (Noll et al. 2012), while [S III]  $\lambda 9069$  is not. This is the most common case in the literature with particular exceptions such as the Orion Nebula (Baldwin et al. 1996). Unfortunately, in a small number of cases, it is not possible to perform this test, as only one of the nebular lines is reported. In these cases, we consider the  $T_e$  results valid. In any case, for this specific work, we only adopt  $T([\text{S III}])$  to determine ionic abundances in the absence of  $T([\text{N II}])$  and  $T([\text{O III}])$ .

Another important case is that of  $T_e([\text{O III}])$ , where [O III]  $\lambda 4363$  can be blended with [Fe II]  $\lambda 4360$  (Curti et al. 2017) when the spectral resolution is intermediate or low. In instances where we have detected this blend, we have discarded the use of [O III]  $\lambda 4363$ , ensuring that we do not introduce spurious overestimations of  $T_e([\text{O III}])$ . The impact of this blend is greater in regions of high metallicity and low ionization degree (Arellano-Córdova & Rodríguez 2020). Most of the star-forming regions with these characteristics analyzed in this work come from the CHAOS sample (Berg et al. 2015), which has taken special care in separating [O III]  $\lambda 4363$  and [Fe II]  $\lambda 4360$  (Berg et al. 2020; Rogers et al. 2021, 2022). Therefore, this potential observational issue will not systematically affect the analysis of the sample presented here. We show our derived physical conditions in Tables D.3 and D.4.

#### 3.2. Ionic abundances

To determine the ionic abundances of  $\text{Fe}^{2+}$ ,  $\text{N}^+$ ,  $\text{O}^+$ , and  $\text{O}^{2+}$ , we use the [Fe III]  $\lambda \lambda 4658, 4702$ , [N II]  $\lambda \lambda 6548, 6584$ , [O II]  $\lambda \lambda 3727, 3729$ , and [O III]  $\lambda \lambda 4959, 5007$  lines. In cases where both lines of each pair are available, we use the sum of their relative intensities to  $\text{H}\beta$ . Otherwise, we use the available line. In cases where [O II]  $\lambda \lambda 3727, 3729$  are not available due to spectral coverage limitations or observational defects in the blue arm, we use the auroral lines [O II]  $\lambda \lambda 7319, 7320, 7330, 7331$  to estimate the abundance of  $\text{O}^+$ . Considering similarities in ionization potential, we adopt a common temperature, representative of low-ionization ions, to estimate the abundances of  $\text{Fe}^{2+}$ ,  $\text{N}^+$ , and  $\text{O}^+$ . In the same manner, to determine the abundance of  $\text{O}^{2+}$ , we adopt a temperature representative of high-ionization.

Ionic abundances are estimated in two ways: considering a nebular homogeneous temperature structure ( $t^2 = 0$ ), known as “the direct method”, and accounting for the effect of an inhomogeneous temperature structure ( $t^2 > 0$ ) (Peimbert 1967). Following the empirical results of Méndez-Delgado et al. (2023b), we performed corrections for temperature inhomogeneities only for highly ionized ions. For  $t^2 = 0$ , we adopt  $T_e([\text{N II}] \lambda 5755/\lambda 6584)$  and the global  $n_e$  in the *getIonAbundance* routine of PyNeb, propagating uncertainties through 100-point Monte Carlo experiments. When  $T_e([\text{N II}] \lambda 5755/\lambda 6584)$  is unavailable, we employ the temperature relations of Garnett (1992) to estimate  $T_e([\text{N II}])$

from  $T_e([\text{O III}] \lambda 4363/\lambda 5007)$  or  $T_e([\text{S III}] \lambda 6312/\lambda 9069)$ , when the first diagnostic is also absent. Similarly, the abundance of  $\text{O}^{2+}$  is determined using  $T_e([\text{O III}] \lambda 4363/\lambda 5007)$  and the derived global average density. In cases where  $T_e([\text{O III}] \lambda 4363/\lambda 5007)$  is not available, we use the temperature relations of Garnett (1992) along with measurements of  $T_e([\text{N II}] \lambda 5755/\lambda 6584)$  and/or  $T_e([\text{S III}] \lambda 6312/\lambda 9069)$ . For  $t^2 > 0$ , the treatment of low-ionization ions is identical to that described above. In the case of  $\text{O}^{2+}$ , we adopt  $T_0(\text{O}^{2+})$ , estimated from Equation (4) of Méndez-Delgado et al. (2023b). To roughly estimate the effect of  $t^2$  when  $T_e([\text{N II}] \lambda 5755/\lambda 6584)$  is not available, we determine  $T_0(\text{O}^{2+})$  by combining Equation (4) of Méndez-Delgado et al. (2023b) with Equation (2) of Garnett (1992).

In the present study, we do not add additional errors when using a temperature relationship to connect one  $T_e$  diagnostic with another (e.g., if we have  $T_e([\text{N II}] \lambda 5755/\lambda 6584)$  with a 15% error, and we use a relationship to infer  $T_e([\text{O III}] \lambda 4363/\lambda 5007)$ , we assume that  $T_e([\text{O III}] \lambda 4363/\lambda 5007)$  also has a 15% error). This is a lower limit to the uncertainties of the inferred temperature, similar to the approach of Skillman et al. (2003). However, we have been particularly careful about the impact of potential systematic errors introduced by the temperature relationships, with special emphasis on what happens in the low-metallicity regime. Under such conditions, the temperature relationships have not been sufficiently tested with empirical determinations, having limited statistics among simultaneous determinations of  $T_e([\text{N II}] \lambda 5755/\lambda 6584)$ ,  $T_e([\text{O III}] \lambda 4363/\lambda 5007)$ , and  $T_0(\text{O}^{2+})$  when  $T_e > 13,000\text{K}$  (Esteban et al. 2009; Berg et al. 2020; Arellano-Córdova et al. 2020; Méndez-Delgado et al. 2023b,a). This is analyzed in greater detail in Sec. B. In general, the potential impact of severe systematic errors in the temperature relationships could be up to  $\sim 0.05$  dex in the Fe/O and Fe/N distributions. The adopted temperatures for determining the ionic abundances are shown in Table D.5. Ionic abundances are shown in Table D.6.

### 3.3. Total abundances

To estimate the total abundance of O/H, we directly sum the contributions of the ionic abundances  $\text{O}^+/\text{H}^+$  and  $\text{O}^{2+}/\text{H}^+$ . The possible contribution of  $\text{O}^{3+}/\text{H}^+$  was not considered, as it is expected to be very small (Amayo et al. 2021). In extremely metal-poor H II regions ( $12+\log(\text{O}/\text{H}) < 7.5$ ), ionization conditions may be harder than expected in photoionization models, leading to relatively strong emissions of He II. Under these conditions, an Ionization Correction Factor (ICF) can be implemented, as is typically done in the study of planetary nebulae (PNe, Torres-Peimbert & Peimbert 1977). However, observational studies on the contribution of  $\text{O}^{3+}/\text{H}^+$  to the total O/H abundance in metal-poor regions often find values up to the order of 5% (Izotov & Thuan 1999; Domínguez-Guzmán et al. 2022). This was also found by Berg et al. (2021) in two Extreme Emission Line Galaxies with direct  $\text{O}^{3+}/\text{H}^+$  abundances measured from the UV O IV] lines. This fraction is small for the purposes of this study and does not affect our conclusions. However, other studies such as those dedicated to estimating the He/O fractions must consider it, as they require a precision better than 1% (Peimbert & Torres-Peimbert 1974; Pagel et al. 1992; Izotov & Thuan 1998a; Peimbert et al. 2002; Aver et al. 2015; Valerdi et al. 2019; Méndez-Delgado et al. 2020; Hsyu et al. 2020; Kurichin et al. 2021; Matsumoto et al. 2022).

The choice of  $t^2 = 0$  or  $t^2 > 0$  in determining the total O/H abundances of our observational sample of star-forming regions has an impact of 0.1-0.2 dex, as shown in Fig. 2. All determinations shown in black dots are based on CELs, following the procedure described in Sec. 3.2. For comparison, the figure displays

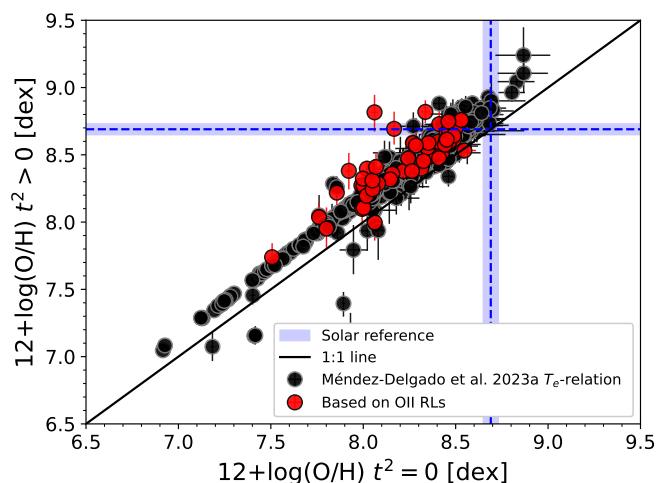


**Fig. 2.** Comparison of O/H abundances in the sample of star-forming regions considering a homogeneous temperature structure ( $t^2 = 0$ ) and considering temperature variations ( $t^2 > 0$ ) following the empirical relations derived by Méndez-Delgado et al. (2023b). Red dots indicate the O/H abundances determined from the ultra-faint O II-RLs, which are insensitive to temperature. The solar O/H abundance from Asplund et al. (2021) is shown as a reference.

abundances estimated with the temperature-insensitive O II RLs (red dots), in objects with the deepest spectra. Additionally, the solar reference by Asplund et al. (2021) is included. The choice of  $t^2 = 0$  or  $t^2 > 0$  results in differences of around 0.1-0.2 dex in the distributions of Fe/O and Fe/N, as discussed in Sec. 4. These differences may be relevant for the absolute values of Fe/O and Fe/N. On the other hand, the shape of the Fe/O and Fe/N distributions seems to remain unchanged, as it is shown in Sec. C.

From the entire sample, 7 regions (Hubble V (Peimbert et al. 2005), NGC 3603 (García-Rojas et al. 2006), POX36, SBS0335-052E, J1205+4551 (Izotov & Thuan 2004; Izotov et al. 2009, 2017, 2021), Tol1214-277 (Guseva et al. 2011) and NGC 5449-2 (Croxall et al. 2016)) showed substantially higher O abundances in the case of  $t^2 = 0$  compared to the case  $t^2 > 0$  using the temperature relation proposed by Méndez-Delgado et al. (2023b). This suggests discrepancies between the values of  $T_e([\text{N II}] \lambda 5755/\lambda 6584)$  and  $T_e([\text{O III}] \lambda 4363/\lambda 5007)$  beyond temperature variations. The most obvious case is NGC 5449-2 (Croxall et al. 2016), where  $[\text{N II}] \lambda 5755/\lambda 6584$  suggest a  $T_e([\text{N II}] > 40,000\text{K}$  (see Table D.4). This could be a non-reported observational error (Croxall et al. 2016) did not report  $T_e([\text{N II}] \lambda 5755/\lambda 6584)$  for this region, but they do not mention any observational problem that would necessitate discarding  $[\text{N II}] \lambda 5755/\lambda 6584$ . In the case of NGC 3603, it may be an aperture effect by not covering the entire Galactic nebula. Other regions like J1205+4551 could have overestimations in  $T_e([\text{N II}] \lambda 5755/\lambda 6584)$  due to some phenomenon related to the presence of WR stars enriching the ISM with N (Izotov et al. 2021). In these cases, we adopt only the  $t^2 = 0$  values for our analysis, exerting no influence on our conclusions.

It is interesting to note that if  $t^2 = 0$  is considered in general, H II regions with abundances clearly higher than solar are rather rare, being only P203 and +30.8+139.0 from the M51 galaxy (Croxall et al. 2015), -35d7+119d6 from NGC 628 (Berg et al. 2015) and +75.7+89.1 and -35.7+119.6 from NGC 3184 (Berg et al. 2020), respectively. This, of course, could be a selection bias of our sample, dedicated to the detection of  $[\text{Fe III}]$  emission lines. However, in the literature, there are only  $\sim 20$  additional examples of regions with  $T_e$ -based metallicity estimations higher

than solar (with  $t^2 = 0$ ) (Castellanos et al. 2002; Rosolowsky & Simon 2008; Bresolin et al. 2005; Bresolin 2007; Croxall et al. 2015, 2016; Lin et al. 2017; Patterson et al. 2012; Berg et al. 2015; Arellano-Córdova et al. 2021; Rogers et al. 2021, 2022). In our Galaxy, only Sh 2-48 and Sh 2-53 (Arellano-Córdova et al. 2021) would reach metallicities close to solar, but they are approximately 4 kpc closer to the Galactic center than the Sun. In contrast, massive O and B-type stars in the solar neighborhood ( $d < 3$  kpc) typically exhibit solar or supersolar metallicities (Simón-Díaz et al. 2006; Nieva & Przybilla 2012; Martins et al. 2015; Weßmayer et al. 2022).

To determine the abundances of N/H and Fe/H, the use of an ICF is required to estimate the contributions of unobserved ionic states. In the case of N, it is necessary to estimate the contribution of  $N^{2+}$  in the ionized gas that does not emit lines in the optical spectrum. To this purpose, we adopt the scheme proposed by Amayo et al. (2021), based on photoionization models by Vale Asari et al. (2016) constructed using CLOUDY (Ferland et al. 2017). The ICF of Amayo et al. (2021) utilizes the similarity between the ionization potentials of  $N^+$  and  $O^+$  as proposed by Peimbert & Costero (1969), while also considering departures dependent on the ionization degree of the gas.

In the case of Fe, it is necessary to consider both the contribution of  $Fe^+$  and  $Fe^{3+}$ . Although there are lines such as [Fe II]  $\lambda 8617$  or [Fe IV]  $\lambda 6740$  optimal for the direct estimation of ionic abundances, these are generally very weak or found in complicated spectral regions affected by telluric absorptions. Therefore, initially one would think of using a classical ICF as those adopted in the case of other elements such as N, S, Ar, Ne (Amayo et al. 2021). Considering the ionization potentials of  $Fe^{2+}$ ,  $O^+$ , and  $N^+$ , the obvious choice would be to construct an ICF scheme considering the predictions of photoionization models on the relative abundances of these ions. However, Fe is a particularly complex element in star-forming nebulae because it is heavily depleted in dust grains. The relationships between the ionic fractions of Fe may be inconsistent with photoionization models if the fraction of Fe depleted in dust grains is different in the volumes where  $Fe^+$ ,  $Fe^{2+}$ , and  $Fe^{3+}$  ions are located. We generally adopt the ICF proposed in Eq. 2 of Rodríguez & Rubin (2005). However, it is important to note that the Fe-ICF is a potentially important source of errors as is discussed in Sec. 4. ICF(N) and ICF(Fe) numerical values are presented in Table D.7 while the total abundances are shown in Table D.8.

#### 4. The problematic calculation of the total gaseous Fe abundances in ionized nebulae

It is well known that different ICF schemes in the literature can yield significantly different results for various elements (e.g., see the discussions by Arellano-Córdova et al. 2020; Amayo et al. 2021; Arellano-Córdova et al. 2024). In the case of Fe, there is a systematic discrepancy between the predictions of Eq. 24 from Izotov et al. (2006) and Eq. 2 from Rodríguez & Rubin (2005). In Fig. 3, we show the comparison between both schemes in our sample of star-forming nebulae. The differences between these two ICFs for Fe can reach a systematic offset of up to  $\sim 0.2$  dex (see also Kojima et al. 2021). To determine whether the ICF model of Izotov et al. (2006) overestimates the Fe abundances or the model of Rodríguez & Rubin (2005) underestimates them, or even the possibility that both models provide incorrect predictions, it is necessary to test both models in regions where direct estimates of all ionization states of Fe expected in the ionized gas are available.

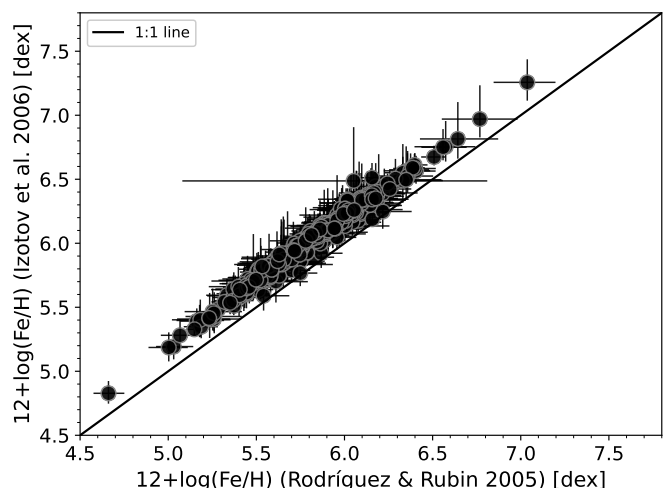


**Fig. 3.** Comparison between the Fe-ICF models of Izotov et al. (2006) and Rodríguez & Rubin (2005) in our adopted sample of star-forming nebulae. Both schemes were derived from photoionization models and are based on the determination of the ionic abundance of  $Fe^{2+}$ .

In Table 1, we present the ionic and total abundances in a sample of nebulae with detections of [Fe IV]  $\lambda 6740$ , which are useful for the direct estimation of  $Fe^{3+}/H^+$  abundance. Other ionization states such as  $Fe^+$  and  $Fe^{4+}$  can be estimated using the lines [Fe II]  $\lambda 8617$ , 8892 (Mendoza et al. 2023) and [Fe V]  $\lambda 4227$ . To calculate the abundances of  $Fe^+$ , we adopted the same temperature used to estimate the abundances of  $O^+$ ,  $N^+$ , and  $Fe^{2+}$ , while for the abundances of  $Fe^{3+}$  and  $Fe^{4+}$ , we adopted the same temperature used for  $O^{2+}$  (see Sec. 3). Note that the contributions of  $Fe^+$  and  $Fe^{4+}$  to the total Fe abundances are generally very small, while the contribution of  $Fe^{3+}$  is always significant. The direct sum of ionic abundances can be compared directly with the predictions of Fe-ICFs by Rodríguez & Rubin (2005) and Izotov et al. (2006), based on the predictions of photoionization models using the measured abundance of  $Fe^{2+}$  and the degree of ionization. This exercise is performed for both  $t^2 = 0$  and  $t^2 > 0$ . In this last case, the ionic abundances of  $Fe^{3+}$  and  $Fe^{4+}$  increase (Méndez-Delgado et al. 2023b), as well as the degree of ionization  $O^{2+}/O^+$ , which modifies the predictions of the Fe-ICF models.

As shown in Figures 4 and 5, both Fe-ICFs exhibit a high dispersion compared to the directly determined values. Notably, the Fe-ICF by Izotov et al. (2006) overestimates the total Fe abundances in almost all cases, showing differences of up to  $\sim 0.7$  dex compared to the directly estimated total value. Discrepancies between the predictions of photoionization models and the directly determined gaseous Fe values, considering  $t^2 = 0$ , have been known since the pioneering work of Rubin et al. (1997). This discrepancy, known as “The [Fe IV] discrepancy” (Rodríguez & Rubin 2005), consists of photoionization models predicting  $Fe^{3+}$  abundances higher than those obtained observationally through the direct method, considering  $t^2 = 0$ . This problem is clearly seen in the upper panels of Figures 4 and 5, where practically all objects show higher Fe abundances in calculations using ICF. This issue appears to improve when considering the effects of temperature inhomogeneities, using the formalism of Peimbert (1967) and the empirical results of Méndez-Delgado et al. (2023b). Under this scheme, empirical abundances of highly ionized ions, such as  $Fe^{3+}$ , increase when correcting the temperature bias introduced by an inhomogeneous



**Table 1.** Ionic and total Fe abundances compared to the predictions of the Fe-ICFs from Rodríguez & Rubin (2005) and Izotov et al. (2006), derived from photoionization models. These values were calculated both considering an homogeneous nebular temperature ( $t^2 = 0$ ) and considering the effect of  $t^2 > 0$ . The abundance values are presented in units of  $12+\log(X/H)$ . The reference number is also shown for consistency with the values in Table D.2.

Ref.	Region	Fe <sup>+</sup> /H <sup>+</sup>	Fe <sup>2+</sup> /H <sup>+</sup>	Fe <sup>3+</sup> /H <sup>+</sup>	Fe <sup>4+</sup> /H <sup>+</sup>	Ionic Sum	ICF R&R05 <sup>g</sup>	ICF I06 <sup>h</sup>
$t^2 = 0$								
D83	HS1851+6933 <sup>a</sup>	-	5.20 <sup>+0.06</sup> <sub>-0.05</sub>	5.59 ± 0.04	4.49 <sup>+0.05</sup> <sub>-0.04</sub>	5.76 ± 0.03	5.88 ± 0.06	6.12 <sup>+0.06</sup> <sub>-0.05</sub>
D451	W1702+18 <sup>a</sup>	-	4.95 <sup>+0.04</sup> <sub>-0.03</sub>	5.28 <sup>+0.06</sup> <sub>-0.05</sub>	4.53 ± 0.05	5.50 ± 0.04	5.81 ± 0.03	6.07 ± 0.03
D224	Orion Nebula <sup>b</sup>	4.69 <sup>+0.04</sup> <sub>-0.05</sub>	5.55 ± 0.03	5.71 ± 0.07	-	5.96 ± 0.04	6.11 ± 0.03	6.32 ± 0.03
D235	NGC2579 <sup>c</sup>	-	5.40 ± 0.03	5.24 <sup>+0.16</sup> <sub>-0.14</sub>	-	5.63 <sup>+0.06</sup> <sub>-0.07</sub>	5.88 ± 0.03	6.11 ± 0.03
D236	NGC3576 <sup>d</sup>	4.59 ± 0.06	5.53 <sup>+0.04</sup> <sub>-0.03</sub>	5.72 <sup>+0.09</sup> <sub>-0.08</sub>	-	5.95 ± 0.05	5.95 ± 0.03	6.18 <sup>+0.04</sup> <sub>-0.03</sub>
D283	Mrk71 <sup>e</sup>	-	4.32 <sup>+0.18</sup> <sub>-0.10</sub>	4.97 <sup>+0.08</sup> <sub>-0.07</sub>	-	5.06 ± 0.06	5.45 ± 0.14	5.72 <sup>+0.18</sup> <sub>-0.10</sub>
D403	SMC-N88A <sup>f</sup>	-	4.99 <sup>+0.04</sup> <sub>-0.03</sub>	5.47 ± 0.04	-	5.59 ± 0.03	6.00 <sup>+0.08</sup> <sub>-0.06</sub>	6.27 <sup>+0.04</sup> <sub>-0.03</sub>
$t^2 > 0$								
D83	HS1851+6933 <sup>a</sup>	-	5.20 <sup>+0.07</sup> <sub>-0.05</sub>	6.48 <sup>+0.13</sup> <sub>-0.09</sub>	5.05 <sup>+0.09</sup> <sub>-0.06</sub>	6.52 <sup>+0.11</sup> <sub>-0.10</sub>	6.29 ± 0.06	6.58 <sup>+0.06</sup> <sub>-0.05</sub>
D451	W1702+18 <sup>a</sup>	-	4.94 ± 0.03	5.63 <sup>+0.07</sup> <sub>-0.05</sub>	4.74 <sup>+0.05</sup> <sub>-0.04</sub>	5.76 <sup>+0.05</sup> <sub>-0.04</sub>	5.98 ± 0.03	6.25 ± 0.03
D224	Orion Nebula <sup>b</sup>	4.69 <sup>+0.05</sup> <sub>-0.04</sub>	5.55 ± 0.03	5.75 <sup>+0.10</sup> <sub>-0.09</sub>	-	5.99 ± 0.05	6.12 ± 0.03	6.34 ± 0.03
D235	NGC2579 <sup>c</sup>	-	5.40 ± 0.03	5.84 ± 0.14	-	5.97 ± 0.10	6.10 ± 0.03	6.31 ± 0.03
D236	NGC3576 <sup>d</sup>	4.59 ± 0.05	5.53 <sup>+0.04</sup> <sub>-0.03</sub>	6.42 <sup>+0.13</sup> <sub>-0.09</sub>	-	6.48 ± 0.09	6.19 ± 0.04	6.40 ± 0.03
D283	Mrk71 <sup>e</sup>	-	4.33 <sup>+0.17</sup> <sub>-0.11</sub>	5.49 <sup>+0.47</sup> <sub>-0.10</sub>	-	5.51 <sup>+0.31</sup> <sub>-0.29</sub>	5.70 ± 0.14	6.03 <sup>+0.19</sup> <sub>-0.11</sub>
D403	SMC-N88A <sup>f</sup>	-	4.99 <sup>+0.04</sup> <sub>-0.03</sub>	5.78 <sup>+0.07</sup> <sub>-0.06</sub>	-	5.84 <sup>+0.07</sup> <sub>-0.06</sub>	6.16 ± 0.04	6.44 <sup>+0.04</sup> <sub>-0.03</sub>

**References.** *a*: Izotov et al. (2021); *b*: Méndez-Delgado et al. (2021a); *c*: Esteban et al. (2013); *d*: García-Rojas et al. (2004); *e*: Esteban et al. (2009); *f*: Domínguez-Guzmán et al. (2022); *g*: Rodríguez & Rubin (2005); *h*: Izotov et al. (2006).

physical conditions structure (Peimbert 1967; Cameron et al. 2023).

Although in the lower panel of Fig. 4, the data points lie both above and below the line (suggesting statistical rather than systematic errors), the dispersion remains very high at around  $\sim 0.2$  dex. This dispersion may be due to various factors, including errors in the atomic models of Fe, as suggested by Rodríguez & Rubin (2005), or to the assumptions made to determine the ionic abundances. However, it is important to mention the possibility that such dispersion may be real, resulting from various physical phenomena. We suggest the possibility that the fraction of Fe trapped in dust may differ between the volume where Fe<sup>2+</sup> and Fe<sup>3+</sup> are present. It is expected that the energy of photons interacting with dust grains is different in the low and high ionization volumes, inducing a different dust grain fragmentation rate. Additionally, shock waves and stellar winds in the different ionization volumes may play a role. If the fraction of Fe trapped in dust grains is higher in the volume where Fe<sup>2+</sup> coexists than where Fe<sup>3+</sup> does, then an ICF based on the gaseous fraction of Fe<sup>2+</sup> and the degree of ionization will underestimate the gaseous abundance of Fe, and vice versa. It is also possible that radiation pressure and stellar winds are capable of moving dust grains (Rodríguez 2002) from one ionization volume to another, inducing concentration variations in the nebulae.

Considering the present discussion, we adopt as default the ICF scheme from Eq. 2 of Rodríguez & Rubin (2005) and the nebular abundances considering  $t^2 > 0$ . However, a greater number of nebulae with detections of the [Fe IV]  $\lambda 6740$  line or another transition of that ion would be highly beneficial for constraining potential errors in the total estimation of gaseous Fe in ionized nebulae.

## 5. Gas phase Fe distributions

### 5.1. Fe and O nebular abundances

In Fig 6, we present the distribution of Fe/O, both in Galactic stellar objects and in Galactic and extragalactic star-forming nebulae. In the stellar panel, the observed distribution is well-known (Amarsi et al. 2019; Kobayashi et al. 2020; Chruślińska et al. 2024) and exhibits an increasing trend with respect to O/H. This is consistent with the predictions from the different enrichment timescales of CCSNe as primary O producers and SNe-Ia as primary Fe producers (e.g., Chruślińska et al. 2024). It is important to note that at the low metallicities covered in our sample, Fe/O remains relatively constant, with  $\log(\text{Fe}/\text{O}) = -1.80 \pm 0.11$ , consistent with the value reported by Amarsi et al. (2019) and Chruślińska et al. (2024) for Galactic low-metallicity dwarf stars. The stellar distribution of Fe/O vs O/H resembles the distribution of N/O versus O/H observed in nebular regions (Henry et al. 2000; Nava et al. 2006; Nicholls et al. 2017). These analogous behaviors can be explained by the similar timescales required to form a white dwarf in a stellar system that gives rise to a SN-Ia (Fe producers) and that required for an intermediate-mass star to release the N produced via CNO processes ( $\sim 40$  Myr).

Although there is a relatively small number of objects (23, see Table 2) with  $12+\log(\text{O}/\text{H}) < 7.6$ , most of the star-forming nebulae in the lower panel of Fig. 6 seem to exhibit a flattening in the Fe/O distribution around  $\log(\text{Fe}/\text{O}) = -1.74 \pm 0.15$ , rather consistent within the errors with the  $\log(\text{Fe}/\text{O}) = -1.80 \pm 0.11$  determined in stellar objects. This may indicate that regions within this range of O/H abundances exhibit a negligible fraction of Fe depleted in dust. Under these conditions, the gaseous abundance of Fe would be representative of the total abundance of this element in ionized nebulae.

In the lower panel of Fig. 6, as the O/H abundance increases beyond  $12+\log(\text{O}/\text{H}) \approx 7.6$ , Fe/O rapidly decreases, in contrast

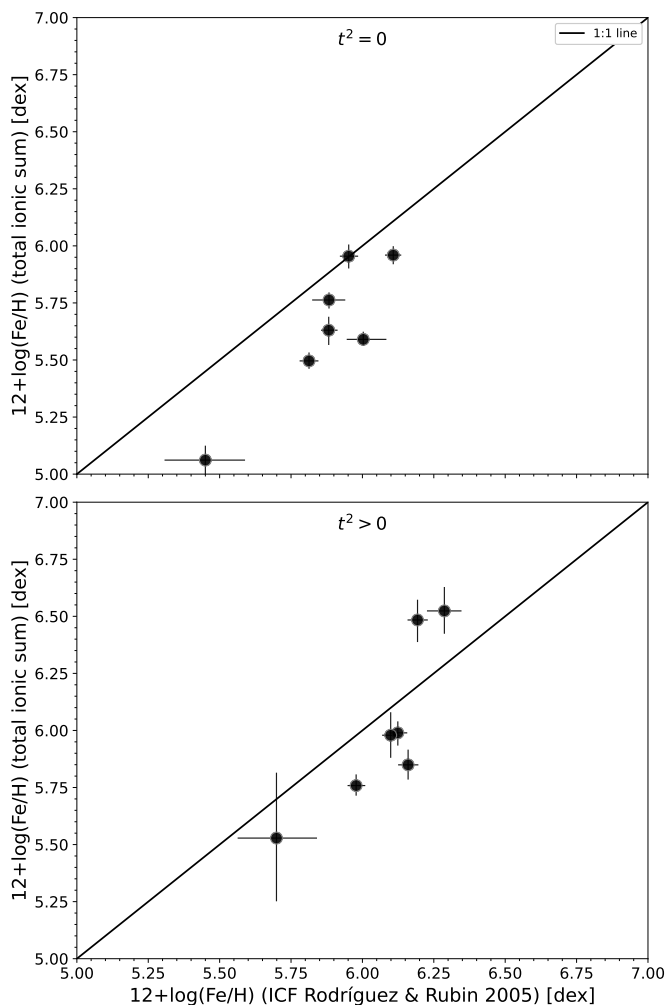


**Fig. 4.** Comparison between the Fe abundances obtained directly from the sum of the ionic abundances present in the gas in the sample of regions of the Table 1 and those determined using the Fe-ICF of Rodríguez & Rubin (2005), derived from photoionization models. Upper panel: the chemical abundances were calculated considering a homogeneous nebular temperature structure ( $t^2 = 0$ ). Lower panel: the chemical abundances were calculated considering the presence of temperature inhomogeneities ( $t^2 > 0$ ).

to the behavior observed in stellar objects. This trend is the result of Fe depletion onto dust grains within the ionized nebulae (Rodríguez 2002; Rodríguez & Rubin 2005; Izotov et al. 2006, 2021). The fraction of Fe trapped in dust grains increases with metallicity mainly due to two factors. First, as metallicity increases, the ionizing sources in the nebulae tend to be softer (Vilchez & Pagel 1988; Stasińska et al. 2015). This makes it less likely for dust grains in the ionized gas to shatter upon being hit by energetic photons (Rodríguez 2002). Secondly, the formation of solid Fe compounds is proportional to the availability of this element. As seen in the upper panel of Fig. 6, the abundance of Fe/H increases more rapidly than O/H at high metallicities.

Although the decreasing trend of Fe/O at high values of O/H is clear, the dispersion is relatively high ( $\sim 0.3$  dex) and the Pearson correlation coefficient is only moderate ( $r = -0.59$ ). Based on Sloan Digital Sky Survey (SDSS) spectra (Abazajian et al. 2005), Izotov et al. (2006) have suggested that the high dispersion in the Fe/O relation may be dominated by the errors in the

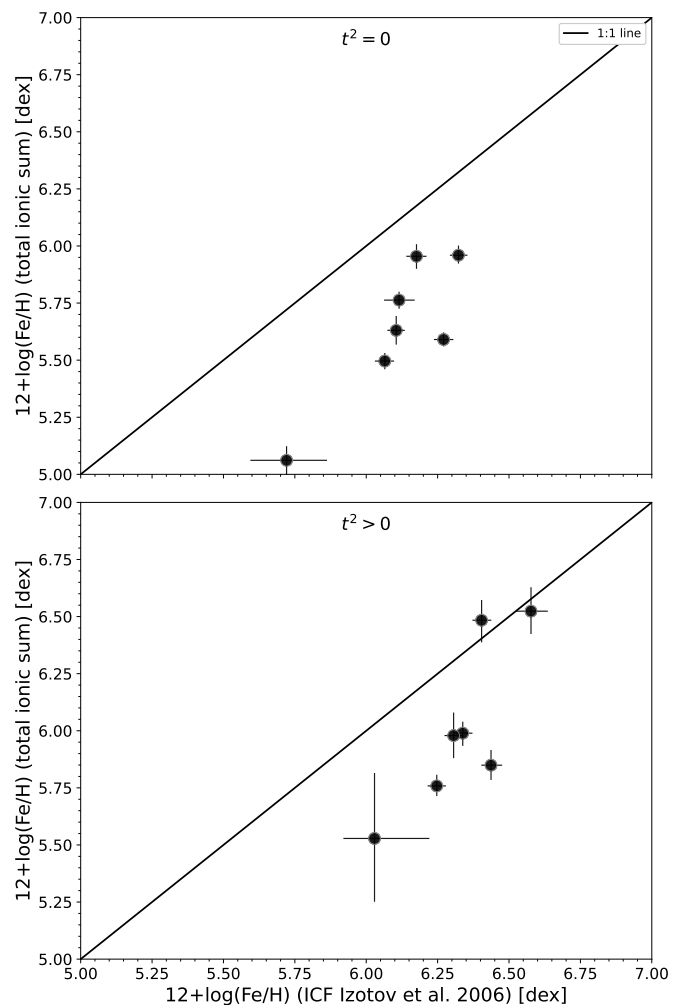


**Fig. 5.** Figure analogous to Fig. 4 but considering the Fe-ICF scheme of Izotov et al. (2006).

flux measurements of the faint [Fe III] lines. In Fig. 7, we consider the subsample of our nebular regions with the deepest spectra, with uncertainties in the [Fe III]  $\lambda 4658$  intensity below 10%. This figure shows a correlation coefficient practically identical to that found in the general sample of nebulae and a relatively high dispersion, suggesting that much of the dispersion is real and caused by a physical reason as those mentioned in Sec. 4.

An important factor that may contribute to the scatter is the presence and propagation of shocks in the nebular gas (Rodríguez 2002). Several studies (Blagrove et al. 2006; Mesa-Delgado et al. 2009; Espíritu et al. 2017; Méndez-Delgado et al. 2022b) have observationally demonstrated the ability of photoionized shocks to break dust grains and release Fe into its gaseous phase. However, we propose that the relationship between Fe/O and O/H does not exhibit a higher linear correlation simply because the phenomena inducing Fe depletion in dust grains are not perfectly linearly related to the abundance of O/H. Although there is a relationship between the radiation hardness and the abundance of O/H, it is not linear (Morisset 2004; Simón-Díaz & Stasińska 2008). In contrast, the effective temperature of the ionizing stars and the importance of their stellar winds depends primarily on Fe rather than O (García et al. 2014; Chruślińska et al. 2024). More importantly, the total abundance of Fe, on which the formation of Fe-rich dust compounds could



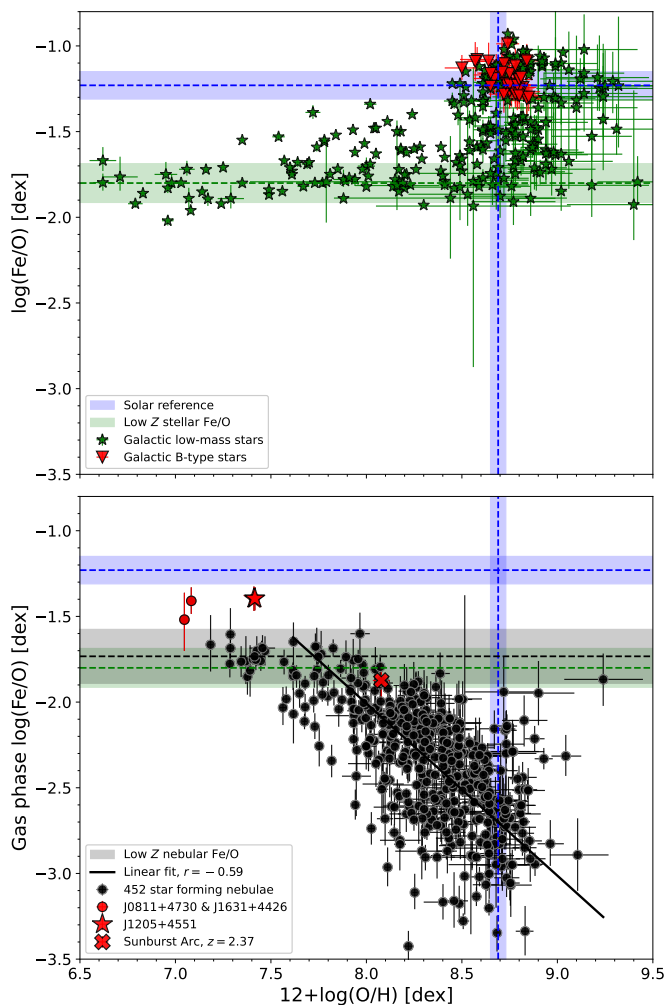


**Fig. 6.** Distribution of  $\log(\text{Fe}/\text{O})$  vs  $12+\log(\text{O}/\text{H})$ . Upper panel: Milky Way stars from the sample described in Sec. 2. Lower panel: Galactic and extragalactic star-forming nebulae. The red dots highlight the position of J0811+4730 (Izotov et al. 2018) and J1631+4426 (Kojima et al. 2021), recently interpreted by Kojima et al. (2021) as enriched in Fe. The red stars indicate the position of J1205+4551 (Izotov et al. 2017, 2021) a galaxy with elevated Fe/O abundances and evidence of WR activity. The red cross points out the location of the Sunburst Arc (Welch et al. 2024), a high-redshift ( $z = 2.37$ ) galaxy recently observed by the JWST. Nebular O/H estimates have considered the influence of nebular temperature variations ( $t^2 > 0$ ). The solar Fe/O and O/H abundances from Asplund et al. (2021) are shown as a reference.  $r$  is the Pearson correlation coefficient of the linear fit.

depends, does not scale linearly with that of O at high metallicity, as shown in the upper panel of Fig. 6.

## 5.2. Fe and N nebular abundances

Considering the hypothesis that the timescale to form a white dwarf in a stellar system that produces a SN-Ia is similar to the timescale over which an intermediate mass star returns secondary N to the ISM, we decided to explore the Fe/N distribution. If this hypothesis holds true, then the production of Fe at high metallicities should be better correlated with that of N rather than O. In Fig. 8, we present the distribution of  $\log(\text{Fe}/\text{N})$  as a function of  $12+\log(\text{N}/\text{H})$  both in Milky Way stars (upper panel) and in star-forming nebulae (lower panel), analogous to what is presented in Fig. 6.

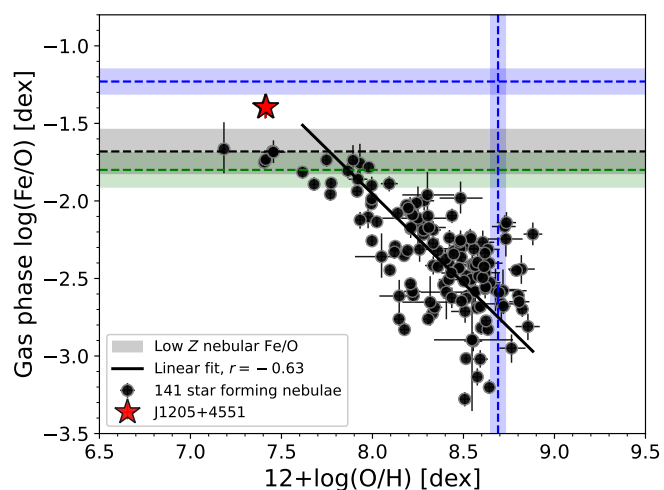


**Fig. 7.** Same as the lower panel of Fig. 6 but considering only regions with errors in the  $[\text{Fe III}] \lambda 4658$  line intensity smaller than 10%.

Despite the significant dispersion in the upper panel of Fig. 8, the observed Fe/N ratio in low-mass stars can mostly be encompassed around a relatively flat band, represented by a green dashed line in Fig. 8 and which corresponding parameters are given in Table 2. This trend can be explained by the findings of different studies where the stellar abundance of Fe scales linearly with that of N even in wider abundance ranges than those considered in this work (Israelian et al. 2004; Ecuivillon et al. 2004; Magrini et al. 2018; Kobayashi et al. 2020; Grisoni et al. 2021). Notably, when examining the B-type stars studied by Nieva & Przybilla (2012) and Weßmayer et al. (2022), shown in red triangles in the upper panel of Fig. 8, a strongly linear Fe/N correlation is observed, contrasting with the Fe/O relationship observed in this same stellar sample. These stars have formed more recently than the lower-mass star sample and have been enriched with metals. It is likely that the N present in these B-type stars in the solar neighborhood has been modified via the CNO cycle and mixing processes (Przybilla et al. 2010). In such case, these stellar N abundances would not be comparable to those of H II regions or other stellar systems. On the other hand, the Fe/H abundance shows little variation, suggesting homogeneous production of Fe/H in the interstellar medium that contributed to the formation of these B stars. This will be further discussed in Sec. 6.4.

In the lower panel of Fig. 8, we show the distribution of gaseous Fe/N in star-forming nebulae, similar to that shown in the lower panel of Fig. 6 for Fe/O. The higher Pearson correlation coefficient suggests that the linear correlation between Fe/N abundance and N/H is stronger than that observed for Fe/O and O/H, although the dispersion remains quite high  $\sim 0.3$  dex, similar to what is found in the Fe/O vs O/H distribution. This could indicate that some of the key factors in the Fe dust depletion have a closer relationship with N abundance than with O. Given the close relationship between the stellar abundances of Fe and N observed in the upper panel of Fig. 8, it seems plausible that the nucleosynthetic production of Fe is better correlated with that of N, due to similarities in the timescales required for SN-Ia production and the evolution of intermediate-mass stars. The use of N as a proxy for Fe would allow us to capture the systematic effect of radiation hardness, which is capable of destroying dust grains in photoionized environments (Rodríguez 2002) and scales with the abundance of Fe/H (García et al. 2014;

**Table 2.** Fitted distributions of the Fe/O and Fe/N abundances shown in Figures 6 and 8.

Abundance ratio	Relation	Range	N	Pearson $r$	$\sigma$ [dex]
Star-forming nebulae					
log(Fe/O)	$-1.74 \pm 0.15$	$12 + \log(\text{O}/\text{H}) < 7.6$	23	-	0.29
	$(-1.00 \pm 0.05) \times [12 + \log(\text{O}/\text{H})] + (6.03 \pm 0.38)$	$12 + \log(\text{O}/\text{H}) \geq 7.6$	429	-0.59	
log(Fe/N)	$-0.45 \pm 0.15$	$12 + \log(\text{N}/\text{H}) < 6.3$	16	-	0.28
	$(-0.91 \pm 0.03) \times [12 + \log(\text{N}/\text{H})] + (5.47 \pm 0.21)$	$12 + \log(\text{N}/\text{H}) \geq 6.3$	382	-0.80	
Low-mass stars					
log(Fe/O)	$-1.80 \pm 0.11$	$12 + \log(\text{O}/\text{H}) < 7.6$	27	-	-
log(Fe/N)	$-0.60 \pm 0.20$	$5.0 \leq 12 + \log(\text{N}/\text{H}) \leq 8.7$	143	-	-
B-type stars					
log(Fe/N)	$(-0.84 \pm 0.04) \times [12 + \log(\text{N}/\text{H})] + (6.25 \pm 0.34)$	$7.7 \leq 12 + \log(\text{N}/\text{H}) \leq 8.7$	34	-0.97	0.06

Chruślińska et al. 2024). Additionally, N exhibits insignificant depletions even in neutral environments of high metallicities (Jenkins 2009).

Similarly to what is presented in Fig. 7 for the Fe/O vs. O/H distribution, in Fig. 9 we show the Fe/N vs. N/H distribution considering only the regions where [Fe III]  $\lambda 4658$  has uncertainties in its intensity lower than 10%. This figure shows that the general distribution observed in Fig. 8 is maintained, although with less dispersion. Additionally, an apparent flattening in the distribution is observed when  $12 + \log(\text{N}/\text{H}) < 6.3$ . This flattening is not observed in the general sample and will be discussed in more detail in Sec. 6.

## 6. Discussion

### 6.1. Possible empirical relations for dust depletion

As shown in Fig. 6 when  $12 + \log(\text{O}/\text{H}) < 7.6$  the nebular gas-phase Fe/O seems to reach a constant value, or at least change the slope of the general trend, being consistent with the abundance one observed in Galactic stars in the same metallicity range. This flattening may suggest that the fraction of Fe trapped into dust in these photoionized nebulae is very small. This could be explained by the fact that the photoionization conditions in metal-poor regions are harder (Vilchez & Pagel 1988; Stasińska et al. 2015), making the destruction of dust grains more efficient. At the same time, the availability of Fe, essential for the formation of some solid compounds, is very low. Determining the metallicity ranges where total Fe can be directly inferred from gaseous Fe is very important because it could point out to significant differences in the impact of dust in local ionized environments (generally of higher metallicity) and those observed in less evolved galaxies, such as those currently detected with the JWST. This could also help to explain why some Fe lines have been detected in high- $z$  galaxies (Arellano-Córdova et al. 2022; Ji et al. 2024; Tacchella et al. 2024; Welch et al. 2024), despite being very weak in local H II regions.

However, the flattening effect is not clearly seen in the general distribution of Fe/N presented in Fig. 8. This is a bit puzzling as it seems well established that nebular N/O abundance reaches a plateau at low metallicities (Garnett 1990; Nava et al. 2006; Skillman et al. 2013; Nicholls et al. 2017) and therefore, one would also expect to observe a flattening in Fe/N if it is present in Fe/O. In our sample, the regions 0556-51991-31, J0811+4730, and SBS-0335-052E (Izotov et al. 2006, 2009, 2018) seem to extend the linear trend between Fe/N and N/H observed at high

metallicities. This could be a consequence of the changes in the gaseous abundance of Fe due to different depletion patterns being small and going unnoticed when compared to the abundance of O, as it is an element much more abundant than N. Alternatively, this could simply be a problem of low statistics when  $12 + \log(\text{N}/\text{H}) < 6.5$ . In fact, such flattening seems to begin to appear in Fig. 9, which shows the Fe/N distribution only in regions with the best signal-to-noise ratio in [Fe III]  $\lambda 4658$ . Notably, in low metallicity regions, the detection of [N II]  $\lambda 6548, 6584$  is more challenging than in the case of [Fe III]  $\lambda 4658$ . In fact, in this work, we have more regions with direct determinations of Fe and O than that of Fe and N. In our DESIRED sample, using the same criteria described in Sec. 3, we determine that when  $12 + \log(\text{O}/\text{H}) < 8.0$ ,  $\log(\text{N}/\text{O}) \sim -1.3$  (Arellano-Córdova et al. in prep.). Therefore, we adopt  $12 + \log(\text{N}/\text{H}) = 6.3$  as equivalent to  $12 + \log(\text{O}/\text{H}) = 7.6$ . However, we find a relatively high dispersion ( $\sim 0.3$  dex) around this value.

If we assume that the total abundance of Fe scales proportionally to that of N, as suggested by stellar abundances and the previous discussion, it is possible to determine an empirical relationship to approximately determine the fraction of Fe trapped in dust as a function of the N/H abundance. In Eq. (1), we present this relation considering only the nebular values given in Table 2. Eq. (1) is valid for high-metallicity nebulae, where  $12 + \log(\text{O}/\text{H}) \geq 7.6$  or  $12 + \log(\text{N}/\text{H}) \geq 6.3$ . For values lower than these,  $\text{Fe}_{\text{Dust}}/\text{Fe}_{\text{Total}} \approx 0$ .

$$\frac{\text{Fe}_{\text{Dust}}}{\text{Fe}_{\text{Total}}} \approx 1 - 1 \times 10^{-5} \times \left(\frac{\text{N}}{\text{H}}\right)^{-0.91}. \quad (1)$$

Eq. (1) implies that the formation of Fe-rich dust grains grows predominantly in proportion to the same Fe abundance. From this equation, the proportionality factor ( $1 \times 10^{-5}$ ) presents the greatest uncertainties as it is mainly based on the Fe/N nebular values when  $12 + \log(\text{N}/\text{H}) < 6.3$ . In contrast, the power ( $-0.91$ ) is much more robust as it represents the slope of the relationship between Fe/N and N/H considering 382 objects with  $12 + \log(\text{N}/\text{H}) > 6.3$ . Considering a solar N abundance of  $12 + \log(\text{N}/\text{H}) = 7.83$  (Asplund et al. 2021), Eq. (1) indicates that approximately  $\sim 95\%$  of the Fe in ionized nebulae is depleted into dust grains. On the other hand, considering the values of the Large Magellanic Cloud (LMC) and the Small Magellanic Cloud (SMC) ( $12 + \log(\text{N}/\text{H}) = 7.1-7.2$  and  $12 + \log(\text{N}/\text{H}) = 6.5-6.7$ , respectively, see Table D.8), the fractions would be approximately  $\sim 75\%$  and  $\sim 35\%$ , respectively. In the case of the SMC, the nitrogen abundance values are at the limit of validity of Eq. (1). The fraction of  $\sim 35\%$  assumes a value of

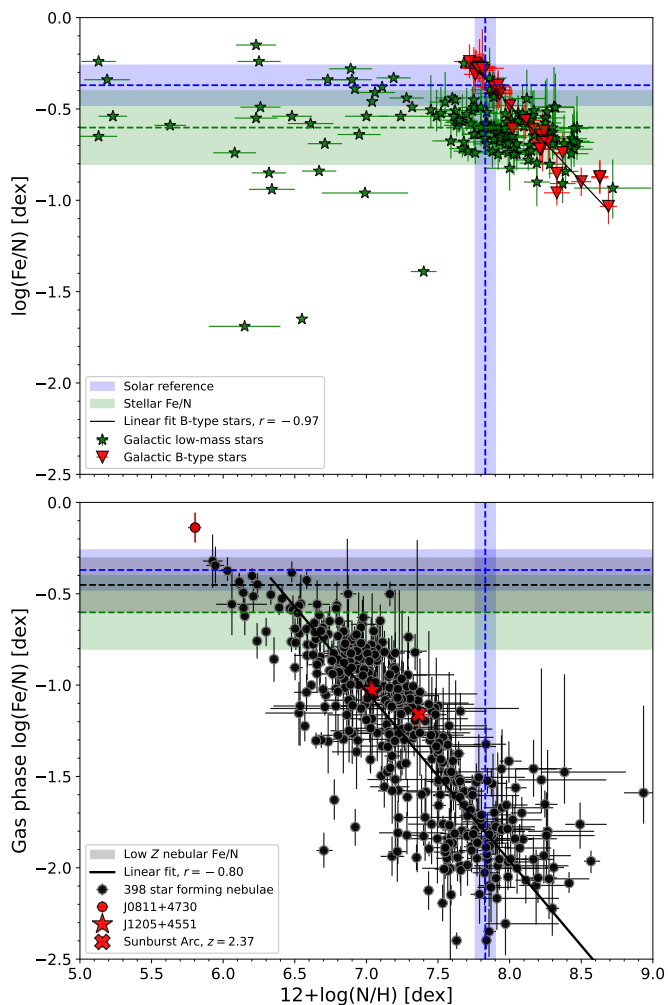


**Fig. 8.** Distribution of  $\log(\text{Fe}/\text{N})$  vs  $12+\log(\text{N}/\text{H})$ . Upper panel: Milky Way stars from the sample described in Sec. 2. Lower panel: Galactic and extragalactic star-forming nebulae. The red dot highlights the position of J0811+4730 (Izotov et al. 2018), recently interpreted by Kojima et al. (2021) as enriched in Fe. The red star indicates the position of J1205+4551 (Izotov et al. 2017, 2021) a galaxy with elevated Fe/O abundances and evidence of WR activity. The red cross points out the location of the Sunburst Arc (Welch et al. 2024), a high-redshift ( $z = 2.37$ ) galaxy recently observed by the JWST. Nebular N/H estimates have considered the influence of nebular temperature variations ( $r^2 > 0$ ). The solar Fe/N and N/H abundances from Asplund et al. (2021) are shown as a reference.  $r$  is the Pearson correlation coefficient of the linear fit.

$12+\log(\text{N}/\text{H})=6.7$ , but a negligible O-dust fraction of  $\sim 1\%$  is expected if  $12+\log(\text{N}/\text{H})=6.5$  is considered. In Fig. 10, we show the total Fe/O abundance in the entire sample of star-forming nebulae, considering the gaseous fraction of Fe/H, measured from the  $[\text{Fe III}]$  emission, and the fraction of Fe/H depleted into dust, inferred from Eq. (1). There is a rather good consistency between the stellar and nebular abundance distributions, as indicated by the binned values marked with red stars and black dots.

Typically, the Fe/O vs. O/H relationship (or more commonly  $[\text{O}/\text{Fe}]$  vs.  $[\text{Fe}/\text{H}]$ <sup>1</sup>) is used to understand the star formation history of a particular galaxy (Kobayashi et al. 2006; Magrini et al.

<sup>1</sup> when dealing with abundances from stellar atmospheres, the typical notation is  $[\text{X}/\text{Y}] = \log(N_{\text{X}}/N_{\text{Y}}) - \log(N_{\text{X}}/N_{\text{Y}})_{\odot}$ , where  $\log(N_{\text{X}}/N_{\text{Y}})_{\odot}$  is the number ratio measured in the Sun.

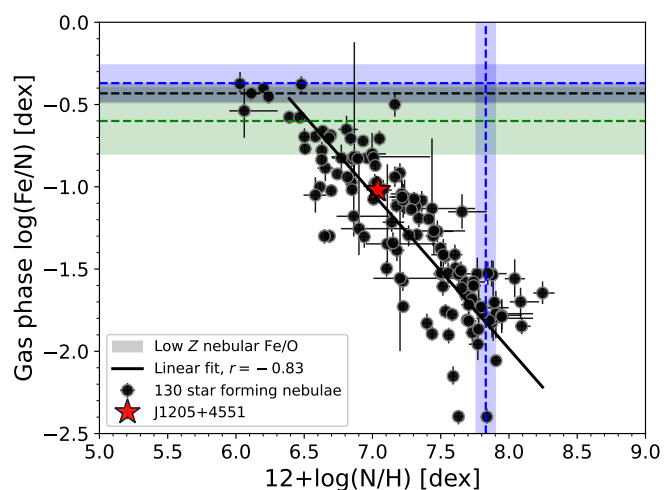


**Fig. 9.** Same as the lower panel of Fig. 8 but considering only regions with errors in the  $[\text{Fe III}] \lambda 4658$  line intensity smaller than 10%.

2010; Matteucci 2012). In this relationship, star formation efficiency and the Initial Mass Function are parameters that play a fundamental role. Similarly, these same parameters govern the N/O vs. O/H relationship (Mollá et al. 2006). Considering a large number of star-forming regions from different galaxies, it is well established observationally that the N/O vs. O/H relationship reaches a plateau at low metallicities ( $12+\log(\text{O}/\text{H}) < 8$ ) (Henry et al. 2000; Nava et al. 2006; Nicholls et al. 2017) determined by the onset of N production from intermediate mass stars (Vincenzo et al. 2016). If there is a close relationship between the production times of Fe and N, one would also expect a plateau in the Fe/O vs. O/H relationship among various star-forming regions, once the fraction of Fe trapped in dust grains has been considered. By looking at the binned nebular values in Fig. 10 we indeed observe a plateau up to roughly  $12+\log(\text{O}/\text{H}) = 8.0$ , with a subsequent rise in the Fe/O ratio. Moreover, the position of this “knee”, which indicates the onset of SNe Ia contribution, also agrees with the one observed in Galactic stars considered in this work. In turn, this means that, on average, star-forming regions in present-day local galaxies share a similar level of efficiency of star formation and Initial Mass Function shape relative to the one already experienced by the Galactic disk, capturing different evolutionary snapshots according to their metallicity. This appears to be at odds with stellar abundances observed in dwarf galaxies of the Local Group. For example, dwarf spheroidal galaxies show an O/Fe plateau (deduced from other  $\alpha$ -elements) roughly from  $12+\log(\text{O}/\text{H}) < 7.5$  (Hendricks et al. 2014; Hill et al. 2019). However, these galaxies are faint, gas-poor, and quiescent in star formation (see e.g. Tolstoy et al. 2009). This indicates that nebular observations of galaxies with low O/H abundance will be biased toward regions of intense star formation corresponding to gas-rich, dwarf irregular galaxies. The position of the O/Fe plateau in irregular dwarf galaxies is still relatively uncertain, as there are very few determinations beyond local systems as the SMC and LMC, which might differ from the conditions of other lower-metallicity systems with a higher star formation rate.

Nonetheless, the position of the “knee” could still show differences relative to the mean trend due to the different evolutionary history in each galaxy. This causes the significant dispersion in the nebular abundances in Fig. 10, in addition to other factors contributing to the uncertainties in Fe, dominated by the correc-



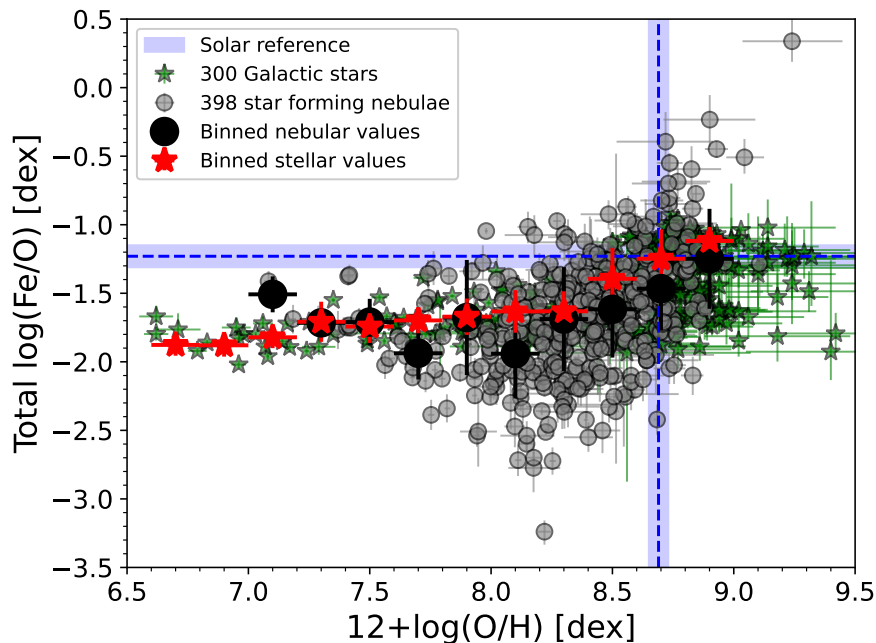


**Fig. 10.** Total Fe/O vs O/H abundance ratios for Galactic stars (green stars) and gas-phase abundance ratios for star-forming nebulae (gray circles). The plotted gas-phase abundances include the contribution from the dust-depleted Fe fraction calculated using Eq. (1). The binned values (with bins of 0.2 dex) appear as red stars and black circles for Galactic stars and star-forming nebulae, respectively.

tion for depletion onto dust grains. In fact, the distribution presented here in Fig. 10 is valid if the possible O/Fe plateau occurs when  $12+\log(\text{O}/\text{H}) < 7.6$ . The precise position of the expected O/Fe-plateau may induce offsets in the nebular distribution of Fe/O observed, but in general, the functional form would not be altered.

Fig. 10 also reinforces the fact that the conversion between stellar metallicities, measured with Fe, and nebular metallicities, measured with O, is not straightforward. Significant biases can be expected when transforming individual stellar Fe abundances to O abundances using the solar reference as in Bresolin et al. (2009, 2016, 2022). In the best case scenario, when indeed we are within the range of solar metallicities, both stars and nebulae exhibit average dispersions of up to  $\sim 0.2$  dex in the Fe/O abundances, resulting from production variations between Fe and O. We think it is important to consider this uncertainty when comparing stellar and nebular metallicities. A much worse situation arises when comparing stellar and nebular galactic abundance gradients using the solar reference of Fe/O as a conversion factor as used in several works (e.g. Gazak et al. 2015; Bresolin et al. 2022), as the entire abundance pattern changes with metallicity. Using the stellar reference of Fe/N that we present in Table 2 could be potentially useful in this latter case. However, a larger statistical sample for stellar Fe and N abundances is required for this purpose. An alternative based on the knowledge of the specific SFR of the system is presented by Chruślińska et al. (2024).

As suggested by Peimbert & Peimbert (2010), in the case that the depletion of O onto dust grains scales with that of Fe, it is possible to derive an upper limit to the O depletion. In the case of the Orion Nebula, it is known that the fraction of dust trapping O is up to  $\sim 0.1$  dex (Mesa-Delgado et al. 2009; Peimbert & Peimbert 2010). Therefore, it can be estimated that in the LMC and SMC there may be up to  $\sim 0.07$  dex and  $\sim 0.03$  dex of O trapped in dust, respectively. The depletion of O onto dust could be negligible at  $12+\log(\text{O}/\text{H}) < 8.0$ , as its contribution is much smaller than the typical uncertainties in the estimation of chemical abundances in ionized nebulae. We remark that these could be considered upper limits to the depletion of O in photoionized environments as they are based on a scaling of the upper limit

derived for the Orion Nebula. Therefore, simply adding 0.1 dex to correct for dust all nebular determinations of O/H, regardless of metallicity and ionization conditions –as it has been done in several works (e.g., Bresolin et al. 2016, 2022)– seems inappropriate.

## 6.2. On the dust composition in H II regions

The precise chemical composition of dust in ionized gas remains a matter of debate (Simón-Díaz & Stasińska 2011), and its impact on the important parameters of ionized nebulae could be significant (Gunasekera et al. 2023). The dust present in H II regions should consist of the grains most resistant to photoionization, formed prior to star formation. This is supported by the fact that we do not observe any connection between the depleted Fe fraction and the electron density, a case that could be expected if a significant fraction of the dust grains were formed within the photoionized environment (Zhukovska et al. 2018). In our Sec. A, we show a weak anticorrelation between optical reddening relative to  $H\beta$  and the Fe/O and Fe/N abundances in a subsample of the regions analyzed in this work. The anticorrelation seems stronger in the case of Fe/N. This reinforces the idea of having an interconnection between the dust found in H II regions and that present in the neutral medium, which may cause most of the optical extinction. Studies of dust in the neutral ISM can provide candidates that may survive photoionization and be present in H II regions. In situ studies of dust in the neutral ISM indicate that it is likely that Fe is mostly locked up in free-flying iron particles and silicate grains (Jones et al. 2017; Choban et al. 2022; Hensley & Draine 2023; Dubois et al. 2024).

Our results from Figs 6 and 8 show that the fraction of Fe trapped in dust grains decreases as metallicity decreases. Our interpretation is that photo-destruction is particularly important at lower metallicities (Rodríguez 2002; Rodríguez & Rubin 2005) because the ionizing spectrum becomes increasingly harder as the amount of Fe in stars decreases (Vilchez & Pagel 1988; Stasińska et al. 2015). In turn, the gas-to-dust fraction in the neutral ISM tends to be higher at lower metallicities (Gioannini

et al. 2017; Galliano et al. 2021; Roman-Duval et al. 2022b,a), which suggests that there is less Fe-rich dust in low-metallicity ionized environments because the fraction of Fe trapped in dust in the neutral ISM is lower prior the star formation. In fact, the relation we find between Fe/O and O/H is similar to the relation found by Gioannini et al. (2017) between Fe/Zn vs Zn/H and Fe/S vs S/H in neutral gas. Both the increased photo-destruction of dust grains in low-metallicity ionized environments and the reduced formation of dust in the low-metallicity neutral ISM are not mutually exclusive and could be acting in the same direction. It is important to mention that spatially resolved studies of the distribution of gaseous Fe/H in H II regions of our Galaxy, as is possible with the SDSS-V Local Volume Mapper (Drory et al. 2024), are of great importance to quantify the impact of dust photo-destruction in ionized environments. Preliminary results from the Orion Nebula (Méndez-Delgado et al. in prep) show an increasing trend of Fe/O and Fe/N when approaching the ionizing star  $\theta^1$  Ori C, suggesting that the impact could be significant.

Photo-destruction should mainly affect the smaller grains, particularly the carbonaceous ones (Jones et al. 2017). Studies of photoionized Herbig-Haro objects in the Orion Nebula (Blagrove et al. 2006; Mesa-Delgado et al. 2009; Méndez-Delgado et al. 2021a,b, 2022b) show dramatic increases in the gaseous abundances of Fe, Ni and Cr at the bowshocks due to the destruction of dust present in the photoionized gas. In contrast, in these objects, the abundances of O and C remain virtually unchanged. This suggests that most of the Fe depleted in grains could be composed of Fe grains decoupled from C and O that could be efficiently destroyed by the ionizing radiation. This could suggest that most of the Fe-dust in ionized environments is composed by free-flying iron particles.

Interestingly, the fact that we find a significant depletion of Fe in dust grains in a large number of objects indicates that these grains were not yet processed by the supernova forward shock, which is predicted to destroy a large fraction of the dust grains (Bocchio et al. 2014; Slavin et al. 2015; Kirchschrager et al. 2022, 2024). However, given the large dispersion observed in the distributions of Fe/N and Fe/O, it cannot be ruled out that supernova shocks are playing a role in some fraction of the regions analyzed here.

### 6.3. On the Fe enrichment on short timescales by very massive stars

Recently, Kojima et al. (2021) reported a puzzlingly high Fe/O in J0811+4730 and J1631+4426, two of the extremely metal-poor local dwarf galaxies in their sample. Such an abundance pattern cannot be explained by enrichment from regular CCSNe, and the inferred young age and very high specific SFR in those galaxies rule out the possibility of significant Fe enrichment by SNe Ia. Kojima et al. (2021) speculate that the high Fe/O could be indicative of enrichment by very massive stars with  $M_{\text{init}} > 300M_{\odot}$ . Other scenarios, involving enrichment by massive pair-instability supernovae and a non-universal IMF, have also been proposed Goswami et al. (2021).

Our results presented in Sec. 4 suggest that Kojima et al. (2021) overestimate the Fe abundances in J0811+4730 and J1631+4426 due to the bias introduced by the Fe-ICF they use (that proposed by Izotov et al. 2006). We argue that these abundances are overestimated by at least  $\sim 0.2$  dex. However, we point out that the adoption of the ICF by Izotov et al. (2006) can introduce overestimations of the Fe abundances of up to  $\sim 0.7$  dex in environments where the  $\text{Fe}^{3+}/\text{Fe}$  fraction is higher,

which are precisely metal-poor regions like J0811+4730 and J1631+4426 (Rodríguez & Rubin 2005).

Additionally, in contrast with the discussion presented by Kojima et al. (2021), we show that the trends observed in Figures 6 and 8 can be explained in terms of the depletion of Fe onto dust grains in ionized environments. The existence of such dust is firmly established by various studies of local nebulae (Rodríguez 1999, 2002; Rodríguez & Rubin 2005; Blagrove et al. 2006; Mesa-Delgado et al. 2009; Méndez-Delgado et al. 2021a) that include direct detections of the dust emissions (Smith et al. 2005). On the other hand, Kojima et al. (2021) did not find any correlation between the dust extinction and the Fe/O ratios. However, although local dust trapping Fe in Galactic nebulae could have some effects on the observed optical extinction due to their proximity to us (Rodríguez 2002), this effect may be negligible in more distant systems where the influence of dust outside the H II region and integrated along the line of sight could play the most significant role.

Although J0811+4730 and J1631+4426 certainly exhibit a slightly elevated Fe/O abundance, they remain basically consistent with values obtained in other regions with low O/H abundances, explained in terms of preferential dust depletion. Therefore, we do not find compelling evidence of Fe overproduction by stars with  $M_{\text{init}} > 300M_{\odot}$  in these objects.

Interestingly, in the lower panel of Fig. 6 two spectra of J1205+4551 highlighted by the red stars (Izotov et al. 2017, 2021), show Fe/O abundances similar to those found by Kojima et al. (2021) in J0811+4730 and J1631+4426. J1205+4551 additionally exhibits signatures of WR stars (Izotov et al. 2021) and a very high N/O abundance for its O/H abundance. In more massive stars, surface nitrogen quickly gets enriched at the expense of oxygen. Strong stellar winds can then lead to an enrichment of the ISM with nitrogen (Meynet & Maeder 2005; Crowther 2007; López-Sánchez et al. 2007). In particular the WN stage can provide an efficient channel here as the products of He burning have not yet reached the stellar surface, but the winds are stronger than for normal O stars. This effect is prominently seen in the abundances of resolved nebulae around massive WN stars (e.g., Kwitter 1984; Stock et al. 2011; Esteban et al. 2016), and consequently predicted for the yields of very massive, hydro-burning stars ( $M_{\text{init}} \geq 100M_{\odot}$ ) that also show WNh-type spectra (e.g., Higgins et al. 2023). The effect of WR stars on Fe is not entirely clear, mainly due to the high depletion of this element onto dust grains at high metallicities.

In contrast to the Fe/O abundance, as shown in Fig. 8, the Fe/N abundance in J1205+4551 does not appear anomalous, but rather consistent with the general trend. Another interesting case is the Sunburst Arc, a galaxy at  $z = 2.37$  recently observed with the JWST and analyzed by Welch et al. (2024). This latter galaxy presents a high N/O abundance, unexpected for its low O/H abundance. However, in Fig. 8, we find that, similarly to the case of J1205+4551, the Sunburst Arc (highlighted by the red cross) shows quite a normal Fe/N abundance. This might indicate that some nebular regions with abnormally high N/O abundances could also contain rather high Fe/O abundances. It is possible to speculate that the high values of Fe/O and N/O in these regions may be due to a lower availability of O resulting from the presence of WR stars. A systematic study of the Fe/H abundance in H II regions with low O/H abundances and high N/O ratios like some particular knots of NGC 5471 (Kennicutt et al. 2003) or Mrk 71 (Esteban et al. 2002), may shed light on this interesting issue.

#### 6.4. Stellar and nebular metallicities

The main idea to interpret the linear relation between gas-phase abundances of Fe and N in star-forming nebulae is that the production timescales of N and Fe are similar, while dust formation trapping Fe scales with its own availability. This seems valid in the range of chemical abundances studied here (Magrini et al. 2018; Xiong et al. 2022; Sun et al. 2023), and is consistent with the assumption of the primary origin of N in CCSNe of massive stars and secondary in intermediate-mass stars through the CNO cycle (Henry et al. 2000; Meynet & Maeder 2002b,a). In general, the different nucleosynthetic origins of N and Fe can add additional complexity to the empirical abundances of both elements. For instance, N enrichment from intermediate-mass stars is known to be sensitive to metallicity (Ventura et al. 2013). Such metallicity-sensitive yields could decouple the gas-phase Fe and N abundances, specially at supersolar metallicities. Nevertheless, within the metallicity range covered by this analysis, which encompasses most of the nebular analyses reported in the literature, such deviations are not observed. The yield predictions from Ventura et al. (2013) appear consistent with observational stellar values within the analyzed metallicity range, as illustrated in Figure 1 of Romano et al. (2019) (corresponding to models MWG06 and MWG07). Our study does not extend beyond the metallicity ranges discussed in these works. Future studies that cover metallicity ranges beyond those examined here could investigate these predictions.

Some authors have suggested the existence of massive stars with high rotation velocities as a source of N observed at low metallicities (Limongi & Chieffi 2018; Prantzos et al. 2018), being able to successfully reproduce the observed flat trends between Fe/N and N/H in Galactic stars (Prantzos et al. 2018; Limongi & Chieffi 2018; Romano et al. 2019). These differences in the precise origin of N at low metallicities do not seem to affect our interpretation, at least within the range of our chemical determinations, as the production timescales remain similar.

As observed in the upper panel of Fig. 8, Galactic B-type stars (Nieva & Przybilla 2012; Weßmayer et al. 2022) show more significant variations in the Fe/N ratio compared to the other stars analyzed here. This trend is not limited to Galactic B-type stars but is also evident in other galaxies (Trundle & Lennon 2005; Trundle et al. 2007; Evans et al. 2007; Hunter et al. 2007). For instance, in the SMC, LMC, and NGC 3109, massive B-type stars (both giants and dwarfs) analyzed by Hunter et al. (2007) and Evans et al. (2007) typically exhibit nitrogen overabundances of more than one order of magnitude compared to nebular values (Peña et al. 2007; Toribio San Cipriano et al. 2017; Domínguez-Guzmán et al. 2022), reflecting that massive stars rapidly reach the so-called “CN” equilibrium as a part of the CNO cycle (Przybilla et al. 2010). Confirmed by recent efforts of the XShootU collaboration (Martins et al. 2024), it seems that in galaxies with lower overall O/H abundance, massive stars exhibit higher N/H overabundances. However, determining whether this is systematic or merely a selection bias towards the brightest stars in these systems goes beyond the scope of this study. Nevertheless, it is important to note that N/Fe and N/O ratios in these stars do not constitute the final value that will be released into the ISM after their death in CCSN.

Interestingly, the very high overabundances of N observed in some extragalactic B-type stars could significantly alter the abundances of C and O. If a significant portion of the N is produced at the expense of O, non-negligible decrements, on the order of  $\sim 0.1 - 0.2$  dex, may be present (Martins et al. 2024). This complicates element-by-element comparisons between the

abundances of C, N, and O among massive B-type stars and H II regions when high precision is required. Studies of individual, unevolved OB stars which do not exhibit significant mixing processes (e.g., Rolleston et al. 2003; Ramachandran et al. 2021; Pauli et al. 2023; Martins et al. 2024) could provide a very useful testbed for the consistency between present-day stellar and nebular abundances. Yet, if achieving high precision in the comparisons between O abundances in stars and nebulae is already complicated, it becomes even more so when dealing with stellar metallicities derived from the analysis of combined absorption lines of various elements (but dominated by Fe-peak elements, Urbaneja et al. 2008; U et al. 2009; Kudritzki et al. 2008, 2012, 2014, 2016; Hosek et al. 2014; Patrick et al. 2015), as done by Bresolin et al. (2016) in several galactic systems using the solar reference to transform Fe-metallicities into O-metallicities. Direct O measurements instead are typically focussed on very slow rotating stars such as the prototypical B-type dwarf AzV 304 (Rolleston et al. 2003). While such stars allow for a high-precision O measurement due to the narrow lines, this limited selection might imply a bias in itself.

We are aware that the number of star-forming nebulae with  $12+\log(\text{O}/\text{H}) < 7.6$  in our sample is somewhat limited, but it already constitutes a significant observational achievement to have direct nebular determinations of Fe, O, and N under such conditions. The change in the slope of the Fe/O abundance ratio in this range of metallicities could be very small. If the value of  $\log(\text{Fe}/\text{O}) \sim -1.74$  is representative of the total Fe/O abundances in these star-forming nebulae in the metallicity range –which correspond to dwarf irregular galaxies– this could indicate similar star formation efficiencies than what was present, in the early stages of the Milky Way (Carigi et al. 2005, 2019; Nomoto et al. 2013; Amarsi et al. 2019; Kobayashi et al. 2006, 2020; Prantzos et al. 2023). In contrast, if new observations of star-forming nebulae were to show a continuation of the anti-correlation between Fe/O and O/H produced by Fe depletion in dust grains, this could indicate lower star formation efficiencies or the presence of some phenomenon such as metal losses through winds (Tolstoy et al. 2009).

A high Fe/O ratio in low O/H environments would imply harder thermal equilibrium in ionized nebulae than what is typically observed in local H II regions. On the one hand, the stellar winds from ionizing stars are more significant as a function of the Fe abundance (e.g., Vink et al. 2001; Garcia et al. 2014; Sander et al. 2020; Chruślińska et al. 2024). On the other hand, gas cooling is mainly driven by the O abundance (Osterbrock & Ferland 2006). However, a potentially high rate of Fe production through SN-Ia events should occur on timescales similar to those of secondary N production in intermediate-mass stars, and it seems well established that in star-forming nebulae with  $12+\log(\text{O}/\text{H}) < 8.0$ , the N/O abundance ratio is subsolar at around  $\sim -0.5$  dex (Henry et al. 2000; Nava et al. 2006; Pilyugin et al. 2010; Nicholls et al. 2017), making this scenario less likely. Certainly, there may be specific star-forming nebulae with high N/O and Fe/O at low O/H due to their star formation history, similar to what is demonstrated by Mollá et al. (2006) in the case of N/O. This could also contribute to the dispersion observed in the Fe/O ratios.

#### 6.5. Limitations of this work and future improvements

One of the main objectives of the DESIRED project (Méndez-Delgado et al. 2023a) is to unveil the chemical and physical properties of ionized nebulae that can be explored with the weakest emission lines, which are generally under-studied. In this case,



the analysis of Fe abundances in the gaseous phase has critical limitations due to the estimation of the ICF, as detailed in Sec. 4. The large dispersion of  $\sim 0.2$  dex shown even in the best case (which uses  $t^2 > 0$  and the ICF of Rodríguez & Rubin 2005) substantially limits our ability to correctly interpret the Fe abundances in individual nebulae such as J0811+4730 and J1631+4426 (Kojima et al. 2021). Clearly, it is necessary to expand the sample of star-forming nebulae with measurements of [Fe IV]  $\lambda 6740$  to refine the ICF. To our knowledge, such emission line has only been detected in 7 H II regions to date, which are analyzed here in Table 1. Given the significance of nebular Fe abundances, as evidenced in this article, allocating telescope time for the detection of weak [Fe IV] emission lines across a range of nebular systems is crucial.

Additionally, it is important to expand the detections of [Fe III] in systems where  $12+\log(\text{O}/\text{H}) < 7.6$  to disentangle whether there is a plateau in the Fe/O ratios at such metallicities. The implications of a corroboration of this flattening, as well as those of a continuation of the anticorrelation between Fe/O and O/H, have been discussed in this article and are highly relevant for understanding the star formation history of galaxies. It is also important to understand if high Fe/O ratios are observed in star-forming nebulae with high N/O at low O/H, as in the case of J1205+4551 (Izotov et al. 2017, 2021). This may potentially be occurring in some areas of NGC 5471 (Kennicutt et al. 2003) or Mrk 71 (Esteban et al. 2002) and could allow us to understand the role of WR stars in the chemical enrichment of the ISM. Finally, expanding the sample of Fe/N ratios in low-metallicity stars could allow us to establish a more robust link between the nucleosynthetic production of both elements.

## 7. Conclusions

Following the philosophy of the DESIRED project (Méndez-Delgado et al. 2023a) of studying the nebular physics related to the weakest emission lines, we have analyzed the largest sample of star-forming regions with simultaneous direct determinations of the gas-phase Fe/H, O/H, and N/H ratios from the literature. We have determined the physical conditions ( $n_e$ ,  $T_e$ ) homogeneously and carefully and have considered the effects of temperature variations in the sample ( $t^2 > 0$ , Peimbert 1967), although our general conclusions are independent of the latter parameter.

We have shown a substantial discrepancy between the predictions of Ionization Correction Factor (ICF) models and the direct estimations of all ionization states of Fe. The greatest discrepancies were obtained with the ICF proposed by Izotov et al. (2006), reaching up to  $\sim 0.7$  dex of difference. In contrast, the ICF by Rodríguez & Rubin (2005) seems to provide more suitable predictions, especially when considering  $t^2 > 0$ , where the differences are reduced to  $\sim 0.2$  dex. To resolve these ICF-discrepancies, an observational sample dedicated to the detection of [Fe IV] emission lines is necessary, which is extremely scarce in the literature.

Our results confirm the existence of dust trapping Fe within photoionized environments, in consistency with previous studies (Rodríguez 2002; Rodríguez & Rubin 2005; Izotov et al. 2006). We estimate that at solar metallicities,  $\sim 95\%$  of the Fe is trapped in dust grains, while at typical metallicities of the LMC, this factor is  $\sim 75\%$ , and for those of the SMC, it is  $\sim 35\%$ . If we consider that O may be trapped in solid compounds along with Fe in the ionized gas, this implies that there is up to  $\sim 0.1$  dex of O trapped in dust at solar metallicity, while in the LMC, this value decreases to  $\sim 0.07$  dex, and in the SMC, it decreases to  $\sim 0.03$  dex. At metallicities lower than those of the SMC, the fraction of

O trapped in dust within H II regions could be negligible considering typical uncertainties in the determination of nebular chemical abundances. These values are upper limits and should be used with caution. Our results are in disagreement with the common assumption of adding 0.1 dex –regardless of the metallicity range or degree of ionization– to nebular O/H determinations to account for the contribution of O trapped in dust grains.

Our distribution of gas-phase Fe/O abundance ratios in star-forming regions follows a moderate linear correlation with O/H abundance. In all cases, we have obtained subsolar values of Fe/O. The observed dispersion does not appear to be solely linked to errors in the [Fe III]  $\lambda 4658$  flux, but to other physical phenomena related to the creation and destruction of dust. When  $12+\log(\text{O}/\text{H}) < 7.6$ , the Fe/O values seem to reach a plateau around  $\log(\text{Fe}/\text{O}) \approx -1.74$ . If this plateau is confirmed by subsequent observations, it indicates that the fraction of dust trapping Fe is negligible at such low metallicities. This could help to explain, at least in part, why these lines have been detected in high- $z$  galaxies revealed by the JWST (Arellano-Córdova et al. 2022). The value to which regions with  $12+\log(\text{O}/\text{H}) < 7.6$  seem to converge is consistent with the observed Fe/O values in metal-poor stars in our Galaxy. This would be consistent with a high star formation efficiencies in these regions, which are dwarf irregular galaxies.

We report a stronger linear correlation between Fe/N and N/H compared to the analogous case involving O. We interpret this finding as indicative that the production timescales of N and Fe are similar, while dust formation trapping Fe scales with its own availability. The hardness of the ionizing radiation also plays an important role destroying dust grains and scales with the Fe abundance. The first hypothesis is consistent with the stellar abundances of Fe/N vs. N/H in the Galaxy, which follow a rather flat pattern in the abundance range covered in this study. Considering this hypothesis, we have derived Eq. (1), which allows us to approximately estimate the fraction of Fe trapped into dust. Using this equation along with the gas-phase Fe/H abundances, we have been able to produce the relation between the total ISM (gas+dust) Fe/O ratio and O/H (see Fig. 10). The use of N as an element that connects stellar and nebular metallicities is certainly a promising idea that requires an expansion of both stellar and nebular simultaneous determinations of Fe, O, and N, especially at low metallicities. On the other hand, directly comparing stellar Fe-metallicities and nebular O-metallicities using the solar reference, regardless of the abundance ranges studied, certainly is inadvisable.

While J0811+4730 and J1631+4426 do show slightly elevated Fe/O abundance ratios, these are consistent with other determinations in regions with similar O/H abundances within the errors and are certainly subsolar. The differences found are of the order of typical uncertainties associated with the Fe-ICF discussed here. Therefore, we do not observe clear evidence supporting the Fe enrichment produced by very massive stars ( $M_{\text{init}} > 300M_{\odot}$ ). However, further observations and a better refinement of the Fe-ICF are necessary to reach solid conclusions on this regard. Finally, our analysis of J1205+4551 (Izotov et al. 2017, 2021) and the Sunburst Arc (Welch et al. 2024), the latter galaxy observed with the JWST at  $z = 2.37$ , suggests that systems with high N/O ratios may also have relatively elevated Fe/O values. Since J1205+4551 exhibits evidence of the presence of WR stars, one would have to ask whether the high values of Fe/O and N/O in these regions may be linked to the WR activity.

*Acknowledgements.* We dedicate this work to the memory of our esteemed colleague and friend Dr. Claudio Mendoza Guardia (1951-2024). Among his many contributions to astronomy, he recently reviewed and improved the radiative

and collisional atomic coefficients of Fe, which now allow us to conduct this study with the required precision. The authors thank the anonymous referee for their careful review and valuable comments. These have substantially helped to improve this article. JEMD and KK gratefully acknowledge funding from the Deutsche Forschungsgemeinschaft (DFG, German Research Foundation) in the form of an Emmy Noether Research Group (grant number KR4598/2-1, PI Kreckel) and the European Research Council's starting grant ERC StG-101077573 ("ISM-METALS"). AACs is supported by the German *Deutsche Forschungsgemeinschaft*, DFG in the form of an Emmy Noether Research Group – Project-ID 445674056 (SA4064/1-1, PI Sander). AACs further acknowledges funding provided by the Federal Ministry of Education and Research (BMBF) and the Baden-Württemberg Ministry of Science as part of the Excellence Strategy of the German Federal and State Governments. CE and JG-R acknowledge support from the Agencia Estatal de Investigación del Ministerio de Ciencia e Innovación (AEI- MCINN) under grant Espectroscopía de campo integral de regiones H II locales. Modelos para el estudio de regiones H II extragalácticas with reference 10.13039/501100011033 and from grant P/308614 financed by funds transferred from the Spanish Ministry of Science, Innovation and Universities, charged to the General State Budgets and with funds transferred from the General Budgets of the Autonomous Community of the Canary Islands by the MCIU. JG-R also acknowledges funds from the Spanish Ministry of Science and Innovation (MICINN) through the Spanish State Research Agency, under Severo Ochoa Centres of Excellence Program 2020-2023 (CEX2019-000920-S). IDL and SvdG acknowledge funding from the European Research Council (ERC) under the European Union's Horizon 2020 research and innovation program DustOrigin (ERC-2019-StG-851622) and from the Flemish Fund for Scientific Research (FWO-Vlaanderen) through the research project G023821N. SFS thanks the PAPIIT-DGAPA AG100622 project and CONACYT grant CF19-39578.

## References

- Abazajian, K., Adelman-McCarthy, J. K., Agüeros, M. A., et al. 2005, *AJ*, 129, 1755
- Amarsi, A. M., Grevesse, N., Asplund, M., & Collet, R. 2021, *A&A*, 656, A113
- Amarsi, A. M., Grevesse, N., Gruber, J., et al. 2020, *A&A*, 636, A120
- Amarsi, A. M., Nissen, P. E., Asplund, M., Lind, K., & Barklem, P. S. 2019, *A&A*, 622, L4
- Amayo, A., Delgado-Inglada, G., & Stasińska, G. 2021, *MNRAS*, 505, 2361
- Arellano-Córdova, K. Z., Berg, D. A., Chisholm, J., et al. 2022, *ApJ*, 940, L23
- Arellano-Córdova, K. Z., Berg, D. A., Mingozi, M., et al. 2024, arXiv e-prints, arXiv:2403.08401
- Arellano-Córdova, K. Z., Esteban, C., García-Rojas, J., & Méndez-Delgado, J. E. 2020, *MNRAS*, 496, 1051
- Arellano-Córdova, K. Z., Esteban, C., García-Rojas, J., & Méndez-Delgado, J. E. 2021, *MNRAS*, 502, 225
- Arellano-Córdova, K. Z. & Rodríguez, M. 2020, *MNRAS*, 497, 672
- Asplund, M. 2005, *ARA&A*, 43, 481
- Asplund, M., Amarsi, A. M., & Grevesse, N. 2021, *A&A*, 653, A141
- Aver, E., Olive, K. A., & Skillman, E. D. 2015, *J. Cosmology Astropart. Phys.*, 2015, 011
- Baldwin, J. A., Crotts, A., Dufour, R. J., et al. 1996, *ApJ*, 468, L115
- Baldwin, J. A., Phillips, M. M., & Terlevich, R. 1981, *PASP*, 93, 5
- Ballance, C. P., Griffin, D. C., & McLoughlin, B. M. 2007, *Journal of Physics B Atomic Molecular Physics*, 40, F327
- Bautista, M. A., Fivet, V., Ballance, C., et al. 2015, *ApJ*, 808, 174
- Bensby, T., Yee, J. C., Feltzing, S., et al. 2013, *A&A*, 549, A147
- Berg, D. A., Chisholm, J., Erb, D. K., et al. 2021, *ApJ*, 922, 170
- Berg, D. A., Pogge, R. W., Skillman, E. D., et al. 2020, *ApJ*, 893, 96
- Berg, D. A., Skillman, E. D., Croxall, K. V., et al. 2015, *ApJ*, 806, 16
- Berg, D. A., Skillman, E. D., Garnett, D. R., et al. 2013, *ApJ*, 775, 128
- Bergerud, B. M., Spangler, S. R., & Beauchamp, K. M. 2020, *MNRAS*, 492, 1142
- Blagrove, K. P. M., Martin, P. G., & Baldwin, J. A. 2006, *ApJ*, 644, 1006
- Bocchio, M., Jones, A. P., & Slavin, J. D. 2014, *A&A*, 570, A32
- Bragança, G. A., Daflon, S., Lanz, T., et al. 2019, *A&A*, 625, A120
- Bresolin, F. 2007, *ApJ*, 656, 186
- Bresolin, F., Gieren, W., Kudritzki, R.-P., et al. 2009, *ApJ*, 700, 309
- Bresolin, F., Kudritzki, R.-P., & Urbaneja, M. A. 2022, *ApJ*, 940, 32
- Bresolin, F., Kudritzki, R.-P., Urbaneja, M. A., et al. 2016, *ApJ*, 830, 64
- Bresolin, F., Schaerer, D., González Delgado, R. M., & Stasińska, G. 2005, *A&A*, 441, 981
- Butler, K. & Zeppen, C. J. 1989, *A&A*, 208, 337
- Calzetti, D., Kinney, A. L., & Storchi-Bergmann, T. 1994, *ApJ*, 429, 582
- Cameron, A. J., Katz, H., & Rey, M. P. 2023, *MNRAS*, 522, L89
- Carigi, L., Peimbert, M., Esteban, C., & García-Rojas, J. 2005, *ApJ*, 623, 213
- Carigi, L., Peimbert, M., & Peimbert, A. 2019, *ApJ*, 873, 107
- Carretta, E., Gratton, R. G., & Sneden, C. 2000, *A&A*, 356, 238
- Castellanos, M., Díaz, A. I., & Terlevich, E. 2002, *MNRAS*, 329, 315
- Cayrel, R., Depagne, E., Spite, M., et al. 2004, *A&A*, 416, 1117
- Chiappini, C., Romano, D., & Matteucci, F. 2003, *MNRAS*, 339, 63
- Choban, C. R., Kereš, D., Hopkins, P. F., et al. 2022, *MNRAS*, 514, 4506
- Chruślińska, M., Pakmor, R., Matthee, J., & Matsuno, T. 2024, *A&A*, 686, A186
- Crowther, P. A. 2007, *ARA&A*, 45, 177
- Croxall, K. V., Pogge, R. W., Berg, D. A., Skillman, E. D., & Moustakas, J. 2015, *ApJ*, 808, 42
- Croxall, K. V., Pogge, R. W., Berg, D. A., Skillman, E. D., & Moustakas, J. 2016, *ApJ*, 830, 4
- Curti, M., Cresci, G., Mannucci, F., et al. 2017, *MNRAS*, 465, 1384
- Deb, N. C. & Hibbert, A. 2009, *Atomic Data and Nuclear Data Tables*, 95, 184
- Delgado-Inglada, G., Mesa-Delgado, A., García-Rojas, J., Rodríguez, M., & Esteban, C. 2016, *MNRAS*, 456, 3855
- Dinerstein, H. L. 1990, in *Astrophysics and Space Science Library*, Vol. 161, *The Interstellar Medium in Galaxies*, ed. J. Thronson, Harley A. & J. M. Shull, 257–285
- Domínguez-Guzmán, G., Rodríguez, M., García-Rojas, J., Esteban, C., & Toribio San Cipriano, L. 2022, *MNRAS*, 517, 4497
- Drory, N., Blanc, G. A., Kreckel, K., et al. 2024, arXiv e-prints, arXiv:2405.01637
- Dubois, Y., Rodríguez Montero, F., Guerra, C., et al. 2024, arXiv e-prints, arXiv:2402.18515
- Ecuvillon, A., Israelian, G., Santos, N. C., et al. 2004, *A&A*, 418, 703
- Egorova, E. S., Egorov, O. V., Moiseev, A. V., et al. 2021, *MNRAS*, 504, 6179
- Espíritu, J. N., Peimbert, A., Delgado-Inglada, G., & Ruiz, M. T. 2017, *Rev. Mexicana Astron. Astrofis.*, 53, 95
- Esteban, C., Bresolin, F., García-Rojas, J., & Toribio San Cipriano, L. 2020, *MNRAS*, 491, 2137
- Esteban, C., Bresolin, F., Peimbert, M., et al. 2009, *ApJ*, 700, 654
- Esteban, C., Carigi, L., Copetti, M. V. F., et al. 2013, *MNRAS*, 433, 382
- Esteban, C., Fang, X., García-Rojas, J., & Toribio San Cipriano, L. 2017, *MNRAS*, 471, 987
- Esteban, C. & García-Rojas, J. 2018, *MNRAS*, 478, 2315
- Esteban, C., García-Rojas, J., Carigi, L., et al. 2014, *MNRAS*, 443, 624
- Esteban, C., Méndez-Delgado, J. E., García-Rojas, J., & Arellano-Córdova, K. Z. 2022, *ApJ*, 931, 92
- Esteban, C., Mesa-Delgado, A., Morisset, C., & García-Rojas, J. 2016, *MNRAS*, 460, 4038
- Esteban, C., Peimbert, M., García-Rojas, J., et al. 2004, *MNRAS*, 355, 229
- Esteban, C., Peimbert, M., Torres-Peimbert, S., & Rodríguez, M. 2002, *ApJ*, 581, 241
- Evans, C. J., Bresolin, F., Urbaneja, M. A., et al. 2007, *ApJ*, 659, 1198
- Ferland, G. J., Chatzikos, M., Guzmán, F., et al. 2017, *Rev. Mexicana Astron. Astrofis.*, 53, 385
- Fernández, V., Amorín, R., Pérez-Montero, E., et al. 2022, *MNRAS*, 511, 2515
- Fernández, V., Terlevich, E., Díaz, A. I., Terlevich, R., & Rosales-Ortega, F. F. 2018, *MNRAS*, 478, 5301
- Fernández-Martín, A., Pérez-Montero, E., Vilchez, J. M., & Mampaso, A. 2017, *A&A*, 597, A84
- Fritzsche, S., Fricke, B., Geschke, D., Heitmann, A., & Sienkiewicz, J. E. 1999, *ApJ*, 518, 994
- Froese Fischer, C., Rubin, R. H., & Rodríguez, M. 2008, *MNRAS*, 391, 1828
- Froese Fischer, C. & Tachiev, G. 2004, *Atomic Data and Nuclear Data Tables*, 87, 1
- Froese Fischer, C., Tachiev, G., & Irimia, A. 2006, *Atomic Data and Nuclear Data Tables*, 92, 607
- Galavís, M. E., Mendoza, C., & Zeppen, C. J. 1995, *A&AS*, 111, 347
- Galliano, F., Nersesian, A., Bianchi, S., et al. 2021, *A&A*, 649, A18
- García, M., Herrero, A., Najarro, F., Lennon, D. J., & Alejandro Urbaneja, M. 2014, *ApJ*, 788, 64
- García-Rojas, J. & Esteban, C. 2007, *ApJ*, 670, 457
- García-Rojas, J., Esteban, C., Peimbert, A., et al. 2005, *MNRAS*, 362, 301
- García-Rojas, J., Esteban, C., Peimbert, A., et al. 2007, *Rev. Mexicana Astron. Astrofis.*, 43, 3
- García-Rojas, J., Esteban, C., Peimbert, M., et al. 2006, *MNRAS*, 368, 253
- García-Rojas, J., Esteban, C., Peimbert, M., et al. 2004, *ApJS*, 153, 501
- García-Rojas, J., Simón-Díaz, S., & Esteban, C. 2014, *A&A*, 571, A93
- Garnett, D. R. 1990, *ApJ*, 363, 142
- Garnett, D. R. 1992, *AJ*, 103, 1330
- Gazak, J. Z., Kudritzki, R., Evans, C., et al. 2015, *ApJ*, 805, 182
- Gioannini, L., Matteucci, F., Vladilo, G., & Calura, F. 2017, *MNRAS*, 464, 985
- Gómez-González, V. M. A., Mayya, Y. D., Zaragoza-Cardiel, J., et al. 2024, *MNRAS*, 529, 4369
- Goswami, S., Silva, L., Bressan, A., et al. 2022, *A&A*, 663, A1
- Goswami, S., Slemmer, A., Marigo, P., et al. 2021, *A&A*, 650, A203
- Gratton, R. G., Carretta, E., Matteucci, F., & Sneden, C. 2000, *A&A*, 358, 671
- Greggio, L. 2005, *A&A*, 441, 1055

- Grieve, M. F. R., Ramsbottom, C. A., Hudson, C. E., & Keenan, F. P. 2014, *ApJ*, 780, 110
- Grisoni, V., Matteucci, F., & Romano, D. 2021, *MNRAS*, 508, 719
- Gunasekera, C. M., Ji, X., Chatzikos, M., Yan, R., & Ferland, G. 2023, *MNRAS*, 520, 4345
- Guseva, N. G., Izotov, Y. I., Stasińska, G., et al. 2011, *A&A*, 529, A149
- Guseva, N. G., Papaderos, P., Meyer, H. T., Izotov, Y. I., & Fricke, K. J. 2009, *A&A*, 505, 63
- Guseva, N. G., Thuan, T. X., & Izotov, Y. I. 2024, *MNRAS*, 527, 3932
- Hägele, G. F., Díaz, Á. I., Terlevich, E., et al. 2008, *MNRAS*, 383, 209
- Hägele, G. F., Firpo, V., Bosch, G., Díaz, Á. I., & Morrell, N. 2012, *MNRAS*, 422, 3475
- Hägele, G. F., García-Benito, R., Pérez-Montero, E., et al. 2011, *MNRAS*, 414, 272
- Hägele, G. F., Pérez-Montero, E., Díaz, Á. I., Terlevich, E., & Terlevich, R. 2006, *MNRAS*, 372, 293
- Hendricks, B., Koch, A., Lanfranchi, G. A., et al. 2014, *ApJ*, 785, 102
- Henry, R. B. C., Edmunds, M. G., & Köppen, J. 2000, *ApJ*, 541, 660
- Hensley, B. S. & Draine, B. T. 2023, *ApJ*, 948, 55
- Higgins, E. R., Vink, J. S., Hirschi, R., Laird, A. M., & Sabhahit, G. N. 2023, *MNRAS*, 526, 534
- Hill, V., Skúladóttir, Á., Tolstoy, E., et al. 2019, *A&A*, 626, A15
- Hosek, Matthew W. J., Kudritzki, R.-P., Bresolin, F., et al. 2014, *ApJ*, 785, 151
- Hsu, T., Cooke, R. J., Prochaska, J. X., & Bolte, M. 2020, *ApJ*, 896, 77
- Hunter, I., Dufton, P. L., Smartt, S. J., et al. 2007, *A&A*, 466, 277
- Irimia, A. & Froese Fischer, C. 2005, *Phys. Scr*, 71, 172
- Isobe, Y., Ouchi, M., Suzuki, A., et al. 2022, *ApJ*, 925, 111
- Israelian, G., Ecuivillon, A., Rebolo, R., et al. 2004, *A&A*, 421, 649
- Izotov, Y. I., Chaffee, F. H., Foltz, C. B., et al. 1999, *ApJ*, 527, 757
- Izotov, Y. I., Guseva, N. G., Fricke, K. J., & Papaderos, P. 2009, *A&A*, 503, 61
- Izotov, Y. I., Stasińska, G., Meynet, G., Guseva, N. G., & Thuan, T. X. 2006, *A&A*, 448, 955
- Izotov, Y. I. & Thuan, T. X. 1998a, *ApJ*, 500, 188
- Izotov, Y. I. & Thuan, T. X. 1998b, *ApJ*, 500, 188
- Izotov, Y. I. & Thuan, T. X. 1999, *ApJ*, 511, 639
- Izotov, Y. I. & Thuan, T. X. 2004, *ApJ*, 602, 200
- Izotov, Y. I., Thuan, T. X., & Guseva, N. G. 2017, *MNRAS*, 471, 548
- Izotov, Y. I., Thuan, T. X., & Guseva, N. G. 2021, *MNRAS*, 508, 2556
- Izotov, Y. I., Thuan, T. X., Guseva, N. G., & Liss, S. E. 2018, *MNRAS*, 473, 1956
- Izotov, Y. I., Thuan, T. X., & Lipovetsky, V. A. 1997, *ApJS*, 108, 1
- Izotov, Y. I., Thuan, T. X., & Prigon, G. 2012, *MNRAS*, 427, 1229
- Jenkins, E. B. 2009, *ApJ*, 700, 1299
- Ji, X., Übler, H., Maiolino, R., et al. 2024, *arXiv e-prints*, arXiv:2404.04148
- Jones, A. P., Köhler, M., Ysard, N., Bocchio, M., & Verstraete, L. 2017, *A&A*, 602, A46
- Kauffmann, G., Heckman, T. M., Tremonti, C., et al. 2003, *MNRAS*, 346, 1055
- Kaufman, V. & Sugar, J. 1986, *Journal of Physical and Chemical Reference Data*, 15, 321
- Kennicutt, Robert C., J., Bresolin, F., & Garnett, D. R. 2003, *ApJ*, 591, 801
- Kirchschlager, F., Mattsson, L., & Gent, F. A. 2022, *MNRAS*, 509, 3218
- Kirchschlager, F., Sartorio, N. S., De Looze, I., et al. 2024, *MNRAS*, 528, 5364
- Kisielius, R., Storey, P. J., Ferland, G. J., & Keenan, F. P. 2009, *MNRAS*, 397, 903
- Kobayashi, C., Karakas, A. I., & Lugaro, M. 2020, *ApJ*, 900, 179
- Kobayashi, C., Umeda, H., Nomoto, K., Tominaga, N., & Ohkubo, T. 2006, *ApJ*, 653, 1145
- Kojima, T., Ouchi, M., Rauch, M., et al. 2021, *ApJ*, 913, 22
- Kudritzki, R. P., Castro, N., Urbaneja, M. A., et al. 2016, *ApJ*, 829, 70
- Kudritzki, R.-P., Urbaneja, M. A., Bresolin, F., Hosek, Matthew W. J., & Przybilla, N. 2014, *ApJ*, 788, 56
- Kudritzki, R.-P., Urbaneja, M. A., Bresolin, F., et al. 2008, *ApJ*, 681, 269
- Kudritzki, R.-P., Urbaneja, M. A., Gazak, Z., et al. 2012, *ApJ*, 747, 15
- Kurichin, O. A., Kisilitsyn, P. A., Klimenko, V. V., Balashev, S. A., & Ivanchik, A. V. 2021, *MNRAS*, 502, 3045
- Kwitter, K. B. 1984, *ApJ*, 287, 840
- Limongi, M. & Chieffi, A. 2018, *ApJS*, 237, 13
- Lin, Z., Hu, N., Kong, X., et al. 2017, *ApJ*, 842, 97
- López-Sánchez, A. R. & Esteban, C. 2009, *A&A*, 508, 615
- López-Sánchez, Á. R., Esteban, C., García-Rojas, J., Peimbert, M., & Rodríguez, M. 2007, *ApJ*, 656, 168
- López-Sánchez, Á. R., Westmeier, T., Esteban, C., & Koribalski, B. S. 2015, *MNRAS*, 450, 3381
- Luridiana, V., Morisset, C., & Shaw, R. A. 2015, *A&A*, 573, A42
- Magrini, L., Stanghellini, L., Corbelli, E., Galli, D., & Villaver, E. 2010, *A&A*, 512, A63
- Magrini, L., Vincenzo, F., Randich, S., et al. 2018, *A&A*, 618, A102
- Maoz, D. & Mannucci, F. 2012, *PASA*, 29, 447
- Martins, F., Bouret, J. C., Hillier, D. J., et al. 2024, *arXiv e-prints*, arXiv:2405.01267
- Martins, F., Hervé, A., Bouret, J. C., et al. 2015, *A&A*, 575, A34
- Matsumoto, A., Ouchi, M., Nakajima, K., et al. 2022, *ApJ*, 941, 167
- Matteucci, F. 2012, *Chemical Evolution of Galaxies*
- Matteucci, F. & Greggio, L. 1986, *A&A*, 154, 279
- Méndez-Delgado, J. E., Amayo, A., Arellano-Córdova, K. Z., et al. 2022a, *MNRAS*, 510, 4436
- Méndez-Delgado, J. E., Esteban, C., García-Rojas, J., et al. 2023a, *MNRAS*, 523, 2952
- Méndez-Delgado, J. E., Esteban, C., García-Rojas, J., Arellano-Córdova, K. Z., & Valerdi, M. 2020, *MNRAS*, 496, 2726
- Méndez-Delgado, J. E., Esteban, C., García-Rojas, J., & Henney, W. J. 2022b, *MNRAS*, 514, 744
- Méndez-Delgado, J. E., Esteban, C., García-Rojas, J., et al. 2021a, *MNRAS*, 502, 1703
- Méndez-Delgado, J. E., Esteban, C., García-Rojas, J., Kreckel, K., & Peimbert, M. 2023b, *Nature*, 618, 249
- Méndez-Delgado, J. E., Esteban, C., García-Rojas, J., Kreckel, K., & Peimbert, M. 2024, *Nature Astronomy*, 8, 275
- Méndez-Delgado, J. E., Henney, W. J., Esteban, C., et al. 2021b, *ApJ*, 918, 27
- Mendoza, C. 1983, in *IAU Symposium*, Vol. 103, *Planetary Nebulae*, ed. L. H. Aller, 143–172
- Mendoza, C., Méndez-Delgado, J. E., Bautista, M., García-Rojas, J., & Morisset, C. 2023, *Atoms*, 11, 63
- Mendoza, C. & Zeppen, C. J. 1982, *MNRAS*, 198, 127
- Mesa-Delgado, A., Esteban, C., García-Rojas, J., et al. 2009, *MNRAS*, 395, 855
- Meynet, G. & Maeder, A. 2002a, *A&A*, 390, 561
- Meynet, G. & Maeder, A. 2002b, *A&A*, 381, L25
- Meynet, G. & Maeder, A. 2005, *A&A*, 429, 581
- Mollá, M., Vilchez, J. M., Gavilán, M., & Díaz, A. I. 2006, *MNRAS*, 372, 1069
- Morisset, C. 2004, *ApJ*, 601, 858
- Nahar, S. N., Delahaye, F., Pradhan, A. K., & Zeppen, C. J. 2000, *A&AS*, 144, 141
- Nava, A., Casebeer, D., Henry, R. B. C., & Jevremovic, D. 2006, *ApJ*, 645, 1076
- Nicholls, D. C., Sutherland, R. S., Dopita, M. A., Kewley, L. J., & Groves, B. A. 2017, *MNRAS*, 466, 4403
- Nieva, M. F. & Przybilla, N. 2012, *A&A*, 539, A143
- Noll, S., Kausch, W., Barden, M., et al. 2012, *A&A*, 543, A92
- Nomoto, K., Kobayashi, C., & Tominaga, N. 2013, *ARA&A*, 51, 457
- Osterbrock, D. E. & Ferland, G. J. 2006, *Astrophysics of gaseous nebulae and active galactic nuclei*
- Osterbrock, D. E., Tran, H. D., & Veilleux, S. 1992, *ApJ*, 389, 305
- Pagel, B. E. J., Simonson, E. A., Terlevich, R. J., & Edmunds, M. G. 1992, *MNRAS*, 255, 325
- Palla, M. 2021, *MNRAS*, 503, 3216
- Patrick, L. R., Evans, C. J., Davies, B., et al. 2015, *ApJ*, 803, 14
- Patterson, M. T., Walterbos, R. A. M., Kennicutt, R. C., Chiappini, C., & Thilker, D. A. 2012, *MNRAS*, 422, 401
- Pauli, D., Oskinova, L. M., Hamann, W. R., et al. 2023, *A&A*, 673, A40
- Peña, M., Stasińska, G., & Richer, M. G. 2007, *A&A*, 476, 745
- Peña-Guerrero, M. A., Peimbert, A., Peimbert, M., & Ruiz, M. T. 2012, *ApJ*, 746, 115
- Peimbert, A. 2003, *ApJ*, 584, 735
- Peimbert, A., Peña-Guerrero, M. A., & Peimbert, M. 2012, *ApJ*, 753, 39
- Peimbert, A. & Peimbert, M. 2010, *ApJ*, 724, 791
- Peimbert, A., Peimbert, M., & Luridiana, V. 2002, *ApJ*, 565, 668
- Peimbert, A., Peimbert, M., & Ruiz, M. T. 2005, *ApJ*, 634, 1056
- Peimbert, M. 1967, *ApJ*, 150, 825
- Peimbert, M. 1971, *Boletín de los Observatorios Tonantzintla y Tacubaya*, 6, 29
- Peimbert, M. & Costero, R. 1969, *Boletín de los Observatorios Tonantzintla y Tacubaya*, 5, 3
- Peimbert, M., Luridiana, V., & Peimbert, A. 2007, *ApJ*, 666, 636
- Peimbert, M., Peimbert, A., & Delgado-Inglada, G. 2017, *PASP*, 129, 082001
- Peimbert, M. & Torres-Peimbert, S. 1974, *ApJ*, 193, 327
- Pilyugin, L. S., Vilchez, J. M., & Thuan, T. X. 2010, *ApJ*, 720, 1738
- Prantzos, N., Abia, C., Chen, T., et al. 2023, *MNRAS*, 523, 2126
- Prantzos, N., Abia, C., Limongi, M., Chieffi, A., & Cristallo, S. 2018, *MNRAS*, 476, 3432
- Przybilla, N., Firnstein, M., Nieva, M. F., Meynet, G., & Maeder, A. 2010, *A&A*, 517, A38
- Ramachandran, V., Oskinova, L. M., & Hamann, W. R. 2021, *A&A*, 646, A16
- Ramsbottom, C. A. & Bell, K. L. 1997, *Atomic Data and Nuclear Data Tables*, 66, 65
- Rickards Vaught, R. J., Sandstrom, K. M., Belfiore, F., et al. 2024, *ApJ*, 966, 130
- Rodríguez, M. 1996, *A&A*, 313, L5
- Rodríguez, M. 1999, *A&A*, 348, 222
- Rodríguez, M. 2002, *A&A*, 389, 556
- Rodríguez, M. & Rubin, R. H. 2005, *ApJ*, 626, 900
- Rogers, N. S. J., Skillman, E. D., Pogge, R. W., et al. 2022, *ApJ*, 939, 44
- Rogers, N. S. J., Skillman, E. D., Pogge, R. W., et al. 2021, *ApJ*, 915, 21
- Rolleston, W. R. J., Venn, K., Tolstoy, E., & Dufton, P. L. 2003, *A&A*, 400, 21



- Roman-Duval, J., Jenkins, E. B., Tchernyshyov, K., et al. 2022a, *ApJ*, 928, 90
- Roman-Duval, J., Jenkins, E. B., Tchernyshyov, K., et al. 2022b, *ApJ*, 935, 105
- Romano, D., Matteucci, F., Zhang, Z.-Y., Ivison, R. J., & Ventura, P. 2019, *MNRAS*, 490, 2838
- Rosolowsky, E. & Simon, J. D. 2008, *ApJ*, 675, 1213
- Rubin, R. H. 1989, *ApJS*, 69, 897
- Rubin, R. H., Dufour, R. J., Ferland, G. J., et al. 1997, *ApJ*, 474, L131
- Sánchez, S. F., Espinosa-Ponce, C., Carigi, L., et al. 2021, *A&A*, 652, L10
- Sander, A. A. C., Vink, J. S., & Hamann, W. R. 2020, *MNRAS*, 491, 4406
- Schaerer, D., Fragos, T., & Izotov, Y. I. 2019, *A&A*, 622, L10
- Simón-Díaz, S., Herrero, A., Esteban, C., & Najarro, F. 2006, *A&A*, 448, 351
- Simón-Díaz, S. & Stasińska, G. 2008, *MNRAS*, 389, 1009
- Simón-Díaz, S. & Stasińska, G. 2011, *A&A*, 526, A48
- Skillman, E. D. 1985, *ApJ*, 290, 449
- Skillman, E. D., Côté, S., & Miller, B. W. 2003, *AJ*, 125, 610
- Skillman, E. D., Salzer, J. J., Berg, D. A., et al. 2013, *AJ*, 146, 3
- Slavin, J. D., Dwek, E., & Jones, A. P. 2015, *ApJ*, 803, 7
- Smith, N., Bally, J., Shuping, R. Y., Morris, M., & Kassis, M. 2005, *AJ*, 130, 1763
- Spite, M., Cayrel, R., Hill, V., et al. 2006, *A&A*, 455, 291
- Stasińska, G. 1978, *A&AS*, 32, 429
- Stasińska, G. 2023, arXiv e-prints, arXiv:2312.01873
- Stasińska, G., Izotov, Y., Morisset, C., & Guseva, N. 2015, *A&A*, 576, A83
- Stasińska, G., Morisset, C., Simón-Díaz, S., et al. 2013, *A&A*, 551, A82
- Stock, D. J., Barlow, M. J., & Wesson, R. 2011, *MNRAS*, 418, 2532
- Storey, P. J. & Hummer, D. G. 1995, *MNRAS*, 272, 41
- Storey, P. J., Sochi, T., & Badnell, N. R. 2014, *MNRAS*, 441, 3028
- Storey, P. J. & Zeippen, C. J. 2000, *MNRAS*, 312, 813
- Sun, T., Ge, Z., Chen, X., et al. 2023, *ApJS*, 268, 29
- Tacchella, S., McClymont, W., Scholtz, J., et al. 2024, arXiv e-prints, arXiv:2404.02194
- Tayal, S. S. 2011, *ApJS*, 195, 12
- Tayal, S. S. & Zatsarinny, O. 2010, *ApJS*, 188, 32
- Thompson, H. M. A., Keenan, F. P., Dufton, P. L., et al. 2008, *MNRAS*, 383, 729
- Thuan, T. X. & Izotov, Y. I. 2005, *ApJS*, 161, 240
- Tolstoy, E., Hill, V., & Tosi, M. 2009, *ARA&A*, 47, 371
- Toribio San Cipriano, L., Domínguez-Guzmán, G., Esteban, C., et al. 2017, *MNRAS*, 467, 3759
- Toribio San Cipriano, L., García-Rojas, J., Esteban, C., Bresolin, F., & Peimbert, M. 2016, *MNRAS*, 458, 1866
- Torres-Peimbert, S. & Peimbert, M. 1977, *Rev. Mexicana Astron. Astrofis.*, 2, 181
- Trundle, C., Dufton, P. L., Hunter, I., et al. 2007, *The VLT-FLAMES survey of massive stars: evolution of surface N abundances and effective temperature scales in the Galaxy and Magellanic Clouds, Astronomy and Astrophysics, Volume 471, Issue 2, August IV 2007, pp.625-643*
- Trundle, C. & Lennon, D. J. 2005, *A&A*, 434, 677
- Tsamis, Y. G., Barlow, M. J., Liu, X. W., Danziger, I. J., & Storey, P. J. 2003, *MNRAS*, 345, 186
- U, V., Urbaneja, M. A., Kudritzki, R.-P., et al. 2009, *ApJ*, 704, 1120
- Urbaneja, M. A., Kudritzki, R.-P., Bresolin, F., et al. 2008, *ApJ*, 684, 118
- Vale Asari, N., Stasińska, G., Morisset, C., & Cid Fernandes, R. 2016, *MNRAS*, 460, 1739
- Valerdi, M., Peimbert, A., & Peimbert, M. 2021, *MNRAS*, 505, 3624
- Valerdi, M., Peimbert, A., Peimbert, M., & Sixtos, A. 2019, *ApJ*, 876, 98
- van den Hoek, L. B. & Groenewegen, M. A. T. 1997, *A&AS*, 123, 305
- Ventura, P., Dell'Agli, F., Tailo, M., et al. 2022, *Universe*, 8, 45
- Ventura, P., Di Criscienzo, M., Carini, R., & D'Antona, F. 2013, *MNRAS*, 431, 3642
- Verner, E. M., Verner, D. A., Baldwin, J. A., Ferland, G. J., & Martin, P. G. 2000, *ApJ*, 543, 831
- Vila-Costas, M. B. & Edmunds, M. G. 1993, *MNRAS*, 265, 199
- Vilchez, J. M. & Pagel, B. E. J. 1988, *MNRAS*, 231, 257
- Vincenzo, F., Belfiore, F., Maiolino, R., Matteucci, F., & Ventura, P. 2016, *MNRAS*, 458, 3466
- Vink, J. S., de Koter, A., & Lamers, H. J. G. L. M. 2001, *A&A*, 369, 574
- Walcher, C. J., Coelho, P., Gallazzi, A., & Charlot, S. 2009, *MNRAS*, 398, L44
- Watanabe, K., Ouchi, M., Nakajima, K., et al. 2024, *ApJ*, 962, 50
- Welch, B., Rivera-Thorsen, T. E., Rigby, J., et al. 2024, arXiv e-prints, arXiv:2405.06631
- Weßmayer, D., Przybilla, N., & Butler, K. 2022, *A&A*, 668, A92
- Wheeler, J. C., Sneden, C., & Truran, James W., J. 1989, *ARA&A*, 27, 279
- Wiese, W. L., Fuhr, J. R., & Deters, T. M. 1996, *Journal of Physical and Chemical Reference Data, Monograph 7*, 403
- Woosley, S. E., Heger, A., & Weaver, T. A. 2002, *Reviews of Modern Physics*, 74, 1015
- Xiong, S., Li, X., & Liao, C. 2022, *ApJS*, 261, 36
- Zhang, H. 1996, *A&AS*, 119, 523
- Zhang, H. L. & Pradhan, A. K. 1997, *A&AS*, 126, 373
- Zhukovska, S., Henning, T., & Dobbs, C. 2018, *ApJ*, 857, 94
- Zurita, A. & Bresolin, F. 2012, *MNRAS*, 427, 1463

## Appendix A: The empirical relationship between metallicity and reddening in star-forming nebulae.

Typically, the reddening corrections in star-forming regions are traced by comparing the observed  $H\alpha/H\beta$  fluxes with the theoretically expected values, using an extinction law suited for each specific region (Calzetti et al. 1994). In a subsample of our star-forming regions, we have access to the observed fluxes before reddening correction. In such regions, we compared the observed  $H\alpha/H\beta$  values with the theoretical predictions of Storey & Hummer (1995), using PyNeb (Luridiana et al. 2015). We considered the density and temperature  $T_e([\text{O III}])$  (the impact of  $t^2$  is negligible in this RL-ratio) adopted for each region, presented in Tables D.3 and D.5, respectively. Then, we compared the ratios between the observed and theoretical  $H\alpha/H\beta$  fluxes with the gas-phase Fe/O and Fe/N values analyzed in this manuscript, as shown in Figs. A.1 and A.2. The numerical values are presented in Table D.9

Unfortunately, not all the reference spectra in Table D.2 explicitly report the observed flux values before reddening correction, and the statistics presented in Figs. A.1 and A.2 are notably less robust than those shown in Figs. 6 and 8. However, there is a weak anticorrelation between Fe/N and the  $H\alpha/H\beta$  flux ratios, as specifically shown in Fig. A.2. This anticorrelation is expected if there is a connection between the dust present within the H II regions and the dust in the surrounding neutral gas, which should cause most of the optical extinction. In the global trend, when  $\log(\text{Fe}/\text{N}) \sim -0.5$  dex,  $H\alpha/H\beta$  appears to reach values consistent with the theoretical fluxes under conditions of no extinction. These Fe/N values are achieved in low-metallicity regions, near the limit of  $12+\log(\text{N}/\text{H}) \sim 6.3$  (see Table 2). A qualitatively similar situation occurs with Fe/O, although the correlation with  $H\alpha/H\beta$  is evidently less strong than in the case of Fe/N. This supports the interpretation made in the present article regarding the distribution of gas-phase Fe/N and Fe/O abundances in terms of dust depletion and the apparent closer correlation between Fe and N compared to Fe and O. Observed flux ( $H\alpha/H\beta$ ) / Theoretical ( $H\alpha/H\beta$ ) is an observational quantity independent of the specific extinction law used to model the reddening coefficient,  $c(H\beta)$ , or the color excess  $E(B - V)$ . However, this can, in turn, increase the observed dispersion.

As a final note of interest, in the general DESIRED sample, we found that statistically, there are higher extinctions in regions with higher O/H abundance, as shown in Fig. A.3. The sample presented in that figure is larger than the one shown in Figs. A.1 and A.2, as it includes regions without detections of  $[\text{Fe III}]\lambda 4658$ . It is notable that although the effect of extinction is certainly lower in regions of lower metallicity, it is still not negligible in most cases. Considering the discussion presented in Sec. 6, this could indicate that H II regions have a lower fraction of Fe trapped in dust than the surrounding neutral clouds. This could support the idea that part of the dust initially present in neutral gas clouds is destroyed during the ionization stage when massive stars form in H II regions. However, a systematic and simultaneous multi-wavelength study of Fe depletions in neutral and ionized gas in a statistically robust sample is necessary to reach more solid conclusions.

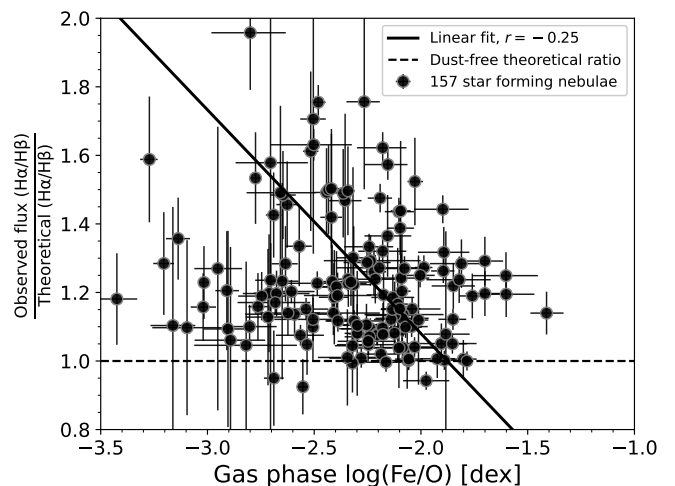


Fig. A.1. Comparison of ratios between the observed and theoretical  $H\alpha/H\beta$  fluxes with the gas-phase Fe/O values analyzed in this manuscript for a subsample with reported flux values prior to reddening correction.

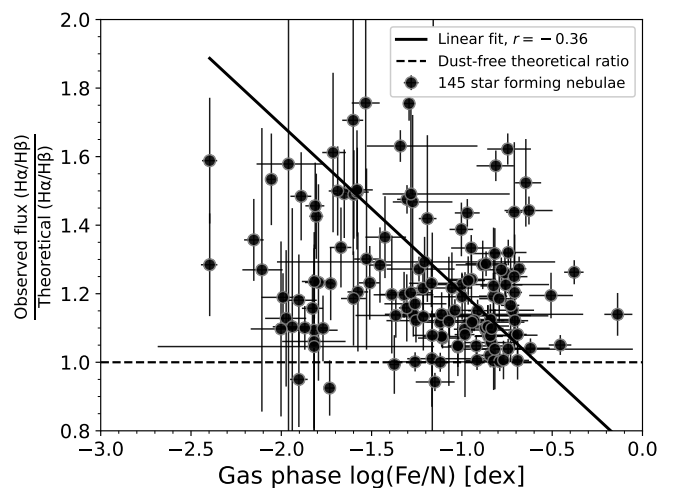
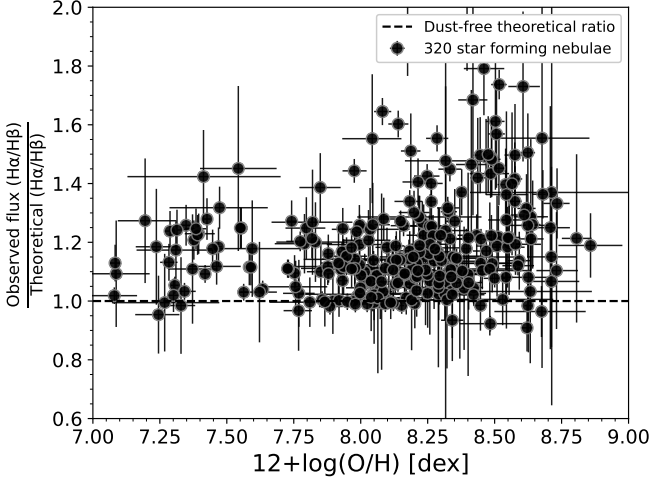


Fig. A.2. Same as Fig. A.1 but for the gas-phase Fe/N abundances.



**Fig. A.3.** Comparison of ratios between the observed and theoretical  $H\alpha/H\beta$  fluxes with the  $12+\log(O/H)$  values for a subsample of the DESIRE database with reported flux values prior to reddening corrections.

## Appendix B: The impact of extrapolating $T_e$ - $T_e$ relations in the Fe/O and Fe/N distributions

Due to their ionization potential,  $Fe^{2+}$ ,  $O^+$ , and  $N^+$  are considered low ionization degree ions. This implies that determining their ionic abundances requires adopting a characteristic temperature for their coexistence volume. Various studies indicate that one of the most reliable diagnostics for this parameter is  $T_e([N\ II] \lambda 5755/\lambda 6584)$  due to its low dependence on  $n_e$  (Esteban et al. 2009; Arellano-Córdova & Rodríguez 2020; Méndez-Delgado et al. 2023a; Rickards Vaught et al. 2024). However, observationally, the detection of  $[N\ II] \lambda 5755$  is particularly challenging for low metallicity regions, which often exhibit high ionization states (Vilchez & Pagel 1988). Because of this, in most cases, a temperature relation is required to connect other temperature diagnostics with  $T_e([N\ II] \lambda 5755/\lambda 6584)$ . As described in Sec. 2, this work adopted the relations proposed by Garnett (1992) and Méndez-Delgado et al. (2023b) to connect  $T_e([O\ III] \lambda 4363/\lambda 5007)$  and/or  $T_e([S\ III] \lambda 6312/\lambda 9069)$  when  $T_e([N\ II] \lambda 5755/\lambda 6584)$  was not measured directly both in the case  $t^2 = 0$  and  $t^2 > 0$ , respectively.

The use of these temperature relations is a potential source of systematic errors if they have significant deviations from what is present in real nebulae. Although this has been studied in several articles (Skillman et al. 2003; Croxall et al. 2015; Berg et al. 2020; Rogers et al. 2021), both in the case of  $t^2 = 0$  (Garnett 1992) and in the case of  $t^2 > 0$  (Méndez-Delgado et al. 2023b), there is a very limited number of low-metallicity regions with simultaneous determinations of  $T_e([N\ II] \lambda 5755/\lambda 6584)$  and  $T_e([O\ III] \lambda 4363/\lambda 5007)$  or  $T_e([S\ III] \lambda 6312/\lambda 9069)$ . These limitations will be alleviated in upcoming studies (Orte-García M. et al., in prep) using the DESIRE sample, but the calibrations still lack statistical robustness for temperatures above 13,000K.

To quantify the impact that a hypothetical systematic deviation between the assumed temperature relations and those actually present in the nebulae could have on our determinations of Fe/N and Fe/O abundances, we can consider the following relation (Stasinska 2023):

$$\frac{Fe^{2+}}{O^+} = \frac{\left( \frac{I([Fe\ III] \lambda 4658)}{I([O\ II] \lambda \lambda 3727 + 3729)} \right)}{\left( \frac{j([Fe\ III] \lambda 4658)}{j([O\ II] \lambda \lambda 3727 + 3729)} \right)}, \quad (B.1)$$

where  $I(\lambda)$  represents the observed line intensity and  $j(\lambda)$  is the emissivity of that line. In most cases,  $[O\ II] \lambda \lambda 3727 + 3729$  is the basis for estimating the abundances of  $O^+/H^+$ , and  $[Fe\ III] \lambda 4658$  is the basis for estimating the abundance of  $Fe^{2+}/H^+$  in all cases. If  $T_e([N\ II])$  presents a systematic error, it will affect both  $j([O\ II] \lambda \lambda 3727 + 3729)$  and  $j([Fe\ III] \lambda 4658)$ . We can quantify that systematic error using PyNeb (Luridiana et al. 2015) and Eq. (B.1) as follows:

$$\frac{(Fe^{2+}/O^+)_{Biased-T_e}}{(Fe^{2+}/O^+)_{True-T_e}} = \frac{\left( \frac{j([Fe\ III] \lambda 4658)}{j([O\ II] \lambda \lambda 3727 + 3729)} \right)_{True-T_e}}{\left( \frac{j([Fe\ III] \lambda 4658)}{j([O\ II] \lambda \lambda 3727 + 3729)} \right)_{Biased-T_e}}. \quad (B.2)$$

We will consider the following case: In low metallicity regions, only  $T_e([O\ III])$  is available and we must use the relationships from Garnett (1992) and Méndez-Delgado et al. (2023b) to determine  $T_e([N\ II])$  and  $T_0(O^{2+})$ . We also assume that the  $T_e$  relationships induce a systematic error of 20%. This value is notably higher than the uncertainties in the slope and intercept of the  $T_e([O\ III]) - T_e([N\ II])$  relations derived by Méndez-Delgado et al. (2023a) and  $T_e([N\ II]) - T_0(O^{2+})$  derived by Méndez-Delgado et al. (2023b), which are around ~5% in the slopes and ~10% in the intercepts.

In Fig. B.1 it is shown that the potential impact of a systematic error in  $T_e$  of 20% on the ionic abundance of  $Fe^{2+}/O^+$  is ~0.05 dex when adopting the nebular lines  $[O\ II] \lambda \lambda 3727 + 3729$ . In this figure,  $n_e = 100\text{ cm}^{-3}$  was considered, although the conclusions do not depend on the value of this parameter. Despite considering systematic errors of several thousand degrees Kelvin, the impact on  $Fe^{2+}/O^+$  is very small due to the similarity between the excitation energies of the  $^3F_4$  atomic level of  $Fe^{2+}$  (~ 2.7 eV) and the  $^2D$  levels of  $O^+$  (~ 3.3 eV). The same is true for the abundance of  $Fe^{2+}/N^+$  (we used  $[N\ II] \lambda 6584$ , which arises from the  $^1D$  level of  $N^+$  (~ 1.9 eV)) as shown in Fig. B.2.

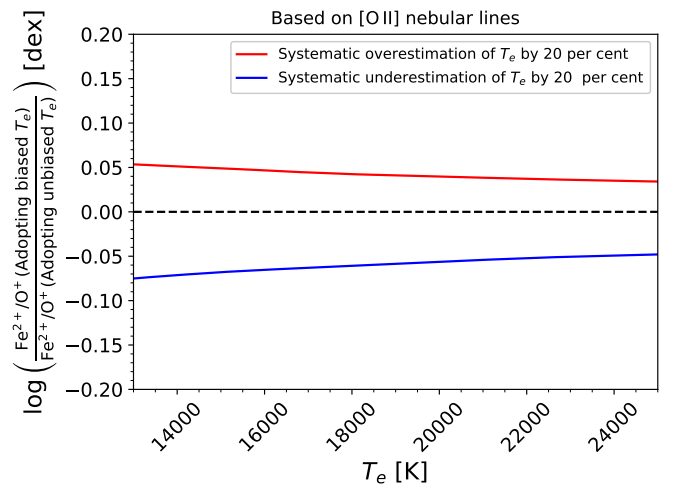


**Fig. B.1.** Upper limits to the systematic errors in the abundance of  $Fe^{2+}/O^+$  considering a hypothetical systematic error in  $T_e$  of 20%. These limits have been calculated using PyNeb (Luridiana et al. 2015) and Eq. (B.2).



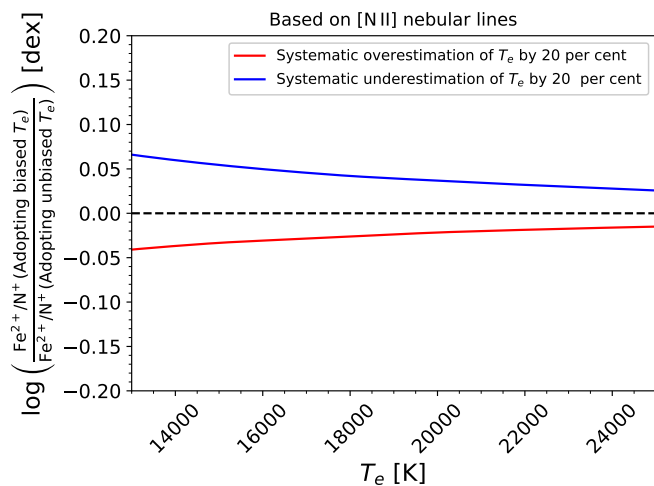


**Fig. B.2.** Same as Fig. B.1 but considering the  $\text{Fe}^{2+}/\text{N}^+$  abundances.

As shown in Fig. B.3, the situation is notably different when the abundance of  $\text{O}^+$  has been determined using the auroral lines of  $[\text{O II}] \lambda\lambda 7319 + 7320 + 7330 + 7331$ . The temperature dependence becomes very significant, potentially introducing systematic errors greater than  $\sim 0.1$  dex. However, only 44 regions ( $<10\%$  of the entire sample) have  $\text{O}^+$  determinations based on these auroral lines of  $[\text{O II}]$ . In Fig. B.4 we demonstrate that these regions do not exhibit anomalies in the observed trends and that our conclusions do not rely particularly on these regions.

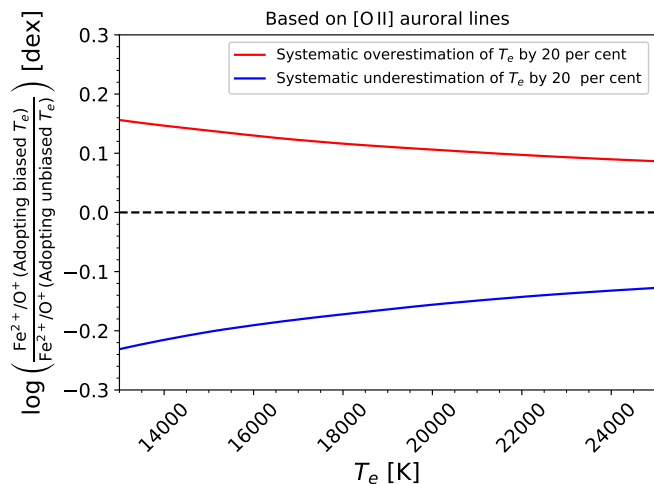


**Fig. B.3.** Same as Fig. B.1 but considering the determination of the  $\text{O}^+/\text{H}^+$  ionic abundances based on the  $[\text{O II}] \lambda\lambda 7319 + 7320 + 7330 + 7331$  auroral lines.

To explore the bias in the total abundances of Fe/O and Fe/N, it is necessary to consider the ICF and its relationship with the ionic abundances of  $\text{O}^+$  and  $\text{O}^{2+}$ , both in the case of  $t^2 = 0$  and  $t^2 > 0$ . In the case of ICF(Fe), we consider the ICF by Rodríguez & Rubin (2005). As shown in Figs. B.5 and B.6, the potential systematic error is smaller than  $\sim 0.04$  dex and acts in the opposite direction to the systematic error in the  $\text{Fe}^{2+}/\text{O}^+$  abundance presented in Fig. B.1, which causes the systematic errors to partially cancel each other when determining  $\text{Fe}/\text{O} = \text{ICF} \times \text{Fe}^{2+}/\text{O}^+$ .

Considering Figures B.1, B.5 and B.6, we can estimate the total impact of a hypothetical bias in  $T_e$  on the Fe/O abundances.

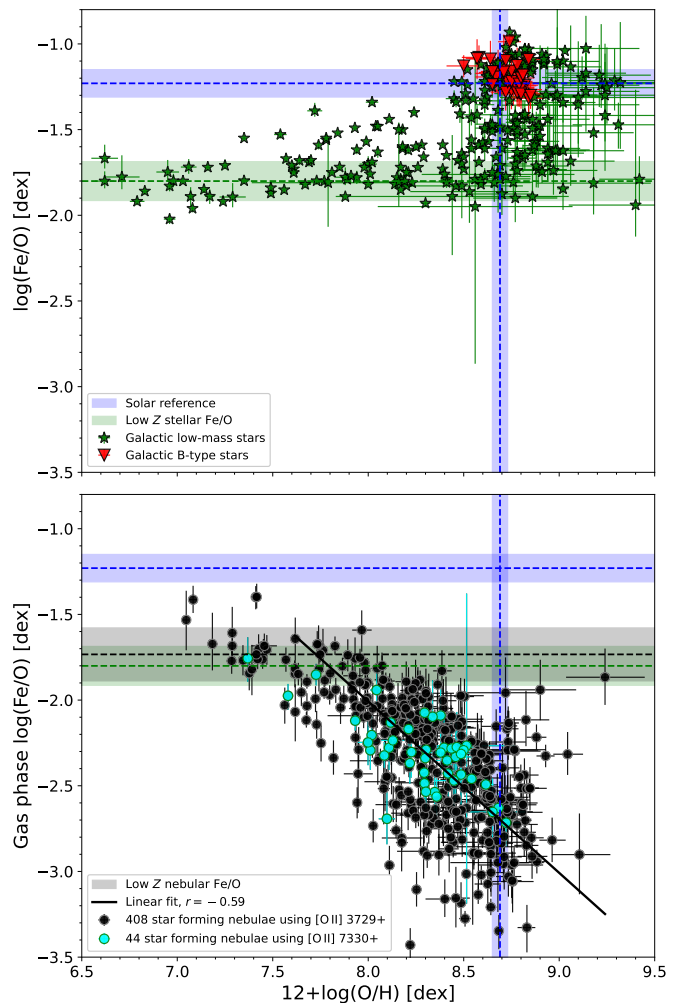


**Fig. B.4.** Same as Fig. 6 but highlighting the subset of objects where the determination of the  $\text{O}^+$  abundance relies on the  $[\text{O II}]$  auroral lines.

This is shown in Figures B.7 and B.8. These figures demonstrate that the potential systematic error induced in the Fe/O abundances due to very large hypothetical errors in  $T_e$  from the extrapolation of the temperature relationships by Garnett (1992) and Méndez-Delgado et al. (2023b) in low-metallicity regions is around  $\sim 0.05$  dex. This rules out the possibility that the apparent plateau observed in the Fe/O distribution at low metallicities (see Fig. 6) is the result of a systematic error in the inferred  $T_e$  ( $[\text{N II}]$ ).

The case of the total Fe/N abundance involves two ICFs: the one from Rodríguez & Rubin (2005) for Fe and the one from Amayo et al. (2021) for N. In the latter case, the equation is a fifth-degree polynomial over  $\omega = \text{O}^{2+}/(\text{O}^+ + \text{O}^{2+})$ . For low metallicity regions,  $\omega$  is expected to be close to 1 (Vilchez & Pagel 1988), minimizing any potential bias in the ionic abundances induced by  $T_e$ -errors. As a good approximation, we can assume that the ICF(N) induce a negligible systematic error due to systematics on  $T_e$ . Such case is presented in figures B.9 and B.10 for the case  $t^2 = 0$  and  $t^2 > 0$ , respectively. The potential systematic bias in the Fe/N distribution is rather similar than in the case of Fe/O, being up to  $\sim 0.05$  dex.

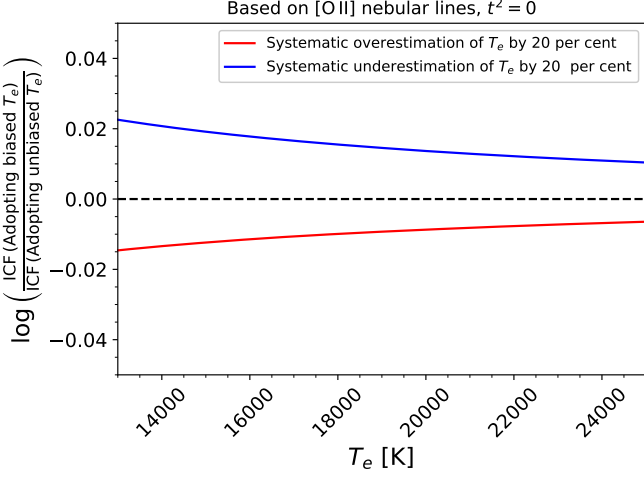


**Fig. B.5.** Upper limits to the systematic errors in ICF(Fe) from Rodríguez & Rubin (2005) considering a hypothetical systematic error in  $T_e$  of 20%. These limits have been calculated using PyNeb (Luridiana et al. 2015) and Eq. (B.2).

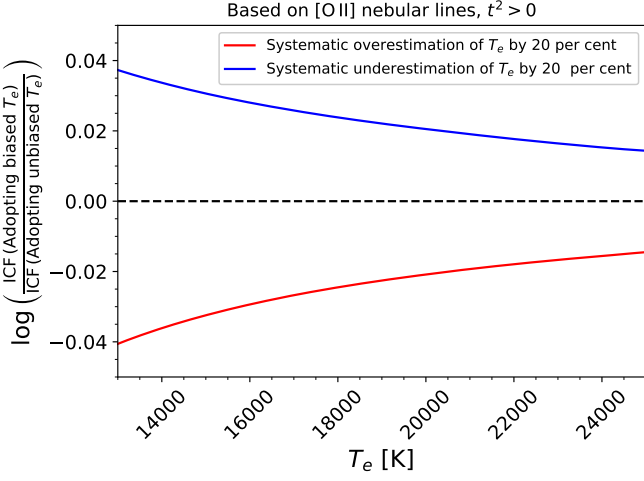


**Fig. B.6.** Same as Fig. B.5 but considering the case  $t^2 > 0$ .

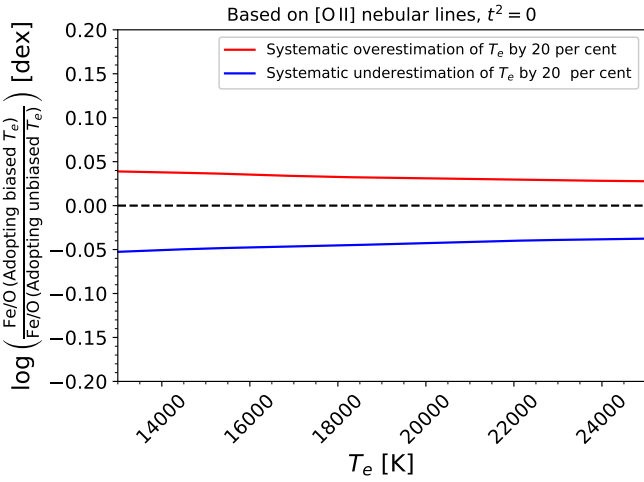


**Fig. B.7.** Same as Fig. B.1 but considering  $\text{Fe}/\text{O} = \text{ICF} \times \text{Fe}^{2+}/\text{O}^+$  and the propagation of their corresponding systematic errors under the case  $t^2 = 0$ .

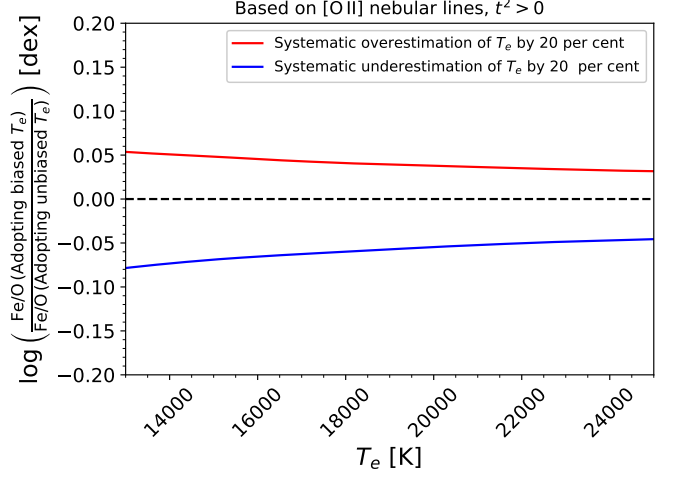


**Fig. B.8.** Same as Fig. B.7 but considering the case  $t^2 > 0$ .

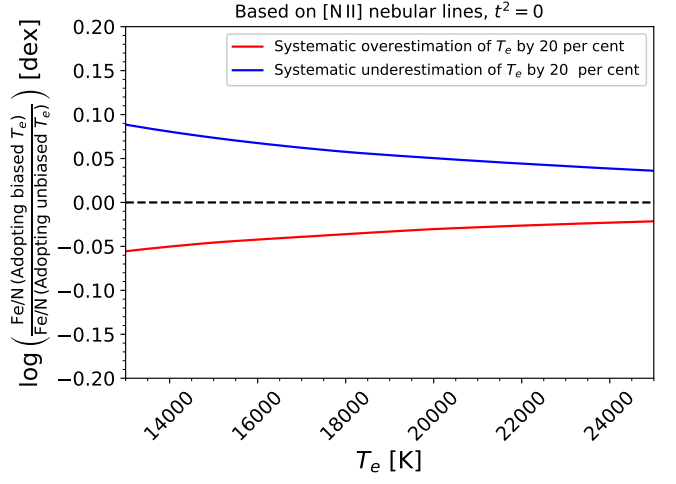


**Fig. B.9.** Same as Fig. B.7 but considering Fe/N under the case  $t^2 = 0$ .

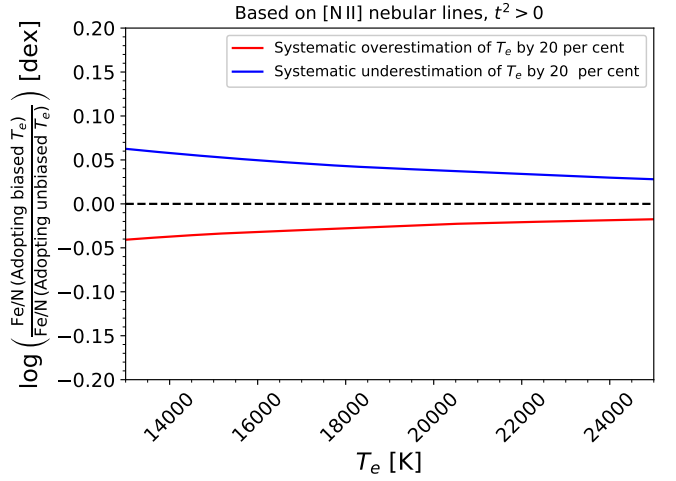


**Fig. B.10.** Same as Fig. B.9 but considering the case  $t^2 > 0$ .

### Appendix C: Fe/O and Fe/N distributions considering $t^2 = 0$

The shape of the Fe/O and Fe/N distributions does not change in the case of  $t^2 = 0$ . In these cases, the observational fits to the star-forming nebulae are as follows:

- For  $12+\log(\text{O}/\text{H}) < 7.6$ :

$$\log(\text{Fe}/\text{O}) = -0.75 \pm 0.19$$

- For  $12+\log(\text{O}/\text{H}) \geq 7.6$ :

$$\log(\text{Fe}/\text{O}) = (-1.02 \pm 0.05) \times [12 + \log(\text{O}/\text{H})] + (5.97 \pm 0.39)$$

- For  $12+\log(\text{N}/\text{H}) < 6.3$ :

$$\log(\text{Fe}/\text{N}) = -0.50 \pm 0.16$$

- For  $12+\log(\text{N}/\text{H}) \geq 6.3$ :

$$\log(\text{Fe}/\text{N}) = (-0.91 \pm 0.03) \times [12 + \log(\text{N}/\text{H})] + (5.20 \pm 0.20)$$

This results in Eq (C.1).

$$\frac{\text{Fe}_{\text{Dust}}}{\text{Fe}_{\text{Total } t^2=0}} \approx 1 - 6 \times 10^{-6} \times \left(\frac{\text{N}}{\text{H}}\right)^{-0.91}. \quad (\text{C.1})$$

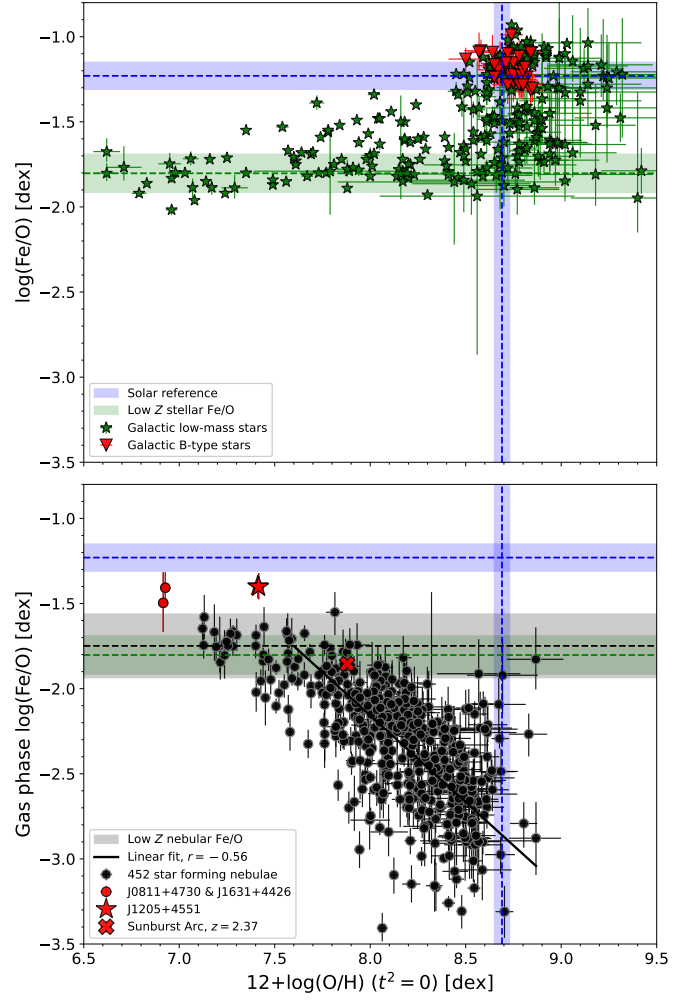


**Fig. C.1.** Same as Fig. 6 but considering an homogeneous nebular temperature  $t^2 = 0$ .



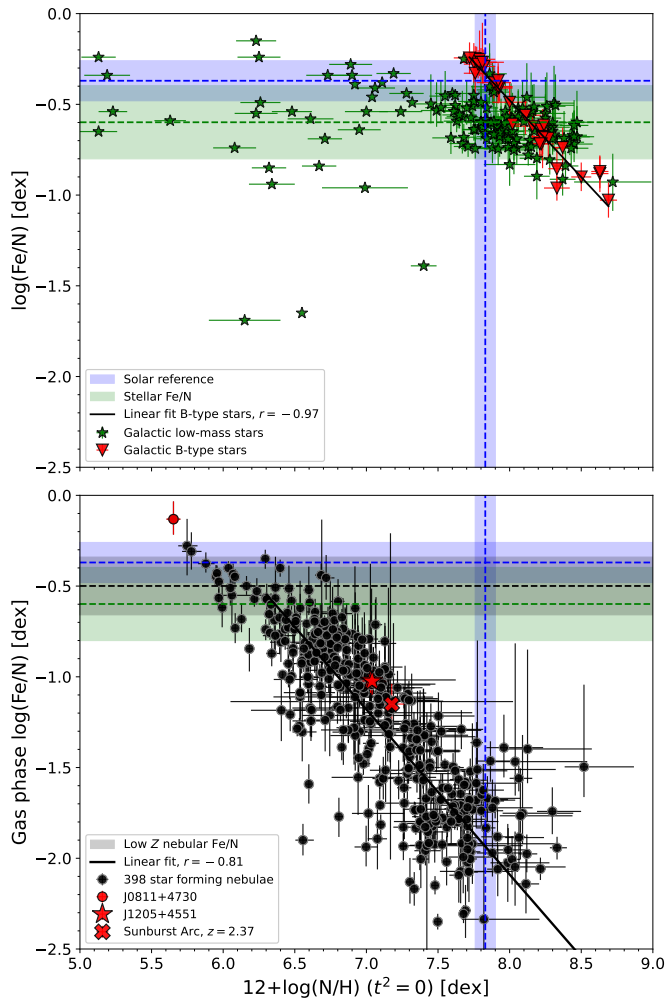


**Fig. C.2.** Same as Fig. 8 but considering an homogeneous nebular temperature  $t^2 = 0$ .

## Appendix D: Tables of values and references

**Table D.1.** Atomic data set used for collisionally excited lines.

Ion	Transition probabilities	Collision strengths
O <sup>+</sup>	<a href="#">Froese Fischer &amp; Tachiev (2004)</a>	<a href="#">Kisielius et al. (2009)</a>
O <sup>2+</sup>	<a href="#">Wiese et al. (1996)</a> , <a href="#">Storey &amp; Zeippen (2000)</a>	<a href="#">Storey et al. (2014)</a>
N <sup>+</sup>	<a href="#">Froese Fischer &amp; Tachiev (2004)</a>	<a href="#">Tayal (2011)</a>
S <sup>+</sup>	<a href="#">Irimia &amp; Froese Fischer (2005)</a>	<a href="#">Tayal &amp; Zatsarinny (2010)</a>
S <sup>2+</sup>	<a href="#">Froese Fischer et al. (2006)</a>	<a href="#">Grieve et al. (2014)</a>
Cl <sup>2+</sup>	<a href="#">Fritzsche et al. (1999)</a>	<a href="#">Butler &amp; Zeippen (1989)</a>
Ar <sup>2+</sup>	<a href="#">Mendoza (1983)</a> , <a href="#">Kaufman &amp; Sugar (1986)</a>	<a href="#">Galavis et al. (1995)</a>
Ar <sup>3+</sup>	<a href="#">Mendoza &amp; Zeippen (1982)</a>	<a href="#">Ramsbottom &amp; Bell (1997)</a>
Fe <sup>+</sup>	<a href="#">Bautista et al. (2015)</a> , <a href="#">Mendoza et al. (2023)</a>	<a href="#">Bautista et al. (2015)</a> , <a href="#">Mendoza et al. (2023)</a>
Fe <sup>2+</sup>	<a href="#">Deb &amp; Hibbert (2009)</a> , <a href="#">Mendoza et al. (2023)</a>	<a href="#">Zhang (1996)</a> , <a href="#">Mendoza et al. (2023)</a>
Fe <sup>3+</sup>	<a href="#">Froese Fischer et al. (2008)</a>	<a href="#">Zhang &amp; Pradhan (1997)</a>
Fe <sup>4+</sup>	<a href="#">Nahar et al. (2000)</a>	<a href="#">Ballance et al. (2007)</a>

**Table D.2.** Reference number, galaxy, region name and references to the sample of nebular objects analyzed in this study.

Reference number	Galaxy	Region	Reference
D1	0275-51910-445	-	Izotov et al. (2006)
D2	0308-51662-081	-	Izotov et al. (2006)
D3	0329-52056-633	-	Izotov et al. (2006)
D4	0330-52370-471	-	Izotov et al. (2006)
D5	0337-51997-097	-	Izotov et al. (2006)
D6	0358-51818-504	-	Izotov et al. (2006)
D7	0364-52000-187	-	Izotov et al. (2006)
D8	0390-51900-445	-	Izotov et al. (2006)
D9	0417-51821-513	-	Izotov et al. (2006)
D10	0445-51873-404	-	Izotov et al. (2006)
D11	0456-51910-076	-	Izotov et al. (2006)
D12	0481-51908-289	-	Izotov et al. (2006)
D13	0485-51909-306	-	Izotov et al. (2006)
D14	0485-51909-550	-	Izotov et al. (2006)
D15	0501-52235-602	-	Izotov et al. (2006)
D16	0516-52017-315	-	Izotov et al. (2006)
D17	0521-52326-073	-	Izotov et al. (2006)
D18	0526-52312-097	-	Izotov et al. (2006)
D19	0549-51981-621	-	Izotov et al. (2006)
D20	0550-51959-092	-	Izotov et al. (2006)
D21	0554-52000-190	-	Izotov et al. (2006)
D22	0556-51991-312	-	Izotov et al. (2006)
D23	0564-52224-216	-	Izotov et al. (2006)
D24	0573-52325-099	-	Izotov et al. (2006)
D25	0575-52319-521	-	Izotov et al. (2006)
D26	0582-52045-440	-	Izotov et al. (2006)
D27	0616-52374-393	-	Izotov et al. (2006)
D28	0723+692A	-	Izotov et al. (1997)
D29	0769-52282-100	-	Izotov et al. (2006)
D30	0775-52295-029	-	Izotov et al. (2006)
D31	0831-52294-526	-	Izotov et al. (2006)
D32	0844-52378-041	-	Izotov et al. (2006)
D33	0844-52378-299	-	Izotov et al. (2006)
D34	0847-52426-040	-	Izotov et al. (2006)
D35	0875-52354-142	-	Izotov et al. (2006)
D36	0899-52620-594	-	Izotov et al. (2006)
D37	0906-52368-534	-	Izotov et al. (2006)
D38	0917+527	-	Izotov et al. (1997)
D39	0920-52411-575	-	Izotov et al. (2006)
D40	0926+606	-	Izotov et al. (1997)
D41	0930+554N	-	Izotov et al. (1997)
D42	0934-52672-369	-	Izotov et al. (2006)
D43	0943-52376-631	-	Izotov et al. (2006)
D44	0946-52407-618	-	Izotov et al. (2006)
D45	0951-52398-600	-	Izotov et al. (2006)
D46	0967-52636-339	-	Izotov et al. (2006)
D47	0999-52636-517	-	Izotov et al. (2006)
D48	1010-52649-328	-	Izotov et al. (2006)
D49	1039-52707-119	-	Izotov et al. (2006)
D50	1048-52736-424	-	Izotov et al. (2006)
D51	1050-52721-402	-	Izotov et al. (2006)
D52	1158-52668-062	-	Izotov et al. (2006)
D53	1222+614	-	Izotov et al. (1997)
D54	1223+487	-	Izotov et al. (1997)
D55	1233-52734-136	-	Izotov et al. (2006)
D56	1256+351	-	Izotov et al. (1997)
D57	1288-52731-390	-	Izotov et al. (2006)
D58	1305-52757-269	-	Izotov et al. (2006)
D59	1319+579A	-	Izotov et al. (1997)
D60	1319+579C	-	Izotov et al. (1997)



**Table D.2.** Reference number, galaxy, region name and references to the sample of nebular objects analyzed in this study.

Reference number	Galaxy	Region	Reference
D61	1321-52764-624	-	Izotov et al. (2006)
D62	1322-52791-470	-	Izotov et al. (2006)
D63	1323-52797-002	-	Izotov et al. (2006)
D64	1323-52797-008	-	Izotov et al. (2006)
D65	1325-52762-353	-	Izotov et al. (2006)
D66	1351-52790-474	-	Izotov et al. (2006)
D67	1358+576	-	Izotov et al. (1997)
D68	1371-52821-059	-	Izotov et al. (2006)
D69	1533+574A	-	Izotov et al. (1997)
D70	1533+574B	-	Izotov et al. (1997)
D71	AM0644-741	ID39	Gómez-González et al. (2024)
D72	CGCG007-025-1	-	Izotov & Thuan (2004)
D73	G1815-6701	-	Guseva et al. (2009)
D74	G2052-6912	1	Guseva et al. (2009)
D75	HS0122+0743	-	Izotov & Thuan (2004)
D76	HS0128+2832	-	Izotov & Thuan (2004)
D77	HS0735+3512	-	Izotov & Thuan (2004)
D78	HS0822+3542	-	Thuan & Izotov (2005)
D79	HS0837+4717-1	-	Thuan & Izotov (2005)
D80	HS0837+4717	-	Thuan & Izotov (2005)
D81	HS0924+3821	-	Izotov & Thuan (2004)
D82	HS1028+3843	-	Izotov & Thuan (2004)
D83	HS1851+6933	-	Izotov et al. (2021)
D84	Haro15	KnotB	Hägele et al. (2012)
D85	He2-10	E	Guseva et al. (2011)
D86	He2-10	-	Esteban et al. (2014)
D87	IIZw40	-	Thuan & Izotov (2005)
D88	IZw18NW	-	Thuan & Izotov (2005)
D89	IZw18SE	-	Thuan & Izotov (2005)
D90	IZw70	-	Fernández et al. (2018)
D91	J0002+1715	-	Kojima et al. (2021)
D92	J0021+005	-	Hägele et al. (2006)
D93	J0032+150	-	Hägele et al. (2006)
D94	J0125+0759	-	Watanabe et al. (2024)
D95	J0126-0038	J0126-0038-1	Guseva et al. (2009)
D96	J0240-0828	-	Thuan & Izotov (2005)
D97	J0338+0013	-	Guseva et al. (2009)
D98	J0519+0007-1	-	Thuan & Izotov (2005)
D99	J0944-0038	-	Thuan & Izotov (2005)
D100	J104457	-	Berg et al. (2021)
D101	J1253-0312	-	Thuan & Izotov (2005)
D102	J1404+5423	-	Thuan & Izotov (2005)
D103	J141851	-	Berg et al. (2021)
D104	J1429-0110	-	Kojima et al. (2021)
D105	J1608+4337	-	Isobe et al. (2022)
D106	J1624-002	-	Hägele et al. (2006)
D107	J1631+4426	-	Kojima et al. (2021)
D108	J1642+2233	-	Kojima et al. (2021)
D109	J1657+321	KnotA	Hägele et al. (2011)
D110	J2115-1734	-	Kojima et al. (2021)
D111	J2253+1116	-	Kojima et al. (2021)
D112	J2302+0049	1	Guseva et al. (2009)
D113	J2310-0211	-	Kojima et al. (2021)
D114	J2327-0200	-	Kojima et al. (2021)
D115	LMC	30Doradus	Peimbert (2003)
D116	LMC	IC2111	Domínguez-Guzmán et al. (2022)
D117	LMC	N11B	Domínguez-Guzmán et al. (2022)
D118	LMC	N44C	Domínguez-Guzmán et al. (2022)
D119	LMC	NGC1714	Domínguez-Guzmán et al. (2022)
D120	M101	H1013	Bresolin (2007)
D121	M101	H1013	Croxall et al. (2016)

**Table D.2.** Reference number, galaxy, region name and references to the sample of nebular objects analyzed in this study.

Reference number	Galaxy	Region	Reference
D122	M101	H1013	<a href="#">Esteban et al. (2009)</a>
D123	M101	H1018	<a href="#">Croxall et al. (2016)</a>
D124	M101	H103	<a href="#">Croxall et al. (2016)</a>
D125	M101	H1040	<a href="#">Croxall et al. (2016)</a>
D126	M101	H1045	<a href="#">Croxall et al. (2016)</a>
D127	M101	H104	<a href="#">Croxall et al. (2016)</a>
D128	M101	H1052	<a href="#">Croxall et al. (2016)</a>
D129	M101	H1122	<a href="#">Croxall et al. (2016)</a>
D130	M101	H1125	<a href="#">Croxall et al. (2016)</a>
D131	M101	H1146	<a href="#">Croxall et al. (2016)</a>
D132	M101	H1148	<a href="#">Croxall et al. (2016)</a>
D133	M101	H1151	<a href="#">Croxall et al. (2016)</a>
D134	M101	H1216	<a href="#">Croxall et al. (2016)</a>
D135	M101	H1216	<a href="#">Esteban et al. (2020)</a>
D136	M101	H143	<a href="#">Croxall et al. (2016)</a>
D137	M101	H167	<a href="#">Croxall et al. (2016)</a>
D138	M101	H185	<a href="#">Croxall et al. (2016)</a>
D139	M101	H203	<a href="#">Croxall et al. (2016)</a>
D140	M101	H206	<a href="#">Croxall et al. (2016)</a>
D141	M101	H219	<a href="#">Croxall et al. (2016)</a>
D142	M101	H237	<a href="#">Croxall et al. (2016)</a>
D143	M101	H246	<a href="#">Croxall et al. (2016)</a>
D144	M101	H260	<a href="#">Croxall et al. (2016)</a>
D145	M101	H27	<a href="#">Croxall et al. (2016)</a>
D146	M101	H321	<a href="#">Croxall et al. (2016)</a>
D147	M101	H336	<a href="#">Croxall et al. (2016)</a>
D148	M101	H399	<a href="#">Croxall et al. (2016)</a>
D149	M101	H46	<a href="#">Croxall et al. (2016)</a>
D150	M101	H493	<a href="#">Croxall et al. (2016)</a>
D151	M101	H504	<a href="#">Croxall et al. (2016)</a>
D152	M101	H618	<a href="#">Croxall et al. (2016)</a>
D153	M101	H641	<a href="#">Croxall et al. (2016)</a>
D154	M101	H681	<a href="#">Croxall et al. (2016)</a>
D155	M101	H699	<a href="#">Croxall et al. (2016)</a>
D156	M101	H71	<a href="#">Croxall et al. (2016)</a>
D157	M101	H798	<a href="#">Croxall et al. (2016)</a>
D158	M101	H875	<a href="#">Croxall et al. (2016)</a>
D159	M101	H8	<a href="#">Croxall et al. (2016)</a>
D160	M101	H949	<a href="#">Croxall et al. (2016)</a>
D161	M101	H953	<a href="#">Croxall et al. (2016)</a>
D162	M101	H959	<a href="#">Croxall et al. (2016)</a>
D163	M101	H969	<a href="#">Croxall et al. (2016)</a>
D164	M101	H972	<a href="#">Croxall et al. (2016)</a>
D165	M101	NGC5447-1	<a href="#">Croxall et al. (2016)</a>
D166	M101	NGC5447-2	<a href="#">Croxall et al. (2016)</a>
D167	M101	NGC5447-3	<a href="#">Croxall et al. (2016)</a>
D168	M101	NGC5447	<a href="#">Esteban et al. (2009)</a>
D169	M101	NGC5449-1	<a href="#">Croxall et al. (2016)</a>
D170	M101	NGC5449-2	<a href="#">Croxall et al. (2016)</a>
D171	M101	NGC5451	<a href="#">Croxall et al. (2016)</a>
D172	M101	NGC5455	<a href="#">Croxall et al. (2016)</a>
D173	M101	NGC5455	<a href="#">Esteban et al. (2020)</a>
D174	M101	NGC5461-2	<a href="#">Croxall et al. (2016)</a>
D175	M101	NGC5461-3	<a href="#">Croxall et al. (2016)</a>
D176	M101	NGC5461	<a href="#">Croxall et al. (2016)</a>
D177	M101	NGC5461	<a href="#">Esteban et al. (2009)</a>
D178	M101	NGC5462-1	<a href="#">Croxall et al. (2016)</a>
D179	M101	NGC5462-2	<a href="#">Croxall et al. (2016)</a>
D180	M101	NGC5471A	<a href="#">Skillman (1985)</a>
D181	M101	NGC5471B	<a href="#">Skillman (1985)</a>
D182	M101	NGC5471	<a href="#">Croxall et al. (2016)</a>

**Table D.2.** Reference number, galaxy, region name and references to the sample of nebular objects analyzed in this study.

Reference number	Galaxy	Region	Reference
D183	M101	NGC5471	<a href="#">Esteban et al. (2020)</a>
D184	M31	BA373	<a href="#">Zurita &amp; Bresolin (2012)</a>
D185	M31	BA379-2	<a href="#">Zurita &amp; Bresolin (2012)</a>
D186	M31	BA423	<a href="#">Zurita &amp; Bresolin (2012)</a>
D187	M31	K160	<a href="#">Esteban et al. (2020)</a>
D188	M31	K932	<a href="#">Esteban et al. (2009)</a>
D189	M33	B0013c	<a href="#">Rogers et al. (2022)</a>
D190	M33	B0017d	<a href="#">Rogers et al. (2022)</a>
D191	M33	B0027b	<a href="#">Rogers et al. (2022)</a>
D192	M33	B0029	<a href="#">Toribio San Cipriano et al. (2016)</a>
D193	M33	B0043b	<a href="#">Toribio San Cipriano et al. (2016)</a>
D194	M33	B0290	<a href="#">Toribio San Cipriano et al. (2016)</a>
D195	M33	B0623	<a href="#">Rogers et al. (2022)</a>
D196	M33	B0691	<a href="#">Rogers et al. (2022)</a>
D197	M33	LGCHII3	<a href="#">Toribio San Cipriano et al. (2016)</a>
D198	M33	NGC588	<a href="#">Toribio San Cipriano et al. (2016)</a>
D199	M33	NGC595	<a href="#">Esteban et al. (2009)</a>
D200	M33	NGC604A	<a href="#">Rogers et al. (2022)</a>
D201	M33	NGC604	<a href="#">Esteban et al. (2009)</a>
D202	M33	-224-437	<a href="#">Rogers et al. (2022)</a>
D203	M33	-267-462	<a href="#">Rogers et al. (2022)</a>
D204	M33	-36+312	<a href="#">Rogers et al. (2022)</a>
D205	M33	-442+797	<a href="#">Rogers et al. (2022)</a>
D206	M33	+209+473	<a href="#">Rogers et al. (2022)</a>
D207	M33	+553+448	<a href="#">Rogers et al. (2022)</a>
D208	M33	+62+354	<a href="#">Rogers et al. (2022)</a>
D209	M51	CCM10	<a href="#">Croxall et al. (2015)</a>
D210	M51	CCM53	<a href="#">Croxall et al. (2015)</a>
D211	M51	CCM54	<a href="#">Croxall et al. (2015)</a>
D212	M51	CCM55	<a href="#">Croxall et al. (2015)</a>
D213	M51	CCM57	<a href="#">Croxall et al. (2015)</a>
D214	M51	CCM72	<a href="#">Croxall et al. (2015)</a>
D215	M51	P203	<a href="#">Croxall et al. (2015)</a>
D216	M51	-82d0-102d7	<a href="#">Croxall et al. (2015)</a>
D217	M51	+30d2+2d2	<a href="#">Croxall et al. (2015)</a>
D218	M51	+30d8+139d0	<a href="#">Croxall et al. (2015)</a>
D219	M51	+56d8+126d5	<a href="#">Croxall et al. (2015)</a>
D220	MilkyWay	M17	<a href="#">García-Rojas et al. (2007)</a>
D221	MilkyWay	M20	<a href="#">García-Rojas et al. (2006)</a>
D222	MilkyWay	M42-1	<a href="#">Méndez-Delgado et al. (2021a)</a>
D223	MilkyWay	M42-1	<a href="#">Méndez-Delgado et al. (2021b)</a>
D224	MilkyWay	M42-2	<a href="#">Méndez-Delgado et al. (2021a)</a>
D225	MilkyWay	M42-2	<a href="#">Méndez-Delgado et al. (2021b)</a>
D226	MilkyWay	M42-2	<a href="#">Méndez-Delgado et al. (2022b)</a>
D227	MilkyWay	M42-3	<a href="#">Méndez-Delgado et al. (2021a)</a>
D228	MilkyWay	M42-3	<a href="#">Méndez-Delgado et al. (2022b)</a>
D229	MilkyWay	M42-4	<a href="#">Méndez-Delgado et al. (2021a)</a>
D230	MilkyWay	M42-NIL	<a href="#">Méndez-Delgado et al. (2021b)</a>
D231	MilkyWay	M42-P1	<a href="#">Delgado-Inglada et al. (2016)</a>
D232	MilkyWay	M42	<a href="#">Esteban et al. (2004)</a>
D233	MilkyWay	M42	<a href="#">Mesa-Delgado et al. (2009)</a>
D234	MilkyWay	M8	<a href="#">García-Rojas et al. (2007)</a>
D235	MilkyWay	NGC2579	<a href="#">Esteban et al. (2013)</a>
D236	MilkyWay	NGC3576	<a href="#">García-Rojas et al. (2004)</a>
D237	MilkyWay	NGC3603	<a href="#">García-Rojas et al. (2006)</a>
D238	MilkyWay	Sh2-100	<a href="#">Esteban et al. (2017)</a>
D239	MilkyWay	Sh2-127	<a href="#">Esteban et al. (2017)</a>
D240	MilkyWay	Sh2-128	<a href="#">Esteban et al. (2017)</a>
D241	MilkyWay	Sh2-152	<a href="#">Esteban &amp; García-Rojas (2018)</a>
D242	MilkyWay	Sh2-156	<a href="#">Fernández-Martín et al. (2017)</a>
D243	MilkyWay	Sh2-212	<a href="#">Esteban et al. (2017)</a>



**Table D.2.** Reference number, galaxy, region name and references to the sample of nebular objects analyzed in this study.

Reference number	Galaxy	Region	Reference
D244	MilkyWay	Sh2-235	Esteban & García-Rojas (2018)
D245	MilkyWay	Sh2-254	Arellano-Córdova et al. (2021)
D246	MilkyWay	Sh2-266	Esteban & García-Rojas (2018)
D247	MilkyWay	Sh2-288	Esteban et al. (2017)
D248	MilkyWay	Sh2-297	Esteban & García-Rojas (2018)
D249	MilkyWay	Sh2-311	García-Rojas et al. (2005)
D250	Mrk1063	-	Izotov & Thuan (2004)
D251	Mrk1089	-	Izotov & Thuan (1998b)
D252	Mrk1236	-	Izotov & Thuan (2004)
D253	Mrk1271	-	Esteban et al. (2014)
D254	Mrk1271	-	Guseva et al. (2011)
D255	Mrk1271	-	Izotov & Thuan (1998b)
D256	Mrk1315	-	Izotov & Thuan (2004)
D257	Mrk1329	-	Izotov & Thuan (2004)
D258	Mrk162	-	Izotov & Thuan (1998b)
D259	Mrk178-2	-	Thuan & Izotov (2005)
D260	Mrk178-3	-	Thuan & Izotov (2005)
D261	Mrk35-1	-	Thuan & Izotov (2005)
D262	Mrk35	-	Izotov & Thuan (2004)
D263	Mrk36	A1	Fernández et al. (2018)
D264	Mrk36	A2	Fernández et al. (2018)
D265	Mrk36	-	Izotov & Thuan (1998b)
D266	Mrk450-1	-	Izotov & Thuan (2004)
D267	Mrk475	-	Fernández et al. (2018)
D268	Mrk59-1	-	Thuan & Izotov (2005)
D269	Mrk59-2	-	Thuan & Izotov (2005)
D270	Mrk5	-	Izotov & Thuan (1998b)
D271	Mrk600	-	Izotov & Thuan (1998b)
D272	Mrk627	-	Fernández et al. (2018)
D273	Mrk67	-	Fernández et al. (2018)
D274	Mrk689	-	Fernández et al. (2018)
D275	Mrk71A	-	Thuan & Izotov (2005)
D276	Mrk71B	-	Thuan & Izotov (2005)
D277	Mrk71CC	-	Thuan & Izotov (2005)
D278	Mrk724	-	Izotov & Thuan (2004)
D279	Mrk930	-	Izotov & Thuan (1998b)
D280	Mrk94	-	Thuan & Izotov (2005)
D281	NGC1510	-	López-Sánchez et al. (2015)
D282	NGC1741	NGC1741-C	Esteban et al. (2009)
D283	NGC2366	Mrk71	Esteban et al. (2009)
D284	NGC2403	HK423	Berg et al. (2013)
D285	NGC2403	VS24	Esteban et al. (2009)
D286	NGC2403	VS38	Esteban et al. (2009)
D287	NGC2403	VS44	Berg et al. (2013)
D288	NGC2403	VS44	Esteban et al. (2009)
D289	NGC2403	VS44	Rogers et al. (2021)
D290	NGC2403	VS9	Berg et al. (2013)
D291	NGC2403	-196+58	Rogers et al. (2021)
D292	NGC2403	-99-59	Rogers et al. (2021)
D293	NGC2403	+125-142	Rogers et al. (2021)
D294	NGC300	R14	Toribio San Cipriano et al. (2016)
D295	NGC300	R23	Toribio San Cipriano et al. (2016)
D296	NGC3125	-	Esteban et al. (2014)
D297	NGC3125	-	Guseva et al. (2011)
D298	NGC3184	-14d9-95d5	Berg et al. (2020)
D299	NGC3184	-172d5-30d2	Berg et al. (2020)
D300	NGC3184	-59d5-37d7	Berg et al. (2020)
D301	NGC3184	-67d3+87d1	Berg et al. (2020)
D302	NGC3184	-82d5+57d7	Berg et al. (2020)
D303	NGC3184	+14d9-139d6	Berg et al. (2020)
D304	NGC3184	+16d4+119d8	Berg et al. (2020)

**Table D.2.** Reference number, galaxy, region name and references to the sample of nebular objects analyzed in this study.

Reference number	Galaxy	Region	Reference
D305	NGC3184	+18d8-115d7	Berg et al. (2020)
D306	NGC3184	+41d9+148d8	Berg et al. (2020)
D307	NGC3184	+48d9+97d3	Berg et al. (2020)
D308	NGC3184	+51d2+60d4	Berg et al. (2020)
D309	NGC3184	+75d7+89d1	Berg et al. (2020)
D310	NGC3184	+80d0-148d2	Berg et al. (2020)
D311	NGC3184	+8d2-132d1	Berg et al. (2020)
D312	NGC4861	-	Esteban et al. (2009)
D313	NGC5253	NGC5253-C2	Guseva et al. (2011)
D314	NGC5253	P1	Guseva et al. (2011)
D315	NGC5253	UV-1	López-Sánchez et al. (2007)
D316	NGC5253	UV-2	López-Sánchez et al. (2007)
D317	NGC5398	Tol89-1	Guseva et al. (2011)
D318	NGC5398	Tol89-2	Guseva et al. (2011)
D319	NGC5408	1	Guseva et al. (2011)
D320	NGC5408	-	Esteban et al. (2014)
D321	NGC628	-130d9+71d8	Berg et al. (2015)
D322	NGC628	-184d7+83d4	Berg et al. (2015)
D323	NGC628	-35d7+119d6	Berg et al. (2015)
D324	NGC628	-42d8-158d2	Berg et al. (2015)
D325	NGC628	-59d6-111d6	Berg et al. (2015)
D326	NGC628	-73d1+27d3	Berg et al. (2015)
D327	NGC628	-90d1+190d2	Berg et al. (2015)
D328	NGC628	-90+186	Berg et al. (2013)
D329	NGC628	+131d9+18d5	Berg et al. (2015)
D330	NGC628	+163d5+64d4	Berg et al. (2015)
D331	NGC628	+176d7-50d0	Berg et al. (2015)
D332	NGC628	+232d7+6d6	Berg et al. (2015)
D333	NGC628	+49d8+48d7	Berg et al. (2015)
D334	NGC6822	HubbleV	Esteban et al. (2014)
D335	NGC6822	HubbleV	Guseva et al. (2011)
D336	NGC6822	HubbleV	Peimbert et al. (2005)
D337	NGC7667	1-m	Guseva et al. (2011)
D338	NGC7667	a	Valerdi et al. (2021)
D339	NGC7667	b	Valerdi et al. (2021)
D340	NGC7667	c	Valerdi et al. (2021)
D341	POX36	-	Izotov & Thuan (2004)
D342	POX4	-	Esteban et al. (2014)
D343	POX4	-	Guseva et al. (2011)
D344	SBS-0335-052E	-	Watanabe et al. (2024)
D345	SBS0335-052E	-	Thuan & Izotov (2005)
D346	SBS0335-052	06NE	Izotov et al. (1999)
D347	SBS0335-052	06SW	Izotov et al. (1999)
D348	SBS0335-052	12NE	Izotov et al. (1999)
D349	SBS0335-052	18NE	Izotov et al. (1999)
D350	SBS0335-052	18SW	Izotov et al. (1999)
D351	SBS0335-052	Center	Izotov et al. (1999)
D352	SBS0335-052E	1+2_h	Izotov et al. (2009)
D353	SBS0335-052E	1+2_l	Izotov et al. (2009)
D354	SBS0335-052E	1+2a	Izotov et al. (2009)
D355	SBS0335-052E	7_h	Izotov et al. (2009)
D356	SBS0911+472	-	Thuan & Izotov (2005)
D357	SBS0926+606A	-	Thuan & Izotov (2005)
D358	SBS0940+544	-	Thuan & Izotov (2005)
D359	SBS1030+583	-	Thuan & Izotov (2005)
D360	SBS1159+545	-	Izotov & Thuan (1998b)
D361	SBS1415+437	-	Izotov & Thuan (1998b)
D362	SBS1420+540	-	Guseva et al. (2024)
D363	J0519+0007	-	Guseva et al. (2009)
D364	J0811+4730	-	Izotov et al. (2018)
D365	J0813+3132	-	Fernández et al. (2018)

**Table D.2.** Reference number, galaxy, region name and references to the sample of nebular objects analyzed in this study.

Reference number	Galaxy	Region	Reference
D366	J0823+0313	-	Fernández et al. (2018)
D367	J0905+0335	-	Izotov et al. (2012)
D368	J1011+1308	-	Fernández et al. (2022)
D369	J1016+3754	-	Izotov et al. (2012)
D370	J1032+4919	-	Izotov et al. (2017)
D371	J1044+0353	-	Izotov et al. (2012)
D372	J1050+1538	-	Izotov et al. (2012)
D373	J1053+5016	-	Izotov et al. (2012)
D374	J1205+4551	-	Izotov et al. (2017)
D375	J1205+4551	-	Izotov et al. (2021)
D376	J1219+1560	-	Fernández et al. (2022)
D377	J1221+2822	-	Fernández et al. (2018)
D378	J1222+3602	-	Izotov et al. (2021)
D379	J1230+1202	-	Izotov et al. (2012)
D380	J1253-0312	-	Esteban et al. (2014)
D381	J1423+2257	-	Izotov et al. (2012)
D382	J1426+3822	-	Izotov et al. (2012)
D383	J1455+3808	-	Hägele et al. (2008)
D384	J1509+4543	-	Hägele et al. (2008)
D385	J1528+3956	-	Hägele et al. (2008)
D386	J1545+0858	-	Izotov et al. (2012)
D387	J1608+3528	-	Izotov et al. (2017)
D388	J1657+3211	-	Hägele et al. (2008)
D389	J2324-0006	-	Guseva et al. (2009)
D390	SHOC133	-	Izotov et al. (2021)
D391	SHOC137	-	Fernández et al. (2018)
D392	SHOC148	-	Fernández et al. (2022)
D393	SHOC220	-	Fernández et al. (2018)
D394	SHOC22	-	Fernández et al. (2018)
D395	SHOC254b	-	Izotov et al. (2012)
D396	SHOC391	-	Guseva et al. (2011)
D397	SHOC486	-	Izotov et al. (2012)
D398	SHOC513	-	Hägele et al. (2008)
D399	SHOC575	-	Hägele et al. (2008)
D400	SHOC579	-	Fernández et al. (2018)
D401	SMC	N66A	Domínguez-Guzmán et al. (2022)
D402	SMC	N81	Domínguez-Guzmán et al. (2022)
D403	SMC	N88A	Domínguez-Guzmán et al. (2022)
D404	SMC	N90	Domínguez-Guzmán et al. (2022)
D405	SMC	NGC346	Valerdi et al. (2019)
D406	SMC	NGC456-1	Peña-Guerrero et al. (2012)
D407	SMC	NGC456-2	Peña-Guerrero et al. (2012)
D408	SMC	NGC456-a-1	Guseva et al. (2011)
D409	SMC	NGC456-a-3-1	Guseva et al. (2011)
D410	SMC	NGC456-a-3-m	Guseva et al. (2011)
D411	SMC	NGC456-a1	Guseva et al. (2011)
D412	SMC	NGC456-a2	Guseva et al. (2011)
D413	TOL1457-262	-	Esteban et al. (2014)
D414	TOL1924-416	-	Esteban et al. (2014)
D415	Tol0357-3915	C	Peimbert et al. (2012)
D416	Tol0357-3915	E	Peimbert et al. (2012)
D417	Tol0357-3915	l	Guseva et al. (2011)
D418	Tol0357-3915	m	Guseva et al. (2011)
D419	Tol0513-393	-	Valerdi et al. (2021)
D420	Tol0513-393	l	Guseva et al. (2011)
D421	Tol0513-393	m	Guseva et al. (2011)
D422	Tol0618-402	-	Guseva et al. (2011)
D423	Tol1214-277	l	Guseva et al. (2011)
D424	Tol1214-277	m	Guseva et al. (2011)
D425	Tol1457-262	-	Guseva et al. (2011)
D426	Tol1924-416	l	Guseva et al. (2011)

**Table D.2.** Reference number, galaxy, region name and references to the sample of nebular objects analyzed in this study.

Reference number	Galaxy	Region	Reference
D427	Tol1924-416	2	<a href="#">Guseva et al. (2011)</a>
D428	Tol2138-405	1	<a href="#">Guseva et al. (2011)</a>
D429	Tol2138-405	3	<a href="#">Guseva et al. (2011)</a>
D430	Tol2138-405	Tol2138-405-1	<a href="#">Guseva et al. (2011)</a>
D431	Tol2146-391	1-l	<a href="#">Guseva et al. (2011)</a>
D432	Tol2146-391	1-m	<a href="#">Guseva et al. (2011)</a>
D433	Tol2146-391	2-l	<a href="#">Guseva et al. (2011)</a>
D434	Tol2146-391	2-m	<a href="#">Guseva et al. (2011)</a>
D435	Tol2146-391	C	<a href="#">Peimbert et al. (2012)</a>
D436	Tol2146-391	E	<a href="#">Peimbert et al. (2012)</a>
D437	Tol2240-384	m	<a href="#">Guseva et al. (2011)</a>
D438	Tol65	1	<a href="#">Guseva et al. (2011)</a>
D439	Tol65	2	<a href="#">Guseva et al. (2011)</a>
D440	UM133	-	<a href="#">Izotov &amp; Thuan (2004)</a>
D441	UM238	-	<a href="#">Izotov &amp; Thuan (2004)</a>
D442	UM254	-	<a href="#">Guseva et al. (2011)</a>
D443	UM286	-	<a href="#">Egorova et al. (2021)</a>
D444	UM396	-	<a href="#">Izotov &amp; Thuan (2004)</a>
D445	UM420	1	<a href="#">Guseva et al. (2011)</a>
D446	UM420	2-m	<a href="#">Guseva et al. (2011)</a>
D447	UM420	B	<a href="#">Valerdi et al. (2021)</a>
D448	UM420	C	<a href="#">Valerdi et al. (2021)</a>
D449	UM439	-	<a href="#">Izotov &amp; Thuan (2004)</a>
D450	UM462	SW	<a href="#">Izotov &amp; Thuan (1998b)</a>
D451	W1702+18	-	<a href="#">Izotov et al. (2021)</a>
D452	SunburstArc	-	<a href="#">Welch et al. (2024)</a>



**Table D.3.** Electron densities derived from the nebular sample.

Reference number	$n_e(\text{[S II]})$ [cm <sup>-3</sup> ]	$n_e(\text{[O II]})$ [cm <sup>-3</sup> ]	$n_e(\text{[Fe III]})$ [cm <sup>-3</sup> ]	$n_e(\text{[Cl III]})$ [cm <sup>-3</sup> ]	$n_e(\text{[Ar IV]})$ [cm <sup>-3</sup> ]	Adopted $n_e$ [cm <sup>-3</sup> ]
D1	-	-	-	-	-	100 ± 100
D2	-	-	-	-	-	100 ± 100
D3	-	-	-	-	-	100 ± 100
D4	-	-	-	-	-	100 ± 100
D5	-	-	-	-	-	100 ± 100
D6	-	-	-	-	-	100 ± 100
D7	-	-	-	-	-	100 ± 100
D8	-	-	-	-	-	100 ± 100
D9	-	-	-	-	-	100 ± 100
D10	-	-	-	-	-	100 ± 100
D11	-	-	-	-	-	100 ± 100
D12	-	-	-	-	-	100 ± 100
D13	-	-	-	-	-	100 ± 100
D14	-	-	-	-	-	100 ± 100
D15	-	-	-	-	-	100 ± 100
D16	-	-	-	-	-	100 ± 100
D17	-	-	-	-	-	100 ± 100
D18	-	-	-	-	-	100 ± 100
D19	-	-	-	-	-	100 ± 100
D20	-	-	-	-	-	100 ± 100
D21	-	-	-	-	-	100 ± 100
D22	-	-	-	-	-	100 ± 100
D23	-	-	-	-	-	100 ± 100
D24	-	-	-	-	-	100 ± 100
D25	-	-	-	-	-	100 ± 100
D26	-	-	-	-	-	100 ± 100
D27	-	-	-	-	-	100 ± 100
D28	90 <sup>+50</sup> <sub>-40</sub>	-	-	-	-	100 ± 100
D29	-	-	-	-	-	100 ± 100
D30	-	-	-	-	-	100 ± 100
D31	-	-	-	-	-	100 ± 100
D32	-	-	-	-	-	100 ± 100
D33	-	-	-	-	-	100 ± 100
D34	-	-	-	-	-	100 ± 100
D35	-	-	-	-	-	100 ± 100
D36	-	-	-	-	-	100 ± 100
D37	-	-	-	-	-	100 ± 100
D38	20 <sup>+20</sup> <sub>-10</sub>	-	-	-	-	100 ± 100
D39	-	-	-	-	-	100 ± 100
D40	170 ± 30	-	-	-	-	170 ± 30
D41	180 <sup>+130</sup> <sub>-80</sub>	-	-	-	-	180 <sup>+130</sup> <sub>-80</sub>
D42	-	-	-	-	-	100 ± 100
D43	-	-	-	-	-	100 ± 100
D44	-	-	-	-	-	100 ± 100
D45	-	-	-	-	-	100 ± 100
D46	-	-	-	-	-	100 ± 100
D47	-	-	-	-	-	100 ± 100
D48	-	-	-	-	-	100 ± 100
D49	-	-	-	-	-	100 ± 100
D50	-	-	-	-	-	100 ± 100
D51	-	-	-	-	-	100 ± 100
D52	-	-	-	-	-	100 ± 100
D53	40 ± 20	-	-	-	-	100 ± 100
D54	60 <sup>+50</sup> <sub>-30</sub>	-	-	-	-	100 ± 100
D55	-	-	-	-	-	100 ± 100
D56	80 ± 10	-	-	-	-	100 ± 100
D57	-	-	-	-	-	100 ± 100
D58	-	-	-	-	-	100 ± 100
D59	130 <sup>+20</sup> <sub>-10</sub>	-	-	-	-	130 <sup>+20</sup> <sub>-10</sub>

**Table D.3.** Electron densities derived from the nebular sample.

Reference number	$n_e([\text{S II}])$ [cm <sup>-3</sup> ]	$n_e([\text{O II}])$ [cm <sup>-3</sup> ]	$n_e([\text{Fe III}])$ [cm <sup>-3</sup> ]	$n_e([\text{Cl III}])$ [cm <sup>-3</sup> ]	$n_e([\text{Ar IV}])$ [cm <sup>-3</sup> ]	Adopted $n_e$ [cm <sup>-3</sup> ]
D60	30 <sup>+30</sup> <sub>-20</sub>	-	-	-	-	100 ± 100
D61	-	-	-	-	-	100 ± 100
D62	-	-	-	-	-	100 ± 100
D63	-	-	-	-	-	100 ± 100
D64	-	-	-	-	-	100 ± 100
D65	-	-	-	-	-	100 ± 100
D66	-	-	-	-	-	100 ± 100
D67	40 <sup>+30</sup> <sub>-20</sub>	-	-	-	-	100 ± 100
D68	-	-	-	-	-	100 ± 100
D69	40 <sup>+30</sup> <sub>-20</sub>	-	-	-	-	100 ± 100
D70	30 <sup>+30</sup> <sub>-20</sub>	-	-	-	-	100 ± 100
D71	60 ± 10	-	-	-	-	100 ± 100
D72	110 <sup>+30</sup> <sub>-50</sub>	-	-	80 <sup>+310</sup> <sub>-60</sub>	-	110 <sup>+30</sup> <sub>-50</sub>
D73	-	-	-	-	-	100 ± 100
D74	-	-	-	-	-	100 ± 100
D75	60 <sup>+60</sup> <sub>-50</sub>	-	-	-	-	100 ± 100
D76	100 ± 30	-	-	3960 <sup>+1960</sup> <sub>-2420</sub>	-	100 ± 100
D77	80 <sup>+30</sup> <sub>-40</sub>	-	-	2970 <sup>+7010</sup> <sub>-1960</sub>	-	100 ± 100
D78	-	-	-	-	-	100 ± 100
D79	370 <sup>+250</sup> <sub>-240</sub>	-	-	-	-	370 <sup>+250</sup> <sub>-240</sub>
D80	-	-	-	-	-	100 ± 100
D81	40 ± 20	-	-	320 ± 80	-	100 ± 100
D82	420 <sup>+120</sup> <sub>-80</sub>	-	-	-	-	420 <sup>+120</sup> <sub>-80</sub>
D83	490 ± 120	-	-	440 <sup>+290</sup> <sub>-260</sub>	-	490 ± 120
D84	-	-	-	-	-	100 ± 100
D85	680 <sup>+70</sup> <sub>-60</sub>	-	-	5690 <sup>+1310</sup> <sub>-1470</sub>	-	680 <sup>+70</sup> <sub>-60</sub>
D86	560 <sup>+150</sup> <sub>-160</sub>	950 <sup>+190</sup> <sub>-180</sub>	-	-	-	750 ± 170
D87	-	-	-	-	-	100 ± 100
D88	-	-	-	-	-	100 ± 100
D89	-	-	-	-	-	100 ± 100
D90	40 <sup>+20</sup> <sub>-10</sub>	-	-	-	-	100 ± 100
D91	-	80 <sup>+10</sup> <sub>-20</sub>	-	-	4500 <sup>+1500</sup> <sub>-1380</sub>	100 ± 100
D92	150 ± 60	-	-	-	-	150 ± 60
D93	60 <sup>+40</sup> <sub>-30</sub>	-	-	-	-	100 ± 100
D94	360 <sup>+60</sup> <sub>-90</sub>	-	-	-	-	360 <sup>+60</sup> <sub>-90</sub>
D95	-	-	-	-	-	100 ± 100
D96	410 <sup>+240</sup> <sub>-190</sub>	-	-	-	-	410 <sup>+240</sup> <sub>-190</sub>
D97	100 ± 40	-	-	-	-	100 ± 40
D98	-	-	-	-	-	100 ± 100
D99	140 ± 70	-	-	-	-	140 ± 70
D100	210 <sup>+50</sup> <sub>-40</sub>	-	-	-	100 ± 50	210 <sup>+50</sup> <sub>-40</sub>
D101	440 ± 60	-	-	-	-	440 ± 60
D102	-	-	-	-	-	100 ± 100
D103	70 ± 50	-	-	-	340 <sup>+260</sup> <sub>-210</sub>	100 ± 100
D104	120 <sup>+20</sup> <sub>-10</sub>	-	-	-	-	120 <sup>+20</sup> <sub>-10</sub>
D105	120 ± 30	-	-	-	-	120 ± 30
D106	60 <sup>+40</sup> <sub>-30</sub>	-	-	-	-	100 ± 100
D107	-	-	-	-	-	100 ± 100
D108	140 ± 20	40 <sup>+20</sup> <sub>-10</sub>	-	-	16430 <sup>+8150</sup> <sub>-9890</sub>	100 ± 100
D109	60 <sup>+50</sup> <sub>-40</sub>	-	-	-	-	100 ± 100
D110	370 ± 30	100 ± 20	-	-	2250 <sup>+850</sup> <sub>-570</sub>	230 ± 20
D111	140 ± 20	80 ± 20	-	-	610 <sup>+140</sup> <sub>-170</sub>	110 ± 20
D112	130 <sup>+40</sup> <sub>-30</sub>	-	-	-	-	130 <sup>+40</sup> <sub>-30</sub>
D113	40 ± 20	130 ± 20	-	-	930 ± 130	100 ± 100
D114	70 ± 20	150 ± 20	-	-	230 <sup>+220</sup> <sub>-170</sub>	100 ± 100
D115	350 ± 20	450 <sup>+20</sup> <sub>-30</sub>	1930 <sup>+2390</sup> <sub>-1770</sub>	390 <sup>+280</sup> <sub>-220</sub>	630 <sup>+620</sup> <sub>-390</sub>	400 ± 20
D116	250 <sup>+130</sup> <sub>-110</sub>	310 <sup>+110</sup> <sub>-120</sub>	3630 <sup>+7150</sup> <sub>-2900</sub>	790 <sup>+390</sup> <sub>-430</sub>	2500 <sup>+2540</sup> <sub>-1580</sub>	280 ± 120

**Table D.3.** Electron densities derived from the nebular sample.

Reference number	$n_e$ ([S II]) [cm <sup>-3</sup> ]	$n_e$ ([O II]) [cm <sup>-3</sup> ]	$n_e$ ([Fe III]) [cm <sup>-3</sup> ]	$n_e$ ([Cl III]) [cm <sup>-3</sup> ]	$n_e$ ([Ar IV]) [cm <sup>-3</sup> ]	Adopted $n_e$ [cm <sup>-3</sup> ]
D117	270 <sup>+50</sup> <sub>-60</sub>	290 <sup>+110</sup> <sub>-100</sub>	2240 <sup>+2180</sup> <sub>-1630</sub>	340 <sup>+120</sup> <sub>-140</sub>	770 <sup>+560</sup> <sub>-430</sub>	280 ± 80
D118	100 ± 40	190 ± 100	3200 <sup>+3550</sup> <sub>-2380</sub>	550 <sup>+280</sup> <sub>-260</sub>	610 <sup>+410</sup> <sub>-360</sub>	140 ± 70
D119	360 <sup>+130</sup> <sub>-120</sub>	440 <sup>+150</sup> <sub>-140</sub>	3880 <sup>+8010</sup> <sub>-3310</sub>	580 <sup>+570</sup> <sub>-350</sub>	1630 <sup>+1410</sup> <sub>-1020</sub>	400 <sup>+140</sup> <sub>-130</sub>
D120	50 <sup>+40</sup> <sub>-30</sub>	-	-	200 <sup>+210</sup> <sub>-120</sub>	-	100 ± 100
D121	60 <sup>+40</sup> <sub>-30</sub>	220 ± 50	-	-	-	100 ± 100
D122	80 <sup>+80</sup> <sub>-50</sub>	90 <sup>+60</sup> <sub>-50</sub>	-	580 <sup>+440</sup> <sub>-390</sub>	-	100 ± 100
D123	30 <sup>+30</sup> <sub>-10</sub>	160 ± 60	-	-	-	100 ± 100
D124	40 <sup>+40</sup> <sub>-30</sub>	180 ± 60	-	-	-	100 ± 100
D125	50 <sup>+50</sup> <sub>-30</sub>	200 <sup>+50</sup> <sub>-40</sub>	-	-	-	100 ± 100
D126	40 <sup>+40</sup> <sub>-20</sub>	310 <sup>+50</sup> <sub>-60</sub>	-	-	-	100 ± 100
D127	40 <sup>+80</sup> <sub>-30</sub>	90 <sup>+50</sup> <sub>-40</sub>	-	-	-	100 ± 100
D128	140 ± 60	280 <sup>+60</sup> <sub>-50</sub>	-	-	-	210 ± 60
D129	40 <sup>+20</sup> <sub>-30</sub>	320 <sup>+50</sup> <sub>-40</sub>	-	-	-	100 ± 100
D130	70 <sup>+60</sup> <sub>-50</sub>	180 <sup>+80</sup> <sub>-90</sub>	-	-	-	100 ± 100
D131	50 <sup>+80</sup> <sub>-40</sub>	210 <sup>+70</sup> <sub>-60</sub>	-	-	-	100 ± 100
D132	50 <sup>+60</sup> <sub>-40</sub>	130 ± 70	-	-	-	100 ± 100
D133	50 ± 30	240 <sup>+60</sup> <sub>-70</sub>	-	-	-	100 ± 100
D134	40 <sup>+40</sup> <sub>-30</sub>	20 ± 10	-	-	-	100 ± 100
D135	50 <sup>+40</sup> <sub>-30</sub>	30 <sup>+30</sup> <sub>-20</sub>	-	250 <sup>+360</sup> <sub>-190</sub>	-	100 ± 100
D136	70 <sup>+50</sup> <sub>-40</sub>	60 <sup>+50</sup> <sub>-30</sub>	-	-	-	100 ± 100
D137	80 <sup>+70</sup> <sub>-50</sub>	220 ± 50	-	-	-	100 ± 100
D138	80 <sup>+60</sup> <sub>-50</sub>	90 <sup>+70</sup> <sub>-50</sub>	-	-	-	100 ± 100
D139	80 <sup>+50</sup> <sub>-30</sub>	40 <sup>+30</sup> <sub>-20</sub>	-	-	-	100 ± 100
D140	40 <sup>+40</sup> <sub>-30</sub>	130 ± 50	-	-	-	100 ± 100
D141	50 ± 30	110 ± 50	-	-	-	100 ± 100
D142	50 <sup>+60</sup> <sub>-30</sub>	130 ± 50	-	-	-	100 ± 100
D143	80 ± 40	290 ± 40	-	-	-	100 ± 100
D144	60 <sup>+50</sup> <sub>-30</sub>	220 ± 50	-	-	-	100 ± 100
D145	70 <sup>+70</sup> <sub>-40</sub>	170 <sup>+60</sup> <sub>-50</sub>	-	-	-	100 ± 100
D146	50 ± 30	100 ± 60	-	-	-	100 ± 100
D147	50 ± 40	320 ± 50	-	-	-	100 ± 100
D148	60 ± 30	110 ± 50	-	-	-	100 ± 100
D149	30 ± 20	220 ± 50	-	-	-	100 ± 100
D150	60 <sup>+40</sup> <sub>-30</sub>	100 <sup>+40</sup> <sub>-30</sub>	-	-	-	100 ± 100
D151	50 ± 30	30 <sup>+30</sup> <sub>-10</sub>	-	-	-	100 ± 100
D152	50 <sup>+40</sup> <sub>-30</sub>	30 ± 20	-	-	-	100 ± 100
D153	40 <sup>+40</sup> <sub>-30</sub>	210 <sup>+80</sup> <sub>-70</sub>	-	-	-	100 ± 100
D154	60 <sup>+40</sup> <sub>-50</sub>	150 <sup>+40</sup> <sub>-60</sub>	-	-	-	100 ± 100
D155	30 <sup>+40</sup> <sub>-20</sub>	-	-	-	-	100 ± 100
D156	50 <sup>+40</sup> <sub>-30</sub>	110 <sup>+60</sup> <sub>-50</sub>	-	-	-	100 ± 100
D157	110 ± 40	60 ± 30	-	-	-	100 ± 100
D158	40 <sup>+40</sup> <sub>-20</sub>	160 ± 50	-	-	-	100 ± 100
D159	20 <sup>+20</sup> <sub>-10</sub>	200 ± 40	-	-	-	100 ± 100
D160	40 <sup>+40</sup> <sub>-20</sub>	290 <sup>+90</sup> <sub>-80</sub>	-	-	-	100 ± 100
D161	50 ± 30	210 ± 60	-	-	-	100 ± 100
D162	50 <sup>+50</sup> <sub>-30</sub>	80 <sup>+40</sup> <sub>-30</sub>	-	-	-	100 ± 100
D163	40 ± 30	150 ± 50	-	-	-	100 ± 100
D164	50 <sup>+40</sup> <sub>-30</sub>	210 ± 40	-	-	-	100 ± 100
D165	60 <sup>+50</sup> <sub>-30</sub>	50 <sup>+50</sup> <sub>-30</sub>	-	-	-	100 ± 100
D166	80 <sup>+50</sup> <sub>-40</sub>	50 <sup>+40</sup> <sub>-30</sub>	-	-	-	100 ± 100
D167	110 ± 60	150 <sup>+50</sup> <sub>-40</sub>	-	-	-	130 ± 50
D168	200 ± 130	-	6990 <sup>+30700</sup> <sub>-5090</sub>	660 <sup>+690</sup> <sub>-410</sub>	1530 <sup>+1500</sup> <sub>-1040</sub>	200 ± 130
D169	50 <sup>+60</sup> <sub>-30</sub>	60 <sup>+50</sup> <sub>-40</sub>	-	-	-	100 ± 100
D170	60 ± 40	390 <sup>+80</sup> <sub>-70</sub>	-	-	-	100 ± 100
D171	60 <sup>+50</sup> <sub>-30</sub>	220 <sup>+80</sup> <sub>-60</sub>	-	-	-	100 ± 100
D172	170 ± 90	390 <sup>+100</sup> <sub>-90</sub>	-	-	-	280 ± 90

**Table D.3.** Electron densities derived from the nebular sample.

Reference number	$n_e$ ([S II]) [cm <sup>-3</sup> ]	$n_e$ ([O II]) [cm <sup>-3</sup> ]	$n_e$ ([Fe III]) [cm <sup>-3</sup> ]	$n_e$ ([Cl III]) [cm <sup>-3</sup> ]	$n_e$ ([Ar IV]) [cm <sup>-3</sup> ]	Adopted $n_e$ [cm <sup>-3</sup> ]
D173	160 ± 40	250 <sup>+60</sup> <sub>-50</sub>	-	90 <sup>+170</sup> <sub>-60</sub>	-	200 ± 50
D174	30 ± 20	210 ± 40	-	-	-	100 ± 100
D175	40 <sup>+40</sup> <sub>-30</sub>	270 <sup>+50</sup> <sub>-60</sub>	-	-	-	100 ± 100
D176	200 <sup>+100</sup> <sub>-90</sub>	320 <sup>+100</sup> <sub>-80</sub>	-	-	-	260 <sup>+100</sup> <sub>-90</sub>
D177	220 ± 130	310 <sup>+80</sup> <sub>-100</sub>	-	410 <sup>+760</sup> <sub>-260</sub>	-	270 ± 110
D178	70 <sup>+50</sup> <sub>-40</sub>	70 <sup>+40</sup> <sub>-50</sub>	-	-	-	100 ± 100
D179	60 ± 40	60 <sup>+50</sup> <sub>-40</sub>	-	-	-	100 ± 100
D180	90 <sup>+70</sup> <sub>-60</sub>	-	-	-	-	100 ± 100
D181	250 ± 100	-	-	-	-	250 ± 100
D182	190 <sup>+80</sup> <sub>-70</sub>	270 <sup>+100</sup> <sub>-70</sub>	-	-	-	230 <sup>+90</sup> <sub>-70</sub>
D183	180 ± 60	210 ± 60	-	230 <sup>+230</sup> <sub>-180</sub>	-	190 ± 60
D184	110 <sup>+100</sup> <sub>-60</sub>	-	-	680 <sup>+570</sup> <sub>-450</sub>	-	110 <sup>+100</sup> <sub>-60</sub>
D185	70 <sup>+70</sup> <sub>-50</sub>	-	-	860 <sup>+840</sup> <sub>-580</sub>	-	100 ± 100
D186	190 <sup>+90</sup> <sub>-80</sub>	-	-	1170 <sup>+600</sup> <sub>-550</sub>	-	190 <sup>+90</sup> <sub>-80</sub>
D187	80 ± 40	80 <sup>+50</sup> <sub>-30</sub>	-	1440 <sup>+1350</sup> <sub>-870</sub>	-	100 ± 100
D188	120 ± 40	250 ± 30	3190 <sup>+5220</sup> <sub>-2430</sub>	810 <sup>+340</sup> <sub>-400</sub>	2490 <sup>+3200</sup> <sub>-1640</sub>	180 <sup>+40</sup> <sub>-30</sub>
D189	100 <sup>+60</sup> <sub>-50</sub>	-	-	790 <sup>+1360</sup> <sub>-510</sub>	-	100 ± 100
D190	90 <sup>+80</sup> <sub>-60</sub>	-	-	700 <sup>+730</sup> <sub>-450</sub>	-	100 ± 100
D191	60 <sup>+40</sup> <sub>-30</sub>	-	-	-	-	100 ± 100
D192	100 <sup>+120</sup> <sub>-70</sub>	110 <sup>+100</sup> <sub>-60</sub>	-	910 <sup>+750</sup> <sub>-520</sub>	-	110 <sup>+110</sup> <sub>-70</sub>
D193	210 <sup>+420</sup> <sub>-130</sub>	400 <sup>+330</sup> <sub>-210</sub>	-	850 <sup>+1060</sup> <sub>-560</sub>	-	310 <sup>+370</sup> <sub>-170</sub>
D194	150 <sup>+160</sup> <sub>-100</sub>	60 <sup>+120</sup> <sub>-40</sub>	-	490 <sup>+490</sup> <sub>-320</sub>	-	110 <sup>+140</sup> <sub>-70</sub>
D195	470 <sup>+170</sup> <sub>-180</sub>	-	-	1870 <sup>+500</sup> <sub>-440</sub>	-	470 <sup>+170</sup> <sub>-180</sub>
D196	220 ± 120	-	-	370 <sup>+350</sup> <sub>-250</sub>	-	220 ± 120
D197	100 <sup>+130</sup> <sub>-60</sub>	50 <sup>+80</sup> <sub>-40</sub>	-	670 <sup>+780</sup> <sub>-550</sub>	-	100 ± 100
D198	100 <sup>+230</sup> <sub>-60</sub>	90 <sup>+90</sup> <sub>-50</sub>	-	670 <sup>+630</sup> <sub>-500</sub>	-	100 ± 100
D199	40 <sup>+30</sup> <sub>-20</sub>	60 ± 20	-	680 <sup>+350</sup> <sub>-290</sub>	-	100 ± 100
D200	110 <sup>+90</sup> <sub>-70</sub>	-	-	200 <sup>+230</sup> <sub>-110</sub>	-	110 <sup>+90</sup> <sub>-70</sub>
D201	40 <sup>+40</sup> <sub>-20</sub>	70 <sup>+20</sup> <sub>-30</sub>	-	560 <sup>+420</sup> <sub>-330</sub>	-	100 ± 100
D202	110 <sup>+90</sup> <sub>-70</sub>	-	-	-	-	110 <sup>+90</sup> <sub>-70</sub>
D203	60 <sup>+60</sup> <sub>-40</sub>	-	-	-	-	100 ± 100
D204	90 <sup>+80</sup> <sub>-50</sub>	-	-	-	-	100 ± 100
D205	100 <sup>+90</sup> <sub>-70</sub>	-	-	510 <sup>+420</sup> <sub>-310</sub>	-	100 <sup>+90</sup> <sub>-70</sub>
D206	120 <sup>+90</sup> <sub>-80</sub>	-	-	470 <sup>+390</sup> <sub>-290</sub>	-	120 <sup>+90</sup> <sub>-80</sub>
D207	200 <sup>+120</sup> <sub>-110</sub>	-	-	900 <sup>+330</sup> <sub>-380</sub>	-	200 <sup>+120</sup> <sub>-110</sub>
D208	130 <sup>+90</sup> <sub>-80</sub>	-	-	520 <sup>+490</sup> <sub>-370</sub>	-	130 <sup>+90</sup> <sub>-80</sub>
D209	40 ± 20	60 <sup>+60</sup> <sub>-40</sub>	-	-	-	100 ± 100
D210	100 ± 30	290 <sup>+80</sup> <sub>-70</sub>	-	-	-	100 ± 100
D211	50 ± 20	40 <sup>+30</sup> <sub>-20</sub>	-	-	-	100 ± 100
D212	110 ± 30	120 ± 30	-	-	-	120 ± 30
D213	50 ± 20	50 ± 30	-	-	-	100 ± 100
D214	130 ± 20	300 <sup>+50</sup> <sub>-40</sub>	-	-	-	210 ± 30
D215	100 <sup>+30</sup> <sub>-20</sub>	350 ± 100	-	-	-	100 ± 100
D216	40 ± 20	390 <sup>+170</sup> <sub>-160</sub>	-	-	-	100 ± 100
D217	380 ± 50	360 ± 70	-	-	-	370 ± 60
D218	80 ± 20	50 ± 30	-	-	-	100 ± 100
D219	50 ± 30	200 ± 90	-	-	-	100 ± 100
D220	400 <sup>+100</sup> <sub>-120</sub>	510 <sup>+90</sup> <sub>-110</sub>	-	360 <sup>+300</sup> <sub>-210</sub>	-	460 <sup>+90</sup> <sub>-120</sub>
D221	270 ± 80	260 <sup>+50</sup> <sub>-60</sub>	-	430 <sup>+360</sup> <sub>-240</sub>	-	270 ± 70
D222	4180 <sup>+990</sup> <sub>-770</sub>	5330 <sup>+680</sup> <sub>-600</sub>	10170 <sup>+3100</sup> <sub>-2670</sub>	6980 <sup>+670</sup> <sub>-680</sub>	4200 <sup>+1430</sup> <sub>-1210</sub>	5640 ± 1260
D223	1310 ± 190	1130 <sup>+100</sup> <sub>-110</sub>	-	1570 <sup>+280</sup> <sub>-260</sub>	-	1210 ± 140
D224	4170 <sup>+1000</sup> <sub>-780</sub>	5130 <sup>+670</sup> <sub>-500</sub>	10240 <sup>+2730</sup> <sub>-1910</sub>	6590 <sup>+550</sup> <sub>-620</sub>	5880 <sup>+700</sup> <sub>-740</sub>	5720 ± 1050
D225	1180 <sup>+200</sup> <sub>-170</sub>	1470 ± 120	-	2100 <sup>+530</sup> <sub>-550</sub>	-	1400 ± 190
D226	3980 <sup>+1260</sup> <sub>-920</sub>	5910 <sup>+840</sup> <sub>-700</sub>	9960 <sup>+2560</sup> <sub>-2000</sub>	7590 <sup>+770</sup> <sub>-720</sub>	6680 <sup>+570</sup> <sub>-580</sub>	6510 ± 1180
D227	4440 <sup>+1260</sup> <sub>-1020</sub>	5440 <sup>+630</sup> <sub>-620</sub>	11170 <sup>+3630</sup> <sub>-2340</sub>	7430 <sup>+810</sup> <sub>-890</sub>	6450 <sup>+1150</sup> <sub>-1350</sub>	6040 ± 1260
D228	4190 <sup>+890</sup> <sub>-690</sub>	5460 <sup>+670</sup> <sub>-710</sub>	7400 <sup>+2680</sup> <sub>-2050</sub>	7730 <sup>+710</sup> <sub>-690</sub>	4680 ± 460	5390 ± 1250



Table D.3. Electron densities derived from the nebular sample.

Reference number	$n_e$ ([S II]) [cm <sup>-3</sup> ]	$n_e$ ([O II]) [cm <sup>-3</sup> ]	$n_e$ ([Fe III]) [cm <sup>-3</sup> ]	$n_e$ ([Cl III]) [cm <sup>-3</sup> ]	$n_e$ ([Ar IV]) [cm <sup>-3</sup> ]	Adopted $n_e$ [cm <sup>-3</sup> ]
D229	4030 <sup>+1160</sup> <sub>-810</sub>	4950 <sup>+580</sup> <sub>-550</sub>	9940 <sup>+3150</sup> <sub>-2410</sub>	7000 <sup>+690</sup> <sub>-740</sub>	5300 <sup>+780</sup> <sub>-760</sub>	5490 ± 1130
D230	290 ± 120	390 <sup>+100</sup> <sub>-80</sub>	-	2720 <sup>+2790</sup> <sub>-1690</sub>	-	340 <sup>+110</sup> <sub>-100</sub>
D231	2810 <sup>+660</sup> <sub>-560</sub>	4760 <sup>+800</sup> <sub>-780</sub>	6760 <sup>+3060</sup> <sub>-2160</sub>	6030 <sup>+1310</sup> <sub>-1280</sub>	6120 <sup>+4120</sup> <sub>-3270</sub>	3960 ± 1300
D232	4850 <sup>+3280</sup> <sub>-1700</sub>	6950 <sup>+2440</sup> <sub>-1700</sub>	9020 <sup>+3710</sup> <sub>-2590</sub>	7000 <sup>+620</sup> <sub>-570</sub>	4930 <sup>+1010</sup> <sub>-1060</sub>	6510 ± 990
D233	1750 <sup>+600</sup> <sub>-540</sub>	2780 <sup>+740</sup> <sub>-600</sub>	-	2190 <sup>+1080</sup> <sub>-1090</sub>	-	2190 ± 470
D234	1240 <sup>+190</sup> <sub>-160</sub>	1750 <sup>+620</sup> <sub>-570</sub>	1980 <sup>+1790</sup> <sub>-1390</sub>	1840 <sup>+290</sup> <sub>-280</sub>	5440 <sup>+5520</sup> <sub>-3490</sub>	1430 ± 310
D235	880 <sup>+180</sup> <sub>-170</sub>	1240 <sup>+310</sup> <sub>-210</sub>	2220 <sup>+2830</sup> <sub>-2010</sub>	1680 <sup>+510</sup> <sub>-430</sub>	5130 <sup>+7340</sup> <sub>-3560</sub>	1060 <sup>+250</sup> <sub>-190</sub>
D236	1070 <sup>+360</sup> <sub>-310</sub>	1700 <sup>+260</sup> <sub>-270</sub>	1670 <sup>+1370</sup> <sub>-1610</sub>	2920 <sup>+660</sup> <sub>-600</sub>	3060 <sup>+1750</sup> <sub>-1380</sub>	1630 ± 550
D237	2850 <sup>+1030</sup> <sub>-800</sub>	2440 <sup>+570</sup> <sub>-490</sub>	10690 <sup>+30430</sup> <sub>-8280</sub>	4340 <sup>+1270</sup> <sub>-1290</sub>	1630 <sup>+1390</sup> <sub>-990</sub>	2620 ± 690
D238	430 <sup>+230</sup> <sub>-170</sub>	-	-	800 <sup>+350</sup> <sub>-390</sub>	-	430 <sup>+230</sup> <sub>-170</sub>
D239	600 <sup>+120</sup> <sub>-90</sub>	-	-	1970 <sup>+760</sup> <sub>-1200</sub>	-	600 <sup>+120</sup> <sub>-90</sub>
D240	480 <sup>+70</sup> <sub>-80</sub>	-	-	760 <sup>+610</sup> <sub>-390</sub>	-	480 <sup>+70</sup> <sub>-80</sub>
D241	750 <sup>+70</sup> <sub>-80</sub>	-	-	1020 <sup>+370</sup> <sub>-350</sub>	-	750 <sup>+70</sup> <sub>-80</sub>
D242	880 ± 40	-	-	2660 <sup>+910</sup> <sub>-970</sub>	-	880 ± 40
D243	90 <sup>+110</sup> <sub>-70</sub>	-	-	2470 <sup>+2150</sup> <sub>-1300</sub>	-	100 ± 100
D244	140 <sup>+40</sup> <sub>-30</sub>	-	-	520 <sup>+720</sup> <sub>-330</sub>	-	140 <sup>+40</sup> <sub>-30</sub>
D245	180 ± 50	-	-	610 <sup>+670</sup> <sub>-420</sub>	-	180 ± 50
D246	330 <sup>+180</sup> <sub>-200</sub>	-	-	-	-	330 <sup>+180</sup> <sub>-200</sub>
D247	460 <sup>+200</sup> <sub>-210</sub>	-	-	460 <sup>+380</sup> <sub>-300</sub>	-	460 <sup>+200</sup> <sub>-210</sub>
D248	110 <sup>+20</sup> <sub>-40</sub>	-	-	930 <sup>+1460</sup> <sub>-660</sub>	-	110 <sup>+20</sup> <sub>-40</sub>
D249	310 ± 80	290 <sup>+70</sup> <sub>-80</sub>	-	-	-	300 ± 80
D250	90 ± 30	-	-	-	-	100 ± 100
D251	90 <sup>+40</sup> <sub>-30</sub>	-	-	-	-	100 ± 100
D252	60 ± 30	-	-	-	-	100 ± 100
D253	180 ± 100	220 ± 100	-	470 <sup>+470</sup> <sub>-320</sub>	850 <sup>+1260</sup> <sub>-600</sub>	200 ± 100
D254	80 <sup>+40</sup> <sub>-30</sub>	-	-	240 <sup>+290</sup> <sub>-150</sub>	-	100 ± 100
D255	60 <sup>+50</sup> <sub>-40</sub>	-	-	-	-	100 ± 100
D256	30 ± 20	-	-	660 <sup>+590</sup> <sub>-440</sub>	-	100 ± 100
D257	30 <sup>+30</sup> <sub>-20</sub>	-	-	400 <sup>+480</sup> <sub>-260</sub>	-	100 ± 100
D258	-	-	-	-	-	100 ± 100
D259	-	-	-	-	-	100 ± 100
D260	-	-	-	-	-	100 ± 100
D261	-	-	-	-	-	100 ± 100
D262	170 <sup>+30</sup> <sub>-40</sub>	-	-	420 <sup>+330</sup> <sub>-290</sub>	-	170 <sup>+30</sup> <sub>-40</sub>
D263	20 <sup>+30</sup> <sub>-20</sub>	-	-	-	-	100 ± 100
D264	90 <sup>+10</sup> <sub>-20</sub>	-	-	220 <sup>+420</sup> <sub>-140</sub>	-	100 ± 100
D265	60 <sup>+60</sup> <sub>-40</sub>	-	-	-	-	100 ± 100
D266	120 <sup>+30</sup> <sub>-40</sub>	-	-	5880 <sup>+2880</sup> <sub>-2510</sub>	-	120 <sup>+30</sup> <sub>-40</sub>
D267	20 ± 20	-	-	440 <sup>+390</sup> <sub>-360</sub>	-	100 ± 100
D268	-	-	-	-	-	100 ± 100
D269	-	-	-	-	-	100 ± 100
D270	50 ± 40	-	-	-	-	100 ± 100
D271	70 <sup>+40</sup> <sub>-30</sub>	-	-	-	-	100 ± 100
D272	60 <sup>+10</sup> <sub>-20</sub>	-	-	-	-	100 ± 100
D273	80 ± 40	-	-	-	-	100 ± 100
D274	50 <sup>+10</sup> <sub>-20</sub>	-	-	-	-	100 ± 100
D275	-	-	-	-	-	100 ± 100
D276	-	-	-	-	-	100 ± 100
D277	-	-	-	-	-	100 ± 100
D278	40 <sup>+30</sup> <sub>-20</sub>	-	-	1720 <sup>+2310</sup> <sub>-1140</sub>	-	100 ± 100
D279	60 <sup>+30</sup> <sub>-20</sub>	-	-	-	-	100 ± 100
D280	-	-	-	-	-	100 ± 100
D281	90 <sup>+90</sup> <sub>-60</sub>	-	-	-	-	100 ± 100
D282	50 <sup>+40</sup> <sub>-30</sub>	150 <sup>+60</sup> <sub>-50</sub>	-	-	-	100 ± 100
D283	170 <sup>+120</sup> <sub>-100</sub>	290 ± 100	9530 <sup>+18210</sup> <sub>-7460</sub>	280 <sup>+400</sup> <sub>-200</sub>	530 <sup>+270</sup> <sub>-300</sub>	230 <sup>+110</sup> <sub>-100</sub>
D284	70 <sup>+60</sup> <sub>-40</sub>	-	-	1520 <sup>+1080</sup> <sub>-960</sub>	-	100 ± 100

**Table D.3.** Electron densities derived from the nebular sample.

Reference number	$n_e$ ([S II]) [cm <sup>-3</sup> ]	$n_e$ ([O II]) [cm <sup>-3</sup> ]	$n_e$ ([Fe III]) [cm <sup>-3</sup> ]	$n_e$ ([Cl III]) [cm <sup>-3</sup> ]	$n_e$ ([Ar IV]) [cm <sup>-3</sup> ]	Adopted $n_e$ [cm <sup>-3</sup> ]
D285	110 <sup>+40</sup> <sub>-50</sub>	240 <sup>+30</sup> <sub>-20</sub>	-	760 <sup>+770</sup> <sub>-500</sub>	-	170 ± 40
D286	60 <sup>+40</sup> <sub>-30</sub>	120 <sup>+40</sup> <sub>-30</sub>	-	240 <sup>+270</sup> <sub>-110</sub>	-	100 ± 100
D287	100 <sup>+70</sup> <sub>-60</sub>	-	-	480 <sup>+350</sup> <sub>-300</sub>	-	100 <sup>+70</sup> <sub>-60</sub>
D288	100 <sup>+30</sup> <sub>-40</sub>	150 ± 20	-	580 <sup>+330</sup> <sub>-400</sub>	-	130 ± 30
D289	140 <sup>+100</sup> <sub>-80</sub>	-	-	-	-	140 <sup>+100</sup> <sub>-80</sub>
D290	160 ± 80	-	-	1120 <sup>+1290</sup> <sub>-710</sub>	-	160 ± 80
D291	70 <sup>+60</sup> <sub>-50</sub>	-	-	-	-	100 ± 100
D292	60 <sup>+50</sup> <sub>-40</sub>	-	-	-	-	100 ± 100
D293	100 <sup>+90</sup> <sub>-70</sub>	-	-	-	-	100 ± 100
D294	110 <sup>+110</sup> <sub>-80</sub>	30 <sup>+60</sup> <sub>-10</sub>	-	-	-	100 ± 100
D295	60 <sup>+60</sup> <sub>-40</sub>	40 <sup>+50</sup> <sub>-30</sub>	-	-	-	100 ± 100
D296	140 <sup>+80</sup> <sub>-70</sub>	170 <sup>+110</sup> <sub>-100</sub>	6200 <sup>+14330</sup> <sub>-4590</sub>	1490 <sup>+900</sup> <sub>-1000</sub>	790 <sup>+1140</sup> <sub>-490</sub>	160 <sup>+90</sup> <sub>-80</sub>
D297	200 ± 40	-	-	340 <sup>+280</sup> <sub>-240</sub>	-	200 ± 40
D298	30 ± 20	-	-	-	-	100 ± 100
D299	50 ± 10	-	-	-	-	100 ± 100
D300	60 ± 10	-	-	-	-	100 ± 100
D301	30 ± 20	-	-	-	-	100 ± 100
D302	20 <sup>+20</sup> <sub>-10</sub>	-	-	-	-	100 ± 100
D303	40 <sup>+10</sup> <sub>-20</sub>	-	-	-	-	100 ± 100
D304	40 ± 20	-	-	-	-	100 ± 100
D305	10 <sup>+10</sup> <sub>-0</sub>	-	-	-	-	100 ± 100
D306	30 <sup>+30</sup> <sub>-20</sub>	-	-	-	-	100 ± 100
D307	40 ± 20	-	-	-	-	100 ± 100
D308	50 ± 10	-	-	-	-	100 ± 100
D309	80 <sup>+30</sup> <sub>-20</sub>	-	-	-	-	100 ± 100
D310	50 <sup>+30</sup> <sub>-20</sub>	-	-	-	-	100 ± 100
D311	20 ± 10	-	-	-	-	100 ± 100
D312	90 <sup>+60</sup> <sub>-50</sub>	140 ± 70	16170 <sup>+37730</sup> <sub>-10870</sub>	450 <sup>+590</sup> <sub>-270</sub>	910 <sup>+800</sup> <sub>-570</sub>	100 ± 100
D313	200 <sup>+40</sup> <sub>-30</sub>	-	-	920 <sup>+410</sup> <sub>-370</sub>	-	200 <sup>+40</sup> <sub>-30</sub>
D314	290 <sup>+40</sup> <sub>-60</sub>	-	-	3060 <sup>+1370</sup> <sub>-1430</sub>	-	290 <sup>+40</sup> <sub>-60</sub>
D315	280 <sup>+80</sup> <sub>-70</sub>	190 ± 70	4800 <sup>+12280</sup> <sub>-3390</sub>	880 <sup>+760</sup> <sub>-540</sub>	2500 <sup>+3030</sup> <sub>-1660</sub>	230 <sup>+80</sup> <sub>-70</sub>
D316	170 ± 60	60 <sup>+50</sup> <sub>-40</sub>	-	-	-	110 <sup>+60</sup> <sub>-50</sub>
D317	110 ± 30	-	-	280 <sup>+170</sup> <sub>-140</sub>	-	110 ± 30
D318	80 <sup>+20</sup> <sub>-30</sub>	-	-	-	-	100 ± 100
D319	280 ± 50	-	-	1130 <sup>+790</sup> <sub>-650</sub>	-	280 ± 50
D320	200 <sup>+110</sup> <sub>-100</sub>	220 ± 90	2730 <sup>+4020</sup> <sub>-2650</sub>	350 <sup>+370</sup> <sub>-250</sub>	1080 <sup>+390</sup> <sub>-520</sub>	210 ± 100
D321	30 ± 20	130 ± 30	-	-	-	100 ± 100
D322	60 ± 30	100 ± 30	-	-	-	100 ± 100
D323	80 <sup>+20</sup> <sub>-30</sub>	280 <sup>+40</sup> <sub>-30</sub>	-	-	-	100 ± 100
D324	50 <sup>+30</sup> <sub>-20</sub>	60 <sup>+70</sup> <sub>-30</sub>	-	-	-	100 ± 100
D325	70 <sup>+30</sup> <sub>-20</sub>	360 <sup>+130</sup> <sub>-100</sub>	-	-	-	100 ± 100
D326	40 ± 20	130 <sup>+30</sup> <sub>-20</sub>	-	-	-	100 ± 100
D327	70 ± 30	360 ± 40	-	-	-	100 ± 100
D328	50 ± 20	-	-	-	-	100 ± 100
D329	290 ± 40	270 ± 40	-	-	-	280 ± 40
D330	70 ± 20	10 ± 0	-	-	-	100 ± 100
D331	30 <sup>+20</sup> <sub>-10</sub>	60 <sup>+60</sup> <sub>-30</sub>	-	-	-	100 ± 100
D332	40 <sup>+20</sup> <sub>-30</sub>	100 <sup>+70</sup> <sub>-60</sub>	-	-	-	100 ± 100
D333	160 ± 30	80 ± 30	-	-	-	120 ± 30
D334	130 <sup>+110</sup> <sub>-80</sub>	150 <sup>+100</sup> <sub>-70</sub>	5770 <sup>+12190</sup> <sub>-4100</sub>	600 <sup>+550</sup> <sub>-360</sub>	530 <sup>+870</sup> <sub>-360</sub>	140 <sup>+100</sup> <sub>-70</sub>
D335	110 ± 30	-	-	80 <sup>+90</sup> <sub>-60</sub>	-	110 ± 30
D336	100 <sup>+60</sup> <sub>-50</sub>	80 <sup>+50</sup> <sub>-30</sub>	-	1610 <sup>+1680</sup> <sub>-1060</sub>	-	100 ± 100
D337	130 ± 30	-	-	2640 <sup>+1130</sup> <sub>-1590</sub>	-	130 ± 30
D338	130 <sup>+120</sup> <sub>-90</sub>	30 <sup>+30</sup> <sub>-20</sub>	-	-	-	100 ± 100
D339	50 <sup>+40</sup> <sub>-30</sub>	40 ± 40	-	-	-	100 ± 100
D340	50 <sup>+60</sup> <sub>-30</sub>	20 <sup>+30</sup> <sub>-10</sub>	-	550 <sup>+780</sup> <sub>-310</sub>	-	100 ± 100
D341	60 <sup>+30</sup> <sub>-20</sub>	-	-	1150 <sup>+1000</sup> <sub>-790</sub>	-	100 ± 100

**Table D.3.** Electron densities derived from the nebular sample.

Reference number	$n_e$ ([S II]) [cm <sup>-3</sup> ]	$n_e$ ([O II]) [cm <sup>-3</sup> ]	$n_e$ ([Fe III]) [cm <sup>-3</sup> ]	$n_e$ ([Cl III]) [cm <sup>-3</sup> ]	$n_e$ ([Ar IV]) [cm <sup>-3</sup> ]	Adopted $n_e$ [cm <sup>-3</sup> ]
D342	70 <sup>+60</sup> <sub>-40</sub>	140 <sup>+80</sup> <sub>-70</sub>	58180 <sup>+555350</sup> <sub>-33870</sub>	1380 <sup>+1250</sup> <sub>-750</sub>	1920 <sup>+890</sup> <sub>-1110</sub>	100 ± 100
D343	130 ± 40	-	-	170 <sup>+180</sup> <sub>-120</sub>	-	130 ± 40
D344	290 <sup>+190</sup> <sub>-160</sub>	-	-	-	-	290 <sup>+190</sup> <sub>-160</sub>
D345	-	-	-	-	-	100 ± 100
D346	440 <sup>+150</sup> <sub>-120</sub>	-	-	-	-	440 <sup>+150</sup> <sub>-120</sub>
D347	620 <sup>+190</sup> <sub>-140</sub>	-	-	-	-	620 <sup>+190</sup> <sub>-140</sub>
D348	170 <sup>+80</sup> <sub>-100</sub>	-	-	-	-	170 <sup>+80</sup> <sub>-100</sub>
D349	220 <sup>+170</sup> <sub>-140</sub>	-	-	-	-	220 <sup>+170</sup> <sub>-140</sub>
D350	310 <sup>+220</sup> <sub>-160</sub>	-	-	-	-	310 <sup>+220</sup> <sub>-160</sub>
D351	480 <sup>+110</sup> <sub>-90</sub>	-	-	-	-	480 <sup>+110</sup> <sub>-90</sub>
D352	310 ± 50	-	-	2000 <sup>+2320</sup> <sub>-1350</sub>	-	310 ± 50
D353	500 <sup>+100</sup> <sub>-90</sub>	-	-	1850 <sup>+1470</sup> <sub>-1440</sub>	-	500 <sup>+100</sup> <sub>-90</sub>
D354	40 <sup>+40</sup> <sub>-30</sub>	-	-	-	-	100 ± 100
D355	140 <sup>+130</sup> <sub>-90</sub>	-	-	-	-	140 <sup>+130</sup> <sub>-90</sub>
D356	-	-	-	-	-	100 ± 100
D357	-	-	-	-	-	100 ± 100
D358	-	-	-	-	-	100 ± 100
D359	-	-	-	-	-	100 ± 100
D360	80 ± 40	-	-	-	-	100 ± 100
D361	80 <sup>+10</sup> <sub>-20</sub>	-	-	-	-	100 ± 100
D362	20 ± 10	-	-	24420 <sup>+53820</sup> <sub>-18560</sub>	-	100 ± 100
D363	460 <sup>+70</sup> <sub>-50</sub>	-	-	-	-	460 <sup>+70</sup> <sub>-50</sub>
D364	360 <sup>+150</sup> <sub>-110</sub>	-	-	-	-	360 <sup>+150</sup> <sub>-110</sub>
D365	60 <sup>+10</sup> <sub>-20</sub>	-	-	-	-	100 ± 100
D366	130 ± 20	-	-	-	-	130 ± 20
D367	-	-	-	-	-	100 ± 100
D368	210 <sup>+50</sup> <sub>-40</sub>	-	-	1830 <sup>+2220</sup> <sub>-1310</sub>	-	210 <sup>+50</sup> <sub>-40</sub>
D369	-	-	-	-	-	100 ± 100
D370	430 <sup>+90</sup> <sub>-100</sub>	-	-	1300 <sup>+1190</sup> <sub>-900</sub>	-	430 <sup>+90</sup> <sub>-100</sub>
D371	-	-	-	-	-	100 ± 100
D372	-	-	-	-	-	100 ± 100
D373	-	-	-	-	-	100 ± 100
D374	640 <sup>+130</sup> <sub>-140</sub>	-	-	-	-	640 <sup>+130</sup> <sub>-140</sub>
D375	600 <sup>+160</sup> <sub>-140</sub>	-	-	-	-	600 <sup>+160</sup> <sub>-140</sub>
D376	490 <sup>+60</sup> <sub>-50</sub>	-	-	-	-	490 <sup>+60</sup> <sub>-50</sub>
D377	60 <sup>+40</sup> <sub>-30</sub>	-	-	-	-	100 ± 100
D378	670 <sup>+220</sup> <sub>-260</sub>	-	-	-	-	670 <sup>+220</sup> <sub>-260</sub>
D379	-	-	-	-	-	100 ± 100
D380	1250 ± 60	320 <sup>+120</sup> <sub>-140</sub>	5620 <sup>+17160</sup> <sub>-4500</sub>	3910 <sup>+4870</sup> <sub>-2730</sub>	-	1090 ± 360
D381	-	-	-	-	-	100 ± 100
D382	-	-	-	-	-	100 ± 100
D383	140 ± 50	-	-	-	-	140 ± 50
D384	90 ± 40	-	-	-	-	100 ± 100
D385	80 <sup>+60</sup> <sub>-50</sub>	-	-	-	-	100 ± 100
D386	-	-	-	-	-	100 ± 100
D387	180 ± 80	-	-	-	-	180 ± 80
D388	50 <sup>+50</sup> <sub>-30</sub>	-	-	-	-	100 ± 100
D389	90 <sup>+30</sup> <sub>-40</sub>	-	-	1440 <sup>+1620</sup> <sub>-970</sub>	-	100 ± 100
D390	450 <sup>+70</sup> <sub>-80</sub>	-	-	-	-	450 <sup>+70</sup> <sub>-80</sub>
D391	70 ± 20	-	-	-	-	100 ± 100
D392	-	-	-	-	-	100 ± 100
D393	130 <sup>+80</sup> <sub>-70</sub>	-	-	-	-	130 <sup>+80</sup> <sub>-70</sub>
D394	40 <sup>+30</sup> <sub>-20</sub>	-	-	-	-	100 ± 100
D395	-	-	-	-	-	100 ± 100
D396	1300 <sup>+110</sup> <sub>-120</sub>	-	-	-	-	1300 <sup>+110</sup> <sub>-120</sub>
D397	-	-	-	-	-	100 ± 100
D398	70 ± 40	-	-	-	-	100 ± 100

**Table D.3.** Electron densities derived from the nebular sample.

Reference number	$n_e([\text{S II}])$ [cm <sup>-3</sup> ]	$n_e([\text{O II}])$ [cm <sup>-3</sup> ]	$n_e([\text{Fe III}])$ [cm <sup>-3</sup> ]	$n_e([\text{Cl III}])$ [cm <sup>-3</sup> ]	$n_e([\text{Ar IV}])$ [cm <sup>-3</sup> ]	Adopted $n_e$ [cm <sup>-3</sup> ]
D399	140 ± 40	-	-	-	-	140 ± 40
D400	150 ± 20	300 <sup>+50</sup> <sub>-40</sub>	-	-	-	230 ± 30
D401	180 ± 80	200 <sup>+110</sup> <sub>-80</sub>	2400 <sup>+2350</sup> <sub>-2260</sub>	410 <sup>+300</sup> <sub>-230</sub>	290 <sup>+390</sup> <sub>-230</sub>	190 <sup>+90</sup> <sub>-80</sub>
D402	350 ± 90	460 <sup>+140</sup> <sub>-130</sub>	2480 ± 1830	450 <sup>+170</sup> <sub>-160</sub>	1000 <sup>+580</sup> <sub>-480</sub>	400 ± 110
D403	1900 <sup>+430</sup> <sub>-330</sub>	2780 <sup>+500</sup> <sub>-460</sub>	7050 <sup>+4660</sup> <sub>-2540</sub>	3990 <sup>+350</sup> <sub>-340</sub>	6160 <sup>+800</sup> <sub>-1000</sub>	3190 ± 1190
D404	110 <sup>+90</sup> <sub>-60</sub>	230 <sup>+290</sup> <sub>-160</sub>	-	-	-	170 <sup>+190</sup> <sub>-110</sub>
D405	30 <sup>+40</sup> <sub>-20</sub>	30 <sup>+30</sup> <sub>-20</sub>	-	2590 <sup>+1070</sup> <sub>-760</sub>	-	100 ± 100
D406	70 <sup>+90</sup> <sub>-50</sub>	130 <sup>+30</sup> <sub>-40</sub>	-	1540 <sup>+1820</sup> <sub>-1120</sub>	-	100 ± 100
D407	220 <sup>+40</sup> <sub>-60</sub>	210 ± 20	-	490 <sup>+820</sup> <sub>-340</sub>	-	210 <sup>+30</sup> <sub>-40</sub>
D408	220 <sup>+50</sup> <sub>-30</sub>	-	-	220 <sup>+360</sup> <sub>-170</sub>	-	220 <sup>+50</sup> <sub>-30</sub>
D409	100 ± 30	-	-	2330 <sup>+860</sup> <sub>-1060</sub>	-	100 ± 100
D410	110 ± 30	-	-	590 <sup>+400</sup> <sub>-350</sub>	-	110 ± 30
D411	300 <sup>+50</sup> <sub>-40</sub>	-	-	1150 <sup>+250</sup> <sub>-270</sub>	-	300 <sup>+50</sup> <sub>-40</sub>
D412	70 ± 30	-	-	1010 <sup>+460</sup> <sub>-520</sub>	-	100 ± 100
D413	110 <sup>+50</sup> <sub>-80</sub>	220 ± 100	7340 <sup>+25130</sup> <sub>-5530</sub>	2960 <sup>+2590</sup> <sub>-1740</sub>	780 <sup>+380</sup> <sub>-410</sub>	170 <sup>+80</sup> <sub>-90</sub>
D414	110 ± 80	130 <sup>+100</sup> <sub>-70</sub>	6790 <sup>+15650</sup> <sub>-5320</sub>	2280 <sup>+2100</sup> <sub>-1320</sub>	750 <sup>+740</sup> <sub>-490</sub>	120 <sup>+90</sup> <sub>-70</sub>
D415	120 <sup>+90</sup> <sub>-60</sub>	120 <sup>+40</sup> <sub>-30</sub>	-	1140 <sup>+1820</sup> <sub>-730</sub>	-	120 <sup>+60</sup> <sub>-40</sub>
D416	140 <sup>+110</sup> <sub>-80</sub>	180 <sup>+60</sup> <sub>-50</sub>	-	-	-	160 <sup>+80</sup> <sub>-70</sub>
D417	220 <sup>+80</sup> <sub>-60</sub>	-	-	17770 <sup>+43770</sup> <sub>-14210</sub>	-	220 <sup>+80</sup> <sub>-60</sub>
D418	200 <sup>+40</sup> <sub>-50</sub>	-	-	1010 <sup>+1580</sup> <sub>-670</sub>	-	200 <sup>+40</sup> <sub>-50</sub>
D419	270 ± 110	210 <sup>+60</sup> <sub>-50</sub>	-	410 <sup>+780</sup> <sub>-310</sub>	-	240 <sup>+90</sup> <sub>-80</sub>
D420	190 <sup>+30</sup> <sub>-40</sub>	-	-	640 <sup>+1230</sup> <sub>-480</sub>	-	190 <sup>+30</sup> <sub>-40</sub>
D421	250 ± 50	-	-	400 <sup>+50</sup> <sub>-10</sub>	-	250 ± 50
D422	-	-	-	-	-	100 ± 100
D423	-	-	-	-	-	100 ± 100
D424	250 <sup>+70</sup> <sub>-60</sub>	-	-	-	-	250 <sup>+70</sup> <sub>-60</sub>
D425	90 ± 30	-	-	670 <sup>+520</sup> <sub>-470</sub>	-	100 ± 100
D426	110 <sup>+30</sup> <sub>-40</sub>	-	-	230 <sup>+300</sup> <sub>-170</sub>	-	110 <sup>+30</sup> <sub>-40</sub>
D427	150 ± 30	-	-	100 <sup>+20</sup> <sub>-10</sub>	-	150 ± 30
D428	320 <sup>+30</sup> <sub>-40</sub>	-	-	-	-	320 <sup>+30</sup> <sub>-40</sub>
D429	50 <sup>+50</sup> <sub>-20</sub>	-	-	-	-	100 ± 100
D430	300 <sup>+40</sup> <sub>-50</sub>	-	-	590 <sup>+710</sup> <sub>-470</sub>	-	300 <sup>+40</sup> <sub>-50</sub>
D431	180 <sup>+40</sup> <sub>-60</sub>	-	-	-	-	180 <sup>+40</sup> <sub>-60</sub>
D432	150 <sup>+40</sup> <sub>-30</sub>	-	-	510 <sup>+710</sup> <sub>-330</sub>	-	150 <sup>+40</sup> <sub>-30</sub>
D433	100 ± 60	-	-	-	-	100 ± 60
D434	150 <sup>+30</sup> <sub>-40</sub>	-	-	1030 <sup>+1490</sup> <sub>-590</sub>	-	150 <sup>+30</sup> <sub>-40</sub>
D435	150 <sup>+50</sup> <sub>-40</sub>	50 ± 30	-	-	-	100 ± 40
D436	130 <sup>+80</sup> <sub>-90</sub>	60 ± 40	-	380 <sup>+300</sup> <sub>-230</sub>	-	100 ± 100
D437	320 ± 60	-	-	-	-	320 ± 60
D438	170 <sup>+30</sup> <sub>-40</sub>	-	-	-	-	170 <sup>+30</sup> <sub>-40</sub>
D439	20 <sup>+10</sup> <sub>-20</sub>	-	-	-	-	100 ± 100
D440	30 <sup>+30</sup> <sub>-20</sub>	-	-	-	-	100 ± 100
D441	240 <sup>+50</sup> <sub>-40</sub>	-	-	-	-	240 <sup>+50</sup> <sub>-40</sub>
D442	-	-	-	-	-	100 ± 100
D443	30 ± 10	-	-	-	-	100 ± 100
D444	50 <sup>+30</sup> <sub>-20</sub>	-	-	-	-	100 ± 100
D445	50 ± 30	-	-	-	-	100 ± 100
D446	60 <sup>+40</sup> <sub>-30</sub>	-	-	-	-	100 ± 100
D447	160 ± 90	180 ± 60	-	-	-	170 <sup>+80</sup> <sub>-70</sub>
D448	140 <sup>+130</sup> <sub>-80</sub>	60 <sup>+70</sup> <sub>-30</sub>	-	-	-	100 ± 100
D449	170 <sup>+30</sup> <sub>-50</sub>	-	-	26350 <sup>+76720</sup> <sub>-18600</sub>	-	170 <sup>+30</sup> <sub>-50</sub>
D450	10 <sup>+10</sup> <sub>-0</sub>	-	-	-	-	100 ± 100
D451	290 <sup>+80</sup> <sub>-70</sub>	-	-	-	-	290 <sup>+80</sup> <sub>-70</sub>
D452	830 <sup>+380</sup> <sub>-280</sub>	1530 <sup>+1050</sup> <sub>-700</sub>	-	-	6550 <sup>+6790</sup> <sub>-4250</sub>	1180 <sup>+710</sup> <sub>-490</sub>



**Table D.4.** Measured electron temperatures from the nebular sample.

Reference number	$T_e(\text{[N II]})$ [K]	$T_e(\text{[S III]})$ [K]	$T_e(\text{[O III]})$ [K]
D1	-	-	11410 <sup>+320</sup> <sub>-220</sub>
D2	-	-	13070 <sup>+200</sup> <sub>-260</sub>
D3	-	14340 <sup>+430</sup> <sub>-780</sub>	14310 <sup>+230</sup> <sub>-150</sub>
D4	-	13970 <sup>+1160</sup> <sub>-1440</sub>	14430 <sup>+430</sup> <sub>-360</sub>
D5	-	-	13300 <sup>+130</sup> <sub>-160</sub>
D6	-	-	12490 <sup>+130</sup> <sub>-290</sub>
D7	-	-	11590 <sup>+190</sup> <sub>-230</sub>
D8	-	-	11450 <sup>+490</sup> <sub>-530</sub>
D9	-	-	12090 <sup>+300</sup> <sub>-310</sub>
D10	-	12780 <sup>+450</sup> <sub>-420</sub>	12780 <sup>+230</sup> <sub>-150</sub>
D11	-	12150 <sup>+360</sup> <sub>-320</sub>	13420 <sup>+220</sup> <sub>-200</sub>
D12	-	-	12260 <sup>+180</sup> <sub>-200</sub>
D13	-	-	10120 <sup>+820</sup> <sub>-700</sub>
D14	-	13270 <sup>+670</sup> <sub>-680</sub>	13070 <sup>+270</sup> <sub>-310</sub>
D15	-	-	11520 <sup>+300</sup> <sub>-430</sub>
D16	-	-	13010 <sup>+570</sup> <sub>-590</sub>
D17	-	-	11930 <sup>+410</sup> <sub>-440</sub>
D18	-	-	9700 <sup>+790</sup> <sub>-700</sub>
D19	-	-	18860 <sup>+450</sup> <sub>-570</sub>
D20	-	-	19120 <sup>+600</sup> <sub>-470</sub>
D21	-	13290 <sup>+1070</sup> <sub>-860</sub>	14270 <sup>+250</sup> <sub>-310</sub>
D22	-	19060 <sup>+4600</sup> <sub>-4190</sub>	17380 <sup>+570</sup> <sub>-520</sub>
D23	-	-	11690 <sup>+440</sup> <sub>-510</sub>
D24	-	-	11720 <sup>+440</sup> <sub>-430</sub>
D25	-	-	14650 <sup>+380</sup> <sub>-350</sub>
D26	-	-	10200 <sup>+760</sup> <sub>-1320</sub>
D27	-	11490 <sup>+470</sup> <sub>-440</sub>	12470 <sup>+200</sup> <sub>-240</sub>
D28	-	-	15660 <sup>+100</sup> <sub>-70</sub>
D29	-	-	12960 <sup>+340</sup> <sub>-290</sub>
D30	-	-	12340 <sup>+480</sup> <sub>-390</sub>
D31	-	-	12780 <sup>+480</sup> <sub>-490</sub>
D32	-	17350 <sup>+620</sup> <sub>-920</sub>	9970 <sup>+290</sup> <sub>-280</sub>
D33	-	-	9960 <sup>+1000</sup> <sub>-1090</sub>
D34	-	9940 <sup>+1520</sup> <sub>-1060</sub>	10660 <sup>+1000</sup> <sub>-1150</sub>
D35	-	12560 <sup>+660</sup> <sub>-750</sub>	13400 <sup>+350</sup> <sub>-280</sub>
D36	-	-	12550 <sup>+250</sup> <sub>-280</sub>
D37	-	-	10190 <sup>+950</sup> <sub>-1310</sub>
D38	-	-	14970 <sup>+290</sup> <sub>-220</sub>
D39	-	-	12940 <sup>+250</sup> <sub>-280</sub>
D40	-	-	14190 <sup>+200</sup> <sub>-190</sub>
D41	-	-	20000 <sup>+380</sup> <sub>-330</sub>
D42	-	11230 <sup>+830</sup> <sub>-650</sub>	11200 <sup>+330</sup> <sub>-370</sub>
D43	-	10410 <sup>+840</sup> <sub>-890</sub>	10190 <sup>+610</sup> <sub>-1210</sub>
D44	-	12250 <sup>+630</sup> <sub>-1010</sub>	10920 <sup>+350</sup> <sub>-450</sub>
D45	-	9430 <sup>+1490</sup> <sub>-1260</sub>	-
D46	-	-	10630 <sup>+330</sup> <sub>-350</sub>
D47	-	-	9920 <sup>+930</sup> <sub>-970</sub>
D48	-	8960 <sup>+390</sup> <sub>-280</sub>	9830 <sup>+260</sup> <sub>-350</sub>
D49	-	-	10320 <sup>+420</sup> <sub>-380</sub>
D50	-	-	13040 <sup>+460</sup> <sub>-440</sub>
D51	-	-	10700 <sup>+500</sup> <sub>-350</sub>
D52	-	-	13910 <sup>+470</sup> <sub>-580</sub>
D53	-	-	14090 <sup>+100</sup> <sub>-110</sub>
D54	-	-	16040 <sup>+130</sup> <sub>-120</sub>
D55	-	-	11110 <sup>+580</sup> <sub>-800</sub>

**Table D.4.** Measured electron temperatures from the nebular sample.

Reference number	$T_e([\text{N II}])$ [K]	$T_e([\text{S III}])$ [K]	$T_e([\text{O III}])$ [K]
D56	-	-	13440 <sup>+60</sup> <sub>-50</sub>
D57	-	10200 <sup>+380</sup> <sub>-630</sub>	10240 <sup>+510</sup> <sub>-620</sub>
D58	-	11340 <sup>+370</sup> <sub>-420</sub>	11190 ± 210
D59	-	-	12880 <sup>+140</sup> <sub>-90</sub>
D60	-	-	11190 <sup>+420</sup> <sub>-360</sub>
D61	-	-	11230 <sup>+450</sup> <sub>-460</sub>
D62	-	-	10750 <sup>+390</sup> <sub>-480</sub>
D63	-	9810 <sup>+250</sup> <sub>-270</sub>	9340 <sup>+180</sup> <sub>-160</sub>
D64	-	9340 <sup>+260</sup> <sub>-250</sub>	8940 <sup>+420</sup> <sub>-350</sub>
D65	-	12670 <sup>+300</sup> <sub>-540</sub>	18370 <sup>+280</sup> <sub>-480</sub>
D66	-	-	13640 <sup>+470</sup> <sub>-390</sub>
D67	-	-	14520 <sup>+170</sup> <sub>-160</sub>
D68	-	9300 <sup>+270</sup> <sub>-290</sub>	9660 <sup>+220</sup> <sub>-270</sub>
D69	-	-	14220 <sup>+450</sup> <sub>-420</sub>
D70	-	-	12310 <sup>+340</sup> <sub>-290</sub>
D71	7760 <sup>+510</sup> <sub>-680</sub>	6880 <sup>+680</sup> <sub>-870</sub>	-
D72	-	-	16390 <sup>+170</sup> <sub>-180</sub>
D73	-	-	14040 <sup>+320</sup> <sub>-220</sub>
D74	-	-	10850 ± 70
D75	-	-	17640 <sup>+260</sup> <sub>-230</sub>
D76	-	-	12450 <sup>+130</sup> <sub>-100</sub>
D77	-	-	11950 <sup>+160</sup> <sub>-170</sub>
D78	-	-	18110 <sup>+170</sup> <sub>-220</sub>
D79	-	-	19070 ± 450
D80	-	-	19020 <sup>+270</sup> <sub>-250</sub>
D81	14540 <sup>+1980</sup> <sub>-2750</sub>	-	12460 <sup>+210</sup> <sub>-220</sub>
D82	-	-	15780 <sup>+140</sup> <sub>-190</sub>
D83	12020 <sup>+460</sup> <sub>-570</sub>	15270 <sup>+500</sup> <sub>-490</sub>	16170 <sup>+250</sup> <sub>-290</sub>
D84	-	11900 <sup>+1210</sup> <sub>-1440</sub>	12460 <sup>+300</sup> <sub>-380</sub>
D85	-	7210 ± 140	7390 <sup>+280</sup> <sub>-330</sub>
D86	-	8050 <sup>+270</sup> <sub>-300</sub>	8040 <sup>+290</sup> <sub>-350</sub>
D87	-	-	12930 <sup>+70</sup> <sub>-110</sub>
D88	-	-	19890 <sup>+260</sup> <sub>-230</sub>
D89	-	-	18050 <sup>+300</sup> <sub>-320</sub>
D90	-	10890 <sup>+470</sup> <sub>-340</sub>	12910 <sup>+670</sup> <sub>-690</sub>
D91	-	-	11770 ± 50
D92	11100 <sup>+360</sup> <sub>-380</sub>	12970 <sup>+360</sup> <sub>-400</sub>	12500 <sup>+240</sup> <sub>-230</sub>
D93	-	13270 ± 520	12740 <sup>+320</sup> <sub>-290</sub>
D94	-	-	18390 <sup>+100</sup> <sub>-140</sub>
D95	-	-	14060 <sup>+290</sup> <sub>-300</sub>
D96	-	-	15480 <sup>+310</sup> <sub>-380</sub>
D97	-	-	17860 <sup>+210</sup> <sub>-190</sub>
D98	-	-	19230 <sup>+260</sup> <sub>-210</sub>
D99	-	14820 <sup>+620</sup> <sub>-1020</sub>	15330 <sup>+210</sup> <sub>-200</sub>
D100	-	17950 <sup>+350</sup> <sub>-520</sub>	19160 <sup>+250</sup> <sub>-220</sub>
D101	12120 <sup>+1270</sup> <sub>-1500</sub>	-	13370 ± 130
D102	-	-	13320 <sup>+80</sup> <sub>-120</sub>
D103	-	17890 <sup>+1160</sup> <sub>-970</sub>	17820 <sup>+220</sup> <sub>-180</sub>
D104	-	-	13160 <sup>+180</sup> <sub>-170</sub>
D105	-	-	16180 ± 310
D106	14330 <sup>+590</sup> <sub>-550</sub>	12650 <sup>+390</sup> <sub>-350</sub>	12360 <sup>+150</sup> <sub>-130</sub>
D107	-	-	24430 <sup>+470</sup> <sub>-600</sub>
D108	-	-	12110 ± 80
D109	-	14230 <sup>+600</sup> <sub>-540</sub>	12280 <sup>+250</sup> <sub>-200</sub>
D110	-	-	18010 <sup>+120</sup> <sub>-170</sub>
D111	-	-	14760 <sup>+70</sup> <sub>-80</sub>

**Table D.4.** Measured electron temperatures from the nebular sample.

Reference number	$T_e(\text{[N II]})$ [K]	$T_e(\text{[S III]})$ [K]	$T_e(\text{[O III]})$ [K]
D112	-	-	17180 <sup>+220</sup> <sub>-150</sub>
D113	-	-	16270 <sup>+100</sup> <sub>-130</sub>
D114	-	-	15600 ± 130
D115	10340 <sup>+210</sup> <sub>-230</sub>	10040 ± 80	9900 ± 70
D116	9800 ± 350	9300 <sup>+250</sup> <sub>-230</sub>	9120 <sup>+120</sup> <sub>-130</sub>
D117	9830 <sup>+70</sup> <sub>-110</sub>	10550 <sup>+190</sup> <sub>-270</sub>	9160 <sup>+120</sup> <sub>-110</sub>
D118	10510 <sup>+300</sup> <sub>-370</sub>	11510 <sup>+300</sup> <sub>-350</sub>	11330 <sup>+150</sup> <sub>-130</sub>
D119	10180 <sup>+500</sup> <sub>-460</sub>	9540 <sup>+320</sup> <sub>-340</sub>	9530 <sup>+170</sup> <sub>-190</sub>
D120	8140 <sup>+180</sup> <sub>-170</sub>	7590 <sup>+590</sup> <sub>-760</sub>	7620 ± 210
D121	7570 <sup>+180</sup> <sub>-130</sub>	6920 ± 160	7380 <sup>+170</sup> <sub>-150</sub>
D122	7790 <sup>+330</sup> <sub>-400</sub>	-	7250 <sup>+510</sup> <sub>-570</sub>
D123	7540 <sup>+380</sup> <sub>-390</sub>	7630 <sup>+340</sup> <sub>-390</sub>	-
D124	9360 <sup>+800</sup> <sub>-760</sub>	11350 <sup>+740</sup> <sub>-860</sub>	9010 <sup>+230</sup> <sub>-360</sub>
D125	7380 <sup>+370</sup> <sub>-490</sub>	7550 <sup>+250</sup> <sub>-260</sub>	-
D126	7630 <sup>+350</sup> <sub>-360</sub>	7400 <sup>+330</sup> <sub>-370</sub>	-
D127	-	-	10860 <sup>+320</sup> <sub>-420</sub>
D128	8420 <sup>+150</sup> <sub>-230</sub>	8990 <sup>+130</sup> <sub>-220</sub>	7760 <sup>+60</sup> <sub>-70</sub>
D129	-	8900 <sup>+390</sup> <sub>-500</sub>	9080 <sup>+180</sup> <sub>-190</sub>
D130	-	-	11940 <sup>+230</sup> <sub>-220</sub>
D131	-	-	10740 ± 130
D132	-	-	11080 <sup>+230</sup> <sub>-210</sub>
D133	-	-	10770 <sup>+180</sup> <sub>-220</sub>
D134	9990 <sup>+1210</sup> <sub>-1630</sub>	9920 <sup>+270</sup> <sub>-240</sub>	10670 <sup>+70</sup> <sub>-80</sub>
D135	10820 ± 260	-	10570 <sup>+130</sup> <sub>-150</sub>
D136	9500 <sup>+370</sup> <sub>-390</sub>	11200 <sup>+270</sup> <sub>-320</sub>	9760 <sup>+70</sup> <sub>-80</sub>
D137	-	-	11060 <sup>+150</sup> <sub>-210</sub>
D138	8870 <sup>+710</sup> <sub>-750</sub>	9160 <sup>+930</sup> <sub>-810</sub>	8990 <sup>+330</sup> <sub>-220</sub>
D139	-	7710 <sup>+390</sup> <sub>-460</sub>	-
D140	8590 <sup>+320</sup> <sub>-340</sub>	7500 <sup>+390</sup> <sub>-490</sub>	8420 <sup>+230</sup> <sub>-270</sub>
D141	10960 <sup>+610</sup> <sub>-860</sub>	9380 ± 290	9650 <sup>+210</sup> <sub>-150</sub>
D142	7920 <sup>+720</sup> <sub>-690</sub>	8090 <sup>+440</sup> <sub>-490</sub>	-
D143	7930 <sup>+500</sup> <sub>-580</sub>	-	-
D144	-	-	8260 <sup>+150</sup> <sub>-180</sub>
D145	-	14960 <sup>+720</sup> <sub>-1160</sub>	12940 <sup>+120</sup> <sub>-150</sub>
D146	-	-	8430 ± 70
D147	7020 <sup>+370</sup> <sub>-300</sub>	-	-
D148	7230 <sup>+280</sup> <sub>-290</sub>	-	-
D149	-	12810 <sup>+900</sup> <sub>-510</sub>	11480 <sup>+130</sup> <sub>-120</sub>
D150	6300 <sup>+400</sup> <sub>-420</sub>	5720 <sup>+440</sup> <sub>-430</sub>	-
D151	7640 <sup>+460</sup> <sub>-820</sub>	-	-
D152	8460 <sup>+390</sup> <sub>-510</sub>	-	-
D153	-	-	13300 <sup>+160</sup> <sub>-250</sub>
D154	-	-	13290 <sup>+190</sup> <sub>-180</sub>
D155	6830 <sup>+410</sup> <sub>-460</sub>	-	-
D156	10610 <sup>+1110</sup> <sub>-1300</sub>	14680 <sup>+560</sup> <sub>-620</sub>	11360 <sup>+110</sup> <sub>-150</sub>
D157	8420 <sup>+340</sup> <sub>-330</sub>	9470 <sup>+280</sup> <sub>-380</sub>	8560 <sup>+100</sup> <sub>-110</sub>
D158	8220 <sup>+390</sup> <sub>-430</sub>	8050 <sup>+430</sup> <sub>-400</sub>	8940 <sup>+480</sup> <sub>-530</sub>
D159	-	16030 <sup>+950</sup> <sub>-1050</sub>	13590 <sup>+150</sup> <sub>-130</sub>
D160	7300 <sup>+410</sup> <sub>-580</sub>	7970 <sup>+850</sup> <sub>-1060</sub>	-
D161	7180 <sup>+380</sup> <sub>-380</sub>	7110 <sup>+540</sup> <sub>-510</sub>	-
D162	7350 <sup>+430</sup> <sub>-520</sub>	7930 <sup>+490</sup> <sub>-630</sub>	-
D163	8030 <sup>+310</sup> <sub>-410</sub>	-	-
D164	7410 <sup>+310</sup> <sub>-370</sub>	6710 <sup>+160</sup> <sub>-220</sub>	-
D165	9450 <sup>+380</sup> <sub>-320</sub>	11160 <sup>+260</sup> <sub>-330</sub>	9760 <sup>+70</sup> <sub>-90</sub>
D166	9210 <sup>+230</sup> <sub>-250</sub>	11090 <sup>+330</sup> <sub>-180</sub>	9280 <sup>+70</sup> <sub>-60</sub>
D167	9400 <sup>+330</sup> <sub>-350</sub>	11210 ± 260	9560 <sup>+80</sup> <sub>-60</sub>

**Table D.4.** Measured electron temperatures from the nebular sample.

Reference number	$T_e(\text{[N II]})$ [K]	$T_e(\text{[S III]})$ [K]	$T_e(\text{[O III]})$ [K]
D168	10520 <sup>+420</sup> <sub>-500</sub>	-	9190 <sup>+140</sup> <sub>-160</sub>
D169	8620 <sup>+380</sup> <sub>-540</sub>	7790 <sup>+410</sup> <sub>-340</sub>	9680 <sup>+130</sup> <sub>-150</sub>
D170	40020 <sup>+13350</sup> <sub>-5930</sub>	-	9440 ± 430
D171	-	-	8830 <sup>+200</sup> <sub>-240</sub>
D172	9730 <sup>+250</sup> <sub>-320</sub>	-	9410 <sup>+70</sup> <sub>-60</sub>
D173	10220 <sup>+190</sup> <sub>-170</sub>	-	9580 <sup>+80</sup> <sub>-100</sub>
D174	8370 <sup>+350</sup> <sub>-400</sub>	9010 <sup>+130</sup> <sub>-190</sub>	8520 <sup>+150</sup> <sub>-110</sub>
D175	8500 <sup>+530</sup> <sub>-550</sub>	8740 <sup>+460</sup> <sub>-500</sub>	9170 <sup>+180</sup> <sub>-200</sub>
D176	8800 <sup>+200</sup> <sub>-140</sub>	9420 <sup>+310</sup> <sub>-320</sub>	8730 <sup>+50</sup> <sub>-60</sub>
D177	9090 <sup>+340</sup> <sub>-350</sub>	-	8450 <sup>+280</sup> <sub>-180</sub>
D178	-	-	9510 <sup>+100</sup> <sub>-70</sub>
D179	-	-	9150 ± 80
D180	-	-	13210 <sup>+150</sup> <sub>-200</sub>
D181	-	-	13750 <sup>+300</sup> <sub>-360</sub>
D182	11050 <sup>+910</sup> <sub>-710</sub>	-	12740 <sup>+180</sup> <sub>-160</sub>
D183	-	-	13790 <sup>+150</sup> <sub>-170</sub>
D184	9240 <sup>+250</sup> <sub>-340</sub>	-	11190 <sup>+240</sup> <sub>-220</sub>
D185	9680 <sup>+380</sup> <sub>-400</sub>	9740 <sup>+360</sup> <sub>-460</sub>	9520 <sup>+330</sup> <sub>-450</sub>
D186	7530 <sup>+160</sup> <sub>-170</sub>	7580 <sup>+220</sup> <sub>-160</sub>	12440 <sup>+340</sup> <sub>-300</sub>
D187	8090 <sup>+210</sup> <sub>-320</sub>	-	7950 <sup>+570</sup> <sub>-750</sub>
D188	9280 <sup>+170</sup> <sub>-160</sub>	-	8340 ± 160
D189	9100 <sup>+740</sup> <sub>-890</sub>	8020 <sup>+200</sup> <sub>-190</sub>	7660 <sup>+370</sup> <sub>-490</sub>
D190	8050 <sup>+330</sup> <sub>-220</sub>	7960 <sup>+230</sup> <sub>-180</sub>	8940 <sup>+970</sup> <sub>-870</sub>
D191	7840 <sup>+200</sup> <sub>-310</sub>	-	-
D192	7690 <sup>+390</sup> <sub>-390</sub>	-	-
D193	8500 <sup>+810</sup> <sub>-560</sub>	-	-
D194	9640 <sup>+560</sup> <sub>-570</sub>	-	8250 <sup>+400</sup> <sub>-350</sub>
D195	11010 <sup>+400</sup> <sub>-460</sub>	10520 ± 220	11260 <sup>+230</sup> <sub>-190</sub>
D196	9670 <sup>+240</sup> <sub>-390</sub>	11840 <sup>+430</sup> <sub>-460</sub>	9060 ± 180
D197	10620 <sup>+1120</sup> <sub>-730</sub>	-	-
D198	10720 <sup>+700</sup> <sub>-650</sub>	-	10710 <sup>+360</sup> <sub>-340</sub>
D199	8340 <sup>+140</sup> <sub>-150</sub>	-	7310 <sup>+340</sup> <sub>-290</sub>
D200	8930 <sup>+260</sup> <sub>-240</sub>	8600 <sup>+230</sup> <sub>-240</sub>	8360 <sup>+140</sup> <sub>-160</sub>
D201	8720 <sup>+170</sup> <sub>-230</sub>	-	8110 <sup>+170</sup> <sub>-180</sub>
D202	8120 <sup>+940</sup> <sub>-1220</sub>	7310 <sup>+400</sup> <sub>-470</sub>	-
D203	7440 <sup>+290</sup> <sub>-210</sub>	7380 <sup>+360</sup> <sub>-210</sub>	-
D204	-	10700 <sup>+730</sup> <sub>-710</sub>	-
D205	10490 <sup>+490</sup> <sub>-530</sub>	-	9850 <sup>+250</sup> <sub>-270</sub>
D206	8420 <sup>+230</sup> <sub>-270</sub>	9400 <sup>+150</sup> <sub>-160</sub>	8150 <sup>+150</sup> <sub>-210</sub>
D207	9210 <sup>+340</sup> <sub>-300</sub>	8730 <sup>+160</sup> <sub>-130</sub>	8800 ± 130
D208	7750 <sup>+290</sup> <sub>-340</sub>	7920 <sup>+200</sup> <sub>-300</sub>	7780 ± 500
D209	6710 <sup>+170</sup> <sub>-200</sub>	6420 <sup>+360</sup> <sub>-320</sub>	-
D210	6960 <sup>+150</sup> <sub>-200</sub>	6270 <sup>+120</sup> <sub>-140</sub>	-
D211	7310 <sup>+350</sup> <sub>-320</sub>	6410 <sup>+390</sup> <sub>-460</sub>	-
D212	6580 <sup>+70</sup> <sub>-80</sub>	5840 <sup>+100</sup> <sub>-120</sub>	-
D213	6740 <sup>+140</sup> <sub>-250</sub>	5960 <sup>+240</sup> <sub>-280</sub>	-
D214	6020 <sup>+110</sup> <sub>-130</sub>	5430 <sup>+180</sup> <sub>-230</sub>	-
D215	5640 <sup>+300</sup> <sub>-370</sub>	-	-
D216	6430 <sup>+550</sup> <sub>-580</sub>	-	-
D217	8970 <sup>+230</sup> <sub>-240</sub>	7530 ± 580	21620 <sup>+1890</sup> <sub>-3170</sub>
D218	6280 <sup>+190</sup> <sub>-370</sub>	7130 <sup>+360</sup> <sub>-490</sub>	-
D219	6550 <sup>+410</sup> <sub>-570</sub>	-	-
D220	8900 <sup>+200</sup> <sub>-210</sub>	8160 <sup>+120</sup> <sub>-150</sub>	7960 <sup>+80</sup> <sub>-100</sub>
D221	8240 <sup>+130</sup> <sub>-140</sub>	8310 <sup>+210</sup> <sub>-180</sub>	7800 <sup>+250</sup> <sub>-270</sub>
D222	9980 <sup>+190</sup> <sub>-230</sub>	9230 <sup>+190</sup> <sub>-240</sub>	8420 <sup>+60</sup> <sub>-50</sub>
D223	8530 <sup>+150</sup> <sub>-90</sub>	8100 <sup>+110</sup> <sub>-130</sub>	8010 <sup>+50</sup> <sub>-40</sub>



**Table D.4.** Measured electron temperatures from the nebular sample.

Reference number	$T_e([\text{N II}])$ [K]	$T_e([\text{S III}])$ [K]	$T_e([\text{O III}])$ [K]
D224	9930 <sup>+190</sup> <sub>-210</sub>	9170 <sup>+140</sup> <sub>-230</sub>	8410 ± 60
D225	8490 <sup>+110</sup> <sub>-120</sub>	8030 <sup>+170</sup> <sub>-150</sub>	8100 <sup>+90</sup> <sub>-70</sub>
D226	9800 <sup>+200</sup> <sub>-140</sub>	8730 <sup>+170</sup> <sub>-220</sub>	8510 ± 60
D227	10140 <sup>+190</sup> <sub>-210</sub>	9090 <sup>+220</sup> <sub>-260</sub>	8530 <sup>+50</sup> <sub>-80</sub>
D228	9910 <sup>+200</sup> <sub>-170</sub>	9010 <sup>+200</sup> <sub>-190</sub>	8400 ± 50
D229	9930 <sup>+220</sup> <sub>-160</sub>	8770 <sup>+130</sup> <sub>-190</sub>	8340 <sup>+50</sup> <sub>-60</sub>
D230	8220 <sup>+160</sup> <sub>-260</sub>	7950 <sup>+290</sup> <sub>-250</sub>	-
D231	9550 <sup>+220</sup> <sub>-260</sub>	9140 <sup>+300</sup> <sub>-270</sub>	8340 <sup>+60</sup> <sub>-80</sub>
D232	9980 <sup>+240</sup> <sub>-250</sub>	9540 <sup>+360</sup> <sub>-470</sub>	8370 ± 50
D233	9580 <sup>+400</sup> <sub>-420</sub>	9180 <sup>+250</sup> <sub>-220</sub>	8160 <sup>+200</sup> <sub>-220</sub>
D234	8380 <sup>+100</sup> <sub>-110</sub>	8650 <sup>+180</sup> <sub>-150</sub>	8030 <sup>+70</sup> <sub>-80</sub>
D235	-	10980 <sup>+200</sup> <sub>-240</sub>	9310 <sup>+170</sup> <sub>-140</sub>
D236	8810 <sup>+160</sup> <sub>-210</sub>	8780 <sup>+450</sup> <sub>-360</sub>	8450 <sup>+30</sup> <sub>-40</sub>
D237	11270 <sup>+620</sup> <sub>-600</sub>	9070 <sup>+230</sup> <sub>-300</sub>	9020 <sup>+140</sup> <sub>-160</sub>
D238	8650 <sup>+250</sup> <sub>-350</sub>	-	8210 <sup>+130</sup> <sub>-120</sub>
D239	9830 <sup>+120</sup> <sub>-150</sub>	-	-
D240	10590 <sup>+260</sup> <sub>-280</sub>	-	9990 <sup>+260</sup> <sub>-380</sub>
D241	8200 ± 90	-	-
D242	9310 <sup>+430</sup> <sub>-420</sub>	8250 <sup>+80</sup> <sub>-110</sub>	9080 <sup>+290</sup> <sub>-380</sub>
D243	-	-	11470 <sup>+820</sup> <sub>-1290</sub>
D244	8100 <sup>+150</sup> <sub>-230</sub>	-	-
D245	7470 <sup>+250</sup> <sub>-240</sub>	-	-
D246	8320 <sup>+410</sup> <sub>-460</sub>	-	-
D247	9510 <sup>+340</sup> <sub>-350</sub>	-	9220 <sup>+330</sup> <sub>-410</sub>
D248	7790 <sup>+130</sup> <sub>-220</sub>	-	-
D249	9290 <sup>+210</sup> <sub>-200</sub>	9280 <sup>+170</sup> <sub>-210</sub>	8920 <sup>+130</sup> <sub>-90</sub>
D250	-	-	10150 <sup>+530</sup> <sub>-550</sub>
D251	-	-	10990 <sup>+840</sup> <sub>-760</sub>
D252	12480 <sup>+1970</sup> <sub>-1990</sub>	-	12120 <sup>+100</sup> <sub>-110</sub>
D253	-	14630 <sup>+840</sup> <sub>-770</sub>	13290 <sup>+230</sup> <sub>-260</sub>
D254	-	-	13340 <sup>+60</sup> <sub>-80</sub>
D255	-	-	13950 ± 150
D256	12060 <sup>+1710</sup> <sub>-1930</sub>	-	10920 ± 70
D257	10880 <sup>+1020</sup> <sub>-1070</sub>	-	10690 <sup>+70</sup> <sub>-60</sub>
D258	-	-	11820 <sup>+450</sup> <sub>-390</sub>
D259	-	-	15280 <sup>+130</sup> <sub>-150</sub>
D260	-	-	10010 ± 100
D261	-	-	9990 ± 100
D262	11170 <sup>+420</sup> <sub>-560</sub>	-	10100 <sup>+120</sup> <sub>-140</sub>
D263	-	15110 <sup>+650</sup> <sub>-710</sub>	14830 <sup>+660</sup> <sub>-760</sub>
D264	-	12980 <sup>+320</sup> <sub>-300</sub>	15950 <sup>+300</sup> <sub>-350</sub>
D265	-	-	15070 <sup>+380</sup> <sub>-340</sub>
D266	10790 <sup>+1330</sup> <sub>-1110</sub>	-	11570 <sup>+120</sup> <sub>-120</sub>
D267	-	13410 <sup>+330</sup> <sub>-300</sub>	14370 <sup>+340</sup> <sub>-420</sub>
D268	-	-	13430 <sup>+110</sup> <sub>-120</sub>
D269	-	-	13690 <sup>+320</sup> <sub>-300</sub>
D270	-	-	12060 <sup>+510</sup> <sub>-460</sub>
D271	-	-	15660 <sup>+240</sup> <sub>-210</sub>
D272	-	10410 <sup>+380</sup> <sub>-500</sub>	11290 <sup>+890</sup> <sub>-740</sub>
D273	-	12620 <sup>+450</sup> <sub>-420</sub>	14760 <sup>+550</sup> <sub>-500</sub>
D274	-	10230 <sup>+300</sup> <sub>-380</sub>	11190 <sup>+890</sup> <sub>-850</sub>
D275	-	-	15600 <sup>+100</sup> <sub>-130</sub>
D276	-	-	14640 <sup>+150</sup> <sub>-180</sub>
D277	-	-	13780 <sup>+180</sup> <sub>-170</sub>
D278	-	-	12840 <sup>+100</sup> <sub>-90</sub>
D279	-	-	12250 <sup>+400</sup> <sub>-370</sub>

**Table D.4.** Measured electron temperatures from the nebular sample.

Reference number	$T_e([\text{N II}])$ [K]	$T_e([\text{S III}])$ [K]	$T_e([\text{O III}])$ [K]
D280	-	-	12570 <sup>+110</sup> <sub>-150</sub>
D281	-	-	11670 <sup>+590</sup> <sub>-820</sub>
D282	9660 <sup>+690</sup> <sub>-820</sub>	-	8440 <sup>+580</sup> <sub>-560</sub>
D283	13350 <sup>+1520</sup> <sub>-1480</sub>	-	16010 <sup>+390</sup> <sub>-360</sub>
D284	10740 <sup>+1140</sup> <sub>-2120</sub>	-	11280 <sup>+120</sup> <sub>-160</sub>
D285	8380 <sup>+220</sup> <sub>-330</sub>	-	8110 <sup>+380</sup> <sub>-390</sub>
D286	8110 <sup>+410</sup> <sub>-450</sub>	-	8730 <sup>+300</sup> <sub>-310</sub>
D287	8990 <sup>+470</sup> <sub>-420</sub>	-	8650 <sup>+110</sup> <sub>-150</sub>
D288	8890 <sup>+250</sup> <sub>-320</sub>	-	8210 <sup>+230</sup> <sub>-150</sub>
D289	9110 <sup>+860</sup> <sub>-1000</sub>	9420 <sup>+300</sup> <sub>-390</sub>	8510 ± 240
D290	-	-	11050 <sup>+110</sup> <sub>-120</sub>
D291	8540 <sup>+840</sup> <sub>-940</sub>	8810 <sup>+290</sup> <sub>-240</sub>	8220 ± 300
D292	8660 <sup>+730</sup> <sub>-560</sub>	8990 <sup>+310</sup> <sub>-350</sub>	8790 <sup>+230</sup> <sub>-310</sub>
D293	8980 <sup>+1080</sup> <sub>-970</sub>	8070 <sup>+170</sup> <sub>-320</sub>	7990 ± 300
D294	-	9600 <sup>+390</sup> <sub>-700</sub>	8260 <sup>+310</sup> <sub>-440</sub>
D295	8710 <sup>+1030</sup> <sub>-1140</sub>	8260 <sup>+480</sup> <sub>-600</sub>	7870 <sup>+360</sup> <sub>-520</sub>
D296	-	11310 <sup>+420</sup> <sub>-570</sub>	10310 <sup>+140</sup> <sub>-210</sub>
D297	-	9830 <sup>+120</sup> <sub>-100</sub>	11000 ± 80
D298	6990 <sup>+570</sup> <sub>-650</sub>	9570 <sup>+1000</sup> <sub>-1370</sub>	-
D299	-	-	9630 <sup>+230</sup> <sub>-260</sub>
D300	6200 <sup>+450</sup> <sub>-500</sub>	-	-
D301	7810 <sup>+270</sup> <sub>-380</sub>	6800 <sup>+360</sup> <sub>-380</sub>	-
D302	7330 <sup>+380</sup> <sub>-340</sub>	-	-
D303	-	-	9490 <sup>+330</sup> <sub>-320</sub>
D304	8060 <sup>+410</sup> <sub>-430</sub>	6740 <sup>+230</sup> <sub>-270</sub>	-
D305	8150 <sup>+270</sup> <sub>-310</sub>	-	-
D306	8740 <sup>+620</sup> <sub>-470</sub>	8560 <sup>+590</sup> <sub>-520</sub>	-
D307	7820 <sup>+490</sup> <sub>-620</sub>	6630 <sup>+400</sup> <sub>-350</sub>	-
D308	6590 <sup>+430</sup> <sub>-370</sub>	-	-
D309	6920 <sup>+220</sup> <sub>-300</sub>	-	-
D310	-	-	9050 <sup>+560</sup> <sub>-610</sub>
D311	8180 <sup>+340</sup> <sub>-400</sub>	-	-
D312	12030 <sup>+1710</sup> <sub>-1890</sub>	-	12740 <sup>+250</sup> <sub>-160</sub>
D313	11080 <sup>+290</sup> <sub>-320</sub>	11570 <sup>+160</sup> <sub>-200</sub>	10180 ± 60
D314	-	11380 <sup>+130</sup> <sub>-220</sub>	-
D315	10060 <sup>+630</sup> <sub>-680</sub>	10860 <sup>+630</sup> <sub>-560</sub>	10860 <sup>+190</sup> <sub>-170</sub>
D316	-	11170 <sup>+960</sup> <sub>-1070</sub>	10820 <sup>+440</sup> <sub>-420</sub>
D317	10720 <sup>+400</sup> <sub>-490</sub>	10080 <sup>+130</sup> <sub>-140</sub>	10190 <sup>+50</sup> <sub>-60</sub>
D318	-	7280 <sup>+140</sup> <sub>-130</sub>	9330 <sup>+140</sup> <sub>-200</sub>
D319	13730 <sup>+100</sup> <sub>-90</sub>	17790 <sup>+280</sup> <sub>-390</sub>	15510 <sup>+90</sup> <sub>-100</sub>
D320	11870 <sup>+680</sup> <sub>-840</sub>	14030 <sup>+620</sup> <sub>-520</sub>	15570 <sup>+360</sup> <sub>-390</sub>
D321	7770 <sup>+440</sup> <sub>-480</sub>	7020 <sup>+180</sup> <sub>-210</sub>	-
D322	7970 <sup>+340</sup> <sub>-410</sub>	7120 <sup>+150</sup> <sub>-190</sub>	9390 <sup>+450</sup> <sub>-280</sub>
D323	7040 <sup>+480</sup> <sub>-580</sub>	6510 <sup>+310</sup> <sub>-350</sub>	-
D324	8260 <sup>+500</sup> <sub>-490</sub>	7260 <sup>+190</sup> <sub>-290</sub>	8370 <sup>+350</sup> <sub>-460</sub>
D325	7270 <sup>+380</sup> <sub>-450</sub>	6430 <sup>+230</sup> <sub>-270</sub>	-
D326	-	6470 <sup>+420</sup> <sub>-450</sub>	-
D327	8520 <sup>+530</sup> <sub>-560</sub>	8100 <sup>+200</sup> <sub>-310</sub>	8810 <sup>+410</sup> <sub>-510</sub>
D328	8850 <sup>+180</sup> <sub>-190</sub>	-	9880 <sup>+310</sup> <sub>-300</sub>
D329	7800 <sup>+390</sup> <sub>-380</sub>	6890 <sup>+260</sup> <sub>-330</sub>	10800 <sup>+390</sup> <sub>-420</sub>
D330	7680 <sup>+370</sup> <sub>-340</sub>	6860 <sup>+220</sup> <sub>-230</sub>	-
D331	-	7750 <sup>+560</sup> <sub>-740</sub>	-
D332	-	7720 <sup>+860</sup> <sub>-680</sub>	10180 <sup>+1050</sup> <sub>-1080</sub>
D333	7290 <sup>+300</sup> <sub>-390</sub>	6430 <sup>+270</sup> <sub>-200</sub>	-
D334	11430 <sup>+1340</sup> <sub>-1360</sub>	14630 <sup>+660</sup> <sub>-860</sub>	11550 <sup>+180</sup> <sub>-230</sub>

**Table D.4.** Measured electron temperatures from the nebular sample.

Reference number	$T_e(\text{[N II]})$ [K]	$T_e(\text{[S III]})$ [K]	$T_e(\text{[O III]})$ [K]
D335	11970 <sup>+460</sup> <sub>-570</sub>	11330 ± 140	11320 <sup>+100</sup> <sub>-80</sub>
D336	14330 <sup>+2370</sup> <sub>-1870</sub>	-	11770 <sup>+280</sup> <sub>-190</sub>
D337	-	-	13980 <sup>+160</sup> <sub>-120</sub>
D338	-	-	13790 <sup>+470</sup> <sub>-410</sub>
D339	-	-	13090 <sup>+440</sup> <sub>-690</sub>
D340	-	-	11720 <sup>+460</sup> <sub>-330</sub>
D341	15590 <sup>+2800</sup> <sub>-3280</sub>	-	12510 <sup>+280</sup> <sub>-370</sub>
D342	-	16000 <sup>+780</sup> <sub>-900</sub>	13140 <sup>+210</sup> <sub>-250</sub>
D343	-	14050 <sup>+240</sup> <sub>-180</sub>	13000 <sup>+60</sup> <sub>-70</sub>
D344	-	-	20420 <sup>+120</sup> <sub>-180</sub>
D345	-	-	19930 <sup>+120</sup> <sub>-140</sub>
D346	-	-	20140 <sup>+310</sup> <sub>-240</sub>
D347	-	-	21420 <sup>+350</sup> <sub>-300</sub>
D348	-	-	20900 <sup>+340</sup> <sub>-270</sub>
D349	-	-	20940 <sup>+520</sup> <sub>-430</sub>
D350	-	-	22180 <sup>+590</sup> <sub>-510</sub>
D351	-	-	20250 <sup>+320</sup> <sub>-280</sub>
D352	24120 <sup>+3640</sup> <sub>-3690</sub>	-	21300 <sup>+260</sup> <sub>-250</sub>
D353	-	-	20500 <sup>+310</sup> <sub>-240</sub>
D354	-	13230 <sup>+450</sup> <sub>-410</sub>	20460 <sup>+190</sup> <sub>-160</sub>
D355	-	-	19230 <sup>+380</sup> <sub>-420</sub>
D356	-	-	12700 <sup>+110</sup> <sub>-120</sub>
D357	-	-	13000 <sup>+130</sup> <sub>-120</sub>
D358	-	-	18960 <sup>+230</sup> <sub>-160</sub>
D359	-	-	15290 <sup>+230</sup> <sub>-180</sub>
D360	-	-	18380 <sup>+160</sup> <sub>-190</sub>
D361	-	-	16870 <sup>+90</sup> <sub>-130</sub>
D362	-	17540 <sup>+540</sup> <sub>-680</sub>	17510 <sup>+240</sup> <sub>-280</sub>
D363	19000 <sup>+1430</sup> <sub>-1740</sub>	-	20140 ± 280
D364	-	20550 <sup>+2680</sup> <sub>-3350</sub>	21710 <sup>+480</sup> <sub>-490</sub>
D365	-	12300 <sup>+540</sup> <sub>-640</sub>	14940 <sup>+320</sup> <sub>-280</sub>
D366	-	13340 <sup>+250</sup> <sub>-400</sub>	13820 <sup>+130</sup> <sub>-160</sub>
D367	-	-	16030 <sup>+260</sup> <sub>-280</sub>
D368	-	-	14840 <sup>+530</sup> <sub>-700</sub>
D369	-	-	17770 <sup>+210</sup> <sub>-200</sub>
D370	-	18580 <sup>+790</sup> <sub>-850</sub>	19160 <sup>+460</sup> <sub>-440</sub>
D371	-	-	19910 <sup>+290</sup> <sub>-260</sub>
D372	-	-	14760 <sup>+170</sup> <sub>-100</sub>
D373	-	-	14060 <sup>+150</sup> <sub>-130</sub>
D374	25510 <sup>+2430</sup> <sub>-2110</sub>	21900 <sup>+1560</sup> <sub>-1230</sub>	19010 <sup>+480</sup> <sub>-470</sub>
D375	25450 <sup>+2870</sup> <sub>-2160</sub>	23600 <sup>+1180</sup> <sub>-1490</sub>	18970 <sup>+340</sup> <sub>-480</sub>
D376	-	-	16030 <sup>+110</sup> <sub>-70</sub>
D377	-	12920 <sup>+320</sup> <sub>-490</sub>	12950 <sup>+280</sup> <sub>-400</sub>
D378	-	-	20620 <sup>+370</sup> <sub>-500</sub>
D379	-	-	16580 <sup>+270</sup> <sub>-250</sub>
D380	-	13060 <sup>+560</sup> <sub>-550</sub>	13340 <sup>+320</sup> <sub>-360</sub>
D381	-	-	17340 <sup>+190</sup> <sub>-200</sub>
D382	-	-	15940 <sup>+180</sup> <sub>-150</sub>
D383	-	13630 <sup>+430</sup> <sub>-460</sub>	13960 ± 200
D384	-	10420 ± 260	10830 <sup>+190</sup> <sub>-220</sub>
D385	-	12250 ± 520	11530 <sup>+190</sup> <sub>-160</sub>
D386	-	-	16900 <sup>+190</sup> <sub>-140</sub>
D387	-	30810 <sup>+2270</sup> <sub>-2310</sub>	17200 <sup>+310</sup> <sub>-430</sub>
D388	-	14150 <sup>+650</sup> <sub>-500</sub>	12320 <sup>+240</sup> <sub>-220</sub>
D389	-	-	14210 ± 100
D390	15520 <sup>+780</sup> <sub>-630</sub>	-	15730 <sup>+250</sup> <sub>-300</sub>

**Table D.4.** Measured electron temperatures from the nebular sample.

Reference number	$T_e(\text{[N II]})$ [K]	$T_e(\text{[S III]})$ [K]	$T_e(\text{[O III]})$ [K]
D391	-	12230 <sup>+400</sup> <sub>-480</sub>	12750 <sup>+340</sup> <sub>-230</sub>
D392	13630 <sup>+1420</sup> <sub>-1670</sub>	-	15090 <sup>+350</sup> <sub>-460</sub>
D393	-	17800 <sup>+970</sup> <sub>-1510</sub>	19610 <sup>+120</sup> <sub>-140</sub>
D394	-	11490 <sup>+940</sup> <sub>-500</sub>	12110 ± 510
D395	-	-	14410 <sup>+100</sup> <sub>-150</sub>
D396	-	12900 <sup>+140</sup> <sub>-180</sub>	13740 <sup>+60</sup> <sub>-70</sub>
D397	-	-	13390 <sup>+200</sup> <sub>-170</sub>
D398	-	9850 <sup>+380</sup> <sub>-250</sub>	11250 <sup>+170</sup> <sub>-310</sub>
D399	13150 <sup>+680</sup> <sub>-800</sub>	11390 <sup>+430</sup> <sub>-340</sub>	12530 <sup>+310</sup> <sub>-220</sub>
D400	10770 <sup>+840</sup> <sub>-730</sub>	-	12420 <sup>+60</sup> <sub>-40</sub>
D401	12080 <sup>+320</sup> <sub>-400</sub>	16290 <sup>+580</sup> <sub>-540</sub>	12520 <sup>+220</sup> <sub>-200</sub>
D402	11930 <sup>+230</sup> <sub>-270</sub>	16010 <sup>+610</sup> <sub>-840</sub>	12810 <sup>+180</sup> <sub>-240</sub>
D403	13120 <sup>+390</sup> <sub>-350</sub>	21720 <sup>+1080</sup> <sub>-1280</sub>	13880 <sup>+290</sup> <sub>-180</sub>
D404	-	13380 <sup>+880</sup> <sub>-780</sub>	12050 <sup>+220</sup> <sub>-150</sub>
D405	-	-	12800 <sup>+120</sup> <sub>-90</sub>
D406	-	-	12550 <sup>+300</sup> <sub>-370</sub>
D407	11110 <sup>+1410</sup> <sub>-840</sub>	-	12060 <sup>+140</sup> <sub>-190</sub>
D408	11550 ± 80	-	12190 <sup>+90</sup> <sub>-80</sub>
D409	-	-	12000 <sup>+140</sup> <sub>-90</sub>
D410	11990 <sup>+1140</sup> <sub>-810</sub>	-	11970 <sup>+90</sup> <sub>-110</sub>
D411	11920 <sup>+330</sup> <sub>-340</sub>	-	12180 ± 100
D412	11140 <sup>+960</sup> <sub>-1120</sub>	-	11920 <sup>+110</sup> <sub>-90</sub>
D413	-	11040 <sup>+600</sup> <sub>-630</sub>	11330 <sup>+250</sup> <sub>-170</sub>
D414	-	12540 <sup>+300</sup> <sub>-580</sub>	13500 <sup>+230</sup> <sub>-270</sub>
D415	-	-	14660 <sup>+280</sup> <sub>-200</sub>
D416	-	-	14620 <sup>+260</sup> <sub>-310</sub>
D417	-	-	15320 <sup>+130</sup> <sub>-150</sub>
D418	-	-	15000 <sup>+130</sup> <sub>-180</sub>
D419	-	-	15070 <sup>+320</sup> <sub>-300</sub>
D420	-	-	15060 <sup>+120</sup> <sub>-160</sub>
D421	-	-	15050 <sup>+140</sup> <sub>-200</sub>
D422	-	-	11300 <sup>+180</sup> <sub>-290</sub>
D423	-	25260 <sup>+1160</sup> <sub>-1450</sub>	20020 <sup>+180</sup> <sub>-290</sub>
D424	-	-	19600 <sup>+290</sup> <sub>-260</sub>
D425	9360 <sup>+290</sup> <sub>-340</sub>	12520 <sup>+210</sup> <sub>-160</sub>	11790 <sup>+30</sup> <sub>-60</sub>
D426	-	12150 <sup>+170</sup> <sub>-230</sub>	12360 <sup>+140</sup> <sub>-90</sub>
D427	-	13430 <sup>+150</sup> <sub>-220</sub>	12160 <sup>+60</sup> <sub>-50</sub>
D428	-	-	13020 <sup>+140</sup> <sub>-150</sub>
D429	-	-	14330 <sup>+240</sup> <sub>-190</sub>
D430	11940 <sup>+880</sup> <sub>-1090</sub>	-	13810 <sup>+140</sup> <sub>-120</sub>
D431	-	-	15920 ± 140
D432	-	-	15720 <sup>+170</sup> <sub>-160</sub>
D433	-	-	16450 <sup>+250</sup> <sub>-280</sub>
D434	-	-	15940 <sup>+170</sup> <sub>-190</sub>
D435	-	-	15640 <sup>+210</sup> <sub>-150</sub>
D436	-	-	15760 <sup>+200</sup> <sub>-240</sub>
D437	24970 <sup>+3620</sup> <sub>-3040</sub>	-	14430 <sup>+130</sup> <sub>-140</sub>
D438	-	-	17760 ± 200
D439	-	-	17480 <sup>+260</sup> <sub>-380</sub>
D440	-	-	16630 <sup>+380</sup> <sub>-230</sub>
D441	-	-	12380 ± 150
D442	-	-	10620 <sup>+170</sup> <sub>-260</sub>
D443	11080 <sup>+1120</sup> <sub>-1170</sub>	-	9630 <sup>+820</sup> <sub>-670</sub>
D444	-	-	11220 <sup>+180</sup> <sub>-130</sub>
D445	-	-	12050 <sup>+440</sup> <sub>-410</sub>
D446	-	-	13510 <sup>+310</sup> <sub>-290</sub>

**Table D.4.** Measured electron temperatures from the nebular sample.

Reference number	$T_e([\text{N II}])$ [K]	$T_e([\text{S III}])$ [K]	$T_e([\text{O III}])$ [K]
D447	-	-	$13070^{+800}_{-620}$
D448	-	-	$15960^{+770}_{-920}$
D449	-	-	$13960 \pm 120$
D450	-	-	$13650^{+140}_{-200}$
D451	-	$16010^{+600}_{-430}$	$16950^{+310}_{-270}$
D452	-	$10440^{+550}_{-460}$	$15170^{+600}_{-370}$



**Table D.5.** Adopted electron temperatures for the nebular sample. The information in this table is derived from the values in Table D.4 and the  $T_e$  relations from Garnett (1992) and Méndez-Delgado et al. (2023b).

Reference number	$T_e$ ([N II]) [K]	$T_e$ ([O III]) [K]	$T_0$ (O <sup>2+</sup> ) [K]
D1	10990 <sup>+310</sup> <sub>-210</sub>	11410 <sup>+320</sup> <sub>-220</sub>	9510 <sup>+270</sup> <sub>-180</sub>
D2	12150 <sup>+190</sup> <sub>-240</sub>	13070 <sup>+200</sup> <sub>-260</sub>	10880 <sup>+170</sup> <sub>-220</sub>
D3	13020 <sup>+210</sup> <sub>-140</sub>	14310 <sup>+230</sup> <sub>-150</sub>	11890 <sup>+190</sup> <sub>-130</sub>
D4	13100 <sup>+390</sup> <sub>-330</sub>	14430 <sup>+430</sup> <sub>-360</sub>	11990 <sup>+360</sup> <sub>-300</sub>
D5	12310 <sup>+120</sup> <sub>-150</sub>	13300 <sup>+130</sup> <sub>-160</sub>	11060 <sup>+110</sup> <sub>-140</sub>
D6	11740 <sup>+150</sup> <sub>-270</sub>	12490 <sup>+150</sup> <sub>-290</sub>	10400 <sup>+130</sup> <sub>-240</sub>
D7	11110 <sup>+180</sup> <sub>-220</sub>	11590 <sup>+190</sup> <sub>-230</sub>	9660 <sup>+150</sup> <sub>-190</sub>
D8	11010 <sup>+470</sup> <sub>-510</sub>	11450 <sup>+490</sup> <sub>-530</sub>	9540 <sup>+410</sup> <sub>-440</sub>
D9	11460 ± 290	12090 <sup>+300</sup> <sub>-310</sub>	10070 <sup>+250</sup> <sub>-260</sub>
D10	11950 <sup>+220</sup> <sub>-140</sub>	12780 <sup>+230</sup> <sub>-150</sub>	10640 <sup>+190</sup> <sub>-130</sub>
D11	12390 <sup>+200</sup> <sub>-190</sub>	13420 <sup>+220</sup> <sub>-200</sub>	11160 <sup>+180</sup> <sub>-170</sub>
D12	11580 <sup>+170</sup> <sub>-190</sub>	12260 <sup>+180</sup> <sub>-200</sub>	10210 <sup>+150</sup> <sub>-170</sub>
D13	10090 <sup>+820</sup> <sub>-690</sub>	10120 <sup>+820</sup> <sub>-700</sub>	8460 <sup>+690</sup> <sub>-580</sub>
D14	12150 <sup>+250</sup> <sub>-280</sub>	13070 <sup>+270</sup> <sub>-310</sub>	10870 <sup>+230</sup> <sub>-250</sub>
D15	11060 <sup>+290</sup> <sub>-420</sub>	11520 <sup>+300</sup> <sub>-430</sub>	9600 <sup>+250</sup> <sub>-360</sub>
D16	12110 <sup>+530</sup> <sub>-550</sub>	13010 <sup>+570</sup> <sub>-590</sub>	10830 <sup>+470</sup> <sub>-490</sub>
D17	11350 <sup>+390</sup> <sub>-410</sub>	11930 <sup>+410</sup> <sub>-440</sub>	9940 <sup>+340</sup> <sub>-360</sub>
D18	9790 <sup>+790</sup> <sub>-710</sub>	9700 <sup>+790</sup> <sub>-700</sub>	8120 <sup>+660</sup> <sub>-580</sub>
D19	16200 <sup>+390</sup> <sub>-490</sub>	18860 <sup>+450</sup> <sub>-570</sub>	15620 <sup>+380</sup> <sub>-470</sub>
D20	16390 <sup>+520</sup> <sub>-410</sub>	19120 <sup>+600</sup> <sub>-470</sub>	15830 <sup>+500</sup> <sub>-390</sub>
D21	12990 <sup>+230</sup> <sub>-280</sub>	14270 <sup>+250</sup> <sub>-310</sub>	11860 <sup>+210</sup> <sub>-250</sub>
D22	15170 <sup>+500</sup> <sub>-450</sub>	17380 <sup>+570</sup> <sub>-520</sub>	14410 <sup>+480</sup> <sub>-430</sub>
D23	11180 <sup>+420</sup> <sub>-480</sub>	11690 <sup>+440</sup> <sub>-510</sub>	9750 <sup>+360</sup> <sub>-420</sub>
D24	11200 <sup>+420</sup> <sub>-410</sub>	11720 <sup>+440</sup> <sub>-430</sub>	9770 <sup>+370</sup> <sub>-360</sub>
D25	13250 <sup>+340</sup> <sub>-310</sub>	14650 <sup>+380</sup> <sub>-350</sub>	12170 <sup>+310</sup> <sub>-290</sub>
D26	10140 <sup>+760</sup> <sub>-1320</sub>	10200 <sup>+760</sup> <sub>-1320</sub>	8530 <sup>+640</sup> <sub>-1110</sub>
D27	11730 <sup>+190</sup> <sub>-230</sub>	12470 <sup>+200</sup> <sub>-240</sub>	10390 <sup>+170</sup> <sub>-200</sub>
D28	13960 <sup>+90</sup> <sub>-60</sub>	15660 <sup>+100</sup> <sub>-70</sub>	12990 <sup>+80</sup> <sub>-60</sub>
D29	12080 <sup>+310</sup> <sub>-270</sub>	12960 <sup>+340</sup> <sub>-290</sub>	10790 <sup>+280</sup> <sub>-240</sub>
D30	11640 <sup>+450</sup> <sub>-370</sub>	12340 <sup>+480</sup> <sub>-390</sub>	10280 <sup>+400</sup> <sub>-330</sub>
D31	11950 <sup>+450</sup> <sub>-460</sub>	12780 <sup>+480</sup> <sub>-490</sub>	10640 <sup>+400</sup> <sub>-410</sub>
D32	9980 <sup>+290</sup> <sub>-280</sub>	9970 <sup>+290</sup> <sub>-280</sub>	8340 <sup>+250</sup> <sub>-230</sub>
D33	9970 <sup>+1000</sup> <sub>-1090</sub>	9960 <sup>+1000</sup> <sub>-1090</sub>	8330 <sup>+830</sup> <sub>-910</sub>
D34	10460 <sup>+980</sup> <sub>-1130</sub>	10660 <sup>+1000</sup> <sub>-1150</sub>	8900 <sup>+830</sup> <sub>-960</sub>
D35	12380 <sup>+320</sup> <sub>-260</sub>	13400 <sup>+350</sup> <sub>-280</sub>	11140 <sup>+290</sup> <sub>-240</sub>
D36	11790 <sup>+240</sup> <sub>-260</sub>	12550 <sup>+250</sup> <sub>-280</sub>	10450 <sup>+210</sup> <sub>-230</sub>
D37	10140 <sup>+950</sup> <sub>-1300</sub>	10190 <sup>+950</sup> <sub>-1310</sub>	8520 <sup>+800</sup> <sub>-1100</sub>
D38	13480 <sup>+270</sup> <sub>-200</sub>	14970 <sup>+290</sup> <sub>-220</sub>	12430 <sup>+240</sup> <sub>-190</sub>
D39	12060 <sup>+230</sup> <sub>-260</sub>	12940 <sup>+250</sup> <sub>-280</sub>	10770 <sup>+210</sup> <sub>-230</sub>
D40	12930 <sup>+190</sup> <sub>-170</sub>	14190 <sup>+200</sup> <sub>-190</sub>	11790 <sup>+170</sup> <sub>-150</sub>
D41	17000 <sup>+330</sup> <sub>-280</sub>	20000 <sup>+380</sup> <sub>-330</sub>	16550 <sup>+320</sup> <sub>-270</sub>
D42	10840 <sup>+320</sup> <sub>-360</sub>	11200 <sup>+330</sup> <sub>-370</sub>	9340 <sup>+280</sup> <sub>-310</sub>
D43	10140 <sup>+600</sup> <sub>-1210</sub>	10190 <sup>+610</sup> <sub>-1210</sub>	8520 <sup>+510</sup> <sub>-1010</sub>
D44	10640 <sup>+350</sup> <sub>-430</sub>	10920 <sup>+350</sup> <sub>-450</sub>	9110 <sup>+300</sup> <sub>-370</sub>
D45	9590 <sup>+1520</sup> <sub>-1280</sub>	9360 <sup>+1480</sup> <sub>-1250</sub>	7880 <sup>+1250</sup> <sub>-1050</sub>
D46	10440 <sup>+320</sup> <sub>-350</sub>	10630 <sup>+330</sup> <sub>-350</sub>	8880 <sup>+270</sup> <sub>-290</sub>
D47	9940 <sup>+930</sup> <sub>-980</sub>	9920 <sup>+930</sup> <sub>-970</sub>	8290 <sup>+780</sup> <sub>-810</sub>
D48	9880 <sup>+270</sup> <sub>-350</sub>	9830 <sup>+260</sup> <sub>-350</sub>	8220 <sup>+220</sup> <sub>-290</sub>
D49	10220 <sup>+420</sup> <sub>-380</sub>	10320 <sup>+420</sup> <sub>-380</sub>	8620 <sup>+350</sup> <sub>-320</sub>
D50	12130 <sup>+430</sup> <sub>-410</sub>	13040 <sup>+460</sup> <sub>-440</sub>	10850 <sup>+380</sup> <sub>-370</sub>
D51	10490 <sup>+490</sup> <sub>-340</sub>	10700 <sup>+500</sup> <sub>-350</sub>	8930 <sup>+420</sup> <sub>-290</sub>
D52	12740 <sup>+430</sup> <sub>-530</sub>	13910 <sup>+470</sup> <sub>-580</sub>	11560 <sup>+390</sup> <sub>-480</sub>
D53	12860 <sup>+90</sup> <sub>-100</sub>	14090 <sup>+100</sup> <sub>-110</sub>	11710 ± 90
D54	14230 <sup>+110</sup> <sub>-100</sub>	16040 <sup>+130</sup> <sub>-120</sub>	13310 <sup>+110</sup> <sub>-100</sub>

**Table D.5.** Adopted electron temperatures for the nebular sample. The information in this table is derived from the values in Table D.4 and the  $T_e$  relations from Garnett (1992) and Méndez-Delgado et al. (2023b).

Reference number	$T_e$ ([N II]) [K]	$T_e$ ([O III]) [K]	$T_0$ (O <sup>2+</sup> ) [K]
D55	10780 <sup>+560</sup> <sub>-770</sub>	11110 <sup>+580</sup> <sub>-800</sub>	9270 <sup>+480</sup> <sub>-670</sub>
D56	12410 <sup>+60</sup> <sub>-50</sub>	13440 <sup>+60</sup> <sub>-50</sub>	11180 <sup>+50</sup> <sub>-40</sub>
D57	10170 <sup>+510</sup> <sub>-620</sub>	10240 <sup>+510</sup> <sub>-620</sub>	8550 <sup>+430</sup> <sub>-520</sub>
D58	10840 ± 200	11190 ± 210	9340 ± 170
D59	12020 <sup>+130</sup> <sub>-90</sub>	12880 <sup>+140</sup> <sub>-90</sub>	10720 <sup>+120</sup> <sub>-80</sub>
D60	10840 <sup>+410</sup> <sub>-350</sub>	11190 <sup>+420</sup> <sub>-360</sub>	9340 <sup>+350</sup> <sub>-300</sub>
D61	10860 <sup>+430</sup> <sub>-440</sub>	11230 <sup>+450</sup> <sub>-460</sub>	9360 <sup>+370</sup> <sub>-380</sub>
D62	10530 <sup>+380</sup> <sub>-470</sub>	10750 <sup>+390</sup> <sub>-480</sub>	8980 <sup>+320</sup> <sub>-400</sub>
D63	9540 <sup>+180</sup> <sub>-160</sub>	9340 <sup>+180</sup> <sub>-160</sub>	7820 <sup>+150</sup> <sub>-130</sub>
D64	9260 <sup>+430</sup> <sub>-360</sub>	8940 <sup>+420</sup> <sub>-350</sub>	7490 <sup>+350</sup> <sub>-290</sub>
D65	15860 <sup>+240</sup> <sub>-410</sub>	18370 <sup>+280</sup> <sub>-480</sub>	15210 <sup>+230</sup> <sub>-400</sub>
D66	12550 <sup>+430</sup> <sub>-360</sub>	13640 <sup>+470</sup> <sub>-390</sub>	11340 <sup>+390</sup> <sub>-330</sub>
D67	13170 ± 150	14520 <sup>+170</sup> <sub>-160</sub>	12060 <sup>+140</sup> <sub>-130</sub>
D68	9760 <sup>+220</sup> <sub>-270</sub>	9660 <sup>+220</sup> <sub>-270</sub>	8080 <sup>+180</sup> <sub>-220</sub>
D69	12960 <sup>+410</sup> <sub>-390</sub>	14220 <sup>+450</sup> <sub>-420</sub>	11820 <sup>+380</sup> <sub>-380</sub>
D70	11620 <sup>+270</sup> <sub>-270</sub>	12310 <sup>+320</sup> <sub>-290</sub>	10250 <sup>+320</sup> <sub>-240</sub>
D71	7760 <sup>+510</sup> <sub>-680</sub>	6820 <sup>+450</sup> <sub>-600</sub>	5740 ± 380
D72	14470 <sup>+150</sup> <sub>-160</sub>	16390 <sup>+170</sup> <sub>-180</sub>	13590 <sup>+140</sup> <sub>-150</sub>
D73	12830 <sup>+300</sup> <sub>-200</sub>	14040 <sup>+320</sup> <sub>-220</sub>	11670 <sup>+270</sup> <sub>-180</sub>
D74	10600 <sup>+70</sup> <sub>-60</sub>	10850 ± 70	9060 ± 60
D75	15350 <sup>+230</sup> <sub>-200</sub>	17640 <sup>+260</sup> <sub>-230</sub>	14620 <sup>+220</sup> <sub>-190</sub>
D76	11720 <sup>+120</sup> <sub>-90</sub>	12450 <sup>+130</sup> <sub>-100</sub>	10370 <sup>+110</sup> <sub>-80</sub>
D77	11370 <sup>+150</sup> <sub>-160</sub>	11950 <sup>+160</sup> <sub>-170</sub>	9960 <sup>+130</sup> <sub>-140</sub>
D78	15680 <sup>+140</sup> <sub>-190</sub>	18110 <sup>+170</sup> <sub>-220</sub>	15000 <sup>+140</sup> <sub>-180</sub>
D79	16350 <sup>+390</sup> <sub>-380</sub>	19070 ± 450	15790 ± 370
D80	16310 <sup>+230</sup> <sub>-220</sub>	19020 <sup>+270</sup> <sub>-250</sub>	15750 <sup>+220</sup> <sub>-210</sub>
D81	14540 <sup>+1980</sup> <sub>-2750</sub>	12460 <sup>+210</sup> <sub>-220</sub>	13680 ± 1860
D82	14040 <sup>+120</sup> <sub>-170</sub>	15780 <sup>+140</sup> <sub>-190</sub>	13090 <sup>+120</sup> <sub>-160</sub>
D83	12020 <sup>+460</sup> <sub>-570</sub>	16170 <sup>+250</sup> <sub>-290</sub>	10720 ± 410
D84	11720 <sup>+280</sup> <sub>-360</sub>	12460 <sup>+300</sup> <sub>-380</sub>	10380 <sup>+250</sup> <sub>-310</sub>
D85	8170 <sup>+310</sup> <sub>-370</sub>	7390 <sup>+280</sup> <sub>-330</sub>	6220 <sup>+230</sup> <sub>-280</sub>
D86	8620 <sup>+310</sup> <sub>-380</sub>	8040 <sup>+290</sup> <sub>-350</sub>	6750 <sup>+240</sup> <sub>-300</sub>
D87	12050 <sup>+70</sup> <sub>-100</sub>	12930 <sup>+70</sup> <sub>-110</sub>	10760 <sup>+60</sup> <sub>-90</sub>
D88	16920 <sup>+220</sup> <sub>-200</sub>	19890 <sup>+260</sup> <sub>-230</sub>	16460 <sup>+220</sup> <sub>-190</sub>
D89	15630 <sup>+260</sup> <sub>-270</sub>	18050 <sup>+300</sup> <sub>-320</sub>	14950 <sup>+240</sup> <sub>-260</sub>
D90	12040 <sup>+630</sup> <sub>-640</sub>	12910 <sup>+670</sup> <sub>-690</sub>	10740 <sup>+560</sup> <sub>-570</sub>
D91	11240 ± 50	11770 ± 50	9810 ± 40
D92	11100 <sup>+360</sup> <sub>-380</sub>	12500 <sup>+240</sup> <sub>-230</sub>	9650 ± 320
D93	11920 <sup>+300</sup> <sub>-270</sub>	12740 <sup>+320</sup> <sub>-290</sub>	10600 <sup>+260</sup> <sub>-240</sub>
D94	15870 <sup>+90</sup> <sub>-100</sub>	18390 <sup>+100</sup> <sub>-110</sub>	15230 <sup>+80</sup> <sub>-90</sub>
D95	12840 <sup>+270</sup> <sub>-280</sub>	14060 <sup>+290</sup> <sub>-300</sub>	11680 <sup>+240</sup> <sub>-250</sub>
D96	13840 <sup>+280</sup> <sub>-340</sub>	15480 <sup>+310</sup> <sub>-380</sub>	12850 <sup>+260</sup> <sub>-310</sub>
D97	15500 <sup>+190</sup> <sub>-220</sub>	17860 <sup>+210</sup> <sub>-260</sub>	14800 <sup>+180</sup> <sub>-210</sub>
D98	16460 <sup>+160</sup> <sub>-220</sub>	19230 <sup>+190</sup> <sub>-260</sub>	15920 <sup>+160</sup> <sub>-210</sub>
D99	13730 <sup>+190</sup> <sub>-180</sub>	15330 <sup>+210</sup> <sub>-200</sub>	12730 <sup>+180</sup> <sub>-170</sub>
D100	16420 <sup>+210</sup> <sub>-190</sub>	19160 <sup>+250</sup> <sub>-220</sub>	15870 <sup>+200</sup> <sub>-180</sub>
D101	12120 <sup>+1270</sup> <sub>-1500</sub>	13370 ± 130	10840 ± 1140
D102	12330 <sup>+70</sup> <sub>-110</sub>	13320 <sup>+80</sup> <sub>-120</sub>	11080 <sup>+60</sup> <sub>-100</sub>
D103	15470 <sup>+190</sup> <sub>-150</sub>	17820 <sup>+220</sup> <sub>-180</sub>	14760 <sup>+180</sup> <sub>-150</sub>
D104	12210 ± 160	13160 <sup>+180</sup> <sub>-170</sub>	10950 <sup>+150</sup> <sub>-140</sub>
D105	14320 ± 270	16180 ± 310	13420 <sup>+230</sup> <sub>-260</sub>
D106	14330 <sup>+590</sup> <sub>-550</sub>	12360 <sup>+150</sup> <sub>-130</sub>	13430 ± 560
D107	20100 <sup>+390</sup> <sub>-490</sub>	24430 <sup>+470</sup> <sub>-600</sub>	20180 <sup>+390</sup> <sub>-490</sub>
D108	11480 <sup>+80</sup> <sub>-70</sub>	12110 ± 80	10090 <sup>+70</sup> <sub>-60</sub>
D109	11600 <sup>+240</sup> <sub>-190</sub>	12280 <sup>+250</sup> <sub>-200</sub>	10230 <sup>+210</sup> <sub>-170</sub>

**Table D.5.** Adopted electron temperatures for the nebular sample. The information in this table is derived from the values in Table D.4 and the  $T_e$  relations from Garnett (1992) and Méndez-Delgado et al. (2023b).

Reference number	$T_e$ ([N II]) [K]	$T_e$ ([O III]) [K]	$T_0$ (O <sup>2+</sup> ) [K]
D110	15600 <sup>+110</sup> <sub>-150</sub>	18010 <sup>+120</sup> <sub>-170</sub>	14920 <sup>+100</sup> <sub>-140</sub>
D111	13330 <sup>+60</sup> <sub>-70</sub>	14760 <sup>+70</sup> <sub>-80</sub>	12260 ± 60
D112	15020 <sup>+190</sup> <sub>-140</sub>	17180 <sup>+220</sup> <sub>-150</sub>	14240 <sup>+180</sup> <sub>-130</sub>
D113	14390 <sup>+90</sup> <sub>-120</sub>	16270 <sup>+100</sup> <sub>-130</sub>	13490 <sup>+80</sup> <sub>-110</sub>
D114	13920 ± 110	15600 ± 130	12950 <sup>+100</sup> <sub>-110</sub>
D115	10340 <sup>+210</sup> <sub>-230</sub>	9900 ± 70	8750 ± 180
D116	9800 ± 350	9120 <sup>+120</sup> <sub>-130</sub>	8120 ± 290
D117	9830 <sup>+70</sup> <sub>-110</sub>	9160 <sup>+120</sup> <sub>-110</sub>	8160 ± 60
D118	10510 <sup>+300</sup> <sub>-370</sub>	11330 <sup>+150</sup> <sub>-130</sub>	8950 ± 250
D119	10180 <sup>+500</sup> <sub>-460</sub>	9530 <sup>+170</sup> <sub>-190</sub>	8570 ± 420
D120	8140 <sup>+180</sup> <sub>-170</sub>	7620 ± 210	6180 ± 130
D121	7570 <sup>+180</sup> <sub>-130</sub>	7380 <sup>+170</sup> <sub>-150</sub>	5520 ± 130
D122	7790 <sup>+330</sup> <sub>-400</sub>	7250 <sup>+510</sup> <sub>-570</sub>	5770 ± 250
D123	7540 <sup>+380</sup> <sub>-390</sub>	6500 <sup>+320</sup> <sub>-330</sub>	5480 ± 270
D124	9360 <sup>+800</sup> <sub>-760</sub>	9010 <sup>+230</sup> <sub>-360</sub>	7620 ± 650
D125	7380 <sup>+370</sup> <sub>-490</sub>	6270 <sup>+310</sup> <sub>-410</sub>	5290 ± 270
D126	7630 <sup>+350</sup> <sub>-360</sub>	6620 ± 310	5590 ± 260
D127	10600 <sup>+310</sup> <sub>-410</sub>	10860 <sup>+320</sup> <sub>-420</sub>	9060 <sup>+260</sup> <sub>-350</sub>
D128	8420 <sup>+150</sup> <sub>-230</sub>	7760 <sup>+60</sup> <sub>-70</sub>	6510 ± 110
D129	9350 <sup>+180</sup> <sub>-190</sub>	9080 <sup>+180</sup> <sub>-190</sub>	7600 <sup>+150</sup> <sub>-160</sub>
D130	11360 <sup>+220</sup> <sub>-210</sub>	11940 <sup>+230</sup> <sub>-220</sub>	9950 <sup>+190</sup> <sub>-180</sub>
D131	10520 <sup>+130</sup> <sub>-120</sub>	10740 ± 130	8970 ± 110
D132	10760 <sup>+230</sup> <sub>-200</sub>	11080 <sup>+230</sup> <sub>-210</sub>	9250 <sup>+190</sup> <sub>-170</sub>
D133	10540 <sup>+170</sup> <sub>-210</sub>	10770 <sup>+180</sup> <sub>-220</sub>	8990 <sup>+150</sup> <sub>-180</sub>
D134	9990 <sup>+1210</sup> <sub>-1630</sub>	10670 <sup>+70</sup> <sub>-80</sub>	8350 ± 1010
D135	10820 ± 260	10570 <sup>+130</sup> <sub>-150</sub>	9320 ± 230
D136	9500 <sup>+370</sup> <sub>-390</sub>	9760 <sup>+70</sup> <sub>-80</sub>	7780 ± 300
D137	10740 <sup>+150</sup> <sub>-210</sub>	11060 <sup>+150</sup> <sub>-210</sub>	9230 <sup>+130</sup> <sub>-180</sub>
D138	8870 <sup>+710</sup> <sub>-750</sub>	8990 <sup>+330</sup> <sub>-220</sub>	7040 ± 560
D139	8130 <sup>+410</sup> <sub>-480</sub>	7280 <sup>+370</sup> <sub>-430</sub>	6170 <sup>+310</sup> <sub>-370</sub>
D140	8590 <sup>+320</sup> <sub>-340</sub>	8420 <sup>+230</sup> <sub>-270</sub>	6710 ± 250
D141	10960 <sup>+610</sup> <sub>-860</sub>	9650 <sup>+210</sup> <sub>-150</sub>	9480 ± 530
D142	7920 <sup>+720</sup> <sub>-690</sub>	7040 <sup>+640</sup> <sub>-620</sub>	5920 ± 540
D143	7930 <sup>+500</sup> <sub>-580</sub>	7050 <sup>+440</sup> <sub>-510</sub>	5930 ± 370
D144	8780 <sup>+160</sup> <sub>-190</sub>	8260 <sup>+150</sup> <sub>-180</sub>	6930 <sup>+130</sup> <sub>-150</sub>
D145	12060 <sup>+110</sup> <sub>-140</sub>	12940 <sup>+120</sup> <sub>-150</sub>	10770 <sup>+100</sup> <sub>-130</sub>
D146	8900 ± 70	8430 ± 70	7080 <sup>+50</sup> <sub>-60</sub>
D147	7020 <sup>+370</sup> <sub>-300</sub>	5750 <sup>+300</sup> <sub>-250</sub>	4870 ± 250
D148	7230 <sup>+280</sup> <sub>-290</sub>	6050 ± 240	5110 ± 200
D149	11030 <sup>+130</sup> <sub>-110</sub>	11480 <sup>+130</sup> <sub>-120</sub>	9570 <sup>+110</sup> <sub>-100</sub>
D150	6300 <sup>+400</sup> <sub>-420</sub>	4730 <sup>+300</sup> <sub>-320</sub>	4030 ± 250
D151	7640 <sup>+460</sup> <sub>-820</sub>	6640 <sup>+400</sup> <sub>-710</sub>	5600 ± 340
D152	8460 <sup>+390</sup> <sub>-510</sub>	7810 <sup>+360</sup> <sub>-470</sub>	6550 ± 310
D153	12310 <sup>+150</sup> <sub>-230</sub>	13300 <sup>+160</sup> <sub>-250</sub>	11060 <sup>+140</sup> <sub>-200</sub>
D154	12310 <sup>+180</sup> <sub>-170</sub>	13290 <sup>+190</sup> <sub>-180</sub>	11060 <sup>+160</sup> <sub>-150</sub>
D155	6830 <sup>+410</sup> <sub>-460</sub>	5480 <sup>+330</sup> <sub>-370</sub>	4650 ± 280
D156	10610 <sup>+1110</sup> <sub>-1300</sub>	11360 <sup>+110</sup> <sub>-150</sub>	9070 ± 950
D157	8420 <sup>+340</sup> <sub>-330</sub>	8560 <sup>+100</sup> <sub>-110</sub>	6510 ± 270
D158	8220 <sup>+390</sup> <sub>-430</sub>	8940 <sup>+480</sup> <sub>-530</sub>	6270 ± 300
D159	12510 <sup>+140</sup> <sub>-120</sub>	13590 <sup>+150</sup> <sub>-130</sub>	11300 <sup>+130</sup> <sub>-110</sub>
D160	7300 <sup>+410</sup> <sub>-580</sub>	6150 <sup>+350</sup> <sub>-480</sub>	5200 ± 290
D161	7180 <sup>+410</sup> <sub>-380</sub>	5980 <sup>+340</sup> <sub>-320</sub>	5060 ± 290
D162	7350 <sup>+380</sup> <sub>-520</sub>	6220 <sup>+370</sup> <sub>-440</sub>	5260 ± 310
D163	8030 <sup>+370</sup> <sub>-410</sub>	7190 <sup>+460</sup> <sub>-370</sub>	6050 ± 390
D164	7410 <sup>+310</sup> <sub>-370</sub>	6310 <sup>+260</sup> <sub>-320</sub>	5330 ± 220

**Table D.5.** Adopted electron temperatures for the nebular sample. The information in this table is derived from the values in Table D.4 and the  $T_e$  relations from Garnett (1992) and Méndez-Delgado et al. (2023b).

Reference number	$T_e$ ([N II]) [K]	$T_e$ ([O III]) [K]	$T_0$ (O <sup>2+</sup> ) [K]
D165	9450 <sup>+380</sup> <sub>-320</sub>	9760 <sup>+70</sup> <sub>-90</sub>	7720 ± 310
D166	9210 <sup>+230</sup> <sub>-250</sub>	9280 <sup>+70</sup> <sub>-60</sub>	7430 ± 190
D167	9400 <sup>+330</sup> <sub>-350</sub>	9560 <sup>+80</sup> <sub>-60</sub>	7660 ± 270
D168	10520 <sup>+420</sup> <sub>-500</sub>	9190 <sup>+140</sup> <sub>-160</sub>	8970 ± 360
D169	8620 <sup>+380</sup> <sub>-540</sub>	9680 <sup>+130</sup> <sub>-150</sub>	6740 ± 300
D170	40020 <sup>+13350</sup> <sub>-5930</sub>	9440 ± 430	43480 ± 14510
D171	9180 <sup>+210</sup> <sub>-250</sub>	8830 <sup>+200</sup> <sub>-240</sub>	7400 <sup>+170</sup> <sub>-200</sub>
D172	9730 <sup>+250</sup> <sub>-320</sub>	9410 <sup>+70</sup> <sub>-60</sub>	8040 ± 210
D173	10220 <sup>+190</sup> <sub>-170</sub>	9580 <sup>+80</sup> <sub>-100</sub>	8620 ± 160
D174	8370 <sup>+350</sup> <sub>-400</sub>	8520 <sup>+150</sup> <sub>-110</sub>	6450 ± 270
D175	8500 <sup>+530</sup> <sub>-550</sub>	9170 <sup>+180</sup> <sub>-200</sub>	6610 ± 410
D176	8800 <sup>+200</sup> <sub>-140</sub>	8730 <sup>+50</sup> <sub>-60</sub>	6960 ± 160
D177	9090 <sup>+340</sup> <sub>-350</sub>	8450 <sup>+280</sup> <sub>-180</sub>	7290 ± 270
D178	9660 <sup>+100</sup> <sub>-70</sub>	9510 <sup>+100</sup> <sub>-70</sub>	7960 <sup>+90</sup> <sub>-60</sub>
D179	9410 ± 80	9150 ± 80	7670 ± 70
D180	12250 <sup>+140</sup> <sub>-180</sub>	13210 <sup>+150</sup> <sub>-200</sub>	10990 <sup>+130</sup> <sub>-170</sub>
D181	12620 <sup>+280</sup> <sub>-300</sub>	13750 <sup>+300</sup> <sub>-360</sub>	11430 <sup>+250</sup> <sub>-300</sub>
D182	11050 <sup>+910</sup> <sub>-710</sub>	12740 <sup>+180</sup> <sub>-160</sub>	9580 ± 790
D183	12650 <sup>+130</sup> <sub>-160</sub>	13790 <sup>+150</sup> <sub>-170</sub>	11470 <sup>+120</sup> <sub>-140</sub>
D184	9240 <sup>+250</sup> <sub>-340</sub>	11190 <sup>+240</sup> <sub>-220</sub>	7480 ± 200
D185	9680 <sup>+380</sup> <sub>-400</sub>	9520 <sup>+330</sup> <sub>-450</sub>	7990 ± 310
D186	7530 <sup>+160</sup> <sub>-170</sub>	12440 <sup>+340</sup> <sub>-300</sub>	5480 ± 120
D187	8090 <sup>+210</sup> <sub>-320</sub>	7950 <sup>+570</sup> <sub>-750</sub>	6130 ± 160
D188	9280 <sup>+170</sup> <sub>-160</sub>	8340 ± 160	7520 ± 140
D189	9100 <sup>+740</sup> <sub>-890</sub>	7660 <sup>+370</sup> <sub>-490</sub>	7310 ± 590
D190	8050 <sup>+330</sup> <sub>-230</sub>	8940 <sup>+970</sup> <sub>-870</sub>	6080 ± 250
D191	7840 <sup>+220</sup> <sub>-200</sub>	6920 <sup>+190</sup> <sub>-180</sub>	5830 ± 160
D192	7690 <sup>+310</sup> <sub>-390</sub>	6720 <sup>+270</sup> <sub>-340</sub>	5660 ± 230
D193	8500 <sup>+810</sup> <sub>-560</sub>	7880 <sup>+750</sup> <sub>-520</sub>	6610 ± 630
D194	9640 <sup>+560</sup> <sub>-570</sub>	8250 <sup>+400</sup> <sub>-350</sub>	7930 ± 460
D195	11010 <sup>+400</sup> <sub>-460</sub>	11260 <sup>+230</sup> <sub>-190</sub>	9540 ± 350
D196	9670 <sup>+240</sup> <sub>-390</sub>	9060 ± 180	7970 ± 200
D197	10620 <sup>+1120</sup> <sub>-730</sub>	10910 <sup>+1150</sup> <sub>-750</sub>	9090 ± 960
D198	10720 <sup>+700</sup> <sub>-650</sub>	10710 <sup>+360</sup> <sub>-340</sub>	9200 ± 600
D199	8340 <sup>+140</sup> <sub>-150</sub>	7310 <sup>+340</sup> <sub>-290</sub>	6420 ± 110
D200	8930 <sup>+260</sup> <sub>-240</sub>	8360 <sup>+140</sup> <sub>-160</sub>	7110 ± 200
D201	8720 <sup>+170</sup> <sub>-230</sub>	8110 <sup>+170</sup> <sub>-180</sub>	6860 ± 130
D202	8120 <sup>+940</sup> <sub>-1220</sub>	7320 <sup>+850</sup> <sub>-1100</sub>	6160 ± 710
D203	7440 <sup>+290</sup> <sub>-210</sub>	6360 <sup>+250</sup> <sub>-180</sub>	5370 ± 210
D204	10670 <sup>+730</sup> <sub>-710</sub>	10900 <sup>+740</sup> <sub>-720</sub>	9140 <sup>+620</sup> <sub>-610</sub>
D205	10490 <sup>+490</sup> <sub>-530</sub>	9850 <sup>+250</sup> <sub>-270</sub>	8930 ± 410
D206	8420 <sup>+230</sup> <sub>-270</sub>	8150 <sup>+150</sup> <sub>-210</sub>	6510 ± 180
D207	9210 <sup>+340</sup> <sub>-300</sub>	8800 ± 130	7440 ± 270
D208	7750 <sup>+290</sup> <sub>-340</sub>	7780 ± 500	5730 ± 220
D209	6710 <sup>+170</sup> <sub>-200</sub>	5310 <sup>+140</sup> <sub>-150</sub>	4510 ± 120
D210	6960 <sup>+150</sup> <sub>-200</sub>	5660 <sup>+120</sup> <sub>-170</sub>	4800 ± 100
D211	7310 <sup>+350</sup> <sub>-320</sub>	6170 <sup>+300</sup> <sub>-270</sub>	5210 ± 250
D212	6580 <sup>+70</sup> <sub>-80</sub>	5120 <sup>+50</sup> <sub>-60</sub>	4360 ± 40
D213	6740 <sup>+140</sup> <sub>-250</sub>	5350 <sup>+110</sup> <sub>-200</sub>	4540 ± 90
D214	6020 <sup>+110</sup> <sub>-130</sub>	4320 <sup>+80</sup> <sub>-90</sub>	3700 ± 70
D215	5640 <sup>+300</sup> <sub>-370</sub>	3780 <sup>+200</sup> <sub>-250</sub>	3260 ± 170
D216	6430 <sup>+350</sup> <sub>-580</sub>	4900 <sup>+440</sup> <sub>-440</sub>	4180 ± 360
D217	8970 <sup>+230</sup> <sub>-240</sub>	21620 <sup>+1890</sup> <sub>-3170</sub>	7150 ± 190
D218	6280 <sup>+370</sup> <sub>-410</sub>	4700 <sup>+140</sup> <sub>-280</sub>	4010 ± 120
D219	6550 <sup>+410</sup> <sub>-570</sub>	5090 <sup>+320</sup> <sub>-440</sub>	4330 ± 270

**Table D.5.** Adopted electron temperatures for the nebular sample. The information in this table is derived from the values in Table D.4 and the  $T_e$  relations from Garnett (1992) and Méndez-Delgado et al. (2023b).

Reference number	$T_e$ ([N II]) [K]	$T_e$ ([O III]) [K]	$T_0$ (O <sup>2+</sup> ) [K]
D220	8900 <sup>+200</sup> <sub>-210</sub>	7960 <sup>+80</sup> <sub>-100</sub>	7070 ± 160
D221	8240 <sup>+130</sup> <sub>-140</sub>	7800 <sup>+250</sup> <sub>-270</sub>	6300 ± 100
D222	9980 <sup>+190</sup> <sub>-230</sub>	8420 <sup>+60</sup> <sub>-50</sub>	8340 ± 150
D223	8530 <sup>+150</sup> <sub>-90</sub>	8010 <sup>+50</sup> <sub>-40</sub>	6640 ± 120
D224	9930 <sup>+190</sup> <sub>-210</sub>	8410 ± 60	8280 ± 160
D225	8490 <sup>+110</sup> <sub>-120</sub>	8100 <sup>+90</sup> <sub>-70</sub>	6600 ± 80
D226	9800 <sup>+200</sup> <sub>-140</sub>	8510 ± 60	8130 ± 170
D227	10140 <sup>+190</sup> <sub>-210</sub>	8530 <sup>+50</sup> <sub>-80</sub>	8520 ± 160
D228	9910 <sup>+200</sup> <sub>-170</sub>	8400 ± 50	8250 ± 170
D229	9930 <sup>+220</sup> <sub>-160</sub>	8340 <sup>+50</sup> <sub>-60</sub>	8280 ± 180
D230	8220 <sup>+160</sup> <sub>-260</sub>	7470 <sup>+140</sup> <sub>-240</sub>	6280 ± 120
D231	9550 <sup>+220</sup> <sub>-260</sub>	8340 <sup>+60</sup> <sub>-80</sub>	7840 ± 180
D232	9980 <sup>+240</sup> <sub>-250</sub>	8370 ± 50	8340 ± 200
D233	9580 <sup>+400</sup> <sub>-420</sub>	8160 <sup>+200</sup> <sub>-220</sub>	7870 ± 330
D234	8380 <sup>+100</sup> <sub>-110</sub>	8030 <sup>+70</sup> <sub>-80</sub>	6460 ± 80
D235	9520 <sup>+170</sup> <sub>-140</sub>	9310 <sup>+170</sup> <sub>-140</sub>	7800 <sup>+140</sup> <sub>-120</sub>
D236	8810 <sup>+160</sup> <sub>-210</sub>	8450 <sup>+30</sup> <sub>-40</sub>	6970 ± 130
D237	11270 <sup>+620</sup> <sub>-600</sub>	9020 <sup>+140</sup> <sub>-160</sub>	9850 ± 540
D238	8650 <sup>+250</sup> <sub>-350</sub>	8210 <sup>+130</sup> <sub>-120</sub>	6780 ± 200
D239	9830 <sup>+120</sup> <sub>-150</sub>	9770 <sup>+120</sup> <sub>-150</sub>	8160 ± 100
D240	10590 <sup>+260</sup> <sub>-280</sub>	9990 <sup>+260</sup> <sub>-380</sub>	9050 ± 220
D241	8200 ± 90	7440 ± 80	6250 ± 70
D242	9310 <sup>+430</sup> <sub>-420</sub>	9080 <sup>+290</sup> <sub>-380</sub>	7550 ± 350
D243	11030 <sup>+790</sup> <sub>-1240</sub>	11470 <sup>+820</sup> <sub>-1290</sub>	9560 <sup>+690</sup> <sub>-1070</sub>
D244	8100 <sup>+150</sup> <sub>-230</sub>	7290 <sup>+130</sup> <sub>-200</sub>	6130 ± 110
D245	7470 <sup>+250</sup> <sub>-240</sub>	6400 ± 210	5400 ± 180
D246	8320 <sup>+410</sup> <sub>-460</sub>	7620 <sup>+380</sup> <sub>-420</sub>	6400 ± 320
D247	9510 <sup>+340</sup> <sub>-350</sub>	9220 <sup>+330</sup> <sub>-410</sub>	7780 ± 280
D248	7790 <sup>+130</sup> <sub>-220</sub>	6860 <sup>+120</sup> <sub>-190</sub>	5780 ± 100
D249	9290 <sup>+210</sup> <sub>-200</sub>	8920 <sup>+130</sup> <sub>-90</sub>	7530 ± 170
D250	10100 <sup>+520</sup> <sub>-550</sub>	10150 <sup>+530</sup> <sub>-550</sub>	8480 <sup>+440</sup> <sub>-460</sub>
D251	10700 <sup>+820</sup> <sub>-740</sub>	10990 <sup>+840</sup> <sub>-760</sub>	9170 <sup>+710</sup> <sub>-640</sub>
D252	12480 <sup>+1970</sup> <sub>-1990</sub>	12120 <sup>+100</sup> <sub>-110</sub>	11260 ± 1770
D253	12300 <sup>+210</sup> <sub>-240</sub>	13290 <sup>+230</sup> <sub>-260</sub>	11060 <sup>+190</sup> <sub>-220</sub>
D254	12340 <sup>+60</sup> <sub>-70</sub>	13340 <sup>+60</sup> <sub>-80</sub>	11090 <sup>+50</sup> <sub>-70</sub>
D255	12760 ± 140	13950 ± 150	11590 ± 130
D256	12060 <sup>+1710</sup> <sub>-1930</sub>	10920 ± 70	10770 ± 1520
D257	10880 <sup>+1020</sup> <sub>-1070</sub>	10690 <sup>+70</sup> <sub>-60</sub>	9380 ± 880
D258	11270 <sup>+430</sup> <sub>-380</sub>	11820 <sup>+450</sup> <sub>-390</sub>	9850 <sup>+370</sup> <sub>-330</sub>
D259	13700 <sup>+120</sup> <sub>-130</sub>	15280 <sup>+130</sup> <sub>-150</sub>	12680 <sup>+110</sup> <sub>-120</sub>
D260	10010 ± 100	10010 ± 100	8370 ± 80
D261	9990 ± 100	9990 ± 100	8350 ± 80
D262	11170 <sup>+420</sup> <sub>-560</sub>	10100 <sup>+120</sup> <sub>-140</sub>	9720 ± 370
D263	13380 <sup>+600</sup> <sub>-690</sub>	14830 <sup>+660</sup> <sub>-760</sub>	12310 <sup>+550</sup> <sub>-630</sub>
D264	14170 <sup>+260</sup> <sub>-310</sub>	15950 <sup>+300</sup> <sub>-350</sub>	13240 <sup>+250</sup> <sub>-290</sub>
D265	13550 <sup>+340</sup> <sub>-300</sub>	15070 <sup>+380</sup> <sub>-340</sub>	12510 <sup>+320</sup> <sub>-280</sub>
D266	10790 <sup>+1330</sup> <sub>-1110</sub>	11570 <sup>+130</sup> <sub>-120</sub>	9290 ± 1140
D267	13060 <sup>+310</sup> <sub>-390</sub>	14370 <sup>+340</sup> <sub>-420</sub>	11940 <sup>+280</sup> <sub>-350</sub>
D268	12400 <sup>+100</sup> <sub>-110</sub>	13430 <sup>+110</sup> <sub>-120</sub>	11170 <sup>+90</sup> <sub>-100</sub>
D269	12580 <sup>+290</sup> <sub>-280</sub>	13690 <sup>+320</sup> <sub>-300</sub>	11380 <sup>+270</sup> <sub>-250</sub>
D270	11440 <sup>+490</sup> <sub>-440</sub>	12060 <sup>+510</sup> <sub>-460</sub>	10050 <sup>+430</sup> <sub>-380</sub>
D271	13960 <sup>+210</sup> <sub>-190</sub>	15660 <sup>+240</sup> <sub>-210</sub>	12990 <sup>+200</sup> <sub>-180</sub>
D272	10900 <sup>+860</sup> <sub>-720</sub>	11290 <sup>+890</sup> <sub>-740</sub>	9420 <sup>+740</sup> <sub>-620</sub>
D273	13330 <sup>+490</sup> <sub>-450</sub>	14760 <sup>+550</sup> <sub>-500</sub>	12260 <sup>+450</sup> <sub>-420</sub>
D274	10840 <sup>+860</sup> <sub>-830</sub>	11190 <sup>+890</sup> <sub>-850</sub>	9340 <sup>+740</sup> <sub>-710</sub>

**Table D.5.** Adopted electron temperatures for the nebular sample. The information in this table is derived from the values in Table D.4 and the  $T_e$  relations from Garnett (1992) and Méndez-Delgado et al. (2023b).

Reference number	$T_e$ ([N II]) [K]	$T_e$ ([O III]) [K]	$T_0$ (O <sup>2+</sup> ) [K]
D275	13920 <sup>+90</sup> <sub>-120</sub>	15600 <sup>+100</sup> <sub>-130</sub>	12950 <sup>+90</sup> <sub>-110</sub>
D276	13240 <sup>+130</sup> <sub>-170</sub>	14640 <sup>+150</sup> <sub>-180</sub>	12160 <sup>+120</sup> <sub>-150</sub>
D277	12650 <sup>+170</sup> <sub>-160</sub>	13780 <sup>+180</sup> <sub>-170</sub>	11460 <sup>+150</sup> <sub>-140</sub>
D278	11990 ± 90	12840 <sup>+100</sup> <sub>-90</sub>	10690 ± 80
D279	11580 <sup>+380</sup> <sub>-350</sub>	12250 <sup>+400</sup> <sub>-370</sub>	10200 <sup>+330</sup> <sub>-310</sub>
D280	11800 <sup>+100</sup> <sub>-140</sub>	12570 <sup>+110</sup> <sub>-150</sub>	10470 <sup>+90</sup> <sub>-130</sub>
D281	11170 <sup>+570</sup> <sub>-780</sub>	11670 <sup>+590</sup> <sub>-820</sub>	9720 <sup>+500</sup> <sub>-680</sub>
D282	9660 <sup>+690</sup> <sub>-820</sub>	8440 <sup>+580</sup> <sub>-560</sub>	7960 ± 570
D283	13350 <sup>+1520</sup> <sub>-1480</sub>	16010 <sup>+390</sup> <sub>-360</sub>	12280 ± 1400
D284	10740 <sup>+1140</sup> <sub>-2120</sub>	11280 <sup>+120</sup> <sub>-160</sub>	9230 ± 980
D285	8380 <sup>+220</sup> <sub>-330</sub>	8110 <sup>+380</sup> <sub>-390</sub>	6460 ± 170
D286	8110 <sup>+410</sup> <sub>-450</sub>	8730 <sup>+300</sup> <sub>-310</sub>	6150 ± 310
D287	8990 <sup>+470</sup> <sub>-420</sub>	8650 <sup>+110</sup> <sub>-150</sub>	7180 ± 380
D288	8890 <sup>+250</sup> <sub>-320</sub>	8210 <sup>+230</sup> <sub>-150</sub>	7060 ± 200
D289	9110 <sup>+860</sup> <sub>-1000</sub>	8510 ± 240	7310 ± 690
D290	10740 <sup>+100</sup> <sub>-120</sub>	11050 <sup>+110</sup> <sub>-120</sub>	9220 <sup>+90</sup> <sub>-100</sub>
D291	8540 <sup>+840</sup> <sub>-940</sub>	8220 ± 300	6650 ± 660
D292	8660 <sup>+730</sup> <sub>-560</sub>	8790 <sup>+230</sup> <sub>-310</sub>	6790 ± 570
D293	8980 <sup>+1080</sup> <sub>-970</sub>	7990 ± 300	7160 ± 860
D294	8780 <sup>+320</sup> <sub>-470</sub>	8260 <sup>+310</sup> <sub>-440</sub>	6930 <sup>+260</sup> <sub>-370</sub>
D295	8710 <sup>+1030</sup> <sub>-1140</sub>	7870 <sup>+360</sup> <sub>-520</sub>	6850 ± 810
D296	10220 <sup>+140</sup> <sub>-210</sub>	10310 <sup>+140</sup> <sub>-210</sub>	8610 <sup>+120</sup> <sub>-170</sub>
D297	10700 ± 80	11000 ± 80	9180 ± 70
D298	6990 <sup>+570</sup> <sub>-650</sub>	5710 <sup>+470</sup> <sub>-530</sub>	4840 ± 390
D299	9740 <sup>+230</sup> <sub>-270</sub>	9630 <sup>+230</sup> <sub>-260</sub>	8050 <sup>+190</sup> <sub>-220</sub>
D300	6200 <sup>+450</sup> <sub>-500</sub>	4580 <sup>+330</sup> <sub>-370</sub>	3910 ± 280
D301	7810 <sup>+270</sup> <sub>-380</sub>	6890 <sup>+240</sup> <sub>-330</sub>	5800 ± 200
D302	7330 <sup>+380</sup> <sub>-340</sub>	6200 <sup>+320</sup> <sub>-290</sub>	5240 ± 270
D303	9650 ± 330	9490 <sup>+330</sup> <sub>-320</sub>	7950 <sup>+280</sup> <sub>-270</sub>
D304	8060 <sup>+410</sup> <sub>-430</sub>	7250 <sup>+370</sup> <sub>-390</sub>	6090 ± 310
D305	8150 <sup>+270</sup> <sub>-310</sub>	7360 <sup>+250</sup> <sub>-280</sub>	6190 ± 210
D306	8740 <sup>+620</sup> <sub>-470</sub>	8210 <sup>+580</sup> <sub>-440</sub>	6880 ± 490
D307	7820 <sup>+490</sup> <sub>-620</sub>	6900 <sup>+430</sup> <sub>-550</sub>	5810 ± 360
D308	6590 <sup>+430</sup> <sub>-370</sub>	5140 <sup>+330</sup> <sub>-290</sub>	4370 ± 280
D309	6920 <sup>+220</sup> <sub>-300</sub>	5610 <sup>+180</sup> <sub>-240</sub>	4750 ± 150
D310	9330 <sup>+580</sup> <sub>-630</sub>	9050 <sup>+560</sup> <sub>-610</sub>	7580 <sup>+470</sup> <sub>-510</sub>
D311	8180 <sup>+340</sup> <sub>-400</sub>	7410 <sup>+310</sup> <sub>-360</sub>	6230 ± 260
D312	12030 <sup>+1710</sup> <sub>-1890</sub>	12740 <sup>+250</sup> <sub>-160</sub>	10740 ± 1520
D313	11080 <sup>+290</sup> <sub>-320</sub>	10180 ± 60	9620 ± 250
D314	11250 <sup>+130</sup> <sub>-210</sub>	11720 <sup>+140</sup> <sub>-220</sub>	9820 <sup>+120</sup> <sub>-190</sub>
D315	10060 <sup>+630</sup> <sub>-680</sub>	10860 <sup>+190</sup> <sub>-170</sub>	8420 ± 530
D316	10580 <sup>+430</sup> <sub>-410</sub>	10820 <sup>+440</sup> <sub>-420</sub>	9040 <sup>+370</sup> <sub>-350</sub>
D317	10720 <sup>+400</sup> <sub>-490</sub>	10190 <sup>+50</sup> <sub>-60</sub>	9200 ± 350
D318	9530 <sup>+150</sup> <sub>-200</sub>	9330 <sup>+140</sup> <sub>-200</sub>	7810 <sup>+120</sup> <sub>-160</sub>
D319	13730 <sup>+100</sup> <sub>-90</sub>	15510 <sup>+90</sup> <sub>-100</sub>	12720 ± 90
D320	11870 <sup>+680</sup> <sub>-840</sub>	15570 <sup>+360</sup> <sub>-390</sub>	10550 ± 610
D321	7770 <sup>+440</sup> <sub>-480</sub>	6820 <sup>+390</sup> <sub>-420</sub>	5750 ± 330
D322	7970 <sup>+340</sup> <sub>-410</sub>	9390 <sup>+450</sup> <sub>-280</sub>	5990 ± 260
D323	7040 <sup>+480</sup> <sub>-580</sub>	5780 <sup>+400</sup> <sub>-480</sub>	4890 ± 340
D324	8260 <sup>+300</sup> <sub>-490</sub>	8370 <sup>+350</sup> <sub>-460</sub>	6320 ± 380
D325	7270 <sup>+380</sup> <sub>-450</sub>	6110 <sup>+320</sup> <sub>-390</sub>	5160 ± 270
D326	7080 <sup>+430</sup> <sub>-490</sub>	5780 <sup>+370</sup> <sub>-400</sub>	4940 <sup>+320</sup> <sub>-340</sub>
D327	8520 <sup>+330</sup> <sub>-560</sub>	8810 <sup>+110</sup> <sub>-110</sub>	6630 ± 410
D328	8850 <sup>+180</sup> <sub>-190</sub>	9880 <sup>+310</sup> <sub>-300</sub>	7010 ± 140
D329	7800 <sup>+390</sup> <sub>-380</sub>	10800 <sup>+390</sup> <sub>-420</sub>	5790 ± 290



**Table D.5.** Adopted electron temperatures for the nebular sample. The information in this table is derived from the values in Table D.4 and the  $T_e$  relations from Garnett (1992) and Méndez-Delgado et al. (2023b).

Reference number	$T_e$ ([N II]) [K]	$T_e$ ([O III]) [K]	$T_0$ (O <sup>2+</sup> ) [K]
D330	7680 <sup>+370</sup> <sub>-340</sub>	6700 <sup>+320</sup> <sub>-300</sub>	5650 ± 270
D331	8160 <sup>+590</sup> <sub>-780</sub>	7330 <sup>+530</sup> <sub>-700</sub>	6210 <sup>+450</sup> <sub>-600</sub>
D332	10120 <sup>+1050</sup> <sub>-1070</sub>	10180 <sup>+1050</sup> <sub>-1080</sub>	8500 <sup>+880</sup> <sub>-900</sub>
D333	7290 <sup>+300</sup> <sub>-390</sub>	6140 <sup>+250</sup> <sub>-330</sub>	5190 ± 210
D334	11430 <sup>+1340</sup> <sub>-1360</sub>	11550 <sup>+180</sup> <sub>-230</sub>	10030 ± 1170
D335	11970 <sup>+460</sup> <sub>-570</sub>	11320 <sup>+100</sup> <sub>-80</sub>	10660 ± 410
D336	14330 <sup>+2370</sup> <sub>-1870</sub>	11770 <sup>+280</sup> <sub>-190</sub>	13430 ± 2220
D337	12790 <sup>+150</sup> <sub>-110</sub>	13980 <sup>+160</sup> <sub>-120</sub>	11620 <sup>+130</sup> <sub>-100</sub>
D338	12650 <sup>+430</sup> <sub>-380</sub>	13790 <sup>+470</sup> <sub>-410</sub>	11470 <sup>+390</sup> <sub>-340</sub>
D339	12160 <sup>+410</sup> <sub>-640</sub>	13090 <sup>+440</sup> <sub>-690</sub>	10890 <sup>+370</sup> <sub>-580</sub>
D340	11200 <sup>+440</sup> <sub>-320</sub>	11720 <sup>+460</sup> <sub>-330</sub>	9770 <sup>+380</sup> <sub>-280</sub>
D341	15590 <sup>+2800</sup> <sub>-3280</sub>	12510 <sup>+280</sup> <sub>-370</sub>	14900 ± 2670
D342	12200 <sup>+200</sup> <sub>-230</sub>	13140 <sup>+210</sup> <sub>-250</sub>	10930 <sup>+170</sup> <sub>-210</sub>
D343	12100 ± 60	13000 <sup>+60</sup> <sub>-70</sub>	10820 <sup>+50</sup> <sub>-60</sub>
D344	17290 <sup>+100</sup> <sub>-160</sub>	20420 <sup>+120</sup> <sub>-180</sub>	16890 <sup>+100</sup> <sub>-150</sub>
D345	16950 <sup>+100</sup> <sub>-120</sub>	19930 <sup>+120</sup> <sub>-140</sub>	16490 <sup>+100</sup> <sub>-120</sub>
D346	17100 <sup>+270</sup> <sub>-210</sub>	20140 <sup>+310</sup> <sub>-240</sub>	16670 <sup>+260</sup> <sub>-200</sub>
D347	18000 <sup>+250</sup> <sub>-250</sub>	21420 <sup>+350</sup> <sub>-300</sub>	17720 <sup>+290</sup> <sub>-280</sub>
D348	17630 <sup>+230</sup> <sub>-230</sub>	20900 <sup>+340</sup> <sub>-270</sub>	17290 <sup>+280</sup> <sub>-230</sub>
D349	17650 <sup>+440</sup> <sub>-390</sub>	20940 <sup>+520</sup> <sub>-430</sub>	17320 <sup>+430</sup> <sub>-360</sub>
D350	18520 <sup>+420</sup> <sub>-270</sub>	22180 <sup>+510</sup> <sub>-310</sub>	18330 <sup>+420</sup> <sub>-260</sub>
D351	17170 <sup>+240</sup> <sub>-240</sub>	20250 <sup>+280</sup> <sub>-260</sub>	16750 <sup>+260</sup> <sub>-230</sub>
D352	24120 <sup>+3640</sup> <sub>-3690</sub>	21300 <sup>+260</sup> <sub>-250</sub>	24880 ± 3750
D353	17350 <sup>+260</sup> <sub>-200</sub>	20500 <sup>+310</sup> <sub>-240</sub>	16960 <sup>+260</sup> <sub>-200</sub>
D354	17320 <sup>+160</sup> <sub>-140</sub>	20460 <sup>+190</sup> <sub>-160</sub>	16920 <sup>+160</sup> <sub>-140</sub>
D355	16460 <sup>+320</sup> <sub>-360</sub>	19230 <sup>+380</sup> <sub>-420</sub>	15920 <sup>+310</sup> <sub>-350</sub>
D356	11890 <sup>+100</sup> <sub>-110</sub>	12700 <sup>+110</sup> <sub>-120</sub>	10570 <sup>+90</sup> <sub>-100</sub>
D357	12100 <sup>+140</sup> <sub>-110</sub>	13000 <sup>+150</sup> <sub>-120</sub>	10820 <sup>+120</sup> <sub>-100</sub>
D358	16270 <sup>+140</sup> <sub>-190</sub>	18960 <sup>+160</sup> <sub>-230</sub>	15700 <sup>+140</sup> <sub>-190</sub>
D359	13710 <sup>+170</sup> <sub>-140</sub>	15290 <sup>+180</sup> <sub>-160</sub>	12690 <sup>+150</sup> <sub>-130</sub>
D360	15860 <sup>+170</sup> <sub>-230</sub>	18380 <sup>+190</sup> <sub>-260</sub>	15220 <sup>+160</sup> <sub>-220</sub>
D361	14810 <sup>+80</sup> <sub>-110</sub>	16870 <sup>+90</sup> <sub>-130</sub>	13990 <sup>+80</sup> <sub>-110</sub>
D362	15260 <sup>+210</sup> <sub>-250</sub>	17510 <sup>+240</sup> <sub>-280</sub>	14510 <sup>+200</sup> <sub>-240</sub>
D363	19000 <sup>+1430</sup> <sub>-1740</sub>	20140 ± 280	18890 ± 1420
D364	18200 <sup>+400</sup> <sub>-410</sub>	21710 <sup>+480</sup> <sub>-490</sub>	17950 ± 400
D365	13460 <sup>+290</sup> <sub>-260</sub>	14940 <sup>+320</sup> <sub>-280</sub>	12410 <sup>+270</sup> <sub>-240</sub>
D366	12670 <sup>+120</sup> <sub>-150</sub>	13820 <sup>+130</sup> <sub>-160</sub>	11490 <sup>+110</sup> <sub>-140</sub>
D367	14220 <sup>+230</sup> <sub>-250</sub>	16030 <sup>+260</sup> <sub>-280</sub>	13300 <sup>+210</sup> <sub>-230</sub>
D368	13380 <sup>+480</sup> <sub>-640</sub>	14840 <sup>+530</sup> <sub>-700</sub>	12320 <sup>+440</sup> <sub>-580</sub>
D369	15440 ± 180	17770 <sup>+210</sup> <sub>-200</sub>	14730 ± 170
D370	16420 <sup>+390</sup> <sub>-380</sub>	19160 <sup>+460</sup> <sub>-440</sub>	15870 <sup>+380</sup> <sub>-360</sub>
D371	16940 <sup>+250</sup> <sub>-220</sub>	19910 <sup>+290</sup> <sub>-260</sub>	16470 <sup>+240</sup> <sub>-220</sub>
D372	13330 <sup>+150</sup> <sub>-90</sub>	14760 <sup>+170</sup> <sub>-100</sub>	12250 <sup>+140</sup> <sub>-80</sub>
D373	12840 <sup>+130</sup> <sub>-120</sub>	14060 <sup>+150</sup> <sub>-130</sub>	11680 <sup>+120</sup> <sub>-110</sub>
D374	25510 <sup>+2430</sup> <sub>-2110</sub>	19010 <sup>+480</sup> <sub>-470</sub>	26500 ± 2530
D375	25450 <sup>+2870</sup> <sub>-2160</sub>	18970 <sup>+340</sup> <sub>-480</sub>	26430 ± 2980
D376	14220 <sup>+100</sup> <sub>-60</sub>	16030 <sup>+110</sup> <sub>-70</sub>	13300 <sup>+90</sup> <sub>-50</sub>
D377	12070 <sup>+260</sup> <sub>-380</sub>	12950 <sup>+280</sup> <sub>-400</sub>	10780 <sup>+230</sup> <sub>-340</sub>
D378	17430 <sup>+310</sup> <sub>-420</sub>	20620 <sup>+370</sup> <sub>-500</sub>	17050 <sup>+310</sup> <sub>-410</sub>
D379	14610 <sup>+240</sup> <sub>-220</sub>	16580 <sup>+270</sup> <sub>-250</sub>	13750 <sup>+230</sup> <sub>-200</sub>
D380	12340 <sup>+300</sup> <sub>-330</sub>	13340 <sup>+320</sup> <sub>-360</sub>	11090 <sup>+270</sup> <sub>-300</sub>
D381	15140 <sup>+160</sup> <sub>-180</sub>	17340 <sup>+190</sup> <sub>-200</sub>	14370 <sup>+160</sup> <sub>-170</sub>
D382	14160 <sup>+160</sup> <sub>-140</sub>	15940 <sup>+180</sup> <sub>-150</sub>	13230 <sup>+150</sup> <sub>-130</sub>
D383	12770 <sup>+190</sup> <sub>-180</sub>	13960 ± 200	11600 <sup>+170</sup> <sub>-160</sub>

**Table D.5.** Adopted electron temperatures for the nebular sample. The information in this table is derived from the values in Table D.4 and the  $T_e$  relations from Garnett (1992) and Méndez-Delgado et al. (2023b).

Reference number	$T_e$ ([N II]) [K]	$T_e$ ([O III]) [K]	$T_0$ (O <sup>2+</sup> ) [K]
D384	10580 <sup>+180</sup> <sub>-210</sub>	10830 <sup>+190</sup> <sub>-220</sub>	9040 <sup>+160</sup> <sub>-180</sub>
D385	11070 <sup>+180</sup> <sub>-150</sub>	11530 <sup>+190</sup> <sub>-160</sub>	9610 <sup>+160</sup> <sub>-130</sub>
D386	14830 <sup>+170</sup> <sub>-120</sub>	16900 <sup>+190</sup> <sub>-140</sub>	14010 <sup>+160</sup> <sub>-110</sub>
D387	15040 <sup>+270</sup> <sub>-380</sub>	17200 <sup>+310</sup> <sub>-430</sub>	14260 <sup>+260</sup> <sub>-360</sub>
D388	11620 <sup>+230</sup> <sub>-210</sub>	12320 <sup>+240</sup> <sub>-220</sub>	10260 <sup>+200</sup> <sub>-180</sub>
D389	12950 ± 90	14210 ± 100	11810 <sup>+80</sup> <sub>-90</sub>
D390	15520 <sup>+780</sup> <sub>-630</sub>	15730 <sup>+250</sup> <sub>-300</sub>	14820 ± 750
D391	11920 <sup>+310</sup> <sub>-210</sub>	12750 <sup>+340</sup> <sub>-230</sub>	10610 <sup>+280</sup> <sub>-190</sub>
D392	13630 <sup>+1420</sup> <sub>-1670</sub>	15090 <sup>+350</sup> <sub>-460</sub>	12610 ± 1310
D393	16730 <sup>+100</sup> <sub>-120</sub>	19610 <sup>+120</sup> <sub>-140</sub>	16230 <sup>+100</sup> <sub>-120</sub>
D394	11480 <sup>+480</sup> <sub>-490</sub>	12110 ± 510	10090 ± 430
D395	13090 <sup>+90</sup> <sub>-130</sub>	14410 <sup>+100</sup> <sub>-150</sub>	11970 <sup>+80</sup> <sub>-120</sub>
D396	12620 <sup>+60</sup> <sub>-70</sub>	13740 <sup>+60</sup> <sub>-70</sub>	11420 <sup>+50</sup> <sub>-60</sub>
D397	12370 <sup>+190</sup> <sub>-160</sub>	13390 <sup>+200</sup> <sub>-170</sub>	11130 <sup>+170</sup> <sub>-140</sub>
D398	10880 <sup>+170</sup> <sub>-300</sub>	11250 <sup>+170</sup> <sub>-310</sub>	9380 <sup>+150</sup> <sub>-260</sub>
D399	13150 <sup>+680</sup> <sub>-800</sub>	12530 <sup>+310</sup> <sub>-220</sub>	12050 ± 630
D400	10770 <sup>+840</sup> <sub>-730</sub>	12420 <sup>+60</sup> <sub>-40</sub>	9260 ± 730
D401	12080 <sup>+320</sup> <sub>-400</sub>	12520 <sup>+220</sup> <sub>-200</sub>	10790 ± 280
D402	11930 <sup>+230</sup> <sub>-270</sub>	12810 <sup>+180</sup> <sub>-240</sub>	10620 ± 200
D403	13120 <sup>+350</sup> <sub>-210</sub>	13880 <sup>+240</sup> <sub>-180</sub>	12010 ± 360
D404	11430 <sup>+150</sup> <sub>-110</sub>	12050 <sup>+220</sup> <sub>-150</sub>	10040 <sup>+180</sup> <sub>-130</sub>
D405	11960 <sup>+110</sup> <sub>-90</sub>	12800 <sup>+120</sup> <sub>-90</sub>	10650 <sup>+100</sup> <sub>-80</sub>
D406	11790 <sup>+290</sup> <sub>-350</sub>	12550 <sup>+300</sup> <sub>-370</sub>	10450 <sup>+250</sup> <sub>-310</sub>
D407	11110 <sup>+1410</sup> <sub>-840</sub>	12060 <sup>+140</sup> <sub>-190</sub>	9660 ± 1230
D408	11550 ± 80	12190 <sup>+90</sup> <sub>-80</sub>	10180 ± 70
D409	11400 <sup>+130</sup> <sub>-80</sub>	12000 <sup>+140</sup> <sub>-90</sub>	10000 <sup>+110</sup> <sub>-70</sub>
D410	11990 <sup>+1140</sup> <sub>-810</sub>	11970 <sup>+90</sup> <sub>-110</sub>	10690 ± 1020
D411	11920 <sup>+330</sup> <sub>-340</sub>	12180 ± 100	10610 ± 290
D412	11140 <sup>+960</sup> <sub>-1120</sub>	11920 <sup>+110</sup> <sub>-90</sub>	9690 ± 830
D413	10930 <sup>+240</sup> <sub>-160</sub>	11330 <sup>+250</sup> <sub>-170</sub>	9450 <sup>+210</sup> <sub>-140</sub>
D414	12450 <sup>+210</sup> <sub>-240</sub>	13500 <sup>+230</sup> <sub>-270</sub>	11230 <sup>+190</sup> <sub>-220</sub>
D415	13260 <sup>+250</sup> <sub>-180</sub>	14660 <sup>+280</sup> <sub>-200</sub>	12180 <sup>+230</sup> <sub>-170</sub>
D416	13240 <sup>+240</sup> <sub>-280</sub>	14620 <sup>+260</sup> <sub>-310</sub>	12150 <sup>+220</sup> <sub>-250</sub>
D417	13720 <sup>+110</sup> <sub>-140</sub>	15320 <sup>+130</sup> <sub>-150</sub>	12720 <sup>+110</sup> <sub>-130</sub>
D418	13500 <sup>+140</sup> <sub>-120</sub>	15000 <sup>+160</sup> <sub>-130</sub>	12450 <sup>+130</sup> <sub>-110</sub>
D419	13550 <sup>+290</sup> <sub>-270</sub>	15070 <sup>+320</sup> <sub>-300</sub>	12510 <sup>+270</sup> <sub>-250</sub>
D420	13540 <sup>+100</sup> <sub>-140</sub>	15060 <sup>+120</sup> <sub>-160</sub>	12500 <sup>+100</sup> <sub>-130</sub>
D421	13530 <sup>+120</sup> <sub>-180</sub>	15050 <sup>+140</sup> <sub>-200</sub>	12490 <sup>+110</sup> <sub>-160</sub>
D422	10910 <sup>+170</sup> <sub>-280</sub>	11300 <sup>+180</sup> <sub>-290</sub>	9420 <sup>+150</sup> <sub>-240</sub>
D423	17010 <sup>+150</sup> <sub>-240</sub>	20020 <sup>+180</sup> <sub>-290</sub>	16560 <sup>+150</sup> <sub>-240</sub>
D424	16720 <sup>+250</sup> <sub>-220</sub>	19600 <sup>+290</sup> <sub>-260</sub>	16230 <sup>+240</sup> <sub>-210</sub>
D425	9360 <sup>+290</sup> <sub>-340</sub>	11790 <sup>+30</sup> <sub>-60</sub>	7610 ± 240
D426	11650 <sup>+130</sup> <sub>-80</sub>	12360 <sup>+140</sup> <sub>-90</sub>	10290 <sup>+110</sup> <sub>-70</sub>
D427	11510 <sup>+60</sup> <sub>-50</sub>	12160 <sup>+60</sup> <sub>-50</sub>	10130 <sup>+50</sup> <sub>-40</sub>
D428	12110 <sup>+130</sup> <sub>-140</sub>	13020 <sup>+140</sup> <sub>-150</sub>	10830 <sup>+120</sup> <sub>-130</sub>
D429	13030 <sup>+210</sup> <sub>-170</sub>	14330 <sup>+240</sup> <sub>-190</sub>	11910 <sup>+200</sup> <sub>-160</sub>
D430	11940 <sup>+880</sup> <sub>-1090</sub>	13810 <sup>+140</sup> <sub>-120</sub>	10630 ± 780
D431	14140 <sup>+120</sup> <sub>-130</sub>	15920 ± 140	13210 ± 120
D432	14000 <sup>+150</sup> <sub>-140</sub>	15720 <sup>+170</sup> <sub>-160</sub>	13040 <sup>+140</sup> <sub>-130</sub>
D433	14520 <sup>+220</sup> <sub>-250</sub>	16450 <sup>+250</sup> <sub>-280</sub>	13650 <sup>+210</sup> <sub>-230</sub>
D434	14160 <sup>+150</sup> <sub>-170</sub>	15940 <sup>+170</sup> <sub>-190</sub>	13230 <sup>+140</sup> <sub>-150</sub>
D435	13950 <sup>+180</sup> <sub>-130</sub>	15640 <sup>+210</sup> <sub>-150</sub>	12980 <sup>+170</sup> <sub>-120</sub>
D436	14030 <sup>+180</sup> <sub>-210</sub>	15760 <sup>+200</sup> <sub>-240</sub>	13080 <sup>+170</sup> <sub>-200</sub>
D437	24970 <sup>+3620</sup> <sub>-3040</sub>	14430 <sup>+130</sup> <sub>-140</sub>	25870 ± 3750
D438	15430 <sup>+180</sup> <sub>-170</sub>	17760 ± 200	14720 <sup>+170</sup> <sub>-160</sub>

**Table D.5.** Adopted electron temperatures for the nebular sample. The information in this table is derived from the values in Table D.4 and the  $T_e$  relations from Garnett (1992) and Méndez-Delgado et al. (2023b).

Reference number	$T_e$ ([N II]) [K]	$T_e$ ([O III]) [K]	$T_0$ (O <sup>2+</sup> ) [K]
D439	15230 <sup>+220</sup> <sub>-330</sub>	17480 <sup>+260</sup> <sub>-380</sub>	14480 <sup>+210</sup> <sub>-310</sub>
D440	14640 <sup>+190</sup> <sub>-200</sub>	16630 <sup>+220</sup> <sub>-230</sub>	13790 <sup>+180</sup> <sub>-190</sub>
D441	11670 ± 140	12380 ± 150	10310 <sup>+130</sup> <sub>-120</sub>
D442	10440 <sup>+170</sup> <sub>-250</sub>	10620 <sup>+170</sup> <sub>-260</sub>	8870 <sup>+140</sup> <sub>-220</sub>
D443	11080 <sup>+1120</sup> <sub>-1170</sub>	9630 <sup>+820</sup> <sub>-670</sub>	9620 ± 970
D444	10850 <sup>+170</sup> <sub>-120</sub>	11220 <sup>+180</sup> <sub>-130</sub>	9360 <sup>+150</sup> <sub>-110</sub>
D445	11430 <sup>+420</sup> <sub>-390</sub>	12050 <sup>+440</sup> <sub>-410</sub>	10040 <sup>+370</sup> <sub>-340</sub>
D446	12460 <sup>+280</sup> <sub>-270</sub>	13510 <sup>+310</sup> <sub>-290</sub>	11240 <sup>+260</sup> <sub>-240</sub>
D447	12150 <sup>+740</sup> <sub>-580</sub>	13070 <sup>+800</sup> <sub>-620</sub>	10880 <sup>+660</sup> <sub>-520</sub>
D448	14170 <sup>+680</sup> <sub>-820</sub>	15960 <sup>+770</sup> <sub>-920</sub>	13240 <sup>+630</sup> <sub>-770</sub>
D449	12770 ± 110	13960 ± 120	11600 ± 100
D450	12550 <sup>+130</sup> <sub>-190</sub>	13650 <sup>+140</sup> <sub>-200</sub>	11350 <sup>+120</sup> <sub>-170</sub>
D451	14860 <sup>+270</sup> <sub>-240</sub>	16950 <sup>+310</sup> <sub>-270</sub>	14050 <sup>+250</sup> <sub>-230</sub>
D452	13620 <sup>+540</sup> <sub>-330</sub>	15170 <sup>+600</sup> <sub>-370</sub>	12590 <sup>+500</sup> <sub>-300</sub>

**Table D.6.** Ionic abundances derived from the nebular sample. All values are in  $12+\log(X/H)$  units. \* indicates  $\text{Fe}^{2+}$  abundance determinations based on  $[\text{Fe III}]\lambda 4658$  with flux errors smaller than 10%. \*\* indicates  $\text{O}^+$  abundance determinations based on  $[\text{O II}]\lambda 7319, 7330$  auroral lines.

Reference number	$\text{Fe}^{2+}$	$\text{N}^+$	$\text{O}^+$	$\text{O}^{2+}$		
				$[\text{O III}]\text{-CELs } t^2 = 0$	$[\text{O III}]\text{-CELs } t^2 > 0$	
					$\text{O II-RLs}$	
D1	$5.57^{+0.10}_{-0.09}$	$6.35 \pm 0.03$	$7.61^{+0.05}_{-0.04}$	$8.04^{+0.04}_{-0.03}$	$8.30 \pm 0.04$	-
D2	$5.29^{+0.12}_{-0.11}$	$5.85 \pm 0.03$	$7.08^{+0.04}_{-0.03}$	$7.99 \pm 0.03$	$8.23 \pm 0.03$	-
D3	$4.90^{+0.13}_{-0.12}$	$5.63 \pm 0.02$	$7.09 \pm 0.04^{**}$	$7.73 \pm 0.02$	$7.96 \pm 0.02$	-
D4	$5.41^{+0.15}_{-0.14}$	$5.77 \pm 0.04$	$7.25^{+0.08}_{-0.07}$ **	$7.74^{+0.04}_{-0.03}$	$7.97 \pm 0.04$	-
D5	$5.38^{+0.06}_{-0.05}$	$6.27 \pm 0.02$	$7.12^{+0.03}_{-0.02}$	$8.00^{+0.02}_{-0.01}$	$8.24 \pm 0.02$	-
D6	$5.39^{+0.07}_{-0.06}$	$6.30 \pm 0.02$	$7.21 \pm 0.03$	$8.02 \pm 0.02$	$8.26 \pm 0.03$	-
D7	$5.51^{+0.11}_{-0.09}$	$6.10 \pm 0.02$	$7.56 \pm 0.03$	$8.11 \pm 0.03$	$8.37 \pm 0.03$	-
D8	$5.64 \pm 0.14$	$6.46 \pm 0.05$	$7.64^{+0.09}_{-0.07}$	$8.00^{+0.07}_{-0.05}$	$8.27^{+0.07}_{-0.06}$	-
D9	$5.37^{+0.18}_{-0.16}$	$6.14 \pm 0.03$	$7.57^{+0.08}_{-0.07}$ **	$7.96^{+0.04}_{-0.03}$	$8.22 \pm 0.04$	-
D10	$5.02^{+0.13}_{-0.11}$	$5.89 \pm 0.02$	$7.39^{+0.05}_{-0.04}$ **	$7.99 \pm 0.02$	$8.24 \pm 0.02$	-
D11	$4.97 \pm 0.11$	$5.70^{+0.03}_{-0.02}$	$7.22 \pm 0.04^{**}$	$7.93 \pm 0.02$	$8.17^{+0.03}_{-0.02}$	-
D12	$5.07^{+0.12}_{-0.11}$	$6.07 \pm 0.02$	$7.49^{+0.04}_{-0.05}$ **	$8.03 \pm 0.02$	$8.28^{+0.03}_{-0.02}$	-
D13	$5.76^{+0.22}_{-0.16}$	$6.67^{+0.10}_{-0.07}$	$7.96^{+0.30}_{-0.15}$ **	$8.03^{+0.14}_{-0.09}$	$8.31^{+0.16}_{-0.10}$	-
D14	$5.39^{+0.14}_{-0.13}$	$6.00^{+0.04}_{-0.03}$	$7.45^{+0.08}_{-0.06}$ **	$7.89 \pm 0.03$	$8.12 \pm 0.03$	-
D15	$5.56^{+0.17}_{-0.16}$	$6.22 \pm 0.04$	$7.73^{+0.11}_{-0.08}$ **	$8.03^{+0.05}_{-0.04}$	$8.29 \pm 0.05$	-
D16	$5.57^{+0.17}_{-0.15}$	$6.42^{+0.05}_{-0.04}$	$7.53^{+0.07}_{-0.06}$	$7.80^{+0.06}_{-0.05}$	$8.04^{+0.07}_{-0.06}$	-
D17	$5.78^{+0.14}_{-0.12}$	$6.32^{+0.05}_{-0.04}$	$7.51^{+0.07}_{-0.06}$	$8.07^{+0.05}_{-0.04}$	$8.32^{+0.06}_{-0.05}$	-
D18	$5.84^{+0.20}_{-0.14}$	$6.82^{+0.10}_{-0.07}$	$8.00^{+0.18}_{-0.12}$	$8.14^{+0.16}_{-0.10}$	$8.43^{+0.17}_{-0.11}$	-
D19	$4.92^{+0.14}_{-0.12}$	$5.58 \pm 0.03$	$6.49 \pm 0.04$	$7.55 \pm 0.03$	$7.74 \pm 0.03$	-
D20	$4.96^{+0.12}_{-0.11}$	$5.55 \pm 0.03$	$6.51 \pm 0.04$	$7.53 \pm 0.03$	$7.71 \pm 0.03$	-
D21	$5.07^{+0.17}_{-0.15}$	$5.73 \pm 0.03$	$7.25^{+0.06}_{-0.05}$ **	$7.82 \pm 0.02$	$8.04^{+0.03}_{-0.02}$	-
D22	$4.92^{+0.17}_{-0.15}$	$5.05^{+0.07}_{-0.06}$	$6.59^{+0.09}_{-0.08}$ **	$7.09 \pm 0.03$	$7.29 \pm 0.04$	-
D23	$5.64^{+0.18}_{-0.15}$	$6.47^{+0.05}_{-0.04}$	$7.57^{+0.08}_{-0.06}$	$8.07^{+0.06}_{-0.05}$	$8.32^{+0.07}_{-0.06}$	-
D24	$5.70^{+0.17}_{-0.14}$	$6.22^{+0.05}_{-0.04}$	$7.71^{+0.11}_{-0.09}$ **	$8.02^{+0.06}_{-0.04}$	$8.27^{+0.06}_{-0.05}$	-
D25	$5.44^{+0.14}_{-0.13}$	$5.79 \pm 0.04$	$7.13 \pm 0.04$	$7.77 \pm 0.03$	$7.99^{+0.04}_{-0.03}$	-
D26	$5.92^{+0.27}_{-0.18}$	$6.73^{+0.16}_{-0.10}$	$7.98^{+0.25}_{-0.15}$	$8.03^{+0.20}_{-0.13}$	$8.31^{+0.23}_{-0.12}$	-
D27	$5.14^{+0.11}_{-0.09}$	$5.87 \pm 0.02$	$7.46^{+0.06}_{-0.05}$ **	$7.98^{+0.03}_{-0.02}$	$8.22 \pm 0.03$	-
D28	$4.71^{+0.15}_{-0.14}$	$5.36 \pm 0.02$	$6.81 \pm 0.01$	$7.80 \pm 0.01$	$8.02 \pm 0.01$	-
D29	$5.41^{+0.13}_{-0.14}$	$5.98 \pm 0.03$	$7.38 \pm 0.04$	$7.94 \pm 0.03$	$8.19^{+0.04}_{-0.03}$	-
D30	$5.58^{+0.18}_{-0.17}$	$6.19^{+0.05}_{-0.04}$	$7.51^{+0.07}_{-0.05}$	$7.99^{+0.06}_{-0.04}$	$8.24^{+0.06}_{-0.05}$	-
D31	$5.54^{+0.18}_{-0.17}$	$6.27^{+0.05}_{-0.04}$	$7.50^{+0.07}_{-0.06}$	$7.98^{+0.05}_{-0.04}$	$8.21^{+0.06}_{-0.05}$	-
D32	$5.51^{+0.14}_{-0.13}$	$6.47^{+0.04}_{-0.03}$	$7.89^{+0.10}_{-0.07}$ **	$8.14^{+0.05}_{-0.04}$	$8.43 \pm 0.05$	-
D33	$5.86^{+0.31}_{-0.48}$	$7.03^{+0.15}_{-0.10}$	$7.94^{+0.27}_{-0.14}$	$7.93^{+0.20}_{-0.13}$	$8.22^{+0.25}_{-0.14}$	-
D34	$5.86^{+0.30}_{-0.15}$	$6.69^{+0.14}_{-0.09}$	$7.87^{+0.43}_{-0.18}$ **	$7.88^{+0.19}_{-0.11}$	$8.14^{+0.22}_{-0.13}$	-
D35	$5.16^{+0.16}_{-0.14}$	$5.85 \pm 0.04$	$7.30^{+0.08}_{-0.07}$ **	$7.93 \pm 0.03$	$8.17 \pm 0.04$	-
D36	$5.48^{+0.14}_{-0.12}$	$6.07 \pm 0.03$	$7.57^{+0.04}_{-0.03}$	$7.96 \pm 0.03$	$8.21^{+0.04}_{-0.03}$	-
D37	$5.84^{+0.32}_{-0.20}$	$6.86^{+0.16}_{-0.10}$	$8.04^{+0.43}_{-0.21}$ **	$7.95^{+0.25}_{-0.13}$	$8.23^{+0.27}_{-0.14}$	-
D38	$5.22^{+0.15}_{-0.14}$	$5.77 \pm 0.02$	$7.34 \pm 0.03$	$7.70 \pm 0.02$	$7.92 \pm 0.02$	-
D39	$5.23^{+0.14}_{-0.13}$	$5.89 \pm 0.03$	$7.20^{+0.04}_{-0.03}$	$8.03 \pm 0.03$	$8.27 \pm 0.03$	-
D40	$5.30 \pm 0.09$	$5.97^{+0.02}_{-0.01}$	$7.38 \pm 0.02$	$7.77^{+0.02}_{-0.01}$	$8.00 \pm 0.02$	-
D41	$4.61^{+0.12}_{-0.11}$	$5.02 \pm 0.03$	$6.52^{+0.03}_{-0.02}$	$7.34^{+0.02}_{-0.01}$	$7.52 \pm 0.02$	-
D42	$5.58^{+0.18}_{-0.15}$	$6.45 \pm 0.04$	$7.81^{+0.10}_{-0.08}$ **	$8.05^{+0.05}_{-0.04}$	$8.32^{+0.05}_{-0.04}$	-
D43	$5.75^{+0.25}_{-0.18}$	$6.65^{+0.12}_{-0.08}$	$7.93^{+0.33}_{-0.17}$ **	$8.03^{+0.17}_{-0.10}$	$8.31^{+0.20}_{-0.12}$	-
D44	$5.47^{+0.18}_{-0.16}$	$6.37^{+0.05}_{-0.04}$	$7.80^{+0.12}_{-0.08}$ **	$8.03^{+0.06}_{-0.05}$	$8.30^{+0.07}_{-0.05}$	-
D45	$6.02^{+0.42}_{-0.21}$	$7.02^{+0.27}_{-0.12}$	$8.04^{+0.76}_{-0.24}$ **	$8.04^{+0.37}_{-0.17}$	$8.33^{+0.43}_{-0.19}$	-
D46	$5.68^{+0.14}_{-0.12}$	$6.33 \pm 0.04$	$7.73 \pm 0.06$	$8.13^{+0.05}_{-0.04}$	$8.41^{+0.06}_{-0.05}$	-
D47	$5.80^{+0.25}_{-0.17}$	$7.00^{+0.13}_{-0.09}$	$7.89^{+0.26}_{-0.14}$	$7.95^{+0.19}_{-0.11}$	$8.26^{+0.21}_{-0.13}$	-
D48	$5.83^{+0.07}_{-0.06}$ *	$6.96 \pm 0.04$	$8.05^{+0.10}_{-0.08}$ **	$8.02^{+0.05}_{-0.04}$	$8.31^{+0.06}_{-0.05}$	-
D49	$5.74^{+0.16}_{-0.14}$	$6.48^{+0.05}_{-0.04}$	$7.94^{+0.09}_{-0.07}$	$8.18^{+0.07}_{-0.05}$	$8.46^{+0.07}_{-0.06}$	-
D50	$5.51 \pm 0.17$	$6.13 \pm 0.04$	$7.41^{+0.06}_{-0.05}$	$7.95^{+0.05}_{-0.04}$	$8.19 \pm 0.05$	-
D51	$5.67^{+0.18}_{-0.15}$	$6.66^{+0.05}_{-0.04}$	$7.82^{+0.09}_{-0.06}$	$8.03^{+0.07}_{-0.05}$	$8.31^{+0.07}_{-0.06}$	-
D52	$5.51^{+0.13}_{-0.12}$	$6.15 \pm 0.04$	$7.40^{+0.07}_{-0.05}$	$7.80^{+0.05}_{-0.04}$	$8.03^{+0.06}_{-0.05}$	-
D53	$5.18^{+0.14}_{-0.12}$	-	$7.21 \pm 0.01$	$7.87 \pm 0.01$	$8.10 \pm 0.01$	-
D54	$4.70 \pm 0.15$	-	$6.85 \pm 0.01$	$7.71 \pm 0.01$	$7.91 \pm 0.01$	-

**Table D.6.** Ionic abundances derived from the nebular sample. All values are in  $12+\log(X/H)$  units. \* indicates  $\text{Fe}^{2+}$  abundance determinations based on  $[\text{Fe III}]\lambda 4658$  with flux errors smaller than 10%. \*\* indicates  $\text{O}^+$  abundance determinations based on  $[\text{O II}]\lambda 7319, 7330$  auroral lines.

Reference number	$\text{Fe}^{2+}$	$\text{N}^+$	$\text{O}^+$	$\text{O}^{2+}$		$\text{O}^{2+}$
				$[\text{O III}]\text{-CELs } t^2 = 0$	$[\text{O III}]\text{-CELs } t^2 > 0$	
D55	$5.90^{+0.16}_{-0.12}$	$6.89^{+0.08}_{-0.05}$	$7.81^{+0.13}_{-0.09}$	$7.89^{+0.10}_{-0.07}$	$8.16^{+0.13}_{-0.08}$	-
D56	$5.06^{+0.10}_{-0.09}$	-	$7.24 \pm 0.01$	$7.92 \pm 0.01$	$8.15 \pm 0.01$	-
D57	$5.51^{+0.21}_{-0.17}$	$6.45^{+0.07}_{-0.06}$	$7.88^{+0.19}_{-0.12}$ **	$8.10^{+0.09}_{-0.08}$	$8.37^{+0.12}_{-0.08}$	-
D58	$5.54^{+0.11}_{-0.09}$	$6.21^{+0.02}_{-0.03}$	$7.75^{+0.06}_{-0.05}$ **	$8.13 \pm 0.03$	$8.40 \pm 0.03$	-
D59	$5.17^{+0.08}_{-0.07}$	$5.82 \pm 0.01$	$7.25^{+0.02}_{-0.01}$	$8.03 \pm 0.01$	$8.28 \pm 0.01$	-
D60	$5.62^{+0.18}_{-0.14}$	$6.40 \pm 0.04$	$7.79^{+0.07}_{-0.05}$	$7.93^{+0.05}_{-0.04}$	$8.20^{+0.06}_{-0.05}$	-
D61	$5.69^{+0.15}_{-0.13}$	$6.55^{+0.05}_{-0.04}$	$7.76^{+0.08}_{-0.06}$	$8.06^{+0.06}_{-0.05}$	$8.33^{+0.08}_{-0.06}$	-
D62	$5.93^{+0.11}_{-0.09}$	$6.58 \pm 0.05$	$7.82^{+0.08}_{-0.06}$	$8.12^{+0.07}_{-0.05}$	$8.40^{+0.07}_{-0.06}$	-
D63	$5.57^{+0.10}_{-0.07}$	$6.83^{+0.03}_{-0.02}$	$8.13^{+0.07}_{-0.05}$ **	$8.24 \pm 0.03$	$8.54 \pm 0.03$	-
D64	$5.63^{+0.16}_{-0.14}$	$7.01^{+0.06}_{-0.05}$	$8.27^{+0.15}_{-0.11}$ **	$8.21^{+0.08}_{-0.06}$	$8.54^{+0.09}_{-0.08}$	-
D65	$4.94 \pm 0.07$	$5.66 \pm 0.02$	$6.82^{+0.05}_{-0.04}$ **	$7.31 \pm 0.02$	$7.50^{+0.03}_{-0.02}$	-
D66	$5.41 \pm 0.16$	$5.95 \pm 0.04$	$7.21^{+0.06}_{-0.04}$	$7.93 \pm 0.04$	$8.16^{+0.05}_{-0.04}$	-
D67	$5.38^{+0.09}_{-0.08}$	$6.07 \pm 0.02$	$7.33 \pm 0.02$	$7.75 \pm 0.01$	$7.97^{+0.01}_{-0.02}$	-
D68	$5.54^{+0.09}_{-0.08}$	$6.46 \pm 0.03$	$7.94^{+0.09}_{-0.07}$ **	$8.22 \pm 0.04$	$8.51^{+0.05}_{-0.04}$	-
D69	$5.55^{+0.14}_{-0.13}$	$6.13 \pm 0.03$	$7.52^{+0.05}_{-0.04}$	$7.67^{+0.04}_{-0.03}$	$7.90 \pm 0.04$	-
D70	$5.53^{+0.12}_{-0.11}$	$6.09 \pm 0.03$	$7.61^{+0.05}_{-0.04}$	$7.99 \pm 0.03$	$8.24 \pm 0.04$	-
D71	$5.82^{+0.26}_{-0.17}$	$7.63^{+0.12}_{-0.09}$	$8.43^{+0.42}_{-0.19}$ **	$7.86^{+0.21}_{-0.12}$	$8.25^{+0.19}_{-0.12}$	-
D72	$4.90 \pm 0.06$	$5.46 \pm 0.01$	$7.00^{+0.02}_{-0.01}$	$7.67 \pm 0.01$	$7.88 \pm 0.01$	-
D73	$5.56^{+0.10}_{-0.08}$	-	$7.56 \pm 0.03$	$7.81^{+0.03}_{-0.02}$	$8.04^{+0.03}_{-0.02}$	-
D74	$5.04 \pm 0.15$	-	$7.59^{+0.02}_{-0.01}$	$8.11 \pm 0.01$	$8.38 \pm 0.01$	-
D75	$4.61^{+0.13}_{-0.12}$	$5.26 \pm 0.02$	$6.75 \pm 0.02$	$7.51 \pm 0.01$	$7.71^{+0.02}_{-0.01}$	-
D76	$5.22^{+0.07}_{-0.06}$	$6.01 \pm 0.01$	$7.18 \pm 0.02$	$8.10 \pm 0.01$	$8.35 \pm 0.01$	-
D77	$5.58^{+0.08}_{-0.07}$	$6.22 \pm 0.02$	$7.66 \pm 0.03$	$8.05 \pm 0.02$	$8.31 \pm 0.02$	-
D78	$4.71^{+0.09}_{-0.08}$	-	$6.42 \pm 0.02$	$7.39 \pm 0.01$	$7.59 \pm 0.01$	-
D79	$4.88^{+0.14}_{-0.12}$	$5.53 \pm 0.04$	$6.54^{+0.04}_{-0.03}$	$7.53 \pm 0.02$	$7.71^{+0.03}_{-0.02}$	-
D80	$4.93^{+0.05}_{-0.04}$ *	-	$6.52 \pm 0.02$	$7.54 \pm 0.01$	$7.72^{+0.02}_{-0.01}$	-
D81	$5.22^{+0.27}_{-0.14}$	$6.10^{+0.18}_{-0.12}$	$7.21^{+0.34}_{-0.15}$	$7.95^{+0.03}_{-0.02}$	$7.83^{+0.22}_{-0.12}$	-
D82	$5.11^{+0.07}_{-0.06}$	$5.58 \pm 0.02$	$6.77 \pm 0.02$	$7.84 \pm 0.01$	$8.05 \pm 0.01$	-
D83	$5.20^{+0.06}_{-0.05}$ *	$5.90^{+0.05}_{-0.04}$	$7.05^{+0.08}_{-0.06}$	$7.76 \pm 0.02$	$8.26^{+0.06}_{-0.05}$	-
D84	$5.00^{+0.10}_{-0.09}$	$6.22 \pm 0.03$	$7.36^{+0.05}_{-0.04}$	$7.98^{+0.04}_{-0.03}$	$8.23 \pm 0.04$	-
D85	$6.20^{+0.08}_{-0.07}$ *	-	$8.31^{+0.11}_{-0.08}$	$8.16^{+0.10}_{-0.07}$	$8.52^{+0.10}_{-0.08}$	$8.14^{+0.07}_{-0.06}$
D86	$6.03^{+0.08}_{-0.06}$ *	$7.43^{+0.06}_{-0.05}$	$8.24^{+0.10}_{-0.07}$	$8.03^{+0.09}_{-0.06}$	$8.36^{+0.09}_{-0.08}$	-
D87	$5.08^{+0.09}_{-0.07}$	-	$7.07 \pm 0.02$	$8.08 \pm 0.01$	$8.32 \pm 0.01$	-
D88	$4.69^{+0.08}_{-0.07}$	-	$6.34 \pm 0.02$	$7.05 \pm 0.01$	$7.23 \pm 0.01$	-
D89	$4.92^{+0.10}_{-0.09}$	-	$6.59^{+0.03}_{-0.02}$	$7.07 \pm 0.02$	$7.26 \pm 0.02$	-
D90	$5.36^{+0.14}_{-0.12}$	$6.29^{+0.06}_{-0.04}$	$7.50^{+0.16}_{-0.10}$ **	$7.77^{+0.08}_{-0.06}$	$8.01^{+0.09}_{-0.06}$	-
D91	$5.31^{+0.06}_{-0.04}$ *	$5.94 \pm 0.01$	$7.60 \pm 0.01$	$8.09 \pm 0.01$	$8.35 \pm 0.01$	-
D92	$5.49^{+0.07}_{-0.05}$ *	$6.61 \pm 0.04$	$7.59^{+0.06}_{-0.05}$	$7.88^{+0.03}_{-0.02}$	$8.25 \pm 0.05$	-
D93	$5.37 \pm 0.06$ *	$6.17 \pm 0.03$	$7.46 \pm 0.04$	$7.88 \pm 0.03$	$8.13 \pm 0.03$	-
D94	$5.11^{+0.08}_{-0.07}$	-	$6.66 \pm 0.01$	$7.50 \pm 0.01$	$7.70 \pm 0.01$	-
D95	$5.50^{+0.11}_{-0.09}$	-	$7.52^{+0.04}_{-0.03}$	$7.71^{+0.03}_{-0.02}$	$7.94 \pm 0.03$	-
D96	$5.07 \pm 0.16$	-	$6.80 \pm 0.04$	$7.83^{+0.03}_{-0.02}$	$8.05 \pm 0.03$	-
D97	$4.81^{+0.06}_{-0.05}$	$5.11 \pm 0.02$	$6.65 \pm 0.02$	$7.57 \pm 0.01$	$7.77 \pm 0.01$	-
D98	$4.79 \pm 0.12$	-	$6.28 \pm 0.02$	$7.41 \pm 0.01$	$7.60 \pm 0.01$	-
D99	$4.97^{+0.13}_{-0.11}$	$5.54 \pm 0.03$	$7.07^{+0.05}_{-0.04}$ **	$7.75 \pm 0.02$	$7.97 \pm 0.02$	-
D100	$4.57 \pm 0.04$ *	$4.75 \pm 0.03$	$6.23^{+0.02}_{-0.01}$	$7.41 \pm 0.01$	$7.60 \pm 0.01$	-
D101	$5.35^{+0.21}_{-0.11}$ *	$6.22^{+0.15}_{-0.09}$	$7.18^{+0.26}_{-0.13}$	$7.99 \pm 0.01$	$8.27^{+0.19}_{-0.11}$	-
D102	$5.24^{+0.06}_{-0.04}$ *	-	$7.26^{+0.02}_{-0.01}$	$7.98 \pm 0.01$	$8.21 \pm 0.01$	-
D103	$4.75^{+0.04}_{-0.03}$ *	$5.11 \pm 0.02$	$6.57 \pm 0.02$	$7.54 \pm 0.01$	$7.74 \pm 0.01$	-
D104	$5.36^{+0.07}_{-0.08}$	$5.81 \pm 0.02$	$7.44 \pm 0.02$	$7.97 \pm 0.02$	$8.21 \pm 0.02$	-
D105	$5.35^{+0.16}_{-0.15}$	$5.69 \pm 0.02$	$7.16 \pm 0.03$	$7.63 \pm 0.02$	$7.83 \pm 0.02$	-
D106	$5.16^{+0.07}_{-0.06}$ *	$5.93^{+0.04}_{-0.03}$	$7.14^{+0.07}_{-0.05}$	$8.01 \pm 0.01$	$7.91^{+0.06}_{-0.04}$	-
D107	$4.86^{+0.18}_{-0.17}$	-	$6.27^{+0.04}_{-0.03}$	$6.81^{+0.02}_{-0.01}$	$6.97 \pm 0.02$	-
D108	$5.28^{+0.06}_{-0.05}$ *	$5.88 \pm 0.01$	$7.72 \pm 0.01$	$8.03 \pm 0.01$	$8.29 \pm 0.01$	-
D109	$5.48^{+0.09}_{-0.07}$	$6.31 \pm 0.02$	$7.58 \pm 0.03$	$7.90^{+0.02}_{-0.03}$	$8.15 \pm 0.03$	-

**Table D.6.** Ionic abundances derived from the nebular sample. All values are in  $12+\log(X/H)$  units. \* indicates  $\text{Fe}^{2+}$  abundance determinations based on  $[\text{Fe III}]\lambda 4658$  with flux errors smaller than 10%. \*\* indicates  $\text{O}^+$  abundance determinations based on  $[\text{O II}]\lambda 7319, 7330$  auroral lines.

Reference number	$\text{Fe}^{2+}$	$\text{N}^+$	$\text{O}^+$	$\text{O}^{2+}$		$\text{O}^{2+}$
				$[\text{O III}]\text{-CELs } t^2 = 0$	$[\text{O III}]\text{-CELs } t^2 > 0$	
D110	$5.02 \pm 0.03^*$	$5.39 \pm 0.01$	$6.79 \pm 0.01$	$7.53 \pm 0.01$	$7.72 \pm 0.01$	-
D111	$4.84 \pm 0.02^*$	$5.54 \pm 0.01$	$7.06 \pm 0.01$	$7.92 \pm 0.01$	$8.14 \pm 0.01$	-
D112	$4.83 \pm 0.07$	$5.15^{+0.02}_{-0.01}$	$6.69 \pm 0.02$	$7.64 \pm 0.01$	$7.84 \pm 0.01$	-
D113	$4.85^{+0.04}_{-0.03}$ *	$5.41 \pm 0.01$	$6.99 \pm 0.01$	$7.75 \pm 0.01$	$7.95 \pm 0.01$	-
D114	$5.03^{+0.05}_{-0.03}$ *	$5.51 \pm 0.01$	$7.04 \pm 0.01$	$7.76 \pm 0.01$	$7.98 \pm 0.01$	-
D115	$5.25^{+0.04}_{-0.03}$ *	$6.33 \pm 0.02$	$7.62 \pm 0.04$	$8.27 \pm 0.01$	$8.46^{+0.04}_{-0.03}$	$8.42 \pm 0.05$
D116	$5.21^{+0.07}_{-0.06}$ *	$6.65^{+0.05}_{-0.04}$	$8.05^{+0.08}_{-0.06}$	$8.19^{+0.03}_{-0.02}$	$8.38^{+0.07}_{-0.06}$	$8.32 \pm 0.09$
D117	$5.04^{+0.03}_{-0.02}$ *	$6.62 \pm 0.01$	$7.97 \pm 0.02$	$8.17 \pm 0.02$	$8.37 \pm 0.01$	$8.37 \pm 0.03$
D118	$4.44^{+0.06}_{-0.05}$ *	$6.04 \pm 0.04$	$7.31^{+0.07}_{-0.06}$	$8.22 \pm 0.02$	$8.57^{+0.05}_{-0.04}$	$8.56 \pm 0.04$
D119	$5.05^{+0.08}_{-0.07}$ *	$6.25^{+0.06}_{-0.05}$	$7.67^{+0.10}_{-0.08}$	$8.27^{+0.04}_{-0.03}$	$8.44^{+0.10}_{-0.07}$	$8.45^{+0.07}_{-0.08}$
D120	$5.60 \pm 0.08$	$7.42^{+0.04}_{-0.03}$	$8.33^{+0.08}_{-0.05}$	$8.01^{+0.06}_{-0.05}$	$8.43^{+0.06}_{-0.05}$	-
D121	$5.55^{+0.08}_{-0.07}$	$7.48^{+0.04}_{-0.03}$	$8.44^{+0.06}_{-0.05}$	$8.05 \pm 0.04$	$8.69^{+0.07}_{-0.06}$	-
D122	$5.56^{+0.14}_{-0.09}$	$7.40^{+0.07}_{-0.06}$	$8.22^{+0.12}_{-0.09}$	$8.08^{+0.20}_{-0.11}$	$8.57^{+0.12}_{-0.08}$	-
D123	$5.91^{+0.15}_{-0.11}$	$7.58^{+0.08}_{-0.07}$	$8.38^{+0.14}_{-0.11}$	$7.84^{+0.13}_{-0.09}$	$8.23^{+0.14}_{-0.10}$	-
D124	$5.60^{+0.19}_{-0.13}$	$7.05^{+0.12}_{-0.08}$	$8.19^{+0.23}_{-0.12}$	$7.87^{+0.06}_{-0.05}$	$8.17^{+0.18}_{-0.13}$	-
D125	$6.03^{+0.13}_{-0.11}$	$7.62^{+0.10}_{-0.07}$	$8.51^{+0.17}_{-0.12}$	$8.11^{+0.14}_{-0.11}$	$8.50^{+0.16}_{-0.11}$	-
D126	$6.22^{+0.14}_{-0.10}$	$7.41^{+0.07}_{-0.06}$	$8.32^{+0.14}_{-0.09}$	$8.04^{+0.11}_{-0.08}$	$8.42^{+0.13}_{-0.10}$	-
D127	$5.65^{+0.10}_{-0.08}$	$6.95 \pm 0.04$	$7.95^{+0.07}_{-0.06}$	$7.54^{+0.05}_{-0.04}$	$7.81^{+0.06}_{-0.05}$	-
D128	$5.51^{+0.05}_{-0.04}$ *	$7.12 \pm 0.03$	$8.12^{+0.05}_{-0.04}$	$8.38 \pm 0.02$	$8.73 \pm 0.04$	-
D129	$5.01^{+0.14}_{-0.12}$	$7.02 \pm 0.03$	$8.15 \pm 0.04$	$7.90^{+0.04}_{-0.03}$	$8.21 \pm 0.04$	-
D130	$5.96^{+0.09}_{-0.08}$	$6.46 \pm 0.03$	$7.79 \pm 0.03$	$7.97 \pm 0.03$	$8.23 \pm 0.03$	-
D131	$5.16^{+0.11}_{-0.10}$	$6.62^{+0.03}_{-0.04}$	$7.91 \pm 0.03$	$8.09 \pm 0.02$	$8.36 \pm 0.02$	-
D132	$5.29^{+0.06}_{-0.05}$ *	$6.65 \pm 0.04$	$7.95^{+0.04}_{-0.03}$	$7.83 \pm 0.03$	$8.10 \pm 0.03$	-
D133	$5.14 \pm 0.11$	$6.46^{+0.04}_{-0.03}$	$7.78 \pm 0.04$	$8.00^{+0.03}_{-0.02}$	$8.27 \pm 0.03$	-
D134	$5.13^{+0.33}_{-0.15}$ *	$6.51^{+0.22}_{-0.12}$	$7.88^{+0.41}_{-0.18}$	$8.07 \pm 0.01$	$8.45^{+0.32}_{-0.15}$	-
D135	$5.07 \pm 0.07$	$6.34 \pm 0.03$	$7.61^{+0.05}_{-0.04}$	$8.07 \pm 0.02$	$8.26 \pm 0.04$	-
D136	$5.55^{+0.09}_{-0.06}$ *	$6.93^{+0.06}_{-0.05}$	$8.06^{+0.09}_{-0.07}$	$8.01 \pm 0.01$	$8.39^{+0.08}_{-0.06}$	-
D137	$5.37^{+0.12}_{-0.11}$	$6.81^{+0.04}_{-0.03}$	$7.98 \pm 0.03$	$8.05^{+0.03}_{-0.02}$	$8.32^{+0.03}_{-0.02}$	-
D138	$5.55^{+0.21}_{-0.13}$	$7.25^{+0.12}_{-0.09}$	$8.29^{+0.22}_{-0.13}$	$7.79 \pm 0.05$	$8.23^{+0.19}_{-0.12}$	-
D139	$5.86^{+0.15}_{-0.11}$	$7.54 \pm 0.07$	$8.45^{+0.14}_{-0.10}$	$7.81^{+0.12}_{-0.09}$	$8.14^{+0.16}_{-0.10}$	-
D140	$5.44^{+0.11}_{-0.08}$	$7.33^{+0.06}_{-0.05}$	$8.32^{+0.10}_{-0.07}$	$7.76^{+0.06}_{-0.05}$	$8.19^{+0.09}_{-0.07}$	-
D141	$5.38^{+0.14}_{-0.10}$	$6.82^{+0.08}_{-0.07}$	$8.00^{+0.14}_{-0.11}$	$7.78 \pm 0.03$	$7.81^{+0.10}_{-0.07}$	-
D142	$5.39^{+0.25}_{-0.15}$	$7.34^{+0.16}_{-0.10}$	$8.28^{+0.29}_{-0.16}$	$8.19^{+0.24}_{-0.14}$	$8.57^{+0.32}_{-0.15}$	-
D143	$5.82^{+0.17}_{-0.12}$	$7.55^{+0.10}_{-0.08}$	$8.43^{+0.20}_{-0.11}$	$7.87^{+0.19}_{-0.12}$	$8.23^{+0.21}_{-0.12}$	-
D144	$5.83^{+0.08}_{-0.07}$	$7.06^{+0.05}_{-0.04}$	$8.12 \pm 0.04$	$8.15^{+0.04}_{-0.03}$	$8.48 \pm 0.04$	-
D145	$5.50^{+0.05}_{-0.03}$ *	$6.39 \pm 0.03$	$7.74 \pm 0.02$	$7.65 \pm 0.01$	$7.89 \pm 0.02$	-
D146	$4.88 \pm 0.10$	$6.93 \pm 0.04$	$8.15 \pm 0.02$	$8.21^{+0.02}_{-0.01}$	$8.53 \pm 0.02$	-
D147	$6.32^{+0.13}_{-0.10}$ *	$7.76^{+0.08}_{-0.06}$	$8.53^{+0.15}_{-0.10}$	$7.87^{+0.12}_{-0.10}$	$8.29^{+0.18}_{-0.11}$	-
D148	$6.04^{+0.11}_{-0.08}$ *	$7.62^{+0.07}_{-0.05}$	$8.42^{+0.11}_{-0.08}$	$8.16^{+0.10}_{-0.07}$	$8.59^{+0.12}_{-0.10}$	-
D149	$4.83^{+0.11}_{-0.10}$	$6.48 \pm 0.03$	$7.88 \pm 0.02$	$7.75^{+0.02}_{-0.01}$	$8.01 \pm 0.02$	-
D150	$6.25^{+0.20}_{-0.13}$	$7.94^{+0.13}_{-0.09}$	$8.50^{+0.25}_{-0.15}$	$7.95^{+0.24}_{-0.15}$	$8.41^{+0.28}_{-0.16}$	-
D151	$5.37^{+0.25}_{-0.13}$	$7.56^{+0.14}_{-0.11}$	$8.40^{+0.31}_{-0.15}$	$8.11^{+0.23}_{-0.12}$	$8.50^{+0.17}_{-0.12}$	-
D152	$6.00^{+0.14}_{-0.10}$	$7.46^{+0.08}_{-0.06}$	$8.43^{+0.13}_{-0.09}$	$7.42^{+0.12}_{-0.09}$	$7.76^{+0.11}_{-0.08}$	-
D153	$4.92^{+0.11}_{-0.09}$	-	$7.58^{+0.03}_{-0.02}$	$7.59 \pm 0.02$	$7.83 \pm 0.02$	-
D154	$5.07 \pm 0.09$	$6.17^{+0.03}_{-0.02}$	$7.62^{+0.03}_{-0.02}$	$7.43 \pm 0.02$	$7.66 \pm 0.02$	-
D155	$6.46^{+0.21}_{-0.13}$	$7.79^{+0.12}_{-0.08}$	$8.56^{+0.21}_{-0.13}$	$8.06^{+0.20}_{-0.12}$	$8.53^{+0.21}_{-0.14}$	-
D156	$5.36^{+0.22}_{-0.13}$ *	$6.51^{+0.17}_{-0.10}$	$7.88^{+0.29}_{-0.15}$	$7.94 \pm 0.02$	$8.26^{+0.23}_{-0.12}$	-
D157	$5.54^{+0.10}_{-0.08}$ *	$7.21^{+0.06}_{-0.05}$	$8.26^{+0.10}_{-0.08}$	$8.20 \pm 0.02$	$8.72 \pm 0.09$	-
D158	$6.00^{+0.11}_{-0.08}$ *	$7.40^{+0.08}_{-0.06}$	$8.35^{+0.14}_{-0.09}$	$7.64^{+0.10}_{-0.09}$	$8.31^{+0.11}_{-0.09}$	-
D159	$4.61 \pm 0.11$	$6.07 \pm 0.02$	$7.48 \pm 0.02$	$7.76 \pm 0.01$	$7.99 \pm 0.02$	-
D160	$5.92^{+0.18}_{-0.12}$ *	$7.60^{+0.12}_{-0.09}$	$8.48^{+0.20}_{-0.12}$	$7.84^{+0.19}_{-0.12}$	$8.25^{+0.20}_{-0.13}$	-
D161	$5.75^{+0.15}_{-0.11}$	$7.63^{+0.10}_{-0.07}$	$8.44^{+0.18}_{-0.11}$	$8.11^{+0.15}_{-0.10}$	$8.53^{+0.19}_{-0.12}$	-
D162	$5.99^{+0.17}_{-0.11}$ *	$7.65^{+0.10}_{-0.09}$	$8.52^{+0.21}_{-0.12}$	$7.89^{+0.18}_{-0.12}$	$8.28^{+0.20}_{-0.12}$	-
D163	$5.81^{+0.15}_{-0.11}$	$7.51^{+0.09}_{-0.07}$	$8.48^{+0.16}_{-0.11}$	$7.82^{+0.14}_{-0.11}$	$8.18^{+0.17}_{-0.12}$	-
D164	$5.97^{+0.11}_{-0.09}$ *	$7.64^{+0.07}_{-0.06}$	$8.38^{+0.14}_{-0.09}$	$7.84^{+0.12}_{-0.09}$	$8.24^{+0.13}_{-0.09}$	-



**Table D.6.** Ionic abundances derived from the nebular sample. All values are in  $12+\log(X/H)$  units. \* indicates  $\text{Fe}^{2+}$  abundance determinations based on  $[\text{Fe III}]\lambda 4658$  with flux errors smaller than 10%. \*\* indicates  $\text{O}^+$  abundance determinations based on  $[\text{O II}]\lambda 7319, 7330$  auroral lines.

Reference number	$\text{Fe}^{2+}$	$\text{N}^+$	$\text{O}^+$	$\text{O}^{2+}$		$\text{O}^{2+}$ O II-RLs
				$[\text{O III}]\text{-CELs } t^2 = 0$	$[\text{O III}]\text{-CELs } t^2 > 0$	
D165	$5.56^{+0.07*}_{-0.06}$	$6.94 \pm 0.05$	$8.08^{+0.09}_{-0.07}$	$8.01 \pm 0.01$	$8.40^{+0.08}_{-0.07}$	-
D166	$5.59^{+0.06*}_{-0.05}$	$6.97 \pm 0.04$	$8.10^{+0.06}_{-0.05}$	$8.17 \pm 0.01$	$8.57 \pm 0.05$	-
D167	$5.45^{+0.07*}_{-0.06}$	$6.75^{+0.05}_{-0.04}$	$7.87^{+0.07}_{-0.06}$	$8.19 \pm 0.01$	$8.56^{+0.07}_{-0.06}$	-
D168	$5.41^{+0.09}_{-0.07}$	$6.50^{+0.06}_{-0.05}$	$7.68^{+0.14**}_{-0.11}$	$8.29 \pm 0.03$	$8.33^{+0.07}_{-0.06}$	$8.50 \pm 0.11$
D169	$5.34^{+0.16}_{-0.12}$	$7.24^{+0.09}_{-0.06}$	$8.32^{+0.14}_{-0.09}$	$7.72 \pm 0.02$	$8.37^{+0.10}_{-0.08}$	-
D170	$5.08^{+0.21*}_{-0.07}$	$6.14^{+0.18}_{-0.05}$	$6.70^{+0.23}_{-0.08}$	$7.91^{+0.07}_{-0.06}$	$6.86^{+0.67}_{-0.10}$	-
D171	$5.49^{+0.10}_{-0.09}$	$7.22^{+0.03}_{-0.04}$	$8.12 \pm 0.05$	$7.78 \pm 0.04$	$8.10^{+0.05}_{-0.04}$	-
D172	$5.51^{+0.05*}_{-0.04}$	$6.76 \pm 0.04$	$7.90^{+0.06}_{-0.05}$	$8.23 \pm 0.01$	$8.49^{+0.05}_{-0.04}$	-
D173	$5.50^{+0.04*}_{-0.03}$	$6.69 \pm 0.02$	$7.72 \pm 0.03$	$8.19^{+0.01}_{-0.02}$	$8.36 \pm 0.03$	$8.29 \pm 0.13$
D174	$5.44^{+0.10*}_{-0.08}$	$7.26^{+0.07}_{-0.05}$	$8.32^{+0.12}_{-0.08}$	$8.05 \pm 0.03$	$8.58^{+0.12}_{-0.08}$	-
D175	$5.68^{+0.14*}_{-0.09}$	$7.29^{+0.10}_{-0.07}$	$8.28^{+0.17}_{-0.11}$	$7.89 \pm 0.03$	$8.49^{+0.16}_{-0.11}$	-
D176	$5.68^{+0.04*}_{-0.03}$	$7.03^{+0.04}_{-0.03}$	$8.03^{+0.05}_{-0.04}$	$8.29 \pm 0.01$	$8.71 \pm 0.05$	-
D177	$5.57^{+0.08*}_{-0.07}$	$6.89^{+0.06}_{-0.05}$	$7.77^{+0.09}_{-0.07}$	$8.30^{+0.05}_{-0.04}$	$8.57^{+0.08}_{-0.07}$	$8.68 \pm 0.12$
D178	$5.28^{+0.05*}_{-0.04}$	$6.88 \pm 0.03$	$8.02 \pm 0.02$	$8.17 \pm 0.02$	$8.47 \pm 0.02$	-
D179	$5.20^{+0.05*}_{-0.04}$	$6.79 \pm 0.03$	$7.92 \pm 0.02$	$8.23^{+0.02}_{-0.01}$	$8.54 \pm 0.02$	-
D180	$5.16 \pm 0.15$	$5.89^{+0.06}_{-0.07}$	$7.34 \pm 0.03$	$8.01^{+0.02}_{-0.01}$	$8.25 \pm 0.02$	-
D181	$5.27 \pm 0.10$	$6.19 \pm 0.04$	$7.65^{+0.05}_{-0.04}$	$7.71 \pm 0.03$	$7.94^{+0.04}_{-0.03}$	-
D182	$5.30^{+0.12*}_{-0.09}$	$6.12^{+0.09}_{-0.07}$	$7.47^{+0.15}_{-0.10}$	$8.04^{+0.02}_{-0.01}$	$8.44^{+0.15}_{-0.10}$	-
D183	$5.17 \pm 0.03*$	$5.78 \pm 0.04$	$7.11 \pm 0.02$	$7.93^{+0.01}_{-0.02}$	$8.16 \pm 0.02$	$8.05^{+0.14}_{-0.15}$
D184	$5.80^{+0.07*}_{-0.06}$	$7.21^{+0.05}_{-0.04}$	$8.15 \pm 0.07$	$7.40 \pm 0.03$	$8.05^{+0.06}_{-0.05}$	-
D185	$5.21^{+0.10}_{-0.08}$	$7.04^{+0.06}_{-0.05}$	$7.99^{+0.11}_{-0.08}$	$7.96^{+0.08}_{-0.06}$	$8.26^{+0.09}_{-0.07}$	-
D186	$6.06^{+0.06*}_{-0.04}$	$7.80^{+0.04}_{-0.03}$	$8.35 \pm 0.06$	$6.68 \pm 0.04$	$8.14^{+0.07}_{-0.05}$	-
D187	$6.28^{+0.13}_{-0.10}$	$7.57^{+0.03}_{-0.04}$	$8.38^{+0.08}_{-0.07}$	$7.94^{+0.20}_{-0.14}$	$8.47 \pm 0.06$	-
D188	$5.27 \pm 0.04*$	$6.90^{+0.03}_{-0.02}$	$7.87^{+0.04}_{-0.03}$	$8.29^{+0.04}_{-0.03}$	$8.48 \pm 0.03$	$8.50 \pm 0.07$
D189	$5.44^{+0.27}_{-0.18}$	$7.07^{+0.14}_{-0.09}$	$8.28^{+0.23}_{-0.13}$	$8.15^{+0.12}_{-0.10}$	$8.25^{+0.21}_{-0.13}$	-
D190	$5.67^{+0.13}_{-0.12}$	$7.37 \pm 0.06$	$8.49^{+0.10}_{-0.07}$	$7.54^{+0.22}_{-0.13}$	$8.28^{+0.10}_{-0.08}$	-
D191	$5.28 \pm 0.14$	$7.52 \pm 0.04$	$8.58^{+0.07}_{-0.06}$	$8.10 \pm 0.06$	$8.47^{+0.08}_{-0.06}$	-
D192	$5.47^{+0.14}_{-0.10}$	$7.45^{+0.08}_{-0.07}$	$8.38^{+0.14}_{-0.09}$	$8.05^{+0.11}_{-0.08}$	$8.44^{+0.11}_{-0.09}$	-
D193	$5.48^{+0.21}_{-0.16}$	$7.27^{+0.15}_{-0.11}$	$8.06^{+0.23}_{-0.14}$	$8.19^{+0.19}_{-0.11}$	$8.54^{+0.29}_{-0.15}$	-
D194	$5.09^{+0.14}_{-0.11}$	$6.80^{+0.09}_{-0.07}$	$7.95^{+0.13}_{-0.09}$	$8.11^{+0.09}_{-0.08}$	$8.17^{+0.13}_{-0.09}$	-
D195	$5.23^{+0.07*}_{-0.06}$	$6.39^{+0.06}_{-0.05}$	$7.76^{+0.09}_{-0.06}$	$8.09^{+0.04}_{-0.03}$	$8.33^{+0.07}_{-0.05}$	-
D196	$5.41^{+0.09}_{-0.08}$	$6.57 \pm 0.05$	$7.73^{+0.07}_{-0.06}$	$8.28 \pm 0.04$	$8.50^{+0.06}_{-0.04}$	-
D197	$4.93^{+0.19}_{-0.13}$	$6.56^{+0.12}_{-0.08}$	$7.71^{+0.20}_{-0.12}$	$7.87^{+0.15}_{-0.10}$	$8.16^{+0.25}_{-0.14}$	-
D198	$4.40^{+0.13}_{-0.09}$	$6.14^{+0.09}_{-0.07}$	$7.45^{+0.13}_{-0.10}$	$8.13^{+0.06}_{-0.05}$	$8.36^{+0.13}_{-0.09}$	$8.33 \pm 0.09$
D199	$5.15^{+0.06*}_{-0.04}$	$7.18 \pm 0.02$	$8.24 \pm 0.04$	$8.04^{+0.08}_{-0.07}$	$8.30 \pm 0.04$	$8.34 \pm 0.09$
D200	$5.23 \pm 0.12$	$6.71 \pm 0.05$	$7.96^{+0.07}_{-0.06}$	$8.28 \pm 0.04$	$8.57^{+0.07}_{-0.06}$	-
D201	$5.41^{+0.08*}_{-0.05}$	$6.90 \pm 0.03$	$7.89 \pm 0.05$	$8.21 \pm 0.04$	$8.53 \pm 0.04$	$8.43 \pm 0.07$
D202	$5.56^{+0.36}_{-0.18}$	$7.38^{+0.27}_{-0.14}$	$8.47^{+0.53}_{-0.20}$	$7.90^{+0.43}_{-0.18}$	$8.26^{+0.43}_{-0.18}$	-
D203	$5.62^{+0.13}_{-0.11}$	$7.46^{+0.07}_{-0.06}$	$8.64^{+0.10}_{-0.07}$	$7.63^{+0.08}_{-0.07}$	$8.02^{+0.13}_{-0.09}$	-
D204	$5.52^{+0.21}_{-0.16}$	$7.08^{+0.09}_{-0.07}$	$8.01^{+0.17}_{-0.10}$	$7.05^{+0.12}_{-0.08}$	$7.32^{+0.13}_{-0.09}$	-
D205	$4.65^{+0.17}_{-0.15}$	$6.38 \pm 0.07$	$7.71^{+0.10}_{-0.09}$	$8.22 \pm 0.05$	$8.37^{+0.10}_{-0.07}$	-
D206	$5.34^{+0.14}_{-0.12}$	$7.15^{+0.05}_{-0.04}$	$8.34 \pm 0.07$	$8.11^{+0.05}_{-0.04}$	$8.55^{+0.07}_{-0.06}$	-
D207	$5.33^{+0.10}_{-0.07}$	$6.75^{+0.06}_{-0.05}$	$7.93^{+0.08}_{-0.07}$	$8.31 \pm 0.03$	$8.62^{+0.08}_{-0.07}$	-
D208	$5.59^{+0.12}_{-0.09}$	$7.35^{+0.07}_{-0.05}$	$8.38^{+0.11}_{-0.09}$	$7.98^{+0.15}_{-0.10}$	$8.62^{+0.10}_{-0.08}$	-
D209	$6.41^{+0.08*}_{-0.06}$	$7.92^{+0.05}_{-0.04}$	$8.49^{+0.09}_{-0.07}$	$7.92^{+0.08}_{-0.07}$	$8.36^{+0.09}_{-0.07}$	-
D210	$6.01 \pm 0.10$	$7.88^{+0.04}_{-0.03}$	$8.47^{+0.07}_{-0.06}$	$8.14^{+0.07}_{-0.05}$	$8.58^{+0.06}_{-0.05}$	-
D211	$6.01^{+0.18}_{-0.15}$	$7.83^{+0.08}_{-0.06}$	$8.38^{+0.15}_{-0.10}$	$8.04^{+0.11}_{-0.09}$	$8.43^{+0.15}_{-0.10}$	-
D212	$6.01 \pm 0.06$	$7.96 \pm 0.02$	$8.46^{+0.04}_{-0.03}$	$8.16 \pm 0.03$	$8.62 \pm 0.03$	-
D213	$5.87^{+0.16}_{-0.14}$	$7.97^{+0.05}_{-0.04}$	$8.50^{+0.09}_{-0.07}$	$7.94^{+0.08}_{-0.07}$	$8.39 \pm 0.06$	-
D214	$6.23^{+0.07}_{-0.06}$	$8.07 \pm 0.04$	$8.50^{+0.07}_{-0.06}$	$8.22^{+0.07}_{-0.06}$	$8.73^{+0.07}_{-0.06}$	-
D215	$6.68^{+0.20}_{-0.13}$	$8.06^{+0.12}_{-0.09}$	$8.45^{+0.27}_{-0.14}$	$8.64^{+0.31}_{-0.17}$	$9.19^{+0.31}_{-0.17}$	-
D216	$6.54^{+0.29}_{-0.15}$	$7.91^{+0.20}_{-0.12}$	$8.45^{+0.38}_{-0.18}$	$7.96^{+0.35}_{-0.18}$	$8.39^{+0.41}_{-0.18}$	-
D217	$5.76 \pm 0.12$	$7.58^{+0.04}_{-0.03}$	$7.98^{+0.06}_{-0.05}$	$6.23^{+0.11}_{-0.09}$	$7.67^{+0.06}_{-0.05}$	-
D218	$6.41^{+0.16}_{-0.10}$	$8.05^{+0.08}_{-0.07}$	$8.66^{+0.17}_{-0.10}$	$8.32^{+0.15}_{-0.11}$	$8.80^{+0.12}_{-0.09}$	-

**Table D.6.** Ionic abundances derived from the nebular sample. All values are in  $12+\log(X/H)$  units. \* indicates  $\text{Fe}^{2+}$  abundance determinations based on  $[\text{Fe III}]\lambda 4658$  with flux errors smaller than 10%. \*\* indicates  $\text{O}^+$  abundance determinations based on  $[\text{O II}]\lambda 7319, 7330$  auroral lines.

Reference number	$\text{Fe}^{2+}$	$\text{N}^+$	$\text{O}^+$	$\text{O}^{2+}$		$\text{O}^{2+}$
				$[\text{O III}]\text{-CELs } t^2 = 0$	$[\text{O III}]\text{-CELs } t^2 > 0$	
D219	$6.24^{+0.28}_{-0.18}$	$7.95^{+0.15}_{-0.09}$	$8.49^{+0.27}_{-0.15}$	$7.88^{+0.28}_{-0.14}$	$8.36^{+0.26}_{-0.14}$	-
D220	$5.22 \pm 0.05^*$	$6.83 \pm 0.03$	$7.78^{+0.05}_{-0.04}$	$8.45 \pm 0.02$	$8.67 \pm 0.04$	$8.70^{+0.07}_{-0.08}$
D221	$5.29^{+0.06}_{-0.04}$ *	$7.59^{+0.02}_{-0.03}$	$8.47 \pm 0.04$	$7.73^{+0.07}_{-0.06}$	$8.15 \pm 0.04$	-
D222	$5.50^{+0.04}_{-0.03}$ *	$6.99 \pm 0.03$	$7.86 \pm 0.06$	$8.33 \pm 0.01$	$8.35 \pm 0.03$	$8.48 \pm 0.03$
D223	$5.69^{+0.03}_{-0.02}$ *	$7.33 \pm 0.02$	$8.13^{+0.04}_{-0.03}$	$7.96 \pm 0.01$	$8.32 \pm 0.04$	$8.27 \pm 0.03$
D224	$5.55 \pm 0.03^*$	$6.97 \pm 0.03$	$7.81^{+0.06}_{-0.04}$	$8.35 \pm 0.01$	$8.38 \pm 0.03$	$8.52 \pm 0.01$
D225	$5.68 \pm 0.03^*$	$7.27 \pm 0.02$	$8.16 \pm 0.03$	$8.04 \pm 0.02$	$8.44 \pm 0.03$	$8.40 \pm 0.04$
D226	$5.23 \pm 0.03^*$	$6.85 \pm 0.02$	$7.75 \pm 0.05$	$8.36 \pm 0.01$	$8.44^{+0.04}_{-0.03}$	$8.61 \pm 0.01$
D227	$5.50 \pm 0.03^*$	$6.90 \pm 0.03$	$7.74^{+0.06}_{-0.05}$	$8.35 \pm 0.01$	$8.35 \pm 0.03$	$8.54 \pm 0.03$
D228	$5.15 \pm 0.03^*$	$6.84^{+0.03}_{-0.02}$	$7.69 \pm 0.06$	$8.38 \pm 0.01$	$8.41^{+0.04}_{-0.03}$	$8.63 \pm 0.02$
D229	$5.46 \pm 0.03^*$	$6.97 \pm 0.02$	$7.80^{+0.06}_{-0.05}$	$8.36 \pm 0.01$	$8.37 \pm 0.04$	$8.54 \pm 0.02$
D230	$5.54^{+0.06}_{-0.05}$ *	$7.38^{+0.04}_{-0.03}$	$8.22 \pm 0.06$	$7.38^{+0.05}_{-0.04}$	$7.73 \pm 0.04$	-
D231	$5.49 \pm 0.04^*$	$6.89^{+0.04}_{-0.03}$	$7.81^{+0.08}_{-0.07}$	$8.38 \pm 0.02$	$8.49 \pm 0.04$	$8.55^{+0.05}_{-0.06}$
D232	$5.37 \pm 0.04^*$	$6.91^{+0.04}_{-0.03}$	$7.79^{+0.06}_{-0.05}$	$8.40 \pm 0.01$	$8.41^{+0.05}_{-0.04}$	$8.64 \pm 0.03$
D233	$5.60^{+0.08}_{-0.03}$ *	$7.03^{+0.06}_{-0.04}$	$7.92^{+0.10}_{-0.08}$	$8.35 \pm 0.05$	$8.43^{+0.09}_{-0.07}$	$8.52^{+0.07}_{-0.06}$
D234	$5.60^{+0.03}_{-0.02}$ *	$7.53 \pm 0.02$	$8.33 \pm 0.04$	$7.88 \pm 0.02$	$8.31 \pm 0.03$	$8.25 \pm 0.06$
D235	$5.40 \pm 0.03^*$	$6.74 \pm 0.02$	$7.79 \pm 0.04$	$8.21 \pm 0.03$	$8.51 \pm 0.03$	$8.47 \pm 0.07$
D236	$5.53^{+0.04}_{-0.03}$ *	$7.04^{+0.04}_{-0.03}$	$8.04 \pm 0.05$	$8.36 \pm 0.01$	$8.72^{+0.04}_{-0.03}$	$8.67 \pm 0.03$
D237	$4.86^{+0.10}_{-0.08}$ *	$6.47^{+0.07}_{-0.05}$	$7.31^{+0.12}_{-0.09}$	$8.43 \pm 0.03$	$8.29^{+0.09}_{-0.07}$	$8.74^{+0.10}_{-0.11}$
D238	$5.19^{+0.08}_{-0.06}$ *	$6.75^{+0.06}_{-0.05}$	$7.71^{+0.08}_{-0.07}$	$8.41 \pm 0.03$	$8.77^{+0.07}_{-0.05}$	$8.59^{+0.07}_{-0.08}$
D239	$5.43 \pm 0.04^*$	$7.29 \pm 0.02$	$8.20 \pm 0.03$	$7.35 \pm 0.02$	$7.65 \pm 0.02$	-
D240	$4.99^{+0.08}_{-0.07}$ *	$6.80 \pm 0.03$	$7.83^{+0.05}_{-0.04}$	$7.98^{+0.05}_{-0.04}$	$8.13 \pm 0.04$	-
D241	$5.78 \pm 0.03^*$	$7.57^{+0.02}_{-0.01}$	$8.45 \pm 0.03$	$7.68 \pm 0.02$	$8.04^{+0.03}_{-0.02}$	-
D242	$5.47^{+0.09}_{-0.07}$ *	$7.28^{+0.06}_{-0.05}$	$8.24^{+0.12}_{-0.09}$	$7.66^{+0.06}_{-0.05}$	$7.99^{+0.09}_{-0.07}$	-
D243	$4.91^{+0.21}_{-0.16}$ *	$5.95^{+0.31}_{-0.17}$	$7.61^{+0.21}_{-0.13}$	$7.78^{+0.14}_{-0.09}$	$8.03^{+0.18}_{-0.11}$	-
D244	$5.46^{+0.15}_{-0.13}$ *	$7.55 \pm 0.03$	$8.40^{+0.06}_{-0.05}$	$6.84^{+0.05}_{-0.04}$	$7.20^{+0.05}_{-0.04}$	-
D245	$5.64 \pm 0.13$	$7.57^{+0.05}_{-0.04}$	$8.33^{+0.10}_{-0.08}$	$8.25^{+0.08}_{-0.07}$	$8.64^{+0.10}_{-0.08}$	-
D246	$6.09^{+0.18}_{-0.14}$ *	$7.51^{+0.09}_{-0.07}$	$8.18^{+0.15}_{-0.10}$	$6.01^{+0.19}_{-0.16}$	$6.35^{+0.21}_{-0.16}$	-
D247	$5.72^{+0.07}_{-0.06}$ *	$7.20^{+0.05}_{-0.04}$	$8.19^{+0.09}_{-0.08}$	$7.75^{+0.07}_{-0.06}$	$8.03^{+0.07}_{-0.06}$	$8.12^{+0.15}_{-0.14}$
D248	$5.64 \pm 0.10$	$7.70 \pm 0.03$	$8.46^{+0.06}_{-0.05}$	$6.64^{+0.07}_{-0.05}$	$7.02 \pm 0.06$	-
D249	$5.03^{+0.05}_{-0.04}$ *	$7.30 \pm 0.03$	$8.28^{+0.05}_{-0.04}$	$7.83 \pm 0.02$	$8.12 \pm 0.04$	$8.05 \pm 0.13$
D250	$5.88^{+0.16}_{-0.13}$ *	$6.71^{+0.07}_{-0.06}$	$7.90^{+0.11}_{-0.08}$	$7.99^{+0.09}_{-0.07}$	$8.27^{+0.11}_{-0.08}$	-
D251	$5.67^{+0.23}_{-0.18}$ *	$6.78^{+0.09}_{-0.07}$	$7.83^{+0.15}_{-0.11}$	$7.79^{+0.13}_{-0.08}$	$8.06^{+0.15}_{-0.09}$	-
D252	$5.22^{+0.29}_{-0.15}$ *	$6.10^{+0.21}_{-0.10}$	$7.35^{+0.43}_{-0.16}$	$8.07 \pm 0.01$	$8.16^{+0.38}_{-0.15}$	-
D253	$5.17^{+0.07}_{-0.06}$ *	$5.95 \pm 0.03$	$7.35^{+0.04}_{-0.03}$	$7.97 \pm 0.03$	$8.20 \pm 0.03$	$8.80^{+0.13}_{-0.15}$
D254	$5.02^{+0.05}_{-0.03}$ *	$5.76 \pm 0.01$	$7.22 \pm 0.01$	$7.91 \pm 0.01$	$8.14 \pm 0.01$	$8.24 \pm 0.05$
D255	$5.37^{+0.14}_{-0.11}$ *	$6.02 \pm 0.02$	$7.36 \pm 0.02$	$7.89 \pm 0.01$	$8.12 \pm 0.01$	-
D256	$4.78^{+0.33}_{-0.15}$ *	$5.89^{+0.20}_{-0.12}$	$7.27^{+0.38}_{-0.15}$	$8.20 \pm 0.01$	$8.22^{+0.25}_{-0.15}$	-
D257	$4.97^{+0.19}_{-0.12}$ *	$6.07^{+0.14}_{-0.09}$	$7.50^{+0.23}_{-0.13}$	$8.19 \pm 0.01$	$8.38^{+0.17}_{-0.11}$	-
D258	$5.69^{+0.13}_{-0.11}$ *	$6.49 \pm 0.04$	$7.87^{+0.07}_{-0.06}$	$7.88^{+0.05}_{-0.04}$	$8.14^{+0.06}_{-0.05}$	-
D259	$5.22^{+0.08}_{-0.07}$ *	-	$7.02 \pm 0.02$	$7.72 \pm 0.01$	$7.94 \pm 0.01$	-
D260	$5.70^{+0.06}_{-0.04}$ *	-	$7.84 \pm 0.02$	$8.15 \pm 0.01$	$8.44 \pm 0.02$	-
D261	$5.70^{+0.05}_{-0.04}$ *	-	$7.84 \pm 0.02$	$8.15^{+0.02}_{-0.01}$	$8.44 \pm 0.02$	-
D262	$5.44^{+0.04}_{-0.06}$ *	$6.49^{+0.05}_{-0.04}$	$7.77^{+0.08}_{-0.07}$	$8.13 \pm 0.02$	$8.20^{+0.06}_{-0.05}$	-
D263	$5.01^{+0.13}_{-0.12}$ *	$5.65^{+0.05}_{-0.04}$	$7.15^{+0.11}_{-0.09}$ **	$7.71^{+0.06}_{-0.05}$	$7.93^{+0.07}_{-0.05}$	-
D264	$5.10^{+0.07}_{-0.05}$ *	$5.60 \pm 0.02$	$7.11 \pm 0.05$ **	$7.65^{+0.03}_{-0.02}$	$7.86^{+0.03}_{-0.02}$	-
D265	$5.17^{+0.19}_{-0.15}$ *	$5.73^{+0.04}_{-0.03}$	$7.17^{+0.04}_{-0.03}$	$7.71 \pm 0.03$	$7.93 \pm 0.03$	-
D266	$5.27^{+0.23}_{-0.13}$ *	$6.30^{+0.16}_{-0.10}$	$7.68^{+0.26}_{-0.14}$	$8.05^{+0.01}_{-0.02}$	$8.37^{+0.27}_{-0.14}$	-
D267	$4.95^{+0.08}_{-0.07}$ *	$5.78^{+0.03}_{-0.02}$	$7.16^{+0.07}_{-0.06}$ **	$7.81 \pm 0.03$	$8.03^{+0.04}_{-0.03}$	-
D268	$5.16^{+0.06}_{-0.04}$ *	-	$7.21 \pm 0.02$	$7.93 \pm 0.01$	$8.17 \pm 0.01$	-
D269	$5.38^{+0.14}_{-0.13}$ *	-	$7.27^{+0.04}_{-0.03}$	$7.95 \pm 0.03$	$8.18 \pm 0.03$	-
D270	$5.85^{+0.13}_{-0.12}$ *	$6.31^{+0.05}_{-0.04}$	$7.66^{+0.08}_{-0.06}$	$7.87^{+0.06}_{-0.05}$	$8.12^{+0.07}_{-0.05}$	-
D271	$5.35^{+0.06}_{-0.05}$ *	$5.52 \pm 0.02$	$7.13 \pm 0.02$	$7.72^{+0.02}_{-0.01}$	$7.93 \pm 0.02$	-
D272	$5.54^{+0.17}_{-0.11}$ *	$6.47^{+0.10}_{-0.06}$	$7.75^{+0.28}_{-0.13}$ **	$8.00^{+0.12}_{-0.08}$	$8.27^{+0.15}_{-0.10}$	-
D273	$4.69^{+0.18}_{-0.15}$ *	$5.82^{+0.04}_{-0.03}$	$7.27^{+0.09}_{-0.07}$ **	$7.81 \pm 0.04$	$8.03^{+0.05}_{-0.04}$	-

**Table D.6.** Ionic abundances derived from the nebular sample. All values are in  $12+\log(X/H)$  units. \* indicates  $\text{Fe}^{2+}$  abundance determinations based on  $[\text{Fe III}]\lambda 4658$  with flux errors smaller than 10%. \*\* indicates  $\text{O}^+$  abundance determinations based on  $[\text{O II}]\lambda 7319, 7330$  auroral lines.

Reference number	$\text{Fe}^{2+}$	$\text{N}^+$	$\text{O}^+$	$\text{O}^{2+}$		$\text{O}^{2+}$
				$[\text{O III}]\text{-CELs } t^2 = 0$	$[\text{O III}]\text{-CELs } t^2 > 0$	
D274	$5.42^{+0.17}_{-0.12}$	$6.24^{+0.09}_{-0.07}$	$7.80^{+0.27}_{-0.14}$ **	$8.07^{+0.13}_{-0.09}$	$8.34^{+0.15}_{-0.09}$	-
D275	$4.48^{+0.06}_{-0.05}$	-	$6.65^{+0.02}_{-0.01}$	$7.83 \pm 0.01$	$8.05 \pm 0.01$	-
D276	$4.63 \pm 0.07$	-	$6.95 \pm 0.02$	$7.85 \pm 0.01$	$8.07 \pm 0.01$	-
D277	$4.94^{+0.06}_{-0.03}$ *	-	$7.28^{+0.03}_{-0.02}$	$7.79^{+0.02}_{-0.01}$	$8.02 \pm 0.02$	-
D278	$5.23^{+0.07}_{-0.06}$	$5.89 \pm 0.01$	$7.42^{+0.02}_{-0.01}$	$7.94 \pm 0.01$	$8.18 \pm 0.01$	-
D279	$5.69^{+0.12}_{-0.11}$	$6.31 \pm 0.03$	$7.68 \pm 0.05$	$7.88 \pm 0.04$	$8.13^{+0.05}_{-0.04}$	-
D280	$5.04^{+0.08}_{-0.07}$	-	$7.38 \pm 0.02$	$8.02^{+0.02}_{-0.01}$	$8.26^{+0.02}_{-0.01}$	-
D281	$5.90^{+0.13}_{-0.10}$	$6.56^{+0.08}_{-0.06}$	$7.83^{+0.13}_{-0.10}$	$7.98^{+0.10}_{-0.07}$	$8.25^{+0.11}_{-0.08}$	-
D282	$5.71^{+0.17}_{-0.11}$	$6.76^{+0.10}_{-0.08}$	$7.75^{+0.21}_{-0.12}$	$8.30^{+0.14}_{-0.10}$	$8.41^{+0.15}_{-0.11}$	-
D283	$4.32^{+0.18}_{-0.10}$ *	$5.26^{+0.14}_{-0.09}$	$6.49^{+0.24}_{-0.12}$	$7.74 \pm 0.03$	$8.04^{+0.20}_{-0.12}$	$8.03^{+0.11}_{-0.12}$
D284	$5.32^{+0.33}_{-0.15}$	$6.34^{+0.25}_{-0.12}$	$7.80^{+0.43}_{-0.19}$	$7.98 \pm 0.02$	$8.27^{+0.25}_{-0.12}$	-
D285	$5.45^{+0.09}_{-0.07}$	$7.12^{+0.05}_{-0.04}$	$8.08^{+0.07}_{-0.06}$	$8.05^{+0.10}_{-0.07}$	$8.49^{+0.06}_{-0.05}$	-
D286	$5.33^{+0.14}_{-0.12}$	$7.01^{+0.08}_{-0.06}$	$8.00^{+0.17}_{-0.09}$	$7.94^{+0.06}_{-0.05}$	$8.62^{+0.14}_{-0.09}$	-
D287	$5.74^{+0.11}_{-0.08}$ *	$7.01^{+0.07}_{-0.06}$	$8.16^{+0.13}_{-0.09}$	$8.07 \pm 0.03$	$8.41^{+0.12}_{-0.08}$	-
D288	$5.60^{+0.07}_{-0.05}$ *	$6.94 \pm 0.04$	$7.92^{+0.07}_{-0.08}$	$8.15 \pm 0.04$	$8.44^{+0.06}_{-0.05}$	$8.49 \pm 0.12$
D289	$5.83^{+0.28}_{-0.15}$	$6.99^{+0.17}_{-0.10}$	$8.13^{+0.29}_{-0.16}$	$8.14^{+0.06}_{-0.04}$	$8.40^{+0.27}_{-0.14}$	-
D290	$5.32^{+0.07}_{-0.06}$	$6.37 \pm 0.06$	$7.82 \pm 0.03$	$7.98^{+0.04}_{-0.01}$	$8.25 \pm 0.02$	-
D291	$5.61^{+0.28}_{-0.15}$	$7.01^{+0.17}_{-0.11}$	$8.16^{+0.29}_{-0.17}$	$8.20^{+0.08}_{-0.06}$	$8.61^{+0.30}_{-0.15}$	-
D292	$5.83^{+0.24}_{-0.16}$	$7.17^{+0.12}_{-0.09}$	$8.38^{+0.22}_{-0.12}$	$7.98^{+0.06}_{-0.05}$	$8.46^{+0.25}_{-0.14}$	-
D293	$5.31^{+0.36}_{-0.19}$	$6.83^{+0.21}_{-0.11}$	$8.10^{+0.40}_{-0.18}$	$8.29^{+0.09}_{-0.07}$	$8.51^{+0.36}_{-0.18}$	-
D294	$5.14^{+0.16}_{-0.15}$	$7.02 \pm 0.06$	$8.17^{+0.11}_{-0.09}$	$8.11^{+0.10}_{-0.07}$	$8.44^{+0.11}_{-0.08}$	$8.36 \pm 0.16$
D295	$5.33^{+0.33}_{-0.18}$	$6.95^{+0.22}_{-0.12}$	$8.05^{+0.41}_{-0.17}$	$8.24^{+0.10}_{-0.09}$	$8.49^{+0.40}_{-0.16}$	$8.46^{+0.16}_{-0.18}$
D296	$5.41^{+0.05}_{-0.04}$ *	$6.40 \pm 0.03$	$7.71 \pm 0.03$	$8.22 \pm 0.03$	$8.50 \pm 0.03$	$8.78 \pm 0.09$
D297	$5.28 \pm 0.02$ *	$6.26 \pm 0.01$	$7.42 \pm 0.02$	$8.17 \pm 0.01$	$8.44 \pm 0.01$	$8.43 \pm 0.09$
D298	$6.19^{+0.25}_{-0.15}$	$7.57^{+0.19}_{-0.10}$	$8.44^{+0.33}_{-0.16}$	$8.05^{+0.29}_{-0.15}$	$8.49^{+0.33}_{-0.17}$	-
D299	$5.39^{+0.11}_{-0.10}$	$7.03 \pm 0.03$	$7.98^{+0.06}_{-0.04}$	$7.99 \pm 0.04$	$8.29^{+0.05}_{-0.04}$	-
D300	$6.65^{+0.29}_{-0.15}$	$7.95^{+0.16}_{-0.10}$	$8.55^{+0.33}_{-0.16}$	$8.14^{+0.28}_{-0.16}$	$8.64^{+0.38}_{-0.18}$	-
D301	$5.84^{+0.13}_{-0.10}$	$7.61^{+0.07}_{-0.05}$	$8.26^{+0.12}_{-0.08}$	$7.57^{+0.10}_{-0.08}$	$7.95^{+0.09}_{-0.07}$	-
D302	$5.89^{+0.16}_{-0.11}$	$7.71^{+0.07}_{-0.06}$	$8.44^{+0.13}_{-0.10}$	$7.80^{+0.14}_{-0.09}$	$8.22^{+0.17}_{-0.12}$	-
D303	$5.75^{+0.09}_{-0.07}$ *	$7.25^{+0.05}_{-0.04}$	$8.03^{+0.07}_{-0.06}$	$7.79^{+0.06}_{-0.05}$	$8.09^{+0.07}_{-0.05}$	-
D304	$5.50^{+0.18}_{-0.16}$	$7.45^{+0.08}_{-0.06}$	$8.30^{+0.16}_{-0.10}$	$8.03^{+0.13}_{-0.08}$	$8.38^{+0.15}_{-0.10}$	-
D305	$5.47^{+0.17}_{-0.15}$	$7.50^{+0.05}_{-0.04}$	$8.17^{+0.09}_{-0.07}$	$7.59 \pm 0.07$	$7.95^{+0.09}_{-0.07}$	-
D306	$5.47^{+0.18}_{-0.13}$	$7.24^{+0.08}_{-0.07}$	$8.19^{+0.15}_{-0.11}$	$7.70^{+0.13}_{-0.09}$	$8.03^{+0.18}_{-0.12}$	-
D307	$6.07^{+0.18}_{-0.11}$	$7.58^{+0.12}_{-0.08}$	$8.31^{+0.24}_{-0.13}$	$7.87^{+0.19}_{-0.12}$	$8.26^{+0.18}_{-0.12}$	-
D308	$5.87^{+0.25}_{-0.17}$	$7.85^{+0.11}_{-0.08}$	$8.39^{+0.21}_{-0.14}$	$7.82^{+0.20}_{-0.11}$	$8.28^{+0.28}_{-0.15}$	-
D309	$5.90^{+0.17}_{-0.12}$	$7.83 \pm 0.06$	$8.68^{+0.11}_{-0.08}$	$8.21^{+0.11}_{-0.08}$	$8.64^{+0.10}_{-0.08}$	-
D310	$5.60^{+0.15}_{-0.10}$	$7.31^{+0.09}_{-0.06}$	$8.15^{+0.17}_{-0.11}$	$7.64^{+0.12}_{-0.09}$	$7.95^{+0.15}_{-0.10}$	-
D311	$5.68^{+0.13}_{-0.11}$	$7.47^{+0.07}_{-0.05}$	$8.24^{+0.11}_{-0.09}$	$7.60^{+0.11}_{-0.07}$	$7.95^{+0.11}_{-0.08}$	-
D312	$5.21^{+0.29}_{-0.14}$ *	$5.76^{+0.22}_{-0.12}$	$7.18^{+0.38}_{-0.18}$	$8.00^{+0.32}_{-0.02}$	$8.22^{+0.32}_{-0.15}$	-
D313	$5.38 \pm 0.04$ *	$6.31 \pm 0.03$	$7.56^{+0.05}_{-0.04}$	$8.17 \pm 0.01$	$8.25^{+0.04}_{-0.03}$	$8.31 \pm 0.09$
D314	$5.28^{+0.03}_{-0.02}$ *	$6.17 \pm 0.02$	$7.61 \pm 0.03$	$8.03 \pm 0.02$	$8.28^{+0.03}_{-0.02}$	$8.66^{+0.13}_{-0.14}$
D315	$5.52^{+0.12}_{-0.08}$ *	$6.37^{+0.09}_{-0.06}$	$7.83^{+0.14}_{-0.10}$	$8.10^{+0.03}_{-0.02}$	$8.50^{+0.12}_{-0.09}$	$8.49^{+0.14}_{-0.15}$
D316	$5.90^{+0.09}_{-0.07}$	$6.60^{+0.05}_{-0.04}$	$8.01^{+0.08}_{-0.07}$	$7.92 \pm 0.05$	$8.18^{+0.08}_{-0.05}$	-
D317	$5.26^{+0.07}_{-0.06}$ *	$6.36^{+0.05}_{-0.04}$	$7.62^{+0.08}_{-0.07}$	$8.21 \pm 0.01$	$8.36^{+0.07}_{-0.06}$	-
D318	$5.62^{+0.07}_{-0.06}$ *	$6.51 \pm 0.02$	$7.85^{+0.04}_{-0.03}$	$8.24 \pm 0.03$	$8.54^{+0.04}_{-0.03}$	-
D319	$4.64 \pm 0.02$ *	$5.42 \pm 0.01$	$7.12 \pm 0.01$	$7.96 \pm 0.01$	$8.19 \pm 0.01$	$8.37 \pm 0.06$
D320	$5.04^{+0.10}_{-0.07}$ *	$5.64^{+0.08}_{-0.06}$	$7.22^{+0.13}_{-0.09}$	$7.74 \pm 0.03$	$8.22^{+0.10}_{-0.07}$	$8.18 \pm 0.10$
D321	$5.54^{+0.23}_{-0.18}$	$7.48^{+0.10}_{-0.07}$	$8.43^{+0.18}_{-0.13}$	$8.01^{+0.15}_{-0.09}$	$8.38^{+0.16}_{-0.12}$	-
D322	$5.62^{+0.18}_{-0.13}$	$7.39^{+0.07}_{-0.06}$	$8.48^{+0.13}_{-0.09}$	$7.75^{+0.09}_{-0.06}$	$8.62^{+0.12}_{-0.09}$	-
D323	$5.75^{+0.24}_{-0.17}$	$7.67^{+0.13}_{-0.09}$	$8.59^{+0.26}_{-0.15}$	$8.54^{+0.24}_{-0.14}$	$8.96^{+0.26}_{-0.15}$	-
D324	$5.67^{+0.17}_{-0.12}$	$7.23^{+0.08}_{-0.07}$	$8.22^{+0.16}_{-0.11}$	$8.01^{+0.10}_{-0.07}$	$8.56^{+0.16}_{-0.11}$	-
D325	$5.90^{+0.18}_{-0.12}$	$7.69^{+0.10}_{-0.07}$	$8.43^{+0.19}_{-0.11}$	$8.04^{+0.17}_{-0.10}$	$8.45^{+0.17}_{-0.11}$	-
D326	$6.05^{+0.20}_{-0.13}$	$7.75^{+0.12}_{-0.09}$	$8.38^{+0.24}_{-0.13}$	$7.74^{+0.21}_{-0.12}$	$8.13^{+0.26}_{-0.14}$	-
D327	$5.82^{+0.13}_{-0.10}$	$7.23^{+0.10}_{-0.08}$	$8.33^{+0.18}_{-0.12}$	$7.91^{+0.10}_{-0.08}$	$8.44^{+0.17}_{-0.10}$	-
D328	$5.89^{+0.07}_{-0.06}$ *	$7.18 \pm 0.03$	$8.25^{+0.05}_{-0.04}$	$7.76^{+0.05}_{-0.04}$	$8.36 \pm 0.04$	-

**Table D.6.** Ionic abundances derived from the nebular sample. All values are in  $12+\log(X/H)$  units. \* indicates  $\text{Fe}^{2+}$  abundance determinations based on  $[\text{Fe III}]\lambda 4658$  with flux errors smaller than 10%. \*\* indicates  $\text{O}^+$  abundance determinations based on  $[\text{O II}]\lambda 7319, 7330$  auroral lines.

Reference number	$\text{Fe}^{2+}$	$\text{N}^+$	$\text{O}^+$	$\text{O}^{2+}$		$\text{O}^{2+}$
				$[\text{O III}]\text{-CELs } t^2 = 0$	$[\text{O III}]\text{-CELs } t^2 > 0$	
						$\text{O II-RLs}$
D329	$5.87^{+0.12}_{-0.10}$	$7.53^{+0.08}_{-0.06}$	$8.43^{+0.14}_{-0.10}$	$7.42^{+0.06}_{-0.05}$	$8.56^{+0.14}_{-0.10}$	-
D330	$6.04^{+0.16}_{-0.12}$	$7.57^{+0.08}_{-0.06}$	$8.52^{+0.14}_{-0.09}$	$8.20^{+0.11}_{-0.08}$	$8.58^{+0.13}_{-0.10}$	-
D331	$5.87^{+0.27}_{-0.20}$	$7.27^{+0.14}_{-0.10}$	$8.13^{+0.28}_{-0.14}$	$8.06^{+0.21}_{-0.12}$	$8.41^{+0.29}_{-0.14}$	-
D332	$5.75^{+0.27}_{-0.17}$	$6.90^{+0.14}_{-0.10}$	$7.88^{+0.29}_{-0.14}$	$7.85^{+0.22}_{-0.12}$	$8.13^{+0.27}_{-0.13}$	-
D333	$5.89^{+0.16}_{-0.11}$	$7.75^{+0.08}_{-0.06}$	$8.47^{+0.13}_{-0.10}$	$8.15^{+0.13}_{-0.09}$	$8.56^{+0.13}_{-0.08}$	-
D334	$4.84^{+0.21*}_{-0.13}$	$5.90^{+0.15}_{-0.09}$	$7.40^{+0.30}_{-0.15}$	$8.07 \pm 0.03$	$8.27^{+0.22}_{-0.14}$	$8.31^{+0.08}_{-0.07}$
D335	$4.70^{+0.07*}_{-0.06}$	$5.78 \pm 0.04$	$7.14^{+0.08}_{-0.06}$	$8.10 \pm 0.01$	$8.18^{+0.05}_{-0.04}$	$8.29 \pm 0.05$
D336	$4.58^{+0.27}_{-0.15}$	$5.65^{+0.20}_{-0.10}$	$6.97^{+0.32}_{-0.15}$	$8.05 \pm 0.03$	$7.88^{+0.29}_{-0.14}$	$8.27^{+0.12}_{-0.11}$
D337	$5.16^{+0.05}_{-0.04}$	$5.66 \pm 0.01$	$7.24 \pm 0.02$	$7.84 \pm 0.01$	$8.07 \pm 0.01$	-
D338	$5.20^{+0.13}_{-0.12}$	$5.76 \pm 0.04$	$7.29^{+0.06}_{-0.04}$	$7.84^{+0.04}_{-0.03}$	$8.07^{+0.05}_{-0.04}$	-
D339	$5.37^{+0.13}_{-0.10}$	$5.98^{+0.06}_{-0.05}$	$7.40^{+0.08}_{-0.06}$	$7.86^{+0.06}_{-0.05}$	$8.10 \pm 0.06$	-
D340	$5.54^{+0.11}_{-0.09}$	$6.18 \pm 0.04$	$7.62^{+0.07}_{-0.05}$	$7.92^{+0.05}_{-0.04}$	$8.18^{+0.06}_{-0.05}$	-
D341	$4.96^{+0.32}_{-0.17}$	$5.89^{+0.26}_{-0.11}$	$7.31^{+0.48}_{-0.17}$	$7.84^{+0.04}_{-0.03}$	$7.63^{+0.32}_{-0.15}$	-
D342	$5.21^{+0.06}_{-0.05}$	$5.73 \pm 0.03$	$7.20 \pm 0.03$	$8.02 \pm 0.03$	$8.26 \pm 0.03$	-
D343	$5.06 \pm 0.02^*$	$5.67 \pm 0.01$	$7.14 \pm 0.01$	$8.01 \pm 0.01$	$8.25 \pm 0.01$	$7.93^{+0.15}_{-0.17}$
D344	$4.49^{+0.04*}_{-0.03}$	$4.64 \pm 0.06$	$6.09^{+0.02}_{-0.01}$	$7.21 \pm 0.01$	$7.38 \pm 0.01$	-
D345	$4.62^{+0.05*}_{-0.03}$	-	$6.15 \pm 0.01$	$7.25 \pm 0.01$	$7.43 \pm 0.01$	-
D346	$4.61^{+0.09}_{-0.10}$	-	$6.17 \pm 0.02$	$7.27 \pm 0.01$	$7.45 \pm 0.01$	-
D347	$4.45^{+0.11}_{-0.10}$	-	$6.17 \pm 0.02$	$7.17 \pm 0.01$	$7.35 \pm 0.01$	-
D348	$4.69 \pm 0.09$	-	$6.25 \pm 0.02$	$7.22 \pm 0.01$	$7.40^{+0.02}_{-0.01}$	-
D349	$4.63^{+0.14}_{-0.15}$	-	$6.32 \pm 0.03$	$7.18 \pm 0.02$	$7.35^{+0.03}_{-0.02}$	-
D350	$4.67 \pm 0.14$	-	$6.13 \pm 0.03$	$7.09 \pm 0.02$	$7.26^{+0.02}_{-0.01}$	-
D351	$4.56 \pm 0.06$	-	$6.18 \pm 0.02$	$7.25 \pm 0.01$	$7.42^{+0.02}_{-0.01}$	-
D352	$4.23^{+0.13*}_{-0.09}$	$4.55^{+0.11}_{-0.08}$	$5.74^{+0.22}_{-0.10}$	$7.17 \pm 0.01$	$7.05^{+0.15}_{-0.07}$	-
D353	$4.53 \pm 0.06$	$4.75 \pm 0.02$	$6.14 \pm 0.02$	$7.22 \pm 0.01$	$7.40 \pm 0.01$	-
D354	$4.54^{+0.05*}_{-0.04}$	$4.75 \pm 0.02$	$6.13 \pm 0.01$	$7.21 \pm 0.01$	$7.39 \pm 0.01$	-
D355	$4.66^{+0.11}_{-0.10}$	$4.77 \pm 0.07$	$6.20 \pm 0.03$	$7.07 \pm 0.02$	$7.25 \pm 0.02$	-
D356	$5.46^{+0.06*}_{-0.05}$	-	$7.55 \pm 0.02$	$7.95 \pm 0.01$	$8.19 \pm 0.01$	-
D357	$5.51^{+0.06*}_{-0.04}$	-	$7.45 \pm 0.02$	$7.88 \pm 0.01$	$8.12 \pm 0.01$	-
D358	$4.61^{+0.15}_{-0.17}$	-	$6.55 \pm 0.02$	$7.39 \pm 0.01$	$7.58 \pm 0.01$	-
D359	$5.22^{+0.07}_{-0.06}$	-	$7.02 \pm 0.02$	$7.72 \pm 0.01$	$7.93 \pm 0.01$	-
D360	$4.94 \pm 0.07$	$5.19^{+0.03}_{-0.02}$	$6.68 \pm 0.02$	$7.39 \pm 0.01$	$7.58 \pm 0.01$	-
D361	$4.95^{+0.09}_{-0.07}$	$5.47 \pm 0.01$	$6.99 \pm 0.01$	$7.44 \pm 0.01$	$7.64 \pm 0.01$	-
D362	$4.64^{+0.08}_{-0.07}$	-	$6.49^{+0.03}_{-0.02}$	$7.71 \pm 0.02$	$7.91 \pm 0.02$	-
D363	$4.57^{+0.09*}_{-0.07}$	$5.23^{+0.07}_{-0.05}$	$6.12^{+0.11}_{-0.08}$	$7.38 \pm 0.01$	$7.44^{+0.08}_{-0.06}$	-
D364	$4.65 \pm 0.09$	$4.56^{+0.06}_{-0.05}$	$5.92 \pm 0.03$	$6.88 \pm 0.02$	$7.05 \pm 0.02$	-
D365	$5.22^{+0.07}_{-0.06}$	$5.94 \pm 0.02$	$7.25^{+0.06**}_{-0.05}$	$7.83 \pm 0.02$	$8.05 \pm 0.03$	-
D366	$5.01^{+0.06}_{-0.05}$	-	$7.22 \pm 0.03^{**}$	$8.03 \pm 0.01$	$8.26^{+0.02}_{-0.01}$	-
D367	$5.09^{+0.11}_{-0.12}$	-	$7.01 \pm 0.03$	$7.68 \pm 0.02$	$7.89 \pm 0.02$	-
D368	$5.29^{+0.06*}_{-0.05}$	$5.87 \pm 0.10$	$7.05^{+0.10}_{-0.09}$	$7.83 \pm 0.05$	$8.05^{+0.06}_{-0.05}$	-
D369	$4.82 \pm 0.07$	-	$6.69 \pm 0.02$	$7.49 \pm 0.01$	$7.68 \pm 0.01$	-
D370	$4.60 \pm 0.06$	$4.94 \pm 0.03$	$6.27 \pm 0.03$	$7.60 \pm 0.02$	$7.79 \pm 0.03$	-
D371	$4.63^{+0.08}_{-0.07}$	-	$6.25 \pm 0.02$	$7.37 \pm 0.01$	$7.55 \pm 0.01$	-
D372	$5.26^{+0.07}_{-0.06}$	-	$7.16 \pm 0.02$	$7.86 \pm 0.01$	$8.07 \pm 0.01$	-
D373	$4.89^{+0.09}_{-0.07}$	-	$7.30 \pm 0.02$	$7.87 \pm 0.01$	$8.10 \pm 0.01$	-
D374	$4.42^{+0.08*}_{-0.06}$	$5.20^{+0.06}_{-0.05}$	$5.63^{+0.10}_{-0.06}$	$7.40^{+0.03}_{-0.02}$	$7.14^{+0.08}_{-0.05}$	-
D375	$4.43^{+0.09*}_{-0.06}$	$5.20^{+0.07}_{-0.05}$	$5.64^{+0.10}_{-0.07}$	$7.41 \pm 0.02$	$7.14^{+0.09}_{-0.06}$	-
D376	$5.20 \pm 0.02^*$	$6.10 \pm 0.03$	$6.84 \pm 0.01$	$7.74 \pm 0.01$	$7.95 \pm 0.01$	-
D377	$4.76^{+0.14}_{-0.11}$	$5.66^{+0.03}_{-0.02}$	$7.21 \pm 0.07^{**}$	$8.09^{+0.04}_{-0.03}$	$8.33 \pm 0.04$	-
D378	$4.81 \pm 0.05$	$5.29 \pm 0.03$	$6.33^{+0.04}_{-0.03}$	$7.63 \pm 0.02$	$7.81^{+0.03}_{-0.02}$	-
D379	$5.08^{+0.10}_{-0.09}$	-	$7.03^{+0.03}_{-0.02}$	$7.58 \pm 0.02$	$7.79 \pm 0.02$	-
D380	$5.28^{+0.05*}_{-0.04}$	$6.14 \pm 0.03$	$7.16^{+0.06}_{-0.04}$	$7.97^{+0.04}_{-0.03}$	$8.20 \pm 0.04$	-
D381	$5.01^{+0.08}_{-0.07}$	-	$6.83 \pm 0.02$	$7.58 \pm 0.01$	$7.78 \pm 0.01$	-
D382	$5.17 \pm 0.09$	-	$6.93 \pm 0.02$	$7.71 \pm 0.01$	$7.91 \pm 0.01$	-
D383	$4.76^{+0.07}_{-0.06}$	$5.96^{+0.02}_{-0.01}$	$7.20 \pm 0.02$	$7.90 \pm 0.02$	$8.12 \pm 0.02$	-

**Table D.6.** Ionic abundances derived from the nebular sample. All values are in  $12+\log(X/H)$  units. \* indicates Fe<sup>2+</sup> abundance determinations based on [Fe III] $\lambda$ 4658 with flux errors smaller than 10%. \*\* indicates O<sup>+</sup> abundance determinations based on [O II] $\lambda$ 7319, 7330 auroral lines.

Reference number	Fe <sup>2+</sup>	N <sup>+</sup>	O <sup>+</sup>	O <sup>2+</sup>		O II-RLs
				[O III]-CELs $t^2 = 0$	[O III]-CELs $t^2 > 0$	
D384	5.60 <sup>+0.07</sup> <sub>-0.06</sub>	6.41 <sup>+0.03</sup> <sub>-0.02</sub>	7.64 ± 0.04	8.13 ± 0.03	8.40 ± 0.03	-
D385	5.61 <sup>+0.08</sup> <sub>-0.07</sub>	6.50 ± 0.02	7.74 <sup>+0.03</sup> <sub>-0.02</sub>	8.04 ± 0.02	8.30 <sup>+0.03</sup> <sub>-0.02</sub>	-
D386	5.11 <sup>+0.05</sup> * <sub>-0.04</sub>	-	6.78 <sup>+0.02</sup> <sub>-0.01</sub>	7.63 ± 0.01	7.83 ± 0.01	-
D387	4.58 <sup>+0.06</sup> <sub>-0.05</sub>	4.93 <sup>+0.03</sup> <sub>-0.02</sub>	6.15 <sup>+0.04</sup> <sub>-0.03</sub>	7.75 ± 0.02	7.95 <sup>+0.03</sup> <sub>-0.02</sub>	-
D388	5.48 <sup>+0.08</sup> <sub>-0.07</sub>	6.30 ± 0.02	7.57 ± 0.03	7.89 ± 0.02	8.14 ± 0.03	-
D389	5.09 <sup>+0.06</sup> * <sub>-0.04</sub>	5.73 ± 0.01	7.31 ± 0.01	7.82 ± 0.01	8.05 ± 0.01	-
D390	4.99 <sup>+0.06</sup> * <sub>-0.05</sub>	5.79 <sup>+0.04</sup> <sub>-0.03</sub>	6.72 <sup>+0.07</sup> <sub>-0.05</sub>	7.83 ± 0.02	7.89 <sup>+0.07</sup> <sub>-0.05</sub>	-
D391	5.01 <sup>+0.11</sup> <sub>-0.09</sub>	5.85 ± 0.02	7.44 <sup>+0.07</sup> ** <sub>-0.05</sub>	7.99 ± 0.03	8.24 ± 0.03	-
D392	5.10 <sup>+0.18</sup> <sub>-0.12</sub>	6.15 <sup>+0.16</sup> <sub>-0.10</sub>	7.04 <sup>+0.25</sup> <sub>-0.12</sub>	7.75 ± 0.03	7.97 <sup>+0.17</sup> <sub>-0.10</sub>	-
D393	4.96 <sup>+0.07</sup> <sub>-0.06</sub>	5.67 ± 0.08	6.69 ± 0.03**	7.50 ± 0.01	7.68 ± 0.01	-
D394	5.57 <sup>+0.08</sup> <sub>-0.07</sub>	6.22 <sup>+0.05</sup> <sub>-0.04</sub>	7.54 <sup>+0.14</sup> ** <sub>-0.09</sub>	7.96 <sup>+0.06</sup> <sub>-0.05</sub>	8.21 <sup>+0.07</sup> <sub>-0.06</sub>	-
D395	5.23 <sup>+0.07</sup> <sub>-0.05</sub>	-	7.22 <sup>+0.02</sup> <sub>-0.01</sub>	7.80 ± 0.01	8.03 ± 0.01	-
D396	5.24 ± 0.01*	6.17 <sup>+0.01</sup> <sub>-0.02</sub>	7.17 ± 0.01	7.93 ± 0.01	8.16 ± 0.01	-
D397	5.37 <sup>+0.08</sup> <sub>-0.07</sub>	-	7.19 <sup>+0.03</sup> <sub>-0.02</sub>	7.96 ± 0.02	8.19 ± 0.02	-
D398	5.43 <sup>+0.09</sup> <sub>-0.08</sub>	6.55 <sup>+0.03</sup> <sub>-0.02</sub>	7.75 ± 0.04	7.87 ± 0.03	8.14 ± 0.03	-
D399	5.24 <sup>+0.10</sup> <sub>-0.09</sub>	6.38 <sup>+0.06</sup> <sub>-0.04</sub>	7.35 <sup>+0.09</sup> <sub>-0.07</sub>	7.95 ± 0.03	8.00 <sup>+0.08</sup> <sub>-0.06</sub>	-
D400	5.48 <sup>+0.13</sup> * <sub>-0.02</sub>	6.41 <sup>+0.10</sup> <sub>-0.07</sub>	7.32 <sup>+0.17</sup> <sub>-0.11</sub>	8.04 ± 0.01	8.46 <sup>+0.15</sup> <sub>-0.10</sub>	-
D401	4.82 <sup>+0.05</sup> * <sub>-0.04</sub>	5.95 ± 0.03	7.49 <sup>+0.05</sup> <sub>-0.04</sub>	7.84 ± 0.02	8.04 <sup>+0.04</sup> <sub>-0.03</sub>	7.99 ± 0.05
D402	4.88 <sup>+0.04</sup> * <sub>-0.03</sub>	5.69 ± 0.02	7.30 ± 0.04	7.90 ± 0.02	8.15 ± 0.03	8.22 <sup>+0.03</sup> <sub>-0.02</sub>
D403	4.99 <sup>+0.04</sup> * <sub>-0.03</sub>	5.41 ± 0.03	6.87 <sup>+0.07</sup> <sub>-0.06</sub>	7.99 ± 0.02	8.16 ± 0.04	8.17 ± 0.02
D404	4.38 <sup>+0.09</sup> <sub>-0.08</sub>	6.14 ± 0.03	7.73 <sup>+0.06</sup> <sub>-0.07</sub>	7.79 ± 0.02	8.05 <sup>+0.03</sup> <sub>-0.02</sub>	-
D405	4.89 ± 0.06	5.62 ± 0.09	7.16 <sup>+0.02</sup> <sub>-0.01</sub>	7.93 ± 0.01	8.17 ± 0.01	8.29 ± 0.07
D406	4.99 <sup>+0.12</sup> <sub>-0.10</sub>	6.10 <sup>+0.14</sup> <sub>-0.13</sub>	7.51 <sup>+0.05</sup> <sub>-0.04</sub>	7.77 <sup>+0.04</sup> <sub>-0.03</sub>	8.01 ± 0.04	-
D407	5.00 <sup>+0.20</sup> <sub>-0.13</sub>	6.06 <sup>+0.14</sup> <sub>-0.08</sub>	7.55 <sup>+0.23</sup> <sub>-0.13</sub>	7.88 ± 0.02	8.20 <sup>+0.23</sup> <sub>-0.15</sub>	8.14 ± 0.12
D408	5.10 ± 0.05	6.07 ± 0.01	7.67 ± 0.01	7.85 ± 0.01	8.10 ± 0.01	-
D409	4.98 <sup>+0.07</sup> <sub>-0.06</sub>	-	7.56 ± 0.02	7.89 ± 0.01	8.15 ± 0.01	-
D410	4.96 <sup>+0.13</sup> * <sub>-0.09</sub>	5.84 <sup>+0.10</sup> <sub>-0.07</sub>	7.48 <sup>+0.17</sup> <sub>-0.11</sub>	7.89 ± 0.01	8.05 <sup>+0.17</sup> <sub>-0.11</sub>	-
D411	4.88 <sup>+0.05</sup> * <sub>-0.04</sub>	6.03 ± 0.03	7.63 <sup>+0.05</sup> <sub>-0.04</sub>	7.84 ± 0.01	8.03 ± 0.04	8.20 <sup>+0.12</sup> <sub>-0.11</sub>
D412	4.96 <sup>+0.18</sup> <sub>-0.11</sub>	5.89 <sup>+0.11</sup> <sub>-0.08</sub>	7.50 <sup>+0.21</sup> <sub>-0.12</sub>	7.93 ± 0.01	8.23 <sup>+0.15</sup> <sub>-0.10</sub>	8.34 ± 0.13
D413	5.66 <sup>+0.05</sup> * <sub>-0.04</sub>	6.18 ± 0.03	7.65 <sup>+0.04</sup> <sub>-0.03</sub>	8.09 ± 0.03	8.36 ± 0.03	-
D414	5.34 <sup>+0.05</sup> * <sub>-0.04</sub>	5.84 <sup>+0.02</sup> <sub>-0.03</sub>	7.31 ± 0.03	7.93 <sup>+0.03</sup> <sub>-0.02</sub>	8.16 <sup>+0.03</sup> <sub>-0.02</sub>	-
D415	5.08 <sup>+0.07</sup> <sub>-0.06</sub>	5.78 ± 0.02	7.00 <sup>+0.03</sup> <sub>-0.02</sub>	7.87 ± 0.02	8.09 ± 0.02	8.36 <sup>+0.15</sup> <sub>-0.14</sub>
D416	5.25 ± 0.09	5.79 ± 0.03	7.03 ± 0.03	7.85 ± 0.02	8.08 <sup>+0.03</sup> <sub>-0.02</sub>	-
D417	5.11 ± 0.07	5.66 ± 0.01	6.97 ± 0.02	7.83 ± 0.01	8.04 ± 0.01	-
D418	5.02 ± 0.07	5.69 ± 0.01	7.02 ± 0.02	7.83 ± 0.01	8.05 ± 0.01	-
D419	4.86 <sup>+0.08</sup> <sub>-0.10</sub>	-	6.80 ± 0.03	7.91 ± 0.02	8.13 ± 0.03	-
D420	4.80 ± 0.06	5.52 ± 0.01	6.75 ± 0.02	7.89 ± 0.01	8.11 ± 0.01	-
D421	4.88 ± 0.04*	5.63 ± 0.01	6.82 ± 0.02	7.90 ± 0.01	8.12 ± 0.01	-
D422	5.59 <sup>+0.06</sup> * <sub>-0.04</sub>	6.23 <sup>+0.03</sup> <sub>-0.02</sub>	7.73 ± 0.04	8.06 ± 0.03	8.33 ± 0.03	-
D423	4.44 ± 0.09	4.74 ± 0.02	6.25 <sup>+0.02</sup> <sub>-0.01</sub>	7.45 ± 0.01	7.63 ± 0.01	-
D424	4.53 ± 0.04*	4.76 ± 0.02	6.27 ± 0.02	7.48 ± 0.01	7.66 ± 0.01	7.72 ± 0.12
D425	5.99 <sup>+0.08</sup> * <sub>-0.06</sub>	6.30 ± 0.04	8.10 <sup>+0.08</sup> <sub>-0.06</sub>	8.11 ± 0.01	8.80 <sup>+0.06</sup> <sub>-0.05</sub>	-
D426	5.34 ± 0.02*	6.00 ± 0.01	7.27 ± 0.02	7.89 ± 0.01	8.14 <sup>+0.02</sup> <sub>-0.01</sub>	-
D427	5.39 <sup>+0.02</sup> * <sub>-0.01</sub>	5.91 ± 0.01	7.37 ± 0.01	8.00 ± 0.01	8.25 ± 0.01	-
D428	5.37 <sup>+0.05</sup> <sub>-0.06</sub>	6.18 ± 0.01	7.37 ± 0.02	8.02 ± 0.01	8.26 ± 0.02	-
D429	5.38 <sup>+0.08</sup> <sub>-0.07</sub>	5.80 ± 0.02	7.34 <sup>+0.03</sup> <sub>-0.02</sub>	7.82 ± 0.02	8.05 ± 0.02	-
D430	5.33 <sup>+0.14</sup> * <sub>-0.09</sub>	6.21 <sup>+0.10</sup> <sub>-0.07</sub>	7.38 <sup>+0.17</sup> <sub>-0.11</sub>	7.93 ± 0.01	8.26 <sup>+0.13</sup> <sub>-0.09</sub>	-
D431	5.22 ± 0.05	5.42 ± 0.02	6.91 <sup>+0.02</sup> <sub>-0.01</sub>	7.74 ± 0.01	7.95 ± 0.01	-
D432	5.00 <sup>+0.04</sup> * <sub>-0.03</sub>	5.44 ± 0.01	6.88 <sup>+0.02</sup> <sub>-0.01</sub>	7.75 ± 0.01	7.96 ± 0.01	-
D433	4.95 ± 0.09	5.32 <sup>+0.03</sup> <sub>-0.02</sub>	6.86 <sup>+0.03</sup> <sub>-0.02</sub>	7.69 ± 0.02	7.89 ± 0.02	-
D434	4.94 ± 0.06	5.33 <sup>+0.01</sup> <sub>-0.02</sub>	6.85 ± 0.02	7.72 ± 0.01	7.92 ± 0.01	-
D435	4.96 ± 0.04*	5.42 ± 0.02	6.81 ± 0.02	7.75 ± 0.01	7.97 ± 0.01	7.92 <sup>+0.17</sup> <sub>-0.15</sub>
D436	4.95 <sup>+0.08</sup> <sub>-0.06</sub>	5.44 ± 0.02	6.82 ± 0.02	7.74 <sup>+0.02</sup> <sub>-0.01</sub>	7.95 ± 0.02	-
D437	4.49 <sup>+0.12</sup> * <sub>-0.07</sub>	5.31 <sup>+0.10</sup> <sub>-0.07</sub>	6.03 <sup>+0.16</sup> <sub>-0.09</sub>	7.89 ± 0.01	7.37 <sup>+0.14</sup> <sub>-0.07</sub>	-
D438	4.73 <sup>+0.05</sup> <sub>-0.04</sub>	5.11 ± 0.01	6.73 ± 0.02	7.43 ± 0.01	7.62 ± 0.01	-

**Table D.6.** Ionic abundances derived from the nebular sample. All values are in  $12+\log(X/H)$  units. \* indicates  $\text{Fe}^{2+}$  abundance determinations based on  $[\text{Fe III}]\lambda 4658$  with flux errors smaller than 10%. \*\* indicates  $\text{O}^+$  abundance determinations based on  $[\text{O II}]\lambda\lambda 7319, 7330$  auroral lines.

Reference number	$\text{Fe}^{2+}$	$\text{N}^+$	$\text{O}^+$	$\text{O}^{2+}$		$\text{O}^{2+}$ O II-RLs
				$[\text{O III}]\text{-CELs } t^2 = 0$	$[\text{O III}]\text{-CELs } t^2 > 0$	
D439	$4.97^{+0.08}_{-0.07}$	$5.28^{+0.03}_{-0.02}$	$6.91 \pm 0.03$	$7.40 \pm 0.02$	$7.60 \pm 0.02$	-
D440	$4.96^{+0.10}_{-0.09}$	$5.55 \pm 0.02$	$7.21 \pm 0.02$	$7.49 \pm 0.01$	$7.70 \pm 0.01$	-
D441	$5.08^{+0.12}_{-0.13}$	$6.04 \pm 0.02$	$7.29 \pm 0.02$	$8.12 \pm 0.02$	$8.37 \pm 0.02$	-
D442	$6.03^{+0.06*}_{-0.05}$	$6.85 \pm 0.02$	$8.26 \pm 0.04$	$7.82 \pm 0.03$	$8.10 \pm 0.03$	-
D443	$5.42^{+0.24}_{-0.17}$	$6.52^{+0.14}_{-0.09}$	$7.81^{+0.26}_{-0.14}$	$8.06^{+0.14}_{-0.10}$	$8.06^{+0.23}_{-0.12}$	-
D444	$5.37 \pm 0.10$	$6.13 \pm 0.02$	$7.46 \pm 0.03$	$8.18 \pm 0.02$	$8.44 \pm 0.02$	-
D445	$5.68^{+0.10}_{-0.08}$	$6.53 \pm 0.04$	$7.84^{+0.06}_{-0.05}$	$7.87^{+0.05}_{-0.04}$	$8.12^{+0.06}_{-0.05}$	-
D446	$5.58^{+0.09}_{-0.07}$	$6.15 \pm 0.02$	$7.64^{+0.04}_{-0.03}$	$7.84 \pm 0.03$	$8.08 \pm 0.03$	-
D447	$5.84^{+0.13}_{-0.10}$	$6.50^{+0.06}_{-0.05}$	$7.64^{+0.10}_{-0.08}$	$7.82^{+0.07}_{-0.06}$	$8.06^{+0.09}_{-0.06}$	-
D448	$5.83^{+0.13}_{-0.12}$	$6.16^{+0.07}_{-0.06}$	$7.32^{+0.08}_{-0.07}$	$7.65^{+0.06}_{-0.05}$	$7.85^{+0.07}_{-0.06}$	-
D449	$4.93^{+0.14}_{-0.15}$	$5.70^{+0.01}_{-0.02}$	$7.18^{+0.02}_{-0.01}$	$8.01 \pm 0.01$	$8.24 \pm 0.01$	-
D450	$5.25^{+0.13}_{-0.11}$	$5.94 \pm 0.02$	$7.42 \pm 0.02$	$7.83^{+0.02}_{-0.01}$	$8.06 \pm 0.02$	-
D451	$4.95^{+0.04*}_{-0.03}$	$5.43^{+0.05}_{-0.04}$	$6.75 \pm 0.03$	$7.68 \pm 0.02$	$7.89 \pm 0.02$	-
D452	$5.10^{+0.13}_{-0.11}$	$6.04 \pm 0.04$	$6.83^{+0.07}_{-0.06}$	$7.84^{+0.05}_{-0.04}$	$8.05^{+0.05}_{-0.04}$	-



**Table D.7.** Numerical values of the ICFs adopted in this work for N (Amayo et al. 2021) and Fe (Rodríguez & Rubin 2005). These are on a logarithmic scale, so that  $12+\log(X/H) = \log(\text{ICF}(X)) + 12 + \log(X^{i+}/H^+)$ .

Reference number	$\log(\text{ICF}(N)) (t^2 = 0)$	$\log(\text{ICF}(N)) (t^2 > 0)$	$\log(\text{ICF}(Fe)) (t^2 = 0)$	$\log(\text{ICF}(Fe)) (t^2 > 0)$
D1	0.64	0.84	0.49	0.65
D2	1.04	1.26	0.83	1.04
D3	0.81	1.01	0.63	0.80
D4	0.68	0.88	0.52	0.69
D5	1.02	1.24	0.82	1.02
D6	0.95	1.17	0.75	0.95
D7	0.74	0.95	0.57	0.75
D8	0.58	0.80	0.44	0.62
D9	0.60	0.84	0.46	0.65
D10	0.78	1.00	0.61	0.79
D11	0.87	1.07	0.68	0.85
D12	0.73	0.93	0.56	0.73
D13	0.40	0.57	0.28	0.43
D14	0.64	0.83	0.49	0.65
D15	0.53	0.75	0.40	0.58
D16	0.52	0.71	0.39	0.54
D17	0.74	0.95	0.57	0.75
D18	0.46	0.64	0.34	0.49
D19	1.18	1.40	0.97	1.18
D20	1.13	1.31	0.92	1.09
D21	0.76	0.95	0.59	0.75
D22	0.70	0.88	0.54	0.69
D23	0.70	0.89	0.53	0.70
D24	0.55	0.76	0.41	0.59
D25	0.81	1.02	0.63	0.82
D26	0.40	0.54	0.28	0.40
D27	0.71	0.92	0.54	0.73
D28	1.12	1.31	0.91	1.09
D29	0.74	0.97	0.57	0.77
D30	0.66	0.88	0.51	0.69
D31	0.68	0.90	0.52	0.71
D32	0.51	0.72	0.38	0.56
D33	0.39	0.52	0.26	0.39
D34	0.39	0.51	0.26	0.37
D35	0.81	1.04	0.63	0.83
D36	0.61	0.82	0.46	0.64
D37	0.35	0.46	0.23	0.33
D38	0.58	0.76	0.44	0.59
D39	0.97	1.21	0.77	0.99
D40	0.60	0.80	0.46	0.62
D41	0.97	1.15	0.77	0.93
D42	0.51	0.72	0.38	0.55
D43	0.44	0.60	0.31	0.46
D44	0.51	0.70	0.37	0.53
D45	0.39	0.52	0.26	0.39
D46	0.62	0.86	0.47	0.67
D47	0.41	0.59	0.29	0.45
D48	0.37	0.51	0.24	0.38
D49	0.49	0.72	0.36	0.56
D50	0.71	0.94	0.55	0.74
D51	0.48	0.68	0.35	0.52
D52	0.62	0.82	0.47	0.63
D53	0.84	1.04	0.65	0.83
D54	1.01	1.19	0.80	0.97
D55	0.42	0.58	0.29	0.44
D56	0.85	1.05	0.66	0.84
D57	0.49	0.71	0.36	0.54
D58	0.59	0.81	0.45	0.62
D59	0.94	1.16	0.74	0.94
D60	0.44	0.63	0.32	0.48

**Table D.7.** Numerical values of the ICFs adopted in this work for N (Amayo et al. 2021) and Fe (Rodríguez & Rubin 2005). These are on a logarithmic scale, so that  $12+\log(X/H) = \log(\text{ICF}(X)) + 12 + \log(X^{i+}/H^+)$ .

Reference number	$\log(\text{ICF}(N)) (t^2 = 0)$	$\log(\text{ICF}(N)) (t^2 > 0)$	$\log(\text{ICF}(Fe)) (t^2 = 0)$	$\log(\text{ICF}(Fe)) (t^2 > 0)$
D61	0.54	0.73	0.41	0.56
D62	0.54	0.74	0.40	0.57
D63	0.43	0.62	0.31	0.47
D64	0.35	0.53	0.23	0.40
D65	0.69	0.84	0.53	0.65
D66	0.88	1.07	0.69	0.86
D67	0.63	0.82	0.48	0.64
D68	0.52	0.76	0.39	0.58
D69	0.45	0.60	0.32	0.46
D70	0.60	0.80	0.45	0.62
D71	0.14	0.31	0.10	0.19
D72	0.84	1.03	0.65	0.82
D73	0.50	0.68	0.37	0.52
D74	0.71	0.94	0.55	0.74
D75	0.92	1.09	0.72	0.88
D76	1.05	1.28	0.84	1.06
D77	0.60	0.81	0.46	0.63
D78	1.11	1.27	0.90	1.05
D79	1.12	1.26	0.91	1.04
D80	1.14	1.30	0.93	1.08
D81	0.91	0.72	0.71	0.56
D82	1.20	1.39	0.98	1.17
D83	0.87	1.33	0.68	1.11
D84	0.80	1.00	0.62	0.79
D85	0.32	0.49	0.20	0.36
D86	0.30	0.45	0.18	0.32
D87	1.14	1.36	0.93	1.13
D88	0.88	1.03	0.69	0.82
D89	0.67	0.83	0.51	0.65
D90	0.52	0.70	0.39	0.54
D91	0.68	0.91	0.52	0.71
D92	0.54	0.82	0.41	0.64
D93	0.64	0.83	0.49	0.65
D94	1.00	1.16	0.79	0.95
D95	0.48	0.63	0.35	0.48
D96	1.18	1.35	0.96	1.13
D97	1.05	1.23	0.84	1.01
D98	1.25	1.42	1.03	1.19
D99	0.85	1.05	0.66	0.84
D100	1.28	1.41	1.06	1.19
D101	0.97	1.21	0.77	0.99
D102	0.88	1.09	0.69	0.88
D103	1.09	1.27	0.87	1.05
D104	0.73	0.93	0.56	0.73
D105	0.67	0.85	0.51	0.67
D106	1.00	0.91	0.79	0.71
D107	0.73	0.86	0.56	0.67
D108	0.55	0.75	0.41	0.58
D109	0.56	0.76	0.42	0.58
D110	0.91	1.07	0.71	0.86
D111	1.01	1.21	0.80	0.99
D112	1.09	1.28	0.87	1.06
D113	0.92	1.10	0.73	0.89
D114	0.89	1.08	0.69	0.86
D115	0.82	1.01	0.64	0.80
D116	0.44	0.56	0.31	0.43
D117	0.47	0.61	0.35	0.46
D118	1.05	1.37	0.84	1.15
D119	0.78	0.96	0.60	0.76
D120	0.25	0.43	0.15	0.31

**Table D.7.** Numerical values of the ICFs adopted in this work for N (Amayo et al. 2021) and Fe (Rodríguez & Rubin 2005). These are on a logarithmic scale, so that  $12+\log(X/H) = \log(\text{ICF}(X)) + 12 + \log(X^{i+}/H^+)$ .

Reference number	$\log(\text{ICF}(N)) (t^2 = 0)$	$\log(\text{ICF}(N)) (t^2 > 0)$	$\log(\text{ICF}(Fe)) (t^2 = 0)$	$\log(\text{ICF}(Fe)) (t^2 > 0)$
D121	0.22	0.50	0.13	0.37
D122	0.32	0.57	0.20	0.43
D123	0.16	0.32	0.11	0.20
D124	0.25	0.37	0.15	0.25
D125	0.22	0.38	0.14	0.25
D126	0.27	0.43	0.16	0.30
D127	0.21	0.33	0.13	0.20
D128	0.52	0.79	0.39	0.61
D129	0.28	0.41	0.17	0.28
D130	0.47	0.65	0.34	0.49
D131	0.47	0.66	0.34	0.50
D132	0.33	0.45	0.21	0.33
D133	0.49	0.69	0.36	0.53
D134	0.47	0.75	0.34	0.58
D135	0.68	0.81	0.52	0.63
D136	0.36	0.55	0.24	0.42
D137	0.41	0.57	0.29	0.43
D138	0.17	0.37	0.11	0.24
D139	0.12	0.25	0.10	0.15
D140	0.15	0.33	0.10	0.21
D141	0.29	0.31	0.18	0.19
D142	0.34	0.56	0.22	0.42
D143	0.15	0.31	0.11	0.19
D144	0.39	0.58	0.27	0.44
D145	0.34	0.45	0.22	0.32
D146	0.41	0.60	0.28	0.46
D147	0.11	0.28	0.09	0.17
D148	0.28	0.46	0.17	0.33
D149	0.32	0.44	0.20	0.31
D150	0.15	0.33	0.10	0.20
D151	0.27	0.43	0.16	0.31
D152	0.03	0.11	0.08	0.09
D153	0.38	0.51	0.26	0.38
D154	0.30	0.40	0.19	0.28
D155	0.17	0.38	0.11	0.25
D156	0.40	0.59	0.27	0.45
D157	0.35	0.65	0.23	0.50
D158	0.09	0.35	0.09	0.23
D159	0.53	0.70	0.39	0.54
D160	0.11	0.28	0.09	0.17
D161	0.24	0.43	0.15	0.31
D162	0.12	0.28	0.10	0.17
D163	0.11	0.25	0.09	0.15
D164	0.16	0.32	0.11	0.20
D165	0.35	0.57	0.23	0.43
D166	0.41	0.66	0.29	0.51
D167	0.55	0.84	0.42	0.65
D168	0.79	0.84	0.61	0.65
D169	0.13	0.40	0.10	0.27
D170	1.42	0.03	1.20	0.08
D171	0.24	0.37	0.15	0.25
D172	0.56	0.77	0.42	0.60
D173	0.66	0.80	0.51	0.62
D174	0.27	0.53	0.16	0.39
D175	0.22	0.48	0.13	0.35
D176	0.52	0.85	0.38	0.66
D177	0.70	0.92	0.54	0.73
D178	0.45	0.66	0.32	0.50
D179	0.55	0.79	0.41	0.61
D180	0.85	1.06	0.66	0.85

**Table D.7.** Numerical values of the ICFs adopted in this work for N (Amayo et al. 2021) and Fe (Rodríguez & Rubin 2005). These are on a logarithmic scale, so that  $12+\log(X/H) = \log(\text{ICF}(X)) + 12 + \log(X^{i+}/H^+)$ .

Reference number	$\log(\text{ICF}(N)) (t^2 = 0)$	$\log(\text{ICF}(N)) (t^2 > 0)$	$\log(\text{ICF}(Fe)) (t^2 = 0)$	$\log(\text{ICF}(Fe)) (t^2 > 0)$
D181	0.41	0.54	0.28	0.40
D182	0.76	1.16	0.58	0.94
D183	0.98	1.16	0.78	0.94
D184	0.08	0.34	0.09	0.22
D185	0.37	0.52	0.24	0.39
D186	0.01	0.30	0.10	0.18
D187	0.20	0.42	0.12	0.30
D188	0.64	0.79	0.49	0.61
D189	0.33	0.35	0.20	0.23
D190	0.04	0.29	0.08	0.18
D191	0.18	0.33	0.12	0.21
D192	0.24	0.41	0.15	0.28
D193	0.44	0.62	0.31	0.47
D194	0.45	0.50	0.32	0.37
D195	0.56	0.73	0.42	0.56
D196	0.76	0.94	0.58	0.74
D197	0.48	0.70	0.35	0.53
D198	0.83	1.13	0.65	0.91
D199	0.31	0.41	0.19	0.28
D200	0.56	0.78	0.42	0.60
D201	0.56	0.80	0.42	0.62
D202	0.15	0.30	0.11	0.18
D203	0.03	0.12	0.08	0.10
D204	0.04	0.10	0.08	0.09
D205	0.70	0.85	0.54	0.66
D206	0.29	0.48	0.17	0.36
D207	0.61	0.88	0.46	0.69
D208	0.21	0.48	0.13	0.35
D209	0.14	0.32	0.10	0.20
D210	0.25	0.43	0.15	0.30
D211	0.23	0.41	0.14	0.28
D212	0.26	0.46	0.16	0.33
D213	0.15	0.33	0.10	0.21
D214	0.27	0.51	0.16	0.37
D215	0.47	1.12	0.34	0.90
D216	0.17	0.36	0.11	0.23
D217	0.01	0.25	0.10	0.15
D218	0.24	0.43	0.14	0.30
D219	0.13	0.33	0.10	0.21
D220	0.84	1.08	0.65	0.87
D221	0.09	0.25	0.09	0.15
D222	0.68	0.70	0.52	0.54
D223	0.31	0.47	0.19	0.34
D224	0.72	0.74	0.56	0.57
D225	0.33	0.52	0.21	0.39
D226	0.78	0.86	0.60	0.67
D227	0.79	0.80	0.61	0.62
D228	0.87	0.89	0.68	0.70
D229	0.74	0.76	0.57	0.58
D230	0.06	0.18	0.08	0.12
D231	0.75	0.84	0.58	0.66
D232	0.78	0.81	0.61	0.63
D233	0.65	0.69	0.49	0.53
D234	0.19	0.37	0.12	0.25
D235	0.62	0.88	0.47	0.69
D236	0.56	0.85	0.42	0.66
D237	1.22	0.57	1.00	0.43
D238	0.86	1.14	0.67	0.93
D239	0.06	0.15	0.08	0.11
D240	0.45	0.55	0.32	0.41

**Table D.7.** Numerical values of the ICFs adopted in this work for N (Amayo et al. 2021) and Fe (Rodríguez & Rubin 2005). These are on a logarithmic scale, so that  $12+\log(X/H) = \log(\text{ICF}(X)) + 12 + \log(X^+/H^+)$ .

Reference number	$\log(\text{ICF}(N)) (t^2 = 0)$	$\log(\text{ICF}(N)) (t^2 > 0)$	$\log(\text{ICF}(Fe)) (t^2 = 0)$	$\log(\text{ICF}(Fe)) (t^2 > 0)$
D241	0.08	0.21	0.08	0.13
D242	0.14	0.28	0.10	0.17
D243	0.47	0.65	0.34	0.50
D244	0.01	0.02	0.09	0.08
D245	0.34	0.54	0.22	0.40
D246	0.01	0.01	0.13	0.11
D247	0.19	0.32	0.12	0.20
D248	0.01	0.01	0.11	0.08
D249	0.19	0.32	0.12	0.20
D250	0.41	0.59	0.29	0.44
D251	0.36	0.51	0.24	0.38
D252	0.89	1.10	0.70	0.89
D253	0.80	1.00	0.62	0.79
D254	0.85	1.06	0.67	0.85
D255	0.73	0.93	0.56	0.73
D256	1.07	0.99	0.86	0.78
D257	0.86	0.99	0.67	0.78
D258	0.38	0.52	0.25	0.39
D259	0.88	1.06	0.68	0.85
D260	0.56	0.79	0.42	0.61
D261	0.56	0.79	0.42	0.61
D262	0.60	0.65	0.45	0.49
D263	0.75	0.98	0.58	0.77
D264	0.73	0.92	0.56	0.72
D265	0.72	0.92	0.56	0.72
D266	0.60	0.77	0.45	0.59
D267	0.83	1.02	0.64	0.81
D268	0.89	1.09	0.69	0.88
D269	0.86	1.03	0.67	0.82
D270	0.49	0.70	0.36	0.53
D271	0.76	0.96	0.59	0.76
D272	0.50	0.78	0.37	0.61
D273	0.72	0.94	0.56	0.74
D274	0.53	0.70	0.40	0.54
D275	1.29	1.48	1.07	1.26
D276	1.04	1.24	0.84	1.02
D277	0.71	0.89	0.54	0.70
D278	0.70	0.91	0.54	0.71
D279	0.49	0.65	0.36	0.50
D280	0.81	1.03	0.63	0.83
D281	0.45	0.63	0.32	0.48
D282	0.78	0.87	0.60	0.68
D283	1.33	2.90	1.11	2.60
D284	0.47	0.67	0.34	0.51
D285	0.37	0.63	0.24	0.48
D286	0.35	0.82	0.23	0.63
D287	0.34	0.50	0.22	0.37
D288	0.51	0.70	0.37	0.54
D289	0.39	0.52	0.26	0.39
D290	0.46	0.64	0.33	0.48
D291	0.39	0.70	0.27	0.54
D292	0.22	0.43	0.14	0.30
D293	0.51	0.65	0.38	0.49
D294	0.36	0.52	0.23	0.39
D295	0.48	0.63	0.35	0.48
D296	0.70	0.94	0.54	0.74
D297	0.91	1.16	0.71	0.95
D298	0.21	0.40	0.13	0.28
D299	0.38	0.54	0.26	0.40
D300	0.21	0.42	0.13	0.30

**Table D.7.** Numerical values of the ICFs adopted in this work for N (Amayo et al. 2021) and Fe (Rodríguez & Rubin 2005). These are on a logarithmic scale, so that  $12+\log(X/H) = \log(\text{ICF}(X)) + 12 + \log(X^{i+}/H^+)$ .

Reference number	$\log(\text{ICF}(\text{N})) (t^2 = 0)$	$\log(\text{ICF}(\text{N})) (t^2 > 0)$	$\log(\text{ICF}(\text{Fe})) (t^2 = 0)$	$\log(\text{ICF}(\text{Fe})) (t^2 > 0)$
D301	0.10	0.25	0.09	0.15
D302	0.12	0.29	0.09	0.17
D303	0.28	0.41	0.17	0.28
D304	0.27	0.43	0.16	0.30
D305	0.14	0.29	0.10	0.18
D306	0.18	0.32	0.12	0.20
D307	0.20	0.35	0.13	0.23
D308	0.14	0.34	0.10	0.22
D309	0.19	0.37	0.12	0.24
D310	0.17	0.30	0.11	0.18
D311	0.12	0.26	0.10	0.16
D312	0.99	1.27	0.78	1.05
D313	0.79	0.87	0.61	0.68
D314	0.63	0.84	0.48	0.65
D315	0.52	0.86	0.38	0.68
D316	0.34	0.47	0.22	0.34
D317	0.77	0.88	0.59	0.68
D318	0.60	0.86	0.46	0.67
D319	1.00	1.19	0.79	0.97
D320	0.72	1.14	0.55	0.92
D321	0.20	0.36	0.13	0.23
D322	0.09	0.45	0.09	0.32
D323	0.36	0.64	0.23	0.49
D324	0.29	0.56	0.18	0.42
D325	0.22	0.38	0.13	0.26
D326	0.11	0.29	0.09	0.17
D327	0.21	0.41	0.13	0.29
D328	0.17	0.43	0.11	0.30
D329	0.03	0.44	0.08	0.32
D330	0.25	0.42	0.15	0.30
D331	0.36	0.53	0.23	0.39
D332	0.37	0.51	0.25	0.38
D333	0.25	0.43	0.15	0.30
D334	0.85	1.13	0.67	0.92
D335	1.09	1.18	0.87	0.96
D336	1.22	0.50	1.00	0.37
D337	0.78	0.97	0.61	0.77
D338	0.75	0.96	0.58	0.76
D339	0.66	0.85	0.51	0.67
D340	0.55	0.73	0.41	0.57
D341	0.73	0.38	0.56	0.26
D342	0.96	1.17	0.76	0.95
D343	1.01	1.22	0.80	1.00
D344	1.24	1.38	1.02	1.16
D345	1.22	1.38	1.00	1.16
D346	1.20	1.36	0.98	1.14
D347	1.15	1.28	0.93	1.06
D348	1.11	1.27	0.90	1.05
D349	0.99	1.18	0.79	0.97
D350	1.12	1.24	0.91	1.02
D351	1.18	1.35	0.97	1.13
D352	1.54	0.66	1.32	0.50
D353	1.21	1.38	0.99	1.16
D354	1.20	1.36	0.99	1.14
D355	1.02	1.18	0.81	0.96
D356	0.61	0.81	0.46	0.63
D357	0.65	0.83	0.49	0.65
D358	0.99	1.15	0.79	0.94
D359	0.86	1.07	0.68	0.86
D360	0.88	1.04	0.69	0.83



**Table D.7.** Numerical values of the ICFs adopted in this work for N (Amayo et al. 2021) and Fe (Rodríguez & Rubin 2005). These are on a logarithmic scale, so that  $12+\log(X/H) = \log(\text{ICF}(X)) + 12 + \log(X^{i+}/H^+)$ .

Reference number	$\log(\text{ICF}(\text{N})) (t^2 = 0)$	$\log(\text{ICF}(\text{N})) (t^2 > 0)$	$\log(\text{ICF}(\text{Fe})) (t^2 = 0)$	$\log(\text{ICF}(\text{Fe})) (t^2 > 0)$
D361	0.66	0.82	0.50	0.64
D362	1.33	1.49	1.11	1.27
D363	1.38	1.39	1.15	1.17
D364	1.11	1.26	0.90	1.04
D365	0.76	0.97	0.59	0.76
D366	0.97	1.16	0.77	0.94
D367	0.83	1.03	0.65	0.82
D368	0.91	1.11	0.72	0.89
D369	0.95	1.12	0.75	0.91
D370	1.41	1.54	1.19	1.31
D371	1.22	1.41	1.01	1.19
D372	0.86	1.06	0.67	0.85
D373	0.75	0.96	0.58	0.76
D374	1.83	0.40	1.60	0.28
D375	1.74	0.41	1.50	0.28
D376	1.04	1.22	0.83	1.00
D377	1.02	1.27	0.81	1.05
D378	1.39	1.55	1.16	1.33
D379	0.74	0.92	0.57	0.72
D380	0.95	1.14	0.75	0.93
D381	0.91	1.09	0.72	0.88
D382	0.93	1.12	0.73	0.91
D383	0.87	1.06	0.68	0.85
D384	0.68	0.91	0.52	0.72
D385	0.54	0.75	0.41	0.58
D386	0.99	1.17	0.79	0.95
D387	1.66	1.88	1.43	1.64
D388	0.55	0.76	0.42	0.58
D389	0.71	0.90	0.54	0.71
D390	1.23	1.31	1.01	1.09
D391	0.74	0.93	0.57	0.73
D392	0.90	1.05	0.70	0.84
D393	0.97	1.13	0.77	0.92
D394	0.62	0.83	0.47	0.65
D395	0.76	0.96	0.59	0.76
D396	0.92	1.12	0.73	0.91
D397	0.93	1.15	0.73	0.94
D398	0.44	0.61	0.31	0.46
D399	0.76	0.80	0.59	0.62
D400	0.88	1.20	0.69	0.98
D401	0.58	0.74	0.44	0.57
D402	0.78	1.00	0.60	0.80
D403	1.24	1.38	1.02	1.16
D404	0.41	0.56	0.29	0.42
D405	0.93	1.16	0.73	0.94
D406	0.51	0.70	0.38	0.54
D407	0.57	0.80	0.43	0.62
D408	0.47	0.64	0.34	0.49
D409	0.56	0.76	0.42	0.59
D410	0.62	0.80	0.47	0.62
D411	0.49	0.61	0.36	0.46
D412	0.64	0.92	0.49	0.72
D413	0.65	0.86	0.50	0.68
D414	0.79	1.00	0.61	0.80
D415	1.01	1.19	0.80	0.98
D416	0.98	1.19	0.77	0.97
D417	1.01	1.19	0.80	0.97
D418	0.96	1.16	0.76	0.94
D419	1.23	1.42	1.01	1.19
D420	1.25	1.43	1.03	1.21

**Table D.7.** Numerical values of the ICFs adopted in this work for N (Amayo et al. 2021) and Fe (Rodríguez & Rubin 2005). These are on a logarithmic scale, so that  $12+\log(X/H) = \log(\text{ICF}(X)) + 12 + \log(X^{i+}/H^+)$ .

Reference number	$\log(\text{ICF}(N)) (t^2 = 0)$	$\log(\text{ICF}(N)) (t^2 > 0)$	$\log(\text{ICF}(\text{Fe})) (t^2 = 0)$	$\log(\text{ICF}(\text{Fe})) (t^2 > 0)$
D421	1.21	1.39	0.99	1.16
D422	0.57	0.79	0.43	0.61
D423	1.31	1.45	1.08	1.22
D424	1.34	1.47	1.12	1.25
D425	0.39	0.88	0.26	0.69
D426	0.81	1.01	0.63	0.80
D427	0.80	1.02	0.62	0.82
D428	0.84	1.06	0.65	0.85
D429	0.68	0.87	0.52	0.68
D430	0.73	1.01	0.56	0.81
D431	0.98	1.17	0.78	0.95
D432	1.02	1.19	0.81	0.97
D433	0.98	1.16	0.78	0.94
D434	1.01	1.20	0.81	0.98
D435	1.08	1.28	0.86	1.06
D436	1.06	1.25	0.85	1.03
D437	1.89	0.23	1.65	0.14
D438	0.86	1.04	0.67	0.83
D439	0.69	0.86	0.53	0.67
D440	0.53	0.69	0.40	0.53
D441	0.98	1.21	0.78	0.99
D442	0.20	0.32	0.12	0.20
D443	0.51	0.49	0.38	0.36
D444	0.88	1.11	0.69	0.90
D445	0.39	0.53	0.27	0.39
D446	0.49	0.65	0.36	0.49
D447	0.47	0.62	0.34	0.47
D448	0.55	0.71	0.42	0.55
D449	0.99	1.19	0.79	0.97
D450	0.63	0.82	0.48	0.64
D451	1.09	1.25	0.88	1.03
D452	1.14	1.35	0.93	1.12

**Table D.8.** Total abundances derived from the nebular sample. All values are in  $12+\log(X/H)$  units.

Reference number	Fe		N		O	
	$t^2 = 0$	$t^2 > 0$	$t^2 = 0$	$t^2 > 0$	$t^2 = 0$	$t^2 > 0$
D1	$6.05 \pm 0.10$	$6.22^{+0.10}_{-0.09}$	$6.99 \pm 0.03$	$7.21 \pm 0.03$	$8.18 \pm 0.03$	$8.39^{+0.04}_{-0.03}$
D2	$6.13^{+0.12}_{-0.11}$	$6.34 \pm 0.10$	$6.90 \pm 0.03$	$7.11 \pm 0.03$	$8.04 \pm 0.02$	$8.26 \pm 0.03$
D3	$5.54^{+0.12}_{-0.13}$	$5.71^{+0.12}_{-0.10}$	$6.46^{+0.05}_{-0.04}$	$6.66 \pm 0.04$	$7.82 \pm 0.02$	$8.01 \pm 0.02$
D4	$5.94^{+0.14}_{-0.13}$	$6.10 \pm 0.13$	$6.46 \pm 0.04$	$6.66^{+0.09}_{-0.06}$	$7.86 \pm 0.03$	$8.04^{+0.04}_{-0.03}$
D5	$6.19^{+0.05}_{-0.06}$	$6.39 \pm 0.06$	$7.29 \pm 0.02$	$7.50 \pm 0.02$	$8.05 \pm 0.01$	$8.27 \pm 0.02$
D6	$6.15^{+0.07}_{-0.06}$	$6.35^{+0.06}_{-0.07}$	$7.26 \pm 0.02$	$7.48 \pm 0.02$	$8.08 \pm 0.02$	$8.30 \pm 0.02$
D7	$6.07^{+0.11}_{-0.10}$	$6.27^{+0.10}_{-0.09}$	$6.83 \pm 0.02$	$7.06 \pm 0.02$	$8.21 \pm 0.02$	$8.43^{+0.02}_{-0.03}$
D8	$6.08^{+0.14}_{-0.13}$	$6.24^{+0.16}_{-0.14}$	$7.05 \pm 0.05$	$7.26 \pm 0.05$	$8.16 \pm 0.05$	$8.36^{+0.06}_{-0.05}$
D9	$5.84^{+0.16}_{-0.17}$	$6.01^{+0.17}_{-0.15}$	$6.75^{+0.09}_{-0.08}$	$6.96^{+0.09}_{-0.06}$	$8.11^{+0.04}_{-0.03}$	$8.30 \pm 0.03$
D10	$5.62^{+0.12}_{-0.10}$	$5.81^{+0.11}_{-0.12}$	$6.67^{+0.05}_{-0.04}$	$6.89^{+0.05}_{-0.04}$	$8.09 \pm 0.02$	$8.29 \pm 0.02$
D11	$5.66^{+0.12}_{-0.11}$	$5.85^{+0.11}_{-0.10}$	$6.58 \pm 0.02$	$6.79^{+0.05}_{-0.04}$	$8.01 \pm 0.02$	$8.22 \pm 0.02$
D12	$5.63^{+0.11}_{-0.10}$	$5.81^{+0.10}_{-0.11}$	$6.80^{+0.05}_{-0.04}$	$7.02^{+0.05}_{-0.04}$	$8.14 \pm 0.02$	$8.35 \pm 0.02$
D13	$6.05 \pm 0.20$	$6.17^{+0.19}_{-0.17}$	$7.07^{+0.14}_{-0.14}$	$7.22^{+0.13}_{-0.13}$	$8.30^{+0.11}_{-0.12}$	$8.48^{+0.12}_{-0.11}$
D14	$5.89^{+0.14}_{-0.13}$	$6.05^{+0.14}_{-0.13}$	$6.64^{+0.07}_{-0.06}$	$6.84^{+0.08}_{-0.06}$	$8.02 \pm 0.03$	$8.21 \pm 0.03$
D15	$5.96 \pm 0.16$	$6.12^{+0.17}_{-0.15}$	$6.78^{+0.06}_{-0.08}$	$6.97^{+0.05}_{-0.08}$	$8.21 \pm 0.04$	$8.40 \pm 0.04$
D16	$5.94^{+0.17}_{-0.15}$	$6.11 \pm 0.15$	$6.93 \pm 0.05$	$7.12^{+0.09}_{-0.06}$	$7.98 \pm 0.04$	$8.16 \pm 0.05$
D17	$6.36 \pm 0.13$	$6.55 \pm 0.12$	$7.06^{+0.05}_{-0.04}$	$7.29 \pm 0.04$	$8.17 \pm 0.04$	$8.39 \pm 0.05$
D18	$6.15^{+0.17}_{-0.18}$	$6.32 \pm 0.17$	$7.27^{+0.23}_{-0.12}$	$7.46^{+0.09}_{-0.10}$	$8.38 \pm 0.10$	$8.57^{+0.10}_{-0.11}$
D19	$5.88 \pm 0.13$	$6.05 \pm 0.13$	$6.77 \pm 0.03$	$6.93 \pm 0.03$	$7.59 \pm 0.03$	$7.76 \pm 0.03$
D20	$5.89 \pm 0.12$	$6.06^{+0.10}_{-0.11}$	$6.69 \pm 0.03$	$6.86 \pm 0.03$	$7.57^{+0.02}_{-0.03}$	$7.74 \pm 0.03$
D21	$5.66^{+0.17}_{-0.15}$	$5.83 \pm 0.14$	$6.49^{+0.06}_{-0.05}$	$6.68^{+0.06}_{-0.04}$	$7.92 \pm 0.02$	$8.11 \pm 0.02$
D22	$5.46 \pm 0.15$	$5.61^{+0.13}_{-0.14}$	$5.75^{+0.07}_{-0.06}$	$5.93 \pm 0.07$	$7.21 \pm 0.03$	$7.37^{+0.03}_{-0.04}$
D23	$6.16 \pm 0.18$	$6.34^{+0.18}_{-0.17}$	$7.16 \pm 0.04$	$7.37^{+0.05}_{-0.04}$	$8.19^{+0.04}_{-0.05}$	$8.39^{+0.05}_{-0.06}$
D24	$6.11^{+0.15}_{-0.14}$	$6.29^{+0.14}_{-0.15}$	$6.76^{+0.14}_{-0.08}$	$6.97^{+0.13}_{-0.08}$	$8.19^{+0.04}_{-0.05}$	$8.38 \pm 0.05$
D25	$6.07^{+0.13}_{-0.14}$	$6.23 \pm 0.13$	$6.60 \pm 0.04$	$6.79^{+0.04}_{-0.03}$	$7.86 \pm 0.02$	$8.05 \pm 0.03$
D26	$6.19^{+0.22}_{-0.23}$	$6.35^{+0.24}_{-0.22}$	$7.13^{+0.12}_{-0.14}$	$7.29^{+0.32}_{-0.14}$	$8.31 \pm 0.13$	$8.47^{+0.13}_{-0.14}$
D27	$5.68 \pm 0.10$	$5.87 \pm 0.09$	$6.58^{+0.06}_{-0.05}$	$6.80^{+0.06}_{-0.05}$	$8.09^{+0.02}_{-0.03}$	$8.29 \pm 0.03$
D28	$5.62 \pm 0.15$	$5.80 \pm 0.15$	$6.49 \pm 0.02$	$6.67 \pm 0.02$	$7.84 \pm 0.01$	$8.04 \pm 0.01$
D29	$5.98 \pm 0.14$	$6.16^{+0.13}_{-0.14}$	$6.73 \pm 0.03$	$6.94 \pm 0.03$	$8.05 \pm 0.03$	$8.25 \pm 0.03$
D30	$6.09^{+0.17}_{-0.18}$	$6.27^{+0.16}_{-0.17}$	$6.86 \pm 0.04$	$7.09 \pm 0.04$	$8.11 \pm 0.04$	$8.31 \pm 0.04$
D31	$6.05^{+0.17}_{-0.18}$	$6.22^{+0.18}_{-0.17}$	$6.94 \pm 0.04$	$7.16 \pm 0.04$	$8.10 \pm 0.04$	$8.29 \pm 0.05$
D32	$5.88^{+0.15}_{-0.14}$	$6.08 \pm 0.13$	$6.97^{+0.11}_{-0.07}$	$7.19^{+0.10}_{-0.07}$	$8.33 \pm 0.04$	$8.54 \pm 0.04$
D33	$6.08^{+0.28}_{-0.23}$	$6.25 \pm 0.27$	$7.40^{+0.36}_{-0.14}$	$7.54^{+0.35}_{-0.15}$	$8.23 \pm 0.14$	$8.41^{+0.16}_{-0.15}$
D34	$6.13^{+0.20}_{-0.24}$	$6.25^{+0.21}_{-0.22}$	$7.03^{+0.60}_{-0.20}$	$7.20^{+0.57}_{-0.18}$	$8.18^{+0.16}_{-0.17}$	$8.34^{+0.14}_{-0.15}$
D35	$5.79^{+0.14}_{-0.13}$	$5.93^{+0.18}_{-0.15}$	$6.66^{+0.09}_{-0.06}$	$6.86^{+0.08}_{-0.06}$	$8.02 \pm 0.03$	$8.23 \pm 0.03$
D36	$5.95^{+0.13}_{-0.14}$	$6.09 \pm 0.12$	$6.68 \pm 0.03$	$6.88 \pm 0.03$	$8.11 \pm 0.02$	$8.30 \pm 0.03$
D37	$6.07^{+0.26}_{-0.27}$	$6.14^{+0.28}_{-0.26}$	$7.15^{+0.58}_{-0.18}$	$7.25^{+0.63}_{-0.20}$	$8.30^{+0.20}_{-0.21}$	$8.46^{+0.19}_{-0.20}$
D38	$5.66^{+0.15}_{-0.16}$	$5.82^{+0.14}_{-0.13}$	$6.36 \pm 0.02$	$6.53 \pm 0.02$	$7.86 \pm 0.01$	$8.02 \pm 0.02$
D39	$6.00 \pm 0.14$	$6.21 \pm 0.13$	$6.86 \pm 0.03$	$7.07 \pm 0.03$	$8.09 \pm 0.03$	$8.30 \pm 0.03$
D40	$5.76 \pm 0.09$	$5.91 \pm 0.08$	$6.57 \pm 0.01$	$6.76^{+0.01}_{-0.02}$	$7.92 \pm 0.01$	$8.09 \pm 0.01$
D41	$5.38^{+0.12}_{-0.11}$	$5.53 \pm 0.10$	$5.99 \pm 0.03$	$6.15 \pm 0.03$	$7.40 \pm 0.01$	$7.56^{+0.01}_{-0.02}$
D42	$5.96 \pm 0.17$	$6.14^{+0.15}_{-0.17}$	$6.96^{+0.11}_{-0.07}$	$7.16^{+0.10}_{-0.07}$	$8.25 \pm 0.04$	$8.44 \pm 0.04$
D43	$6.04^{+0.21}_{-0.22}$	$6.20 \pm 0.20$	$7.04^{+0.41}_{-0.16}$	$7.23^{+0.48}_{-0.17}$	$8.28^{+0.14}_{-0.12}$	$8.46 \pm 0.13$
D44	$5.83^{+0.19}_{-0.18}$	$5.98^{+0.18}_{-0.17}$	$6.86^{+0.14}_{-0.08}$	$7.05^{+0.13}_{-0.08}$	$8.23 \pm 0.05$	$8.42 \pm 0.05$
D45	$6.05^{+0.76}_{-0.97}$	$6.19^{+0.85}_{-1.19}$	$7.17^{+0.86}_{-1.12}$	$7.36^{+0.71}_{-1.02}$	$8.32^{+0.31}_{-0.27}$	$8.52 \pm 0.26$
D46	$6.15^{+0.13}_{-0.14}$	$6.34^{+0.12}_{-0.11}$	$6.94 \pm 0.04$	$7.18 \pm 0.04$	$8.27 \pm 0.04$	$8.49 \pm 0.05$
D47	$6.08^{+0.20}_{-0.22}$	$6.25^{+0.23}_{-0.22}$	$7.41^{+0.30}_{-0.14}$	$7.57^{+0.29}_{-0.13}$	$8.22^{+0.12}_{-0.13}$	$8.41^{+0.14}_{-0.13}$
D48	$6.07 \pm 0.07$	$6.21^{+0.07}_{-0.06}$	$7.33^{+0.10}_{-0.07}$	$7.47^{+0.12}_{-0.07}$	$8.33^{+0.06}_{-0.05}$	$8.50 \pm 0.05$
D49	$6.12 \pm 0.15$	$6.28^{+0.14}_{-0.15}$	$6.99 \pm 0.05$	$7.19 \pm 0.05$	$8.38^{+0.04}_{-0.05}$	$8.57^{+0.06}_{-0.05}$
D50	$6.07^{+0.16}_{-0.17}$	$6.27^{+0.16}_{-0.18}$	$6.85 \pm 0.04$	$7.08 \pm 0.04$	$8.06^{+0.03}_{-0.04}$	$8.26 \pm 0.04$
D51	$6.03^{+0.16}_{-0.17}$	$6.19^{+0.17}_{-0.16}$	$7.15 \pm 0.05$	$7.35^{+0.05}_{-0.04}$	$8.24^{+0.04}_{-0.05}$	$8.44 \pm 0.05$
D52	$5.98^{+0.13}_{-0.12}$	$6.13 \pm 0.12$	$6.77 \pm 0.04$	$6.95^{+0.03}_{-0.04}$	$7.95 \pm 0.04$	$8.12^{+0.05}_{-0.04}$
D53	$5.84^{+0.12}_{-0.13}$	$5.99^{+0.14}_{-0.13}$	-	-	$7.96 \pm 0.01$	$8.15 \pm 0.01$
D54	$5.50 \pm 0.16$	$5.66^{+0.14}_{-0.15}$	-	-	$7.76 \pm 0.01$	$7.95 \pm 0.01$
D55	$6.19^{+0.15}_{-0.14}$	$6.33 \pm 0.14$	$7.32^{+0.16}_{-0.09}$	$7.48^{+0.08}_{-0.07}$	$8.15^{+0.06}_{-0.07}$	$8.32^{+0.07}_{-0.08}$

**Table D.8.** Total abundances derived from the nebular sample. All values are in  $12+\log(X/H)$  units.

Reference number	Fe		N		O	
	$t^2 = 0$	$t^2 > 0$	$t^2 = 0$	$t^2 > 0$	$t^2 = 0$	$t^2 > 0$
D56	$5.73 \pm 0.09$	$5.91^{+0.09}_{-0.08}$	-	-	$8.00 \pm 0.01$	$8.20 \pm 0.01$
D57	$5.86^{+0.20}_{-0.18}$	$6.05 \pm 0.17$	$6.94^{+0.26}_{-0.12}$	$7.13^{+0.20}_{-0.11}$	$8.30 \pm 0.08$	$8.49^{+0.09}_{-0.07}$
D58	$5.99 \pm 0.10$	$6.17^{+0.10}_{-0.09}$	$6.80^{+0.07}_{-0.05}$	$7.02^{+0.06}_{-0.05}$	$8.28 \pm 0.03$	$8.49 \pm 0.03$
D59	$5.91 \pm 0.08$	$6.12^{+0.07}_{-0.08}$	$6.76 \pm 0.01$	$6.97 \pm 0.01$	$8.10 \pm 0.01$	$8.32 \pm 0.01$
D60	$5.93 \pm 0.16$	$6.10^{+0.15}_{-0.16}$	$6.85^{+0.08}_{-0.05}$	$7.02 \pm 0.04$	$8.17 \pm 0.04$	$8.34 \pm 0.04$
D61	$6.08^{+0.16}_{-0.15}$	$6.26 \pm 0.14$	$7.09^{+0.04}_{-0.05}$	$7.29^{+0.04}_{-0.05}$	$8.24 \pm 0.04$	$8.43 \pm 0.05$
D62	$6.33^{+0.11}_{-0.10}$	$6.52^{+0.09}_{-0.11}$	$7.13^{+0.04}_{-0.05}$	$7.34 \pm 0.05$	$8.30 \pm 0.04$	$8.50 \pm 0.05$
D63	$5.87 \pm 0.08$	$6.05^{+0.07}_{-0.08}$	$7.26^{+0.07}_{-0.05}$	$7.46 \pm 0.06$	$8.49 \pm 0.03$	$8.68 \pm 0.03$
D64	$5.86 \pm 0.15$	$6.00^{+0.13}_{-0.14}$	$7.37^{+0.19}_{-0.10}$	$7.52^{+0.18}_{-0.10}$	$8.55^{+0.08}_{-0.07}$	$8.72 \pm 0.07$
D65	$5.47 \pm 0.07$	$5.60 \pm 0.07$	$6.34^{+0.05}_{-0.04}$	$6.50^{+0.06}_{-0.04}$	$7.43 \pm 0.02$	$7.58 \pm 0.02$
D66	$6.11 \pm 0.17$	$6.27^{+0.16}_{-0.14}$	$6.84 \pm 0.04$	$7.03 \pm 0.04$	$8.01 \pm 0.03$	$8.21 \pm 0.04$
D67	$5.85^{+0.09}_{-0.08}$	$6.01 \pm 0.08$	$6.70 \pm 0.02$	$6.88 \pm 0.02$	$7.89 \pm 0.01$	$8.06 \pm 0.01$
D68	$5.93 \pm 0.08$	$6.12^{+0.09}_{-0.07}$	$6.98^{+0.09}_{-0.07}$	$7.20^{+0.09}_{-0.06}$	$8.40 \pm 0.04$	$8.62 \pm 0.04$
D69	$5.88 \pm 0.14$	$6.01^{+0.12}_{-0.13}$	$6.58 \pm 0.03$	$6.73 \pm 0.03$	$7.90 \pm 0.03$	$8.05 \pm 0.03$
D70	$5.98^{+0.12}_{-0.11}$	$6.15 \pm 0.11$	$6.69 \pm 0.03$	$6.90 \pm 0.03$	$8.14^{+0.03}_{-0.02}$	$8.33 \pm 0.03$
D71	$5.91^{+0.22}_{-0.20}$	$6.00 \pm 0.21$	$7.74^{+0.58}_{-0.19}$	$7.92^{+0.49}_{-0.17}$	$8.54^{+0.23}_{-0.24}$	$8.65^{+0.17}_{-0.18}$
D72	$5.56^{+0.05}_{-0.06}$	$5.71^{+0.05}_{-0.06}$	$6.30 \pm 0.01$	$6.48 \pm 0.01$	$7.76 \pm 0.01$	$7.93 \pm 0.01$
D73	$5.93 \pm 0.09$	$6.06^{+0.10}_{-0.09}$	-	-	$8.00 \pm 0.02$	$8.16 \pm 0.02$
D74	$5.58 \pm 0.15$	$5.80^{+0.13}_{-0.14}$	-	-	$8.23 \pm 0.01$	$8.45 \pm 0.01$
D75	$5.33 \pm 0.12$	$5.50^{+0.12}_{-0.11}$	$6.18 \pm 0.02$	$6.36 \pm 0.02$	$7.58 \pm 0.01$	$7.75 \pm 0.01$
D76	$6.07 \pm 0.07$	$6.28^{+0.06}_{-0.07}$	$7.06 \pm 0.01$	$7.28 \pm 0.01$	$8.15 \pm 0.01$	$8.38 \pm 0.01$
D77	$6.04 \pm 0.07$	$6.22^{+0.07}_{-0.08}$	$6.83^{+0.01}_{-0.02}$	$7.04 \pm 0.01$	$8.20 \pm 0.01$	$8.39^{+0.02}_{-0.01}$
D78	$5.60^{+0.09}_{-0.08}$	$5.77 \pm 0.08$	-	-	$7.44 \pm 0.01$	$7.62 \pm 0.01$
D79	$5.78^{+0.14}_{-0.12}$	$5.93 \pm 0.14$	$6.65 \pm 0.04$	$6.81 \pm 0.04$	$7.57 \pm 0.02$	$7.74 \pm 0.02$
D80	$5.86^{+0.04}_{-0.05}$	$6.01 \pm 0.04$	-	-	$7.58 \pm 0.01$	$7.75 \pm 0.01$
D81	$5.93^{+0.18}_{-0.21}$	$5.86^{+0.17}_{-0.20}$	$6.99^{+0.43}_{-0.17}$	$6.88^{+0.45}_{-0.17}$	$8.02 \pm 0.04$	$7.94^{+0.14}_{-0.15}$
D82	$6.09^{+0.06}_{-0.07}$	$6.28 \pm 0.06$	$6.78 \pm 0.02$	$6.96 \pm 0.02$	$7.88 \pm 0.01$	$8.07 \pm 0.01$
D83	$5.88 \pm 0.06$	$6.29 \pm 0.06$	$6.77 \pm 0.04$	$7.20 \pm 0.04$	$7.84 \pm 0.02$	$8.28^{+0.06}_{-0.03}$
D84	$5.62 \pm 0.10$	$5.81 \pm 0.09$	$7.02 \pm 0.03$	$7.24 \pm 0.03$	$8.07 \pm 0.03$	$8.29^{+0.03}_{-0.04}$
D85	$6.40 \pm 0.07$	$6.56 \pm 0.07$	-	-	$8.55^{+0.06}_{-0.07}$	$8.73^{+0.06}_{-0.07}$
D86	$6.20 \pm 0.07$	$6.34^{+0.08}_{-0.07}$	$7.72 \pm 0.06$	$7.87^{+0.11}_{-0.07}$	$8.44 \pm 0.06$	$8.61 \pm 0.06$
D87	$6.01^{+0.09}_{-0.08}$	$6.22 \pm 0.08$	-	-	$8.12 \pm 0.01$	$8.35 \pm 0.01$
D88	$5.38^{+0.07}_{-0.08}$	$5.51 \pm 0.08$	-	-	$7.13 \pm 0.01$	$7.29 \pm 0.01$
D89	$5.44 \pm 0.10$	$5.58^{+0.09}_{-0.10}$	-	-	$7.19 \pm 0.01$	$7.34 \pm 0.02$
D90	$5.75 \pm 0.13$	$5.89 \pm 0.13$	$6.82^{+0.18}_{-0.10}$	$6.99^{+0.17}_{-0.10}$	$7.96 \pm 0.06$	$8.13 \pm 0.06$
D91	$5.83 \pm 0.05$	$6.02 \pm 0.05$	$6.62 \pm 0.01$	$6.85 \pm 0.01$	$8.21 \pm 0.01$	$8.42 \pm 0.01$
D92	$5.89^{+0.06}_{-0.05}$	$6.14 \pm 0.06$	$7.15 \pm 0.04$	$7.44^{+0.07}_{-0.06}$	$8.06^{+0.03}_{-0.02}$	$8.33 \pm 0.04$
D93	$5.86 \pm 0.06$	$6.03 \pm 0.06$	$6.81 \pm 0.03$	$7.02 \pm 0.03$	$8.02 \pm 0.02$	$8.21 \pm 0.03$
D94	$5.90^{+0.08}_{-0.07}$	$6.06 \pm 0.08$	-	-	$7.56 \pm 0.01$	$7.73 \pm 0.01$
D95	$5.85 \pm 0.10$	$5.99 \pm 0.09$	-	-	$7.93 \pm 0.02$	$8.08 \pm 0.02$
D96	$6.01^{+0.15}_{-0.17}$	$6.17 \pm 0.17$	-	-	$7.87 \pm 0.02$	$8.07 \pm 0.03$
D97	$5.66 \pm 0.05$	$5.83^{+0.05}_{-0.06}$	$6.16 \pm 0.02$	$6.33 \pm 0.02$	$7.62 \pm 0.01$	$7.80 \pm 0.01$
D98	$5.81^{+0.12}_{-0.11}$	$5.97^{+0.12}_{-0.13}$	-	-	$7.44 \pm 0.01$	$7.62 \pm 0.01$
D99	$5.63 \pm 0.12$	$5.81 \pm 0.12$	$6.39 \pm 0.03$	$6.59 \pm 0.03$	$7.83 \pm 0.02$	$8.02 \pm 0.02$
D100	$5.64 \pm 0.04$	$5.80 \pm 0.04$	$6.04 \pm 0.03$	$6.20 \pm 0.03$	$7.44 \pm 0.01$	$7.62 \pm 0.01$
D101	$6.09^{+0.17}_{-0.15}$	$6.34 \pm 0.14$	$7.19^{+0.35}_{-0.14}$	$7.44^{+0.32}_{-0.14}$	$8.05 \pm 0.03$	$8.30^{+0.15}_{-0.14}$
D102	$5.93 \pm 0.05$	$6.12 \pm 0.04$	-	-	$8.05 \pm 0.01$	$8.26 \pm 0.01$
D103	$5.65 \pm 0.04$	$5.82 \pm 0.04$	$6.22 \pm 0.02$	$6.39 \pm 0.02$	$7.59 \pm 0.01$	$7.77 \pm 0.01$
D104	$5.92^{+0.07}_{-0.08}$	$6.08^{+0.09}_{-0.08}$	$6.54 \pm 0.02$	$6.74 \pm 0.02$	$8.09 \pm 0.01$	$8.28 \pm 0.02$
D105	$5.86^{+0.17}_{-0.16}$	$6.00 \pm 0.15$	$6.37 \pm 0.02$	$6.54 \pm 0.02$	$7.75 \pm 0.02$	$7.92 \pm 0.02$
D106	$5.97 \pm 0.07$	$5.87^{+0.06}_{-0.07}$	$6.95 \pm 0.04$	$6.84 \pm 0.04$	$8.06 \pm 0.01$	$7.98^{+0.05}_{-0.04}$
D107	$5.43^{+0.17}_{-0.19}$	$5.52^{+0.18}_{-0.17}$	-	-	$6.92 \pm 0.01$	$7.05^{+0.01}_{-0.02}$
D108	$5.70^{+0.05}_{-0.06}$	$5.85^{+0.05}_{-0.06}$	$6.43 \pm 0.01$	$6.63 \pm 0.01$	$8.21 \pm 0.01$	$8.39 \pm 0.01$
D109	$5.90^{+0.07}_{-0.08}$	$6.07^{+0.07}_{-0.08}$	$6.86 \pm 0.02$	$7.06 \pm 0.02$	$8.07 \pm 0.02$	$8.25 \pm 0.02$
D110	$5.73 \pm 0.03$	$5.89 \pm 0.03$	$6.30 \pm 0.01$	$6.47 \pm 0.01$	$7.60 \pm 0.01$	$7.77 \pm 0.01$
D111	$5.64 \pm 0.02$	$5.82 \pm 0.02$	$6.55 \pm 0.01$	$6.74 \pm 0.01$	$7.97 \pm 0.01$	$8.17 \pm 0.01$

**Table D.8.** Total abundances derived from the nebular sample. All values are in  $12+\log(X/H)$  units.

Reference number	Fe		N		O	
	$t^2 = 0$	$t^2 > 0$	$t^2 = 0$	$t^2 > 0$	$t^2 = 0$	$t^2 > 0$
D112	$5.71 \pm 0.07$	$5.88 \pm 0.07$	$6.24^{+0.01}_{-0.02}$	$6.41^{+0.01}_{-0.02}$	$7.69 \pm 0.01$	$7.87 \pm 0.01$
D113	$5.57 \pm 0.04$	$5.74 \pm 0.04$	$6.33 \pm 0.01$	$6.51 \pm 0.01$	$7.82 \pm 0.01$	$8.00 \pm 0.01$
D114	$5.72 \pm 0.04$	$5.89 \pm 0.04$	$6.39 \pm 0.01$	$6.58 \pm 0.01$	$7.84 \pm 0.01$	$8.02 \pm 0.01$
D115	$5.88^{+0.03}_{-0.04}$	$6.04 \pm 0.03$	$7.15 \pm 0.02$	$7.33 \pm 0.02$	$8.36 \pm 0.01$	$8.52 \pm 0.03$
D116	$5.53 \pm 0.06$	$5.65 \pm 0.06$	$7.09 \pm 0.04$	$7.22^{+0.04}_{-0.05}$	$8.43^{+0.03}_{-0.04}$	$8.55 \pm 0.05$
D117	$5.39 \pm 0.03$	$5.50 \pm 0.02$	$7.10 \pm 0.01$	$7.22 \pm 0.01$	$8.38^{+0.01}_{-0.02}$	$8.51 \pm 0.01$
D118	$5.28 \pm 0.06$	$5.57 \pm 0.06$	$7.10^{+0.03}_{-0.04}$	$7.40^{+0.03}_{-0.04}$	$8.27 \pm 0.02$	$8.59 \pm 0.04$
D119	$5.67^{+0.07}_{-0.08}$	$5.79^{+0.07}_{-0.08}$	$7.03^{+0.05}_{-0.06}$	$7.18^{+0.06}_{-0.05}$	$8.37 \pm 0.03$	$8.51 \pm 0.08$
D120	$5.75^{+0.08}_{-0.07}$	$5.89 \pm 0.07$	$7.67^{+0.04}_{-0.03}$	$7.85 \pm 0.04$	$8.50 \pm 0.04$	$8.68 \pm 0.04$
D121	$5.69 \pm 0.07$	$5.94 \pm 0.07$	$7.71 \pm 0.04$	$7.99 \pm 0.04$	$8.59^{+0.03}_{-0.04}$	$8.88 \pm 0.04$
D122	$5.76^{+0.12}_{-0.11}$	$6.01 \pm 0.11$	$7.73^{+0.07}_{-0.06}$	$7.99^{+0.15}_{-0.10}$	$8.46 \pm 0.09$	$8.73^{+0.08}_{-0.07}$
D123	$6.01^{+0.13}_{-0.14}$	$6.10^{+0.14}_{-0.13}$	$7.74^{+0.18}_{-0.10}$	$7.90^{+0.21}_{-0.10}$	$8.49 \pm 0.10$	$8.61 \pm 0.09$
D124	$5.75 \pm 0.16$	$5.84^{+0.15}_{-0.13}$	$7.29^{+0.31}_{-0.12}$	$7.42^{+0.25}_{-0.13}$	$8.36^{+0.13}_{-0.12}$	$8.48^{+0.12}_{-0.11}$
D125	$6.17 \pm 0.13$	$6.29 \pm 0.14$	$7.84^{+0.23}_{-0.11}$	$8.02^{+0.20}_{-0.12}$	$8.65 \pm 0.11$	$8.80^{+0.10}_{-0.09}$
D126	$6.38^{+0.10}_{-0.12}$	$6.51 \pm 0.11$	$7.66^{+0.15}_{-0.09}$	$7.83^{+0.14}_{-0.09}$	$8.50 \pm 0.08$	$8.67 \pm 0.08$
D127	$5.78 \pm 0.09$	$5.85 \pm 0.09$	$7.17 \pm 0.04$	$7.28 \pm 0.04$	$8.10 \pm 0.05$	$8.19 \pm 0.04$
D128	$5.89^{+0.05}_{-0.04}$	$6.12^{+0.05}_{-0.04}$	$7.64 \pm 0.03$	$7.91 \pm 0.03$	$8.57 \pm 0.02$	$8.82 \pm 0.03$
D129	$5.18^{+0.14}_{-0.13}$	$5.31^{+0.10}_{-0.12}$	$7.30^{+0.03}_{-0.04}$	$7.43 \pm 0.03$	$8.34 \pm 0.03$	$8.49 \pm 0.03$
D130	$6.29 \pm 0.09$	$6.45^{+0.09}_{-0.10}$	$6.92 \pm 0.03$	$7.10 \pm 0.03$	$8.19 \pm 0.02$	$8.36 \pm 0.02$
D131	$5.51^{+0.10}_{-0.09}$	$5.67 \pm 0.10$	$7.09^{+0.04}_{-0.03}$	$7.29 \pm 0.03$	$8.31^{+0.01}_{-0.02}$	$8.49 \pm 0.02$
D132	$5.49 \pm 0.06$	$5.61 \pm 0.05$	$6.98^{+0.05}_{-0.04}$	$7.10 \pm 0.04$	$8.19^{+0.03}_{-0.02}$	$8.33^{+0.02}_{-0.03}$
D133	$5.50 \pm 0.11$	$5.67 \pm 0.10$	$6.95^{+0.03}_{-0.04}$	$7.15^{+0.04}_{-0.03}$	$8.20 \pm 0.02$	$8.39^{+0.03}_{-0.02}$
D134	$5.48^{+0.23}_{-0.24}$	$5.66^{+0.68}_{-0.19}$	$6.94^{+0.55}_{-0.18}$	$7.20^{+0.39}_{-0.20}$	$8.29 \pm 0.11$	$8.55^{+0.23}_{-0.21}$
D135	$5.58 \pm 0.07$	$5.71 \pm 0.06$	$7.01 \pm 0.03$	$7.17^{+0.04}_{-0.03}$	$8.20 \pm 0.02$	$8.35 \pm 0.03$
D136	$5.79 \pm 0.08$	$5.97 \pm 0.08$	$7.29 \pm 0.06$	$7.50 \pm 0.05$	$8.33^{+0.05}_{-0.04}$	$8.56 \pm 0.06$
D137	$5.66^{+0.12}_{-0.11}$	$5.78^{+0.12}_{-0.11}$	$7.22^{+0.04}_{-0.03}$	$7.38 \pm 0.03$	$8.32 \pm 0.02$	$8.48 \pm 0.02$
D138	$5.67^{+0.18}_{-0.17}$	$5.78^{+0.14}_{-0.16}$	$7.45^{+0.29}_{-0.13}$	$7.59^{+0.30}_{-0.13}$	$8.42^{+0.13}_{-0.14}$	$8.55 \pm 0.13$
D139	$5.95^{+0.14}_{-0.13}$	$6.03^{+0.12}_{-0.13}$	$7.66^{+0.16}_{-0.09}$	$7.77^{+0.18}_{-0.10}$	$8.53 \pm 0.10$	$8.63 \pm 0.10$
D140	$5.55^{+0.10}_{-0.09}$	$5.66^{+0.09}_{-0.10}$	$7.48^{+0.12}_{-0.08}$	$7.66 \pm 0.05$	$8.42 \pm 0.07$	$8.55 \pm 0.06$
D141	$5.56^{+0.11}_{-0.12}$	$5.56 \pm 0.11$	$7.12^{+0.07}_{-0.08}$	$7.12^{+0.18}_{-0.10}$	$8.21^{+0.07}_{-0.08}$	$8.21^{+0.08}_{-0.09}$
D142	$5.62^{+0.18}_{-0.21}$	$5.79^{+0.19}_{-0.20}$	$7.66^{+0.40}_{-0.14}$	$7.91^{+0.43}_{-0.15}$	$8.53^{+0.16}_{-0.14}$	$8.75^{+0.17}_{-0.18}$
D143	$5.93^{+0.12}_{-0.14}$	$6.00^{+0.14}_{-0.15}$	$7.68^{+0.22}_{-0.11}$	$7.84^{+0.23}_{-0.12}$	$8.53^{+0.13}_{-0.12}$	$8.64 \pm 0.12$
D144	$6.10^{+0.07}_{-0.08}$	$6.27 \pm 0.07$	$7.46^{+0.04}_{-0.05}$	$7.64 \pm 0.04$	$8.44 \pm 0.03$	$8.63 \pm 0.03$
D145	$5.72 \pm 0.04$	$5.83 \pm 0.04$	$6.74 \pm 0.03$	$6.85 \pm 0.03$	$8.00 \pm 0.01$	$8.12 \pm 0.01$
D146	$5.16^{+0.10}_{-0.09}$	$5.33^{+0.10}_{-0.11}$	$7.33 \pm 0.04$	$7.53 \pm 0.04$	$8.48 \pm 0.01$	$8.68 \pm 0.01$
D147	$6.41 \pm 0.11$	$6.48 \pm 0.11$	$7.87^{+0.17}_{-0.10}$	$8.04^{+0.08}_{-0.07}$	$8.62 \pm 0.10$	$8.73^{+0.09}_{-0.10}$
D148	$6.21^{+0.09}_{-0.10}$	$6.38 \pm 0.09$	$7.90 \pm 0.06$	$8.09^{+0.14}_{-0.08}$	$8.61^{+0.06}_{-0.07}$	$8.82 \pm 0.07$
D149	$5.03^{+0.11}_{-0.10}$	$5.15 \pm 0.10$	$6.81 \pm 0.03$	$6.92 \pm 0.03$	$8.12 \pm 0.01$	$8.25 \pm 0.01$
D150	$6.36^{+0.14}_{-0.16}$	$6.48^{+0.15}_{-0.17}$	$8.09^{+0.35}_{-0.14}$	$8.27^{+0.33}_{-0.14}$	$8.61^{+0.15}_{-0.16}$	$8.77^{+0.13}_{-0.11}$
D151	$5.53 \pm 0.18$	$5.69 \pm 0.18$	$7.82^{+0.39}_{-0.15}$	$7.97^{+0.37}_{-0.14}$	$8.59 \pm 0.15$	$8.76^{+0.11}_{-0.12}$
D152	$6.08^{+0.11}_{-0.12}$	$6.10^{+0.12}_{-0.11}$	$7.49^{+0.16}_{-0.09}$	$7.57 \pm 0.07$	$8.47 \pm 0.10$	$8.52^{+0.08}_{-0.10}$
D153	$5.19 \pm 0.10$	$5.29 \pm 0.10$	-	-	$7.89 \pm 0.02$	$8.03 \pm 0.02$
D154	$5.26 \pm 0.09$	$5.34^{+0.09}_{-0.08}$	$6.47^{+0.03}_{-0.02}$	$6.57^{+0.03}_{-0.02}$	$7.83 \pm 0.02$	$7.94 \pm 0.02$
D155	$6.57^{+0.17}_{-0.18}$	$6.71^{+0.17}_{-0.15}$	$7.96^{+0.27}_{-0.12}$	$8.17^{+0.27}_{-0.12}$	$8.67 \pm 0.14$	$8.83 \pm 0.12$
D156	$5.65 \pm 0.18$	$5.82^{+0.17}_{-0.18}$	$6.91^{+0.44}_{-0.15}$	$7.11^{+0.43}_{-0.16}$	$8.21 \pm 0.10$	$8.41 \pm 0.14$
D157	$5.77^{+0.09}_{-0.08}$	$6.05^{+0.09}_{-0.08}$	$7.57^{+0.06}_{-0.05}$	$7.88^{+0.07}_{-0.05}$	$8.53^{+0.04}_{-0.05}$	$8.85 \pm 0.07$
D158	$6.09^{+0.09}_{-0.10}$	$6.24 \pm 0.10$	$7.50^{+0.16}_{-0.09}$	$7.77^{+0.15}_{-0.09}$	$8.43^{+0.09}_{-0.10}$	$8.64 \pm 0.07$
D159	$5.00^{+0.11}_{-0.12}$	$5.15 \pm 0.11$	$6.60 \pm 0.02$	$6.78 \pm 0.02$	$7.94 \pm 0.01$	$8.11 \pm 0.01$
D160	$6.04 \pm 0.15$	$6.10^{+0.15}_{-0.14}$	$7.72^{+0.27}_{-0.11}$	$7.88^{+0.29}_{-0.12}$	$8.58^{+0.13}_{-0.14}$	$8.68 \pm 0.13$
D161	$5.91^{+0.12}_{-0.13}$	$6.05^{+0.14}_{-0.13}$	$7.88^{+0.24}_{-0.11}$	$8.05^{+0.21}_{-0.11}$	$8.61^{+0.09}_{-0.11}$	$8.78 \pm 0.11$
D162	$6.09^{+0.15}_{-0.14}$	$6.13^{+0.14}_{-0.15}$	$7.77^{+0.27}_{-0.12}$	$7.90^{+0.27}_{-0.12}$	$8.62^{+0.14}_{-0.13}$	$8.72^{+0.13}_{-0.12}$
D163	$5.91^{+0.14}_{-0.13}$	$5.97^{+0.11}_{-0.12}$	$7.62^{+0.20}_{-0.10}$	$7.76^{+0.19}_{-0.10}$	$8.57 \pm 0.11$	$8.66 \pm 0.10$
D164	$6.07 \pm 0.10$	$6.16 \pm 0.10$	$7.80^{+0.15}_{-0.10}$	$7.95^{+0.15}_{-0.09}$	$8.49 \pm 0.09$	$8.62 \pm 0.08$
D165	$5.79 \pm 0.07$	$5.98^{+0.06}_{-0.07}$	$7.29 \pm 0.05$	$7.50 \pm 0.05$	$8.35 \pm 0.04$	$8.56 \pm 0.06$
D166	$5.87 \pm 0.06$	$6.10 \pm 0.06$	$7.38 \pm 0.04$	$7.63 \pm 0.03$	$8.44^{+0.02}_{-0.03}$	$8.70^{+0.03}_{-0.04}$
D167	$5.86 \pm 0.06$	$6.12 \pm 0.06$	$7.30^{+0.04}_{-0.05}$	$7.61^{+0.05}_{-0.04}$	$8.36^{+0.03}_{-0.02}$	$8.65^{+0.06}_{-0.05}$

**Table D.8.** Total abundances derived from the nebular sample. All values are in  $12+\log(X/H)$  units.

Reference number	Fe		N		O	
	$t^2 = 0$	$t^2 > 0$	$t^2 = 0$	$t^2 > 0$	$t^2 = 0$	$t^2 > 0$
D168	6.01 <sup>+0.07</sup> <sub>-0.08</sub>	6.06 <sup>+0.08</sup> <sub>-0.07</sub>	7.28 <sup>+0.18</sup> <sub>-0.10</sub>	7.33 <sup>+0.19</sup> <sub>-0.09</sub>	8.38 ± 0.03	8.41 ± 0.06
D169	5.44 <sup>+0.13</sup> <sub>-0.14</sub>	5.65 <sup>+0.13</sup> <sub>-0.15</sub>	7.37 <sup>+0.08</sup> <sub>-0.07</sub>	7.66 <sup>+0.08</sup> <sub>-0.07</sub>	8.41 ± 0.10	8.64 ± 0.07
D170	6.18 <sup>+0.14</sup> <sub>-0.13</sub>	6.18 <sup>+0.14</sup> <sub>-0.13</sub>	7.45 <sup>+0.23</sup> <sub>-0.11</sub>	7.45 <sup>+0.23</sup> <sub>-0.11</sub>	7.93 <sup>+0.07</sup> <sub>-0.06</sub>	7.93 <sup>+0.07</sup> <sub>-0.06</sub>
D171	5.64 <sup>+0.09</sup> <sub>-0.10</sub>	5.74 ± 0.10	7.46 ± 0.03	7.60 <sup>+0.03</sup> <sub>-0.04</sub>	8.28 ± 0.04	8.41 ± 0.03
D172	5.93 ± 0.05	6.11 ± 0.05	7.32 ± 0.04	7.53 ± 0.04	8.39 ± 0.02	8.59 ± 0.04
D173	6.01 <sup>+0.03</sup> <sub>-0.04</sub>	6.12 ± 0.04	7.36 ± 0.02	7.50 <sup>+0.03</sup> <sub>-0.02</sub>	8.31 ± 0.01	8.45 ± 0.03
D174	5.60 <sup>+0.08</sup> <sub>-0.09</sub>	5.81 <sup>+0.10</sup> <sub>-0.09</sub>	7.53 <sup>+0.13</sup> <sub>-0.09</sub>	7.77 ± 0.07	8.50 ± 0.07	8.76 <sup>+0.08</sup> <sub>-0.07</sub>
D175	5.82 ± 0.11	6.04 <sup>+0.13</sup> <sub>-0.12</sub>	7.51 <sup>+0.20</sup> <sub>-0.10</sub>	7.78 <sup>+0.22</sup> <sub>-0.11</sub>	8.43 ± 0.10	8.71 ± 0.10
D176	6.06 ± 0.03	6.34 ± 0.04	7.55 <sup>+0.04</sup> <sub>-0.03</sub>	7.88 ± 0.03	8.48 ± 0.02	8.79 ± 0.04
D177	6.12 <sup>+0.08</sup> <sub>-0.07</sub>	6.32 ± 0.07	7.61 ± 0.05	7.84 <sup>+0.06</sup> <sub>-0.05</sub>	8.41 ± 0.04	8.63 ± 0.06
D178	5.60 <sup>+0.05</sup> <sub>-0.04</sub>	5.78 ± 0.04	7.33 ± 0.03	7.54 ± 0.03	8.40 ± 0.01	8.60 ± 0.01
D179	5.61 ± 0.04	5.81 ± 0.04	7.34 ± 0.03	7.58 ± 0.03	8.40 ± 0.01	8.63 ± 0.01
D180	5.82 <sup>+0.15</sup> <sub>-0.16</sub>	6.03 <sup>+0.13</sup> <sub>-0.15</sub>	6.74 ± 0.06	6.94 <sup>+0.06</sup> <sub>-0.07</sub>	8.10 ± 0.01	8.30 ± 0.02
D181	5.55 <sup>+0.10</sup> <sub>-0.11</sub>	5.67 ± 0.10	6.60 ± 0.04	6.72 <sup>+0.05</sup> <sub>-0.04</sub>	7.99 ± 0.03	8.12 ± 0.03
D182	5.88 ± 0.10	6.17 <sup>+0.12</sup> <sub>-0.09</sub>	6.87 ± 0.08	7.21 <sup>+0.07</sup> <sub>-0.08</sub>	8.14 ± 0.03	8.48 ± 0.12
D183	5.94 ± 0.03	6.14 ± 0.03	6.76 ± 0.04	6.96 ± 0.04	7.99 ± 0.01	8.20 <sup>+0.01</sup> <sub>-0.02</sub>
D184	5.89 ± 0.07	6.03 ± 0.06	7.30 ± 0.04	7.55 <sup>+0.05</sup> <sub>-0.04</sub>	8.22 ± 0.06	8.40 ± 0.05
D185	5.46 <sup>+0.08</sup> <sub>-0.09</sub>	5.61 <sup>+0.09</sup> <sub>-0.08</sub>	7.41 <sup>+0.11</sup> <sub>-0.08</sub>	7.56 <sup>+0.11</sup> <sub>-0.07</sub>	8.28 ± 0.06	8.45 <sup>+0.06</sup> <sub>-0.07</sub>
D186	6.16 ± 0.05	6.25 ± 0.05	7.80 <sup>+0.14</sup> <sub>-0.03</sub>	8.09 <sup>+0.02</sup> <sub>-0.05</sub>	8.35 ± 0.06	8.56 ± 0.04
D187	6.40 ± 0.12	6.57 <sup>+0.12</sup> <sub>-0.11</sub>	7.77 ± 0.04	8.00 <sup>+0.09</sup> <sub>-0.06</sub>	8.52 <sup>+0.06</sup> <sub>-0.07</sub>	8.73 ± 0.05
D188	5.75 ± 0.04	5.88 ± 0.04	7.53 ± 0.03	7.69 <sup>+0.02</sup> <sub>-0.03</sub>	8.43 <sup>+0.02</sup> <sub>-0.03</sub>	8.57 ± 0.03
D189	5.64 <sup>+0.22</sup> <sub>-0.24</sub>	5.68 ± 0.23	7.38 <sup>+0.32</sup> <sub>-0.12</sub>	7.41 <sup>+0.34</sup> <sub>-0.15</sub>	8.52 <sup>+0.12</sup> <sub>-0.11</sub>	8.58 ± 0.14
D190	5.75 <sup>+0.14</sup> <sub>-0.13</sub>	5.86 <sup>+0.12</sup> <sub>-0.14</sub>	7.42 ± 0.06	7.67 <sup>+0.07</sup> <sub>-0.06</sub>	8.54 <sup>+0.07</sup> <sub>-0.08</sub>	8.70 ± 0.06
D191	5.40 <sup>+0.14</sup> <sub>-0.15</sub>	5.50 <sup>+0.14</sup> <sub>-0.13</sub>	7.69 ± 0.04	7.86 <sup>+0.05</sup> <sub>-0.04</sub>	8.70 ± 0.05	8.83 <sup>+0.04</sup> <sub>-0.05</sub>
D192	5.63 <sup>+0.11</sup> <sub>-0.12</sub>	5.75 <sup>+0.11</sup> <sub>-0.12</sub>	7.71 ± 0.07	7.86 <sup>+0.08</sup> <sub>-0.07</sub>	8.55 <sup>+0.07</sup> <sub>-0.09</sub>	8.71 ± 0.07
D193	5.79 <sup>+0.18</sup> <sub>-0.17</sub>	5.98 <sup>+0.17</sup> <sub>-0.18</sub>	7.71 <sup>+0.12</sup> <sub>-0.13</sub>	7.93 <sup>+0.14</sup> <sub>-0.12</sub>	8.43 ± 0.12	8.68 <sup>+0.18</sup> <sub>-0.17</sub>
D194	5.43 ± 0.12	5.47 ± 0.12	7.26 <sup>+0.08</sup> <sub>-0.07</sub>	7.28 ± 0.08	8.34 <sup>+0.06</sup> <sub>-0.07</sub>	8.37 ± 0.09
D195	5.65 <sup>+0.06</sup> <sub>-0.07</sub>	5.81 <sup>+0.06</sup> <sub>-0.07</sub>	6.95 <sup>+0.06</sup> <sub>-0.05</sub>	7.15 <sup>+0.05</sup> <sub>-0.06</sub>	8.26 ± 0.03	8.44 <sup>+0.04</sup> <sub>-0.05</sub>
D196	5.97 <sup>+0.09</sup> <sub>-0.08</sub>	6.15 ± 0.08	7.31 ± 0.05	7.50 ± 0.05	8.39 ± 0.04	8.57 <sup>+0.04</sup> <sub>-0.05</sub>
D197	5.26 ± 0.16	5.41 <sup>+0.18</sup> <sub>-0.16</sub>	7.01 <sup>+0.25</sup> <sub>-0.12</sub>	7.22 <sup>+0.32</sup> <sub>-0.13</sub>	8.10 <sup>+0.10</sup> <sub>-0.09</sub>	8.29 <sup>+0.17</sup> <sub>-0.14</sub>
D198	5.07 ± 0.11	5.24 <sup>+0.10</sup> <sub>-0.11</sub>	7.00 ± 0.08	7.18 <sup>+0.09</sup> <sub>-0.08</sub>	8.22 ± 0.05	8.40 ± 0.10
D199	5.33 <sup>+0.06</sup> <sub>-0.05</sub>	5.44 <sup>+0.05</sup> <sub>-0.06</sub>	7.48 ± 0.02	7.59 <sup>+0.02</sup> <sub>-0.03</sub>	8.45 ± 0.04	8.58 ± 0.03
D200	5.65 <sup>+0.11</sup> <sub>-0.12</sub>	5.85 <sup>+0.12</sup> <sub>-0.13</sub>	7.26 ± 0.05	7.50 <sup>+0.05</sup> <sub>-0.04</sub>	8.45 ± 0.03	8.67 ± 0.05
D201	5.82 ± 0.06	6.05 ± 0.06	7.46 ± 0.03	7.72 ± 0.03	8.38 ± 0.03	8.62 ± 0.03
D202	5.65 ± 0.28	5.74 <sup>+0.28</sup> <sub>-0.26</sub>	7.42 <sup>+0.67</sup> <sub>-0.20</sub>	7.59 <sup>+0.62</sup> <sub>-0.20</sub>	8.56 <sup>+0.31</sup> <sub>-0.30</sub>	8.68 <sup>+0.24</sup> <sub>-0.25</sub>
D203	5.70 <sup>+0.11</sup> <sub>-0.12</sub>	5.71 <sup>+0.11</sup> <sub>-0.12</sub>	7.49 ± 0.06	7.58 <sup>+0.06</sup> <sub>-0.07</sub>	8.68 <sup>+0.07</sup> <sub>-0.08</sub>	8.73 ± 0.07
D204	5.61 ± 0.18	5.61 ± 0.17	7.13 <sup>+0.18</sup> <sub>-0.11</sub>	7.18 <sup>+0.19</sup> <sub>-0.10</sub>	8.06 ± 0.12	8.09 ± 0.11
D205	5.18 <sup>+0.17</sup> <sub>-0.16</sub>	5.31 <sup>+0.17</sup> <sub>-0.16</sub>	7.08 ± 0.07	7.22 ± 0.06	8.34 ± 0.04	8.46 ± 0.07
D206	5.52 ± 0.12	5.70 <sup>+0.14</sup> <sub>-0.13</sub>	7.44 ± 0.05	7.64 ± 0.05	8.54 ± 0.05	8.75 <sup>+0.05</sup> <sub>-0.04</sub>
D207	5.79 ± 0.08	6.00 ± 0.09	7.35 <sup>+0.06</sup> <sub>-0.05</sub>	7.61 <sup>+0.05</sup> <sub>-0.06</sub>	8.46 ± 0.03	8.70 ± 0.06
D208	5.74 <sup>+0.10</sup> <sub>-0.09</sub>	5.98 <sup>+0.09</sup> <sub>-0.10</sub>	7.56 <sup>+0.06</sup> <sub>-0.07</sub>	7.85 <sup>+0.14</sup> <sub>-0.08</sub>	8.53 <sup>+0.08</sup> <sub>-0.09</sub>	8.83 ± 0.06
D209	6.51 ± 0.07	6.60 ± 0.07	8.06 <sup>+0.09</sup> <sub>-0.06</sub>	8.25 <sup>+0.09</sup> <sub>-0.07</sub>	8.59 ± 0.06	8.74 ± 0.05
D210	6.15 <sup>+0.11</sup> <sub>-0.10</sub>	6.32 <sup>+0.09</sup> <sub>-0.10</sub>	8.12 <sup>+0.07</sup> <sub>-0.06</sub>	8.31 <sup>+0.07</sup> <sub>-0.06</sub>	8.63 ± 0.05	8.83 ± 0.04
D211	6.17 <sup>+0.18</sup> <sub>-0.16</sub>	6.30 ± 0.15	8.06 <sup>+0.17</sup> <sub>-0.10</sub>	8.24 <sup>+0.19</sup> <sub>-0.10</sub>	8.55 ± 0.09	8.70 ± 0.09
D212	6.16 <sup>+0.07</sup> <sub>-0.06</sub>	6.33 <sup>+0.06</sup> <sub>-0.05</sub>	8.21 <sup>+0.04</sup> <sub>-0.03</sub>	8.41 ± 0.03	8.64 ± 0.02	8.84 ± 0.02
D213	5.96 <sup>+0.16</sup> <sub>-0.15</sub>	6.08 ± 0.15	8.11 <sup>+0.09</sup> <sub>-0.07</sub>	8.30 <sup>+0.05</sup> <sub>-0.04</sub>	8.61 ± 0.06	8.75 ± 0.05
D214	6.39 <sup>+0.07</sup> <sub>-0.06</sub>	6.60 ± 0.06	8.33 <sup>+0.07</sup> <sub>-0.05</sub>	8.57 <sup>+0.06</sup> <sub>-0.05</sub>	8.68 <sup>+0.05</sup> <sub>-0.04</sub>	8.93 ± 0.05
D215	7.04 <sup>+0.16</sup> <sub>-0.19</sub>	7.38 ± 0.16	8.52 <sup>+0.35</sup> <sub>-0.14</sub>	8.94 <sup>+0.40</sup> <sub>-0.14</sub>	8.87 <sup>+0.14</sup> <sub>-0.15</sub>	9.24 <sup>+0.21</sup> <sub>-0.20</sub>
D216	6.64 <sup>+0.23</sup> <sub>-0.21</sub>	6.77 <sup>+0.20</sup> <sub>-0.21</sub>	8.04 <sup>+0.50</sup> <sub>-0.17</sub>	8.22 <sup>+0.45</sup> <sub>-0.17</sub>	8.57 ± 0.22	8.72 ± 0.20
D217	5.87 ± 0.12	5.92 <sup>+0.12</sup> <sub>-0.11</sub>	7.59 <sup>+0.07</sup> <sub>-0.05</sub>	7.84 <sup>+0.06</sup> <sub>-0.05</sub>	7.99 <sup>+0.05</sup> <sub>-0.06</sub>	8.15 ± 0.04
D218	6.56 <sup>+0.13</sup> <sub>-0.12</sub>	6.73 <sup>+0.12</sup> <sub>-0.13</sub>	8.30 <sup>+0.20</sup> <sub>-0.11</sub>	8.49 <sup>+0.19</sup> <sub>-0.10</sub>	8.83 ± 0.10	9.04 <sup>+0.08</sup> <sub>-0.07</sub>
D219	6.33 <sup>+0.23</sup> <sub>-0.26</sub>	6.43 <sup>+0.23</sup> <sub>-0.24</sub>	8.07 <sup>+0.36</sup> <sub>-0.14</sub>	8.26 <sup>+0.34</sup> <sub>-0.14</sub>	8.58 ± 0.17	8.73 <sup>+0.16</sup> <sub>-0.15</sub>
D220	5.87 ± 0.05	6.04 <sup>+0.05</sup> <sub>-0.06</sub>	7.67 ± 0.03	7.86 ± 0.03	8.53 ± 0.02	8.72 ± 0.04
D221	5.37 ± 0.05	5.44 ± 0.05	7.68 ± 0.03	7.84 ± 0.03	8.54 <sup>+0.03</sup> <sub>-0.04</sub>	8.64 ± 0.03
D222	6.01 ± 0.03	6.03 <sup>+0.07</sup> <sub>-0.05</sub>	7.66 <sup>+0.07</sup> <sub>-0.05</sub>	7.68 <sup>+0.07</sup> <sub>-0.05</sub>	8.46 ± 0.02	8.47 ± 0.03
D223	5.88 ± 0.03	6.04 ± 0.03	7.64 ± 0.02	7.80 ± 0.02	8.36 ± 0.02	8.54 ± 0.03

**Table D.8.** Total abundances derived from the nebular sample. All values are in  $12+\log(X/H)$  units.

Reference number	Fe	Fe	N	N	O	O
	$t^2 = 0$	$t^2 > 0$	$t^2 = 0$	$t^2 > 0$	$t^2 = 0$	$t^2 > 0$
D224	6.11 ± 0.03	6.12 ± 0.03	7.71 ± 0.05	7.72 <sup>+0.06</sup> <sub>-0.05</sub>	8.46 ± 0.01	8.49 ± 0.03
D225	5.89 ± 0.03	6.07 ± 0.03	7.60 ± 0.02	7.80 ± 0.02	8.40 ± 0.02	8.62 ± 0.02
D226	5.83 ± 0.03	5.89 <sup>+0.06</sup> <sub>-0.04</sub>	7.63 <sup>+0.06</sup> <sub>-0.04</sub>	7.71 <sup>+0.06</sup> <sub>-0.04</sub>	8.45 ± 0.01	8.52 ± 0.03
D227	6.11 <sup>+0.07</sup> <sub>-0.05</sub>	6.10 ± 0.03	7.69 <sup>+0.07</sup> <sub>-0.05</sub>	7.68 <sup>+0.07</sup> <sub>-0.05</sub>	8.45 <sup>+0.02</sup> <sub>-0.01</sub>	8.45 ± 0.03
D228	5.82 <sup>+0.07</sup> <sub>-0.05</sub>	5.84 <sup>+0.07</sup> <sub>-0.05</sub>	7.71 <sup>+0.07</sup> <sub>-0.05</sub>	7.73 <sup>+0.06</sup> <sub>-0.05</sub>	8.46 ± 0.01	8.49 ± 0.03
D229	6.04 ± 0.03	6.04 ± 0.03	7.72 <sup>+0.06</sup> <sub>-0.05</sub>	7.73 <sup>+0.06</sup> <sub>-0.05</sub>	8.47 <sup>+0.01</sup> <sub>-0.02</sub>	8.48 ± 0.03
D230	5.63 ± 0.05	5.66 ± 0.05	7.44 <sup>+0.04</sup> <sub>-0.03</sub>	7.56 ± 0.04	8.28 ± 0.05	8.34 ± 0.04
D231	6.08 <sup>+0.09</sup> <sub>-0.07</sub>	6.16 ± 0.04	7.64 <sup>+0.08</sup> <sub>-0.06</sub>	7.74 <sup>+0.09</sup> <sub>-0.06</sub>	8.48 ± 0.02	8.58 ± 0.04
D232	5.99 ± 0.04	5.99 ± 0.04	7.71 ± 0.03	7.71 <sup>+0.08</sup> <sub>-0.06</sub>	8.50 ± 0.01	8.50 <sup>+0.03</sup> <sub>-0.04</sub>
D233	6.09 ± 0.07	6.14 ± 0.07	7.68 <sup>+0.12</sup> <sub>-0.08</sub>	7.74 <sup>+0.05</sup> <sub>-0.06</sub>	8.49 ± 0.04	8.55 <sup>+0.06</sup> <sub>-0.07</sub>
D234	5.72 ± 0.03	5.85 <sup>+0.03</sup> <sub>-0.02</sub>	7.72 <sup>+0.05</sup> <sub>-0.04</sub>	7.91 <sup>+0.04</sup> <sub>-0.03</sub>	8.46 ± 0.03	8.62 ± 0.03
D235	5.88 ± 0.03	6.10 ± 0.03	7.37 <sup>+0.02</sup> <sub>-0.03</sub>	7.63 <sup>+0.02</sup> <sub>-0.03</sub>	8.35 ± 0.02	8.58 ± 0.03
D236	5.95 ± 0.03	6.19 ± 0.04	7.60 ± 0.03	7.89 <sup>+0.06</sup> <sub>-0.05</sub>	8.53 ± 0.02	8.80 ± 0.03
D237	5.88 ± 0.09	5.88 ± 0.09	7.71 <sup>+0.14</sup> <sub>-0.09</sub>	7.71 <sup>+0.14</sup> <sub>-0.09</sub>	8.46 ± 0.03	8.46 ± 0.03
D238	5.86 ± 0.07	6.16 ± 0.08	7.61 <sup>+0.06</sup> <sub>-0.05</sub>	7.95 ± 0.05	8.49 ± 0.03	8.81 ± 0.06
D239	5.51 ± 0.04	5.54 ± 0.04	7.34 ± 0.02	7.44 ± 0.02	8.25 ± 0.03	8.31 <sup>+0.02</sup> <sub>-0.03</sub>
D240	5.32 <sup>+0.08</sup> <sub>-0.07</sub>	5.41 ± 0.07	7.26 ± 0.03	7.35 ± 0.03	8.21 ± 0.03	8.31 ± 0.03
D241	5.86 ± 0.03	5.91 ± 0.03	7.65 <sup>+0.02</sup> <sub>-0.01</sub>	7.78 <sup>+0.02</sup> <sub>-0.01</sub>	8.52 ± 0.02	8.59 ± 0.02
D242	5.58 <sup>+0.08</sup> <sub>-0.09</sub>	5.63 <sup>+0.08</sup> <sub>-0.09</sub>	7.43 <sup>+0.13</sup> <sub>-0.08</sub>	7.55 <sup>+0.14</sup> <sub>-0.08</sub>	8.34 <sup>+0.07</sup> <sub>-0.08</sub>	8.43 ± 0.07
D243	5.24 <sup>+0.17</sup> <sub>-0.18</sub>	5.37 <sup>+0.17</sup> <sub>-0.19</sub>	6.41 <sup>+0.22</sup> <sub>-0.21</sub>	6.53 <sup>+0.24</sup> <sub>-0.23</sub>	8.00 <sup>+0.11</sup> <sub>-0.10</sub>	8.18 <sup>+0.11</sup> <sub>-0.10</sub>
D244	5.54 <sup>+0.15</sup> <sub>-0.13</sub>	5.55 ± 0.13	7.56 ± 0.03	7.57 <sup>+0.04</sup> <sub>-0.03</sub>	8.41 <sup>+0.06</sup> <sub>-0.05</sub>	8.42 ± 0.05
D245	5.85 <sup>+0.14</sup> <sub>-0.13</sub>	6.05 <sup>+0.14</sup> <sub>-0.13</sub>	7.92 <sup>+0.11</sup> <sub>-0.07</sub>	8.11 <sup>+0.10</sup> <sub>-0.07</sub>	8.60 ± 0.05	8.82 <sup>+0.06</sup> <sub>-0.07</sub>
D246	6.22 <sup>+0.16</sup> <sub>-0.17</sub>	6.19 <sup>+0.16</sup> <sub>-0.15</sub>	7.52 <sup>+0.16</sup> <sub>-0.10</sub>	7.51 ± 0.08	8.18 ± 0.12	8.18 <sup>+0.13</sup> <sub>-0.12</sub>
D247	5.84 ± 0.06	5.91 ± 0.06	7.39 ± 0.05	7.52 <sup>+0.06</sup> <sub>-0.05</sub>	8.33 <sup>+0.06</sup> <sub>-0.07</sub>	8.42 <sup>+0.05</sup> <sub>-0.06</sub>
D248	5.75 ± 0.10	5.72 ± 0.11	7.71 ± 0.03	7.71 ± 0.03	8.46 ± 0.05	8.47 ± 0.05
D249	5.15 ± 0.04	5.23 ± 0.04	7.50 ± 0.03	7.63 ± 0.03	8.41 ± 0.03	8.51 ± 0.03
D250	6.17 ± 0.15	6.34 <sup>+0.13</sup> <sub>-0.14</sub>	7.13 ± 0.06	7.29 <sup>+0.14</sup> <sub>-0.08</sub>	8.25 ± 0.06	8.43 ± 0.07
D251	5.90 <sup>+0.22</sup> <sub>-0.21</sub>	6.06 <sup>+0.20</sup> <sub>-0.19</sub>	7.15 ± 0.08	7.29 <sup>+0.18</sup> <sub>-0.10</sub>	8.11 <sup>+0.08</sup> <sub>-0.09</sub>	8.26 <sup>+0.09</sup> <sub>-0.08</sub>
D252	5.91 <sup>+0.24</sup> <sub>-0.21</sub>	5.98 <sup>+0.22</sup> <sub>-0.24</sub>	6.92 <sup>+0.55</sup> <sub>-0.18</sub>	7.04 <sup>+0.67</sup> <sub>-0.18</sub>	8.14 ± 0.05	8.22 ± 0.23
D253	5.79 ± 0.06	5.96 ± 0.06	6.74 ± 0.03	6.94 ± 0.03	8.06 ± 0.02	8.26 <sup>+0.03</sup> <sub>-0.02</sub>
D254	5.69 ± 0.04	5.88 <sup>+0.03</sup> <sub>-0.04</sub>	6.61 ± 0.01	6.82 ± 0.01	7.99 ± 0.01	8.19 ± 0.01
D255	5.93 ± 0.12	6.10 <sup>+0.12</sup> <sub>-0.13</sub>	6.75 ± 0.02	6.95 ± 0.02	8.01 ± 0.01	8.19 ± 0.01
D256	5.66 <sup>+0.22</sup> <sub>-0.24</sub>	5.67 <sup>+0.24</sup> <sub>-0.23</sub>	6.92 <sup>+0.49</sup> <sub>-0.17</sub>	6.93 <sup>+0.59</sup> <sub>-0.17</sub>	8.25 ± 0.03	8.27 <sup>+0.18</sup> <sub>-0.19</sub>
D257	5.64 ± 0.15	5.81 <sup>+0.15</sup> <sub>-0.17</sub>	6.91 <sup>+0.25</sup> <sub>-0.12</sub>	7.08 <sup>+0.29</sup> <sub>-0.12</sub>	8.27 ± 0.03	8.45 ± 0.13
D258	5.95 ± 0.12	6.08 ± 0.12	6.88 ± 0.04	7.01 ± 0.04	8.18 <sup>+0.03</sup> <sub>-0.04</sub>	8.32 ± 0.04
D259	5.90 ± 0.08	6.07 ± 0.07	-	-	7.80 ± 0.01	7.99 ± 0.01
D260	6.12 ± 0.05	6.31 ± 0.05	-	-	8.32 ± 0.01	8.54 ± 0.01
D261	6.12 <sup>+0.05</sup> <sub>-0.04</sub>	6.30 <sup>+0.05</sup> <sub>-0.04</sub>	-	-	8.33 ± 0.01	8.54 <sup>+0.01</sup> <sub>-0.02</sub>
D262	5.88 ± 0.07	5.92 ± 0.06	7.08 ± 0.04	7.14 <sup>+0.09</sup> <sub>-0.07</sub>	8.29 ± 0.03	8.33 <sup>+0.05</sup> <sub>-0.04</sub>
D263	5.59 ± 0.12	5.75 <sup>+0.13</sup> <sub>-0.14</sub>	6.40 <sup>+0.14</sup> <sub>-0.08</sub>	6.59 <sup>+0.15</sup> <sub>-0.09</sub>	7.82 <sup>+0.04</sup> <sub>-0.05</sub>	8.00 ± 0.05
D264	5.67 ± 0.06	5.81 <sup>+0.06</sup> <sub>-0.05</sub>	6.32 <sup>+0.06</sup> <sub>-0.04</sub>	6.50 <sup>+0.06</sup> <sub>-0.04</sub>	7.76 ± 0.02	7.93 ± 0.02
D265	5.73 <sup>+0.18</sup> <sub>-0.17</sub>	5.91 <sup>+0.15</sup> <sub>-0.17</sub>	6.45 ± 0.04	6.65 ± 0.03	7.82 ± 0.02	8.00 ± 0.03
D266	5.71 ± 0.18	5.95 ± 0.18	6.87 <sup>+0.31</sup> <sub>-0.14</sub>	7.16 <sup>+0.40</sup> <sub>-0.14</sub>	8.20 <sup>+0.07</sup> <sub>-0.06</sub>	8.45 <sup>+0.18</sup> <sub>-0.19</sub>
D267	5.59 <sup>+0.08</sup> <sub>-0.07</sub>	5.76 <sup>+0.08</sup> <sub>-0.09</sub>	6.60 <sup>+0.08</sup> <sub>-0.05</sub>	6.79 <sup>+0.07</sup> <sub>-0.06</sub>	7.90 ± 0.03	8.08 ± 0.03
D268	5.85 <sup>+0.04</sup> <sub>-0.05</sub>	6.04 ± 0.04	-	-	8.01 ± 0.01	8.21 ± 0.01
D269	6.05 <sup>+0.13</sup> <sub>-0.14</sub>	6.23 <sup>+0.12</sup> <sub>-0.14</sub>	-	-	8.03 ± 0.02	8.23 ± 0.03
D270	6.21 <sup>+0.12</sup> <sub>-0.13</sub>	6.35 <sup>+0.13</sup> <sub>-0.14</sub>	6.80 <sup>+0.04</sup> <sub>-0.05</sub>	6.98 ± 0.05	8.08 <sup>+0.04</sup> <sub>-0.05</sub>	8.25 ± 0.05
D271	5.94 ± 0.05	6.10 <sup>+0.06</sup> <sub>-0.05</sub>	6.29 ± 0.02	6.48 ± 0.02	7.82 ± 0.01	8.00 ± 0.01
D272	5.92 <sup>+0.34</sup> <sub>-0.14</sub>	6.06 ± 0.14	6.98 <sup>+0.36</sup> <sub>-0.15</sub>	7.16 <sup>+0.34</sup> <sub>-0.13</sub>	8.20 ± 0.10	8.38 ± 0.11
D273	5.25 <sup>+0.17</sup> <sub>-0.16</sub>	5.42 <sup>+0.15</sup> <sub>-0.16</sub>	6.55 <sup>+0.10</sup> <sub>-0.07</sub>	6.73 <sup>+0.09</sup> <sub>-0.07</sub>	7.92 <sup>+0.03</sup> <sub>-0.04</sub>	8.10 ± 0.04
D274	5.80 <sup>+0.15</sup> <sub>-0.14</sub>	5.98 <sup>+0.14</sup> <sub>-0.16</sub>	6.75 <sup>+0.40</sup> <sub>-0.14</sub>	6.95 <sup>+0.35</sup> <sub>-0.15</sub>	8.25 <sup>+0.11</sup> <sub>-0.09</sub>	8.45 <sup>+0.11</sup> <sub>-0.10</sub>
D275	5.55 ± 0.05	5.73 ± 0.05	-	-	7.86 ± 0.01	8.06 ± 0.01
D276	5.46 ± 0.07	5.65 ± 0.07	-	-	7.90 ± 0.01	8.10 ± 0.01
D277	5.48 ± 0.04	5.65 ± 0.04	-	-	7.91 ± 0.01	8.10 <sup>+0.01</sup> <sub>-0.02</sub>
D278	5.77 ± 0.07	5.95 ± 0.06	6.60 ± 0.01	6.81 ± 0.01	8.05 ± 0.01	8.25 ± 0.01
D279	6.04 <sup>+0.11</sup> <sub>-0.12</sub>	6.19 <sup>+0.11</sup> <sub>-0.13</sub>	6.79 ± 0.03	6.97 ± 0.04	8.09 <sup>+0.04</sup> <sub>-0.03</sub>	8.27 ± 0.04



**Table D.8.** Total abundances derived from the nebular sample. All values are in  $12+\log(X/H)$  units.

Reference number	Fe		N		O	
	$t^2 = 0$	$t^2 > 0$	$t^2 = 0$	$t^2 > 0$	$t^2 = 0$	$t^2 > 0$
D280	$5.67 \pm 0.07$	$5.85 \pm 0.07$	-	-	$8.11 \pm 0.01$	$8.32 \pm 0.01$
D281	$6.23^{+0.11}_{-0.10}$	$6.38^{+0.12}_{-0.11}$	$7.02^{+0.06}_{-0.07}$	$7.20 \pm 0.07$	$8.22^{+0.06}_{-0.07}$	$8.39 \pm 0.07$
D282	$6.29^{+0.12}_{-0.15}$	$6.36 \pm 0.13$	$7.50^{+0.25}_{-0.12}$	$7.58^{+0.26}_{-0.11}$	$8.41 \pm 0.11$	$8.49 \pm 0.11$
D283	$5.45 \pm 0.14$	$5.70 \pm 0.14$	$6.61^{+0.33}_{-0.12}$	$6.86^{+0.27}_{-0.13}$	$7.76^{+0.02}_{-0.03}$	$8.05 \pm 0.15$
D284	$5.64 \pm 0.25$	$5.83 \pm 0.27$	$6.74^{+0.37}_{-0.19}$	$6.96^{+0.52}_{-0.18}$	$8.20^{+0.13}_{-0.12}$	$8.39^{+0.15}_{-0.16}$
D285	$5.69 \pm 0.07$	$5.93 \pm 0.07$	$7.49 \pm 0.04$	$7.75^{+0.04}_{-0.05}$	$8.37 \pm 0.05$	$8.64^{+0.05}_{-0.04}$
D286	$5.56 \pm 0.13$	$5.91 \pm 0.13$	$7.38^{+0.19}_{-0.11}$	$7.78 \pm 0.07$	$8.27^{+0.08}_{-0.07}$	$8.71^{+0.10}_{-0.09}$
D287	$5.95^{+0.10}_{-0.09}$	$6.11 \pm 0.10$	$7.35^{+0.13}_{-0.09}$	$7.52^{+0.14}_{-0.09}$	$8.42 \pm 0.06$	$8.61 \pm 0.07$
D288	$5.97 \pm 0.06$	$6.14 \pm 0.06$	$7.44 \pm 0.04$	$7.65 \pm 0.04$	$8.35^{+0.04}_{-0.03}$	$8.55^{+0.04}_{-0.05}$
D289	$6.07^{+0.24}_{-0.22}$	$6.20 \pm 0.21$	$7.36^{+0.45}_{-0.15}$	$7.49^{+0.42}_{-0.14}$	$8.43 \pm 0.12$	$8.58^{+0.15}_{-0.14}$
D290	$5.64^{+0.07}_{-0.06}$	$5.81 \pm 0.06$	$6.82 \pm 0.06$	$7.00^{+0.05}_{-0.06}$	$8.21^{+0.01}_{-0.02}$	$8.38 \pm 0.01$
D291	$5.88^{+0.21}_{-0.22}$	$6.08^{+0.20}_{-0.22}$	$7.40^{+0.44}_{-0.16}$	$7.62^{+0.44}_{-0.16}$	$8.48^{+0.11}_{-0.12}$	$8.73^{+0.18}_{-0.19}$
D292	$5.97^{+0.19}_{-0.20}$	$6.12^{+0.22}_{-0.20}$	$7.38^{+0.27}_{-0.12}$	$7.59^{+0.28}_{-0.12}$	$8.52^{+0.13}_{-0.12}$	$8.71 \pm 0.12$
D293	$5.64^{+0.26}_{-0.23}$	$5.79^{+0.24}_{-0.26}$	$7.26^{+0.52}_{-0.18}$	$7.46^{+0.54}_{-0.16}$	$8.50^{+0.13}_{-0.12}$	$8.64 \pm 0.21$
D294	$5.37^{+0.16}_{-0.15}$	$5.55 \pm 0.16$	$7.38 \pm 0.06$	$7.54^{+0.06}_{-0.07}$	$8.44^{+0.07}_{-0.06}$	$8.63 \pm 0.07$
D295	$5.68 \pm 0.26$	$5.81 \pm 0.25$	$7.38^{+0.55}_{-0.18}$	$7.50^{+0.66}_{-0.19}$	$8.45 \pm 0.14$	$8.63^{+0.23}_{-0.24}$
D296	$5.94 \pm 0.05$	$6.15 \pm 0.05$	$7.09 \pm 0.03$	$7.34 \pm 0.03$	$8.34 \pm 0.02$	$8.56 \pm 0.03$
D297	$6.00 \pm 0.02$	$6.21 \pm 0.02$	$7.18 \pm 0.01$	$7.41 \pm 0.01$	$8.24 \pm 0.01$	$8.48 \pm 0.01$
D298	$6.35^{+0.20}_{-0.18}$	$6.47 \pm 0.20$	$7.78^{+0.55}_{-0.15}$	$7.94^{+0.38}_{-0.14}$	$8.60 \pm 0.17$	$8.77 \pm 0.17$
D299	$5.65 \pm 0.10$	$5.81 \pm 0.10$	$7.42^{+0.05}_{-0.05}$	$7.58 \pm 0.03$	$8.29 \pm 0.03$	$8.46^{+0.03}_{-0.04}$
D300	$6.77^{+0.21}_{-0.22}$	$6.96^{+0.19}_{-0.18}$	$8.12^{+0.13}_{-0.13}$	$8.38^{+0.43}_{-0.16}$	$8.69^{+0.18}_{-0.19}$	$8.90 \pm 0.19$
D301	$5.92^{+0.17}_{-0.11}$	$5.99^{+0.13}_{-0.11}$	$7.70^{+0.13}_{-0.08}$	$7.86 \pm 0.06$	$8.34^{+0.09}_{-0.08}$	$8.44 \pm 0.07$
D302	$6.00^{+0.12}_{-0.14}$	$6.06^{+0.14}_{-0.15}$	$7.83 \pm 0.07$	$8.01^{+0.16}_{-0.10}$	$8.54 \pm 0.09$	$8.64^{+0.09}_{-0.10}$
D303	$5.92^{+0.08}_{-0.07}$	$6.04^{+0.08}_{-0.07}$	$7.53 \pm 0.04$	$7.65 \pm 0.04$	$8.23^{+0.04}_{-0.05}$	$8.36 \pm 0.04$
D304	$5.64 \pm 0.17$	$5.76^{+0.20}_{-0.16}$	$7.72^{+0.18}_{-0.09}$	$7.87^{+0.17}_{-0.10}$	$8.49^{+0.10}_{-0.09}$	$8.64 \pm 0.09$
D305	$5.56^{+0.17}_{-0.15}$	$5.65^{+0.17}_{-0.16}$	$7.64^{+0.10}_{-0.07}$	$7.79^{+0.09}_{-0.06}$	$8.27 \pm 0.06$	$8.37^{+0.05}_{-0.06}$
D306	$5.58^{+0.17}_{-0.16}$	$5.67^{+0.16}_{-0.15}$	$7.41^{+0.19}_{-0.10}$	$7.55 \pm 0.09$	$8.31^{+0.10}_{-0.09}$	$8.42^{+0.10}_{-0.09}$
D307	$6.18^{+0.15}_{-0.14}$	$6.28^{+0.13}_{-0.16}$	$7.77^{+0.29}_{-0.12}$	$7.95^{+0.36}_{-0.13}$	$8.44^{+0.14}_{-0.13}$	$8.59^{+0.12}_{-0.11}$
D308	$5.97 \pm 0.21$	$6.09^{+0.22}_{-0.19}$	$7.99^{+0.25}_{-0.12}$	$8.19^{+0.25}_{-0.12}$	$8.50^{+0.13}_{-0.14}$	$8.64^{+0.13}_{-0.14}$
D309	$6.01 \pm 0.14$	$6.14 \pm 0.14$	$8.02 \pm 0.06$	$8.20^{+0.13}_{-0.09}$	$8.80 \pm 0.07$	$8.96 \pm 0.07$
D310	$5.70^{+0.14}_{-0.13}$	$5.79 \pm 0.13$	$7.48^{+0.21}_{-0.10}$	$7.62^{+0.19}_{-0.10}$	$8.27 \pm 0.10$	$8.37^{+0.10}_{-0.09}$
D311	$5.79^{+0.11}_{-0.12}$	$5.83 \pm 0.13$	$7.59^{+0.06}_{-0.07}$	$7.73^{+0.14}_{-0.09}$	$8.32^{+0.09}_{-0.08}$	$8.42 \pm 0.08$
D312	$5.96^{+0.24}_{-0.21}$	$6.14^{+0.19}_{-0.21}$	$6.69^{+0.52}_{-0.18}$	$6.87^{+0.56}_{-0.17}$	$8.06 \pm 0.04$	$8.25^{+0.22}_{-0.20}$
D313	$5.99 \pm 0.04$	$6.06 \pm 0.04$	$7.09 \pm 0.03$	$7.18 \pm 0.03$	$8.26 \pm 0.01$	$8.33 \pm 0.03$
D314	$5.76 \pm 0.03$	$5.93 \pm 0.02$	$6.80 \pm 0.02$	$7.01 \pm 0.02$	$8.17 \pm 0.02$	$8.36 \pm 0.02$
D315	$5.90 \pm 0.10$	$6.18^{+0.11}_{-0.10}$	$6.89 \pm 0.08$	$7.24^{+0.17}_{-0.09}$	$8.29^{+0.04}_{-0.05}$	$8.58^{+0.10}_{-0.09}$
D316	$6.12^{+0.09}_{-0.07}$	$6.23^{+0.08}_{-0.09}$	$6.95 \pm 0.05$	$7.07^{+0.09}_{-0.07}$	$8.27 \pm 0.05$	$8.40 \pm 0.05$
D317	$5.86 \pm 0.06$	$5.97^{+0.07}_{-0.06}$	$7.13 \pm 0.04$	$7.26 \pm 0.04$	$8.31 \pm 0.02$	$8.43 \pm 0.06$
D318	$6.07 \pm 0.06$	$6.28^{+0.07}_{-0.06}$	$7.11 \pm 0.02$	$7.36 \pm 0.02$	$8.39 \pm 0.02$	$8.62 \pm 0.03$
D319	$5.43 \pm 0.02$	$5.61 \pm 0.02$	$6.42 \pm 0.01$	$6.62 \pm 0.01$	$8.02 \pm 0.01$	$8.22 \pm 0.01$
D320	$5.59^{+0.09}_{-0.08}$	$5.95 \pm 0.08$	$6.36^{+0.14}_{-0.09}$	$6.77 \pm 0.07$	$7.86 \pm 0.03$	$8.26^{+0.08}_{-0.07}$
D321	$5.68^{+0.18}_{-0.20}$	$5.79 \pm 0.19$	$7.68^{+0.22}_{-0.10}$	$7.83^{+0.10}_{-0.08}$	$8.57 \pm 0.11$	$8.71 \pm 0.09$
D322	$5.70 \pm 0.15$	$5.94^{+0.14}_{-0.13}$	$7.47^{+0.10}_{-0.08}$	$7.83^{+0.17}_{-0.09}$	$8.55^{+0.10}_{-0.09}$	$8.86 \pm 0.08$
D323	$5.99^{+0.20}_{-0.22}$	$6.21^{+0.22}_{-0.23}$	$8.04^{+0.33}_{-0.14}$	$8.28^{+0.28}_{-0.14}$	$8.87^{+0.13}_{-0.14}$	$9.11^{+0.16}_{-0.14}$
D324	$5.85^{+0.15}_{-0.14}$	$6.10^{+0.14}_{-0.15}$	$7.52^{+0.19}_{-0.10}$	$7.80^{+0.21}_{-0.10}$	$8.43 \pm 0.09$	$8.73 \pm 0.11$
D325	$6.04^{+0.16}_{-0.14}$	$6.18 \pm 0.14$	$7.92^{+0.19}_{-0.11}$	$8.07^{+0.22}_{-0.11}$	$8.58^{+0.11}_{-0.12}$	$8.74 \pm 0.10$
D326	$6.14 \pm 0.17$	$6.20 \pm 0.17$	$7.88^{+0.28}_{-0.13}$	$8.04^{+0.29}_{-0.13}$	$8.47^{+0.15}_{-0.16}$	$8.56 \pm 0.14$
D327	$5.94 \pm 0.12$	$6.12^{+0.13}_{-0.14}$	$7.44^{+0.24}_{-0.12}$	$7.66^{+0.22}_{-0.11}$	$8.47^{+0.12}_{-0.11}$	$8.70^{+0.10}_{-0.09}$
D328	$6.00 \pm 0.07$	$6.19 \pm 0.06$	$7.35 \pm 0.03$	$7.60 \pm 0.03$	$8.38^{+0.03}_{-0.04}$	$8.61 \pm 0.03$
D329	$5.96 \pm 0.11$	$6.20^{+0.10}_{-0.11}$	$7.57^{+0.15}_{-0.09}$	$7.99^{+0.16}_{-0.09}$	$8.47^{+0.11}_{-0.12}$	$8.80^{+0.08}_{-0.09}$
D330	$6.19 \pm 0.14$	$6.33 \pm 0.13$	$7.82^{+0.14}_{-0.10}$	$7.98^{+0.15}_{-0.09}$	$8.69^{+0.09}_{-0.08}$	$8.85^{+0.09}_{-0.08}$
D331	$6.10^{+0.22}_{-0.24}$	$6.28^{+0.26}_{-0.24}$	$7.62^{+0.36}_{-0.14}$	$7.79^{+0.32}_{-0.14}$	$8.39^{+0.13}_{-0.14}$	$8.59 \pm 0.16$
D332	$5.98^{+0.22}_{-0.23}$	$6.11^{+0.24}_{-0.25}$	$7.26^{+0.41}_{-0.15}$	$7.37^{+0.35}_{-0.15}$	$8.17^{+0.13}_{-0.14}$	$8.32^{+0.15}_{-0.14}$
D333	$6.04^{+0.12}_{-0.13}$	$6.21 \pm 0.12$	$7.99^{+0.15}_{-0.09}$	$8.17^{+0.14}_{-0.09}$	$8.64^{+0.09}_{-0.08}$	$8.81^{+0.07}_{-0.08}$
D334	$5.50 \pm 0.17$	$5.66^{+0.16}_{-0.17}$	$6.71^{+0.40}_{-0.15}$	$6.90^{+0.37}_{-0.13}$	$8.16 \pm 0.04$	$8.32^{+0.18}_{-0.15}$
D335	$5.58 \pm 0.06$	$5.64 \pm 0.07$	$6.87^{+0.08}_{-0.07}$	$6.94 \pm 0.04$	$8.15 \pm 0.01$	$8.22^{+0.04}_{-0.05}$

**Table D.8.** Total abundances derived from the nebular sample. All values are in  $12+\log(X/H)$  units.

Reference number	Fe		N		O	
	$t^2 = 0$	$t^2 > 0$	$t^2 = 0$	$t^2 > 0$	$t^2 = 0$	$t^2 > 0$
D336	$5.57^{+0.20}_{-0.18}$	$5.57^{+0.20}_{-0.18}$	$6.84^{+0.45}_{-0.16}$	$6.84^{+0.45}_{-0.16}$	$8.08 \pm 0.03$	$8.08 \pm 0.03$
D337	$5.75^{+0.05}_{-0.04}$	$5.93^{+0.04}_{-0.05}$	$6.44 \pm 0.01$	$6.64 \pm 0.01$	$7.93 \pm 0.01$	$8.13 \pm 0.01$
D338	$5.76^{+0.13}_{-0.12}$	$5.96 \pm 0.12$	$6.50 \pm 0.04$	$6.70 \pm 0.04$	$7.95^{+0.04}_{-0.03}$	$8.14 \pm 0.04$
D339	$5.88 \pm 0.12$	$6.05^{+0.11}_{-0.10}$	$6.64^{+0.05}_{-0.06}$	$6.85^{+0.05}_{-0.06}$	$7.99 \pm 0.04$	$8.18^{+0.05}_{-0.06}$
D340	$5.95 \pm 0.10$	$6.13 \pm 0.10$	$6.72 \pm 0.04$	$6.93 \pm 0.04$	$8.09 \pm 0.04$	$8.29 \pm 0.04$
D341	$5.52^{+0.22}_{-0.24}$	$5.52^{+0.22}_{-0.24}$	$6.54^{+0.55}_{-0.19}$	$6.54^{+0.55}_{-0.19}$	$7.95^{+0.08}_{-0.07}$	$7.95^{+0.08}_{-0.07}$
D342	$5.99 \pm 0.06$	$6.19 \pm 0.05$	$6.71 \pm 0.03$	$6.92 \pm 0.03$	$8.08 \pm 0.02$	$8.29^{+0.02}_{-0.03}$
D343	$5.86 \pm 0.02$	$6.07 \pm 0.02$	$6.68 \pm 0.01$	$6.89 \pm 0.01$	$8.06 \pm 0.01$	$8.28 \pm 0.01$
D344	$5.50 \pm 0.03$	$5.66 \pm 0.04$	$5.88 \pm 0.06$	$6.03 \pm 0.06$	$7.24 \pm 0.01$	$7.41 \pm 0.01$
D345	$5.62 \pm 0.04$	$5.77 \pm 0.04$	-	-	$7.28 \pm 0.01$	$7.45 \pm 0.01$
D346	$5.62^{+0.09}_{-0.10}$	$5.76^{+0.08}_{-0.09}$	-	-	$7.30 \pm 0.01$	$7.47 \pm 0.01$
D347	$5.37 \pm 0.10$	$5.53 \pm 0.10$	-	-	$7.21 \pm 0.01$	$7.38 \pm 0.01$
D348	$5.59^{+0.08}_{-0.09}$	$5.73^{+0.08}_{-0.09}$	-	-	$7.27 \pm 0.01$	$7.43 \pm 0.01$
D349	$5.43^{+0.15}_{-0.14}$	$5.56 \pm 0.15$	-	-	$7.24 \pm 0.02$	$7.39 \pm 0.02$
D350	$5.55^{+0.14}_{-0.12}$	$5.68^{+0.16}_{-0.14}$	-	-	$7.13 \pm 0.02$	$7.29 \pm 0.02$
D351	$5.53 \pm 0.06$	$5.68 \pm 0.06$	-	-	$7.28 \pm 0.01$	$7.45 \pm 0.01$
D352	$5.51^{+0.23}_{-0.11}$	$5.51^{+0.23}_{-0.11}$	$6.06^{+0.24}_{-0.11}$	$6.06^{+0.24}_{-0.11}$	$7.18 \pm 0.01$	$7.18 \pm 0.01$
D353	$5.51^{+0.06}_{-0.05}$	$5.67 \pm 0.06$	$5.95 \pm 0.02$	$6.11 \pm 0.02$	$7.25 \pm 0.01$	$7.42 \pm 0.01$
D354	$5.53 \pm 0.04$	$5.68 \pm 0.04$	$5.96 \pm 0.02$	$6.11 \pm 0.02$	$7.25 \pm 0.01$	$7.41 \pm 0.01$
D355	$5.47 \pm 0.10$	$5.60^{+0.11}_{-0.09}$	$5.78 \pm 0.07$	$5.95 \pm 0.06$	$7.12 \pm 0.02$	$7.29 \pm 0.02$
D356	$5.92 \pm 0.05$	$6.10 \pm 0.05$	-	-	$8.09 \pm 0.01$	$8.28 \pm 0.01$
D357	$6.01 \pm 0.05$	$6.18 \pm 0.05$	-	-	$8.02 \pm 0.01$	$8.21 \pm 0.01$
D358	$5.40^{+0.16}_{-0.17}$	$5.55^{+0.17}_{-0.16}$	-	-	$7.45 \pm 0.01$	$7.62 \pm 0.01$
D359	$5.89 \pm 0.07$	$6.07 \pm 0.07$	-	-	$7.80 \pm 0.01$	$7.98 \pm 0.01$
D360	$5.63^{+0.06}_{-0.07}$	$5.79 \pm 0.07$	$6.07^{+0.02}_{-0.03}$	$6.24 \pm 0.02$	$7.47 \pm 0.01$	$7.63 \pm 0.01$
D361	$5.45 \pm 0.08$	$5.59 \pm 0.08$	$6.13 \pm 0.01$	$6.30 \pm 0.01$	$7.57 \pm 0.01$	$7.73 \pm 0.01$
D362	$5.75^{+0.08}_{-0.07}$	$5.92^{+0.07}_{-0.08}$	-	-	$7.73^{+0.02}_{-0.01}$	$7.92 \pm 0.02$
D363	$5.71^{+0.07}_{-0.08}$	$5.77^{+0.08}_{-0.07}$	$6.60 \pm 0.06$	$6.66 \pm 0.06$	$7.40 \pm 0.01$	$7.46 \pm 0.07$
D364	$5.53 \pm 0.09$	$5.67 \pm 0.08$	$5.65 \pm 0.05$	$5.80^{+0.04}_{-0.05}$	$6.93 \pm 0.02$	$7.08 \pm 0.02$
D365	$5.82^{+0.06}_{-0.07}$	$5.99 \pm 0.06$	$6.71^{+0.06}_{-0.04}$	$6.90^{+0.06}_{-0.05}$	$7.94 \pm 0.02$	$8.12 \pm 0.02$
D366	$5.77^{+0.06}_{-0.05}$	$5.96^{+0.05}_{-0.04}$	-	-	$8.09 \pm 0.01$	$8.30 \pm 0.01$
D367	$5.74^{+0.12}_{-0.11}$	$5.91 \pm 0.11$	-	-	$7.76 \pm 0.01$	$7.94 \pm 0.02$
D368	$6.03 \pm 0.05$	$6.20 \pm 0.05$	$6.80^{+0.09}_{-0.10}$	$7.00 \pm 0.10$	$7.90 \pm 0.04$	$8.09 \pm 0.05$
D369	$5.57 \pm 0.07$	$5.73 \pm 0.07$	-	-	$7.55 \pm 0.01$	$7.72 \pm 0.01$
D370	$5.80 \pm 0.06$	$5.96 \pm 0.06$	$6.36^{+0.02}_{-0.03}$	$6.53 \pm 0.03$	$7.62 \pm 0.02$	$7.80 \pm 0.03$
D371	$5.65 \pm 0.07$	$5.80 \pm 0.07$	-	-	$7.40 \pm 0.01$	$7.57 \pm 0.01$
D372	$5.92^{+0.07}_{-0.06}$	$6.10 \pm 0.07$	-	-	$7.94 \pm 0.01$	$8.12 \pm 0.01$
D373	$5.47^{+0.09}_{-0.08}$	$5.63^{+0.08}_{-0.07}$	-	-	$7.97 \pm 0.01$	$8.16 \pm 0.01$
D374	$6.01 \pm 0.07$	$6.01 \pm 0.07$	$7.03^{+0.10}_{-0.07}$	$7.03^{+0.10}_{-0.07}$	$7.41 \pm 0.02$	$7.41 \pm 0.02$
D375	$6.02^{+0.08}_{-0.07}$	$6.02^{+0.08}_{-0.07}$	$7.04^{+0.10}_{-0.08}$	$7.04^{+0.10}_{-0.08}$	$7.42 \pm 0.02$	$7.42 \pm 0.02$
D376	$6.03 \pm 0.02$	$6.20 \pm 0.02$	$7.14 \pm 0.03$	$7.32 \pm 0.03$	$7.79 \pm 0.01$	$7.98 \pm 0.01$
D377	$5.57 \pm 0.13$	$5.80^{+0.12}_{-0.11}$	$6.68^{+0.08}_{-0.06}$	$6.90^{+0.08}_{-0.06}$	$8.14 \pm 0.03$	$8.36 \pm 0.04$
D378	$5.98^{+0.05}_{-0.04}$	$6.14 \pm 0.05$	$6.68 \pm 0.03$	$6.85 \pm 0.03$	$7.66 \pm 0.02$	$7.83 \pm 0.02$
D379	$5.66 \pm 0.09$	$5.80^{+0.10}_{-0.09}$	-	-	$7.69 \pm 0.01$	$7.86 \pm 0.02$
D380	$6.04 \pm 0.04$	$6.23^{+0.04}_{-0.05}$	$7.10 \pm 0.03$	$7.30 \pm 0.03$	$8.03 \pm 0.03$	$8.24 \pm 0.04$
D381	$5.73^{+0.07}_{-0.08}$	$5.89 \pm 0.07$	-	-	$7.66 \pm 0.01$	$7.83 \pm 0.01$
D382	$5.91^{+0.08}_{-0.09}$	$6.07 \pm 0.08$	-	-	$7.77 \pm 0.01$	$7.96 \pm 0.01$
D383	$5.44 \pm 0.07$	$5.62 \pm 0.07$	$6.83^{+0.01}_{-0.02}$	$7.03^{+0.02}_{-0.01}$	$7.97 \pm 0.01$	$8.17 \pm 0.02$
D384	$6.12^{+0.06}_{-0.07}$	$6.32^{+0.06}_{-0.07}$	$7.09 \pm 0.02$	$7.33^{+0.02}_{-0.03}$	$8.25 \pm 0.02$	$8.47^{+0.02}_{-0.03}$
D385	$6.01^{+0.07}_{-0.08}$	$6.18^{+0.08}_{-0.07}$	$7.04^{+0.02}_{-0.01}$	$7.25 \pm 0.02$	$8.21^{+0.02}_{-0.01}$	$8.40 \pm 0.02$
D386	$5.90 \pm 0.05$	$6.06 \pm 0.05$	-	-	$7.68 \pm 0.01$	$7.87 \pm 0.01$
D387	$6.02 \pm 0.06$	$6.21 \pm 0.05$	$6.61^{+0.02}_{-0.03}$	$6.79^{+0.02}_{-0.03}$	$7.76 \pm 0.02$	$7.96^{+0.03}_{-0.02}$
D388	$5.90 \pm 0.08$	$6.05 \pm 0.08$	$6.86 \pm 0.02$	$7.06 \pm 0.02$	$8.06 \pm 0.02$	$8.25 \pm 0.03$
D389	$5.63^{+0.05}_{-0.04}$	$5.79^{+0.05}_{-0.04}$	$6.43 \pm 0.01$	$6.63 \pm 0.01$	$7.94 \pm 0.01$	$8.12 \pm 0.01$
D390	$6.00^{+0.05}_{-0.06}$	$6.06 \pm 0.06$	$7.02 \pm 0.04$	$7.08 \pm 0.04$	$7.86 \pm 0.02$	$7.92 \pm 0.05$
D391	$5.59^{+0.09}_{-0.10}$	$5.76^{+0.09}_{-0.10}$	$6.59^{+0.07}_{-0.06}$	$6.80^{+0.07}_{-0.05}$	$8.10^{+0.03}_{-0.02}$	$8.30 \pm 0.03$
D392	$5.79^{+0.15}_{-0.14}$	$5.97 \pm 0.16$	$7.03^{+0.32}_{-0.13}$	$7.22^{+0.32}_{-0.12}$	$7.83 \pm 0.04$	$8.02^{+0.11}_{-0.12}$

**Table D.8.** Total abundances derived from the nebular sample. All values are in  $12+\log(X/H)$  units.

Reference number	Fe		N		O	
	$t^2 = 0$	$t^2 > 0$	$t^2 = 0$	$t^2 > 0$	$t^2 = 0$	$t^2 > 0$
D393	$5.73^{+0.06}_{-0.07}$	$5.88^{+0.07}_{-0.06}$	$6.64 \pm 0.07$	$6.81^{+0.07}_{-0.08}$	$7.57 \pm 0.01$	$7.73 \pm 0.01$
D394	$6.06^{+0.07}_{-0.08}$	$6.22 \pm 0.07$	$6.85^{+0.15}_{-0.09}$	$7.06^{+0.12}_{-0.09}$	$8.10 \pm 0.05$	$8.29 \pm 0.06$
D395	$5.82 \pm 0.06$	$5.99 \pm 0.06$	-	-	$7.91 \pm 0.01$	$8.09 \pm 0.01$
D396	$5.96 \pm 0.01$	$6.15 \pm 0.01$	$7.08^{+0.01}_{-0.02}$	$7.29 \pm 0.02$	$8.00 \pm 0.01$	$8.20 \pm 0.01$
D397	$6.10 \pm 0.08$	$6.29^{+0.08}_{-0.07}$	-	-	$8.02 \pm 0.01$	$8.23 \pm 0.02$
D398	$5.75 \pm 0.09$	$5.89 \pm 0.09$	$6.99 \pm 0.02$	$7.16 \pm 0.03$	$8.12^{+0.02}_{-0.03}$	$8.29 \pm 0.03$
D399	$5.85^{+0.10}_{-0.08}$	$5.89^{+0.09}_{-0.10}$	$7.16 \pm 0.05$	$7.20^{+0.12}_{-0.07}$	$8.05 \pm 0.03$	$8.09 \pm 0.06$
D400	$6.17 \pm 0.11$	$6.51^{+0.11}_{-0.10}$	$7.30^{+0.20}_{-0.10}$	$7.66^{+0.18}_{-0.10}$	$8.12 \pm 0.02$	$8.48 \pm 0.12$
D401	$5.26 \pm 0.04$	$5.38 \pm 0.04$	$6.53 \pm 0.03$	$6.68 \pm 0.03$	$8.00 \pm 0.02$	$8.15 \pm 0.03$
D402	$5.48 \pm 0.03$	$5.67 \pm 0.03$	$6.48 \pm 0.02$	$6.70 \pm 0.02$	$8.00 \pm 0.02$	$8.21 \pm 0.03$
D403	$6.00^{+0.08}_{-0.06}$	$6.16 \pm 0.04$	$6.64^{+0.08}_{-0.06}$	$6.81^{+0.08}_{-0.06}$	$8.02 \pm 0.02$	$8.19 \pm 0.04$
D404	$4.66 \pm 0.09$	$4.79 \pm 0.10$	$6.56^{+0.08}_{-0.05}$	$6.70^{+0.06}_{-0.05}$	$8.06 \pm 0.03$	$8.22 \pm 0.03$
D405	$5.62 \pm 0.06$	$5.82 \pm 0.06$	$6.55^{+0.08}_{-0.09}$	$6.76 \pm 0.09$	$8.00 \pm 0.01$	$8.21 \pm 0.01$
D406	$5.37^{+0.12}_{-0.11}$	$5.52 \pm 0.11$	$6.61^{+0.14}_{-0.13}$	$6.80 \pm 0.14$	$7.96^{+0.02}_{-0.03}$	$8.13 \pm 0.03$
D407	$5.43^{+0.14}_{-0.16}$	$5.62^{+0.17}_{-0.16}$	$6.62^{+0.24}_{-0.12}$	$6.88^{+0.31}_{-0.13}$	$8.05 \pm 0.06$	$8.29 \pm 0.15$
D408	$5.45^{+0.04}_{-0.05}$	$5.59 \pm 0.05$	$6.54 \pm 0.01$	$6.71 \pm 0.01$	$8.07 \pm 0.01$	$8.24 \pm 0.01$
D409	$5.41^{+0.06}_{-0.07}$	$5.57 \pm 0.07$	-	-	$8.06 \pm 0.01$	$8.25 \pm 0.01$
D410	$5.45^{+0.10}_{-0.10}$	$5.54^{+0.10}_{-0.11}$	$6.46^{+0.20}_{-0.11}$	$6.58^{+0.08}_{-0.09}$	$8.03 \pm 0.04$	$8.15 \pm 0.11$
D411	$5.23 \pm 0.04$	$5.35^{+0.05}_{-0.04}$	$6.52 \pm 0.03$	$6.65 \pm 0.03$	$8.05 \pm 0.02$	$8.18 \pm 0.03$
D412	$5.46 \pm 0.15$	$5.67^{+0.13}_{-0.14}$	$6.54^{+0.24}_{-0.12}$	$6.79 \pm 0.10$	$8.07 \pm 0.04$	$8.30^{+0.12}_{-0.10}$
D413	$6.16 \pm 0.05$	$6.34 \pm 0.05$	$6.83 \pm 0.03$	$7.05^{+0.02}_{-0.03}$	$8.23 \pm 0.02$	$8.44 \pm 0.03$
D414	$5.96 \pm 0.05$	$6.13 \pm 0.04$	$6.64 \pm 0.02$	$6.84 \pm 0.02$	$8.02 \pm 0.02$	$8.22 \pm 0.02$
D415	$5.89 \pm 0.07$	$6.07 \pm 0.07$	$6.79 \pm 0.02$	$6.98 \pm 0.02$	$7.92^{+0.02}_{-0.01}$	$8.12 \pm 0.02$
D416	$6.02 \pm 0.09$	$6.19^{+0.08}_{-0.09}$	$6.77 \pm 0.03$	$6.96 \pm 0.03$	$7.92 \pm 0.02$	$8.11 \pm 0.02$
D417	$5.91 \pm 0.07$	$6.08 \pm 0.07$	$6.66 \pm 0.01$	$6.85^{+0.01}_{-0.02}$	$7.88 \pm 0.01$	$8.07 \pm 0.01$
D418	$5.78 \pm 0.07$	$5.96 \pm 0.06$	$6.65 \pm 0.01$	$6.84 \pm 0.01$	$7.89 \pm 0.01$	$8.09 \pm 0.01$
D419	$5.86^{+0.09}_{-0.08}$	$6.06 \pm 0.09$	-	-	$7.94 \pm 0.02$	$8.15 \pm 0.03$
D420	$5.84 \pm 0.06$	$6.02 \pm 0.06$	$6.78 \pm 0.01$	$6.97 \pm 0.01$	$7.92 \pm 0.01$	$8.13 \pm 0.01$
D421	$5.87 \pm 0.04$	$6.06 \pm 0.04$	$6.84 \pm 0.01$	$7.03 \pm 0.01$	$7.93 \pm 0.01$	$8.14 \pm 0.01$
D422	$6.01 \pm 0.05$	$6.18 \pm 0.05$	$6.79 \pm 0.02$	$7.01 \pm 0.02$	$8.23^{+0.02}_{-0.03}$	$8.42 \pm 0.03$
D423	$5.53^{+0.09}_{-0.10}$	$5.70^{+0.08}_{-0.09}$	$6.05 \pm 0.02$	$6.21 \pm 0.02$	$7.48 \pm 0.01$	$7.65 \pm 0.01$
D424	$5.63 \pm 0.04$	$5.79 \pm 0.04$	$6.08 \pm 0.02$	$6.24 \pm 0.02$	$7.51 \pm 0.01$	$7.68 \pm 0.01$
D425	$6.24 \pm 0.07$	$6.67 \pm 0.07$	$6.68 \pm 0.04$	$7.16 \pm 0.04$	$8.41^{+0.04}_{-0.03}$	$8.88 \pm 0.05$
D426	$5.96^{+0.02}_{-0.03}$	$6.15^{+0.02}_{-0.03}$	$6.80 \pm 0.01$	$7.02 \pm 0.01$	$7.98 \pm 0.01$	$8.20 \pm 0.01$
D427	$6.01 \pm 0.01$	$6.21 \pm 0.01$	$6.71 \pm 0.01$	$6.93 \pm 0.01$	$8.09 \pm 0.01$	$8.30 \pm 0.01$
D428	$6.02 \pm 0.06$	$6.20^{+0.05}_{-0.06}$	$7.01 \pm 0.01$	$7.22 \pm 0.01$	$8.11 \pm 0.01$	$8.31 \pm 0.01$
D429	$5.90^{+0.07}_{-0.08}$	$6.06^{+0.08}_{-0.07}$	$6.48 \pm 0.02$	$6.67 \pm 0.02$	$7.95 \pm 0.01$	$8.12^{+0.02}_{-0.01}$
D430	$5.91^{+0.11}_{-0.12}$	$6.14 \pm 0.11$	$6.95^{+0.21}_{-0.11}$	$7.22^{+0.09}_{-0.08}$	$8.04 \pm 0.03$	$8.31^{+0.09}_{-0.10}$
D431	$5.99^{+0.04}_{-0.05}$	$6.16^{+0.04}_{-0.05}$	$6.40 \pm 0.02$	$6.58^{+0.01}_{-0.02}$	$7.80 \pm 0.01$	$7.99 \pm 0.01$
D432	$5.80 \pm 0.04$	$5.98 \pm 0.03$	$6.45 \pm 0.01$	$6.64 \pm 0.01$	$7.80 \pm 0.01$	$7.99 \pm 0.01$
D433	$5.73 \pm 0.09$	$5.89 \pm 0.08$	$6.30 \pm 0.03$	$6.49 \pm 0.03$	$7.75^{+0.01}_{-0.02}$	$7.93 \pm 0.02$
D434	$5.74 \pm 0.06$	$5.92 \pm 0.06$	$6.33^{+0.02}_{-0.01}$	$6.52 \pm 0.01$	$7.77 \pm 0.01$	$7.96 \pm 0.01$
D435	$5.83 \pm 0.04$	$6.01 \pm 0.04$	$6.51 \pm 0.02$	$6.70 \pm 0.02$	$7.80 \pm 0.01$	$8.00 \pm 0.01$
D436	$5.80 \pm 0.07$	$5.98^{+0.06}_{-0.07}$	$6.50 \pm 0.02$	$6.69 \pm 0.02$	$7.79 \pm 0.01$	$7.99 \pm 0.02$
D437	$6.16^{+0.10}_{-0.09}$	$6.16^{+0.10}_{-0.09}$	$7.22^{+0.17}_{-0.09}$	$7.22^{+0.17}_{-0.09}$	$7.89 \pm 0.01$	$7.89 \pm 0.01$
D438	$5.41^{+0.04}_{-0.05}$	$5.56 \pm 0.04$	$5.97 \pm 0.01$	$6.14 \pm 0.01$	$7.51 \pm 0.01$	$7.68 \pm 0.01$
D439	$5.50^{+0.08}_{-0.07}$	$5.64^{+0.07}_{-0.08}$	$5.97 \pm 0.02$	$6.14 \pm 0.03$	$7.52^{+0.02}_{-0.01}$	$7.68 \pm 0.02$
D440	$5.35 \pm 0.09$	$5.48^{+0.09}_{-0.11}$	$6.08 \pm 0.02$	$6.24 \pm 0.02$	$7.67 \pm 0.01$	$7.82 \pm 0.01$
D441	$5.86 \pm 0.13$	$6.08^{+0.13}_{-0.12}$	$7.02 \pm 0.02$	$7.24 \pm 0.02$	$8.18 \pm 0.01$	$8.40 \pm 0.02$
D442	$6.16 \pm 0.06$	$6.23 \pm 0.06$	$7.05 \pm 0.02$	$7.16 \pm 0.02$	$8.39 \pm 0.03$	$8.48 \pm 0.03$
D443	$5.78^{+0.22}_{-0.20}$	$5.79 \pm 0.24$	$7.03^{+0.35}_{-0.14}$	$7.03^{+0.31}_{-0.13}$	$8.26^{+0.10}_{-0.11}$	$8.26^{+0.13}_{-0.12}$
D444	$6.05^{+0.10}_{-0.09}$	$6.28 \pm 0.10$	$7.01 \pm 0.02$	$7.25 \pm 0.02$	$8.25 \pm 0.02$	$8.49 \pm 0.02$
D445	$5.95 \pm 0.09$	$6.07^{+0.09}_{-0.08}$	$6.93 \pm 0.04$	$7.06 \pm 0.04$	$8.16^{+0.03}_{-0.04}$	$8.31 \pm 0.04$
D446	$5.94^{+0.07}_{-0.08}$	$6.07 \pm 0.08$	$6.64^{+0.03}_{-0.02}$	$6.80^{+0.03}_{-0.02}$	$8.05^{+0.03}_{-0.02}$	$8.21^{+0.02}_{-0.03}$
D447	$6.18^{+0.13}_{-0.12}$	$6.30 \pm 0.12$	$6.97^{+0.06}_{-0.05}$	$7.13 \pm 0.06$	$8.04^{+0.05}_{-0.06}$	$8.20 \pm 0.06$
D448	$6.26^{+0.12}_{-0.13}$	$6.36^{+0.12}_{-0.13}$	$6.72 \pm 0.06$	$6.87^{+0.06}_{-0.05}$	$7.82^{+0.04}_{-0.05}$	$7.97 \pm 0.05$

**Table D.8.** Total abundances derived from the nebular sample. All values are in  $12+\log(X/H)$  units.

Reference number	Fe		N		O	
	$t^2 = 0$	$t^2 > 0$	$t^2 = 0$	$t^2 > 0$	$t^2 = 0$	$t^2 > 0$
D449	$5.71^{+0.15}_{-0.14}$	$5.89^{+0.15}_{-0.17}$	$6.69^{+0.02}_{-0.01}$	$6.89 \pm 0.01$	$8.07 \pm 0.01$	$8.28 \pm 0.01$
D450	$5.72^{+0.13}_{-0.12}$	$5.89 \pm 0.11$	$6.56 \pm 0.02$	$6.76 \pm 0.02$	$7.97 \pm 0.01$	$8.15 \pm 0.01$
D451	$5.81 \pm 0.03$	$5.98 \pm 0.03$	$6.51 \pm 0.05$	$6.68^{+0.05}_{-0.04}$	$7.73 \pm 0.02$	$7.92 \pm 0.02$
D452	$6.03^{+0.13}_{-0.11}$	$6.20^{+0.10}_{-0.11}$	$7.18^{+0.09}_{-0.06}$	$7.37^{+0.08}_{-0.06}$	$7.88 \pm 0.04$	$8.08 \pm 0.04$

**Table D.9.** Observed  $H\alpha/H\beta$  fluxes prior to reddening correction in a subsample of the references presented in Table D.2 where these values are reported. We also show the theoretical value calculated with PyNeb (Luridiana et al. 2015), using the atomic data from Storey & Hummer (1995) and the Adopted  $n_e$  and  $T_e([\text{O III}])$  ( $t^2$  has no influence on this RL-ratio) from Tables D.3 and D.5, respectively.

Reference number	Observed $H\alpha/H\beta$	Dust-free theoretical $H\alpha/H\beta$
D28	$3.04 \pm 0.03$	2.78
D38	$3.01 \pm 0.03$	2.79
D40	$2.85 \pm 0.03$	2.80
D41	$2.86 \pm 0.03$	2.75
D53	$2.79 \pm 0.03$	2.80
D54	$2.80 \pm 0.03$	2.78
D56	$3.07 \pm 0.03$	2.81
D59	$3.03 \pm 0.03$	2.82
D60	$2.98 \pm 0.03$	2.84
D67	$3.08 \pm 0.03$	2.79
D69	$3.22 \pm 0.03$	2.80
D70	$3.73 \pm 0.04$	2.82
D72	$3.50 \pm 0.07$	2.78
D75	$3.06 \pm 0.06$	2.77
D76	$3.92 \pm 0.08$	2.82
D77	$3.38 \pm 0.07$	2.83
D79	$3.53 \pm 0.07$	2.75
D81	$3.20 \pm 0.06$	2.82
D82	$2.79 \pm 0.06$	2.78
D86	$5.11 \pm 0.26$	2.91
D90	$3.01 \pm 0.03$	2.82
D92	$4.16 \pm 0.04$	2.82
D93	$3.09 \pm 0.03$	2.82
D96	$2.92 \pm 0.06$	2.78
D99	$1.98 \pm 0.04$	2.79
D101	$0.30 \pm 0.01$	2.81
D106	$4.05 \pm 0.04$	2.82
D115	$5.02 \pm 0.05$	2.86
D116	$3.48 \pm 0.17$	2.88
D117	$3.54 \pm 0.11$	2.88
D118	$3.29 \pm 0.10$	2.84
D119	$3.44 \pm 0.17$	2.87
D122	$3.32 \pm 0.20$	2.94
D135	$3.66 \pm 0.11$	2.85
D168	$4.23 \pm 0.25$	2.88
D173	$2.85 \pm 0.09$	2.87
D177	$3.77 \pm 0.26$	2.90
D183	$2.81 \pm 0.08$	2.80
D187	$3.98 \pm 0.12$	2.92
D188	$4.14 \pm 0.12$	2.90
D192	$3.76 \pm 0.41$	2.96
D193	$4.60 \pm 0.78$	2.91
D194	$3.18 \pm 0.29$	2.91
D197	$3.02 \pm 0.27$	2.85
D198	$3.15 \pm 0.35$	2.85
D199	$3.99 \pm 0.12$	2.94
D201	$3.89 \pm 0.12$	2.91
D220	$6.81 \pm 0.27$	2.91
D221	$3.75 \pm 0.15$	2.92
D222	$4.31 \pm 0.13$	2.89
D223	$3.19 \pm 0.10$	2.91
D224	$4.30 \pm 0.13$	2.89
D225	$2.68 \pm 0.08$	2.90
D226	$4.20 \pm 0.13$	2.88
D227	$4.32 \pm 0.13$	2.88
D228	$4.29 \pm 0.13$	2.89
D229	$4.33 \pm 0.13$	2.89
D230	$2.78 \pm 0.14$	2.93
D231	$4.35 \pm 0.17$	2.89

**Table D.9.** Observed  $H\alpha/H\beta$  fluxes prior to reddening correction in a subsample of the references presented in Table D.2 where these values are reported. We also show the theoretical value calculated with PyNeb (Luridiana et al. 2015), using the atomic data from Storey & Hummer (1995) and the Adopted  $n_e$  and  $T_e([\text{O III}])$  ( $t^2$  has no influence on this RL-ratio) from Tables D.3 and D.5, respectively.

Reference number	Observed $H\alpha/H\beta$	Dust-free theoretical $H\alpha/H\beta$
D232	$4.65 \pm 0.23$	2.89
D233	$3.44 \pm 0.14$	2.90
D234	$4.45 \pm 0.13$	2.90
D235	$11.61 \pm 0.46$	2.87
D236	$7.69 \pm 0.38$	2.89
D237	$16.39 \pm 0.82$	2.88
D238	$3.58 \pm 0.29$	2.90
D239	$13.79 \pm 0.41$	2.86
D240	$15.38 \pm 0.46$	2.86
D241	$9.75 \pm 0.20$	2.92
D242	$8.40 \pm 0.08$	2.88
D243	$5.56 \pm 0.17$	2.84
D244	$7.47 \pm 0.15$	2.94
D245	$10.85 \pm 0.33$	2.97
D246	$9.08 \pm 0.82$	2.92
D247	$4.91 \pm 0.39$	2.88
D248	$3.52 \pm 0.07$	2.96
D249	$4.59 \pm 0.18$	2.89
D250	$3.55 \pm 0.07$	2.86
D251	$3.62 \pm 0.04$	2.85
D252	$3.65 \pm 0.07$	2.83
D253	$3.04 \pm 0.18$	2.81
D255	$3.15 \pm 0.03$	2.80
D256	$3.24 \pm 0.06$	2.85
D257	$3.25 \pm 0.07$	2.85
D258	$3.78 \pm 0.04$	2.83
D262	$3.48 \pm 0.07$	2.86
D263	$2.95 \pm 0.06$	2.79
D264	$3.01 \pm 0.06$	2.78
D265	$2.90 \pm 0.03$	2.79
D266	$3.18 \pm 0.06$	2.84
D267	$2.92 \pm 0.06$	2.80
D270	$4.08 \pm 0.04$	2.83
D271	$3.51 \pm 0.04$	2.78
D272	$3.17 \pm 0.03$	2.84
D273	$3.34 \pm 0.07$	2.79
D274	$3.49 \pm 0.03$	2.84
D278	$3.11 \pm 0.06$	2.82
D279	$3.59 \pm 0.04$	2.82
D282	$3.29 \pm 0.10$	2.90
D283	$2.81 \pm 0.14$	2.78
D285	$3.60 \pm 0.11$	2.91
D286	$3.19 \pm 0.06$	2.90
D288	$3.58 \pm 0.11$	2.91
D294	$3.19 \pm 0.26$	2.91
D295	$3.05 \pm 0.24$	2.92
D296	$4.05 \pm 0.24$	2.86
D312	$2.92 \pm 0.12$	2.82
D315	$3.46 \pm 0.10$	2.85
D316	$3.07 \pm 0.09$	2.85
D320	$3.40 \pm 0.17$	2.78
D334	$4.23 \pm 0.25$	2.84
D336	$4.62 \pm 0.05$	2.83
D338	$4.55 \pm 0.05$	2.80
D339	$3.33 \pm 0.07$	2.81
D340	$4.46 \pm 0.04$	2.83
D341	$3.22 \pm 0.06$	2.82
D342	$3.28 \pm 0.16$	2.81
D346	$3.28 \pm 0.07$	2.74

**Table D.9.** Observed  $H\alpha/H\beta$  fluxes prior to reddening correction in a subsample of the references presented in Table D.2 where these values are reported. We also show the theoretical value calculated with PyNeb (Luridiana et al. 2015), using the atomic data from Storey & Hummer (1995) and the Adopted  $n_e$  and  $T_e([\text{O III}])$  ( $t^2$  has no influence on this RL-ratio) from Tables D.3 and D.5, respectively.

Reference number	Observed $H\alpha/H\beta$	Dust-free theoretical $H\alpha/H\beta$
D347	$3.34 \pm 0.07$	2.74
D348	$3.54 \pm 0.07$	2.74
D349	$3.39 \pm 0.07$	2.74
D350	$3.42 \pm 0.07$	2.73
D351	$3.26 \pm 0.07$	2.74
D360	$2.90 \pm 0.03$	2.76
D361	$3.11 \pm 0.03$	2.77
D364	$3.12 \pm 0.06$	2.74
D365	$3.21 \pm 0.03$	2.79
D366	$3.47 \pm 0.03$	2.80
D368	$2.79 \pm 0.03$	2.79
D376	$2.78 \pm 0.03$	2.78
D377	$3.03 \pm 0.03$	2.81
D380	$3.14 \pm 0.19$	2.80
D391	$3.24 \pm 0.03$	2.82
D392	$2.79 \pm 0.03$	2.79
D393	$3.08 \pm 0.03$	2.75
D394	$3.11 \pm 0.03$	2.83
D400	$2.66 \pm 0.03$	2.82
D401	$3.27 \pm 0.10$	2.82
D402	$2.95 \pm 0.09$	2.81
D403	$4.26 \pm 0.13$	2.80
D404	$3.34 \pm 0.13$	2.83
D405	$3.15 \pm 0.03$	2.82
D406	$3.39 \pm 0.03$	2.82
D407	$3.31 \pm 0.03$	2.83
D413	$4.08 \pm 0.20$	2.84
D414	$3.38 \pm 0.17$	2.81
D415	$2.81 \pm 0.03$	2.79
D416	$2.81 \pm 0.06$	2.79
D419	$3.21 \pm 0.03$	2.79
D435	$3.54 \pm 0.04$	2.78
D436	$3.48 \pm 0.03$	2.78
D440	$3.40 \pm 0.07$	2.77
D441	$3.47 \pm 0.07$	2.82
D444	$3.52 \pm 0.07$	2.84
D447	$3.70 \pm 0.07$	2.81
D448	$3.32 \pm 0.07$	2.78
D449	$3.34 \pm 0.07$	2.80
D450	$3.61 \pm 0.04$	2.81
D452	$3.00 \pm 0.30$	2.78